

Julius Maximilians University Würzburg



Influence of the pancreatic extracellular matrix on pancreatic differentiation of human induced pluripotent stem cells and establishment of 3D organ models

Einfluss der Extrazellulärmatrix des Pankreas auf die pankreatische Differenzierung humaner induziert pluripotenter Stammzellen und Etablierung von 3D Organmodellen

Doctoral thesis for a doctoral degree at the Graduate School of Life Sciences,
Julius-Maximilians-Universität Würzburg,
Section Biomedicine

Submitted by

Constantin Berger

From

Bad Soden a.T. (Germany)

Würzburg 2020



Submitted on:

office stamp

Members of the Thesis Committee

Chairperson: Prof. Dr. Manfred Gessler

Primary Supervisor: PD Dr. Marco Metzger

Supervisor (Second): Prof. Dr. Heike Walles

Supervisor (Third): Prof. Dr. Martin Faßnacht-Capeller

Supervisor (Fourth): Dr. Daniela Zdzieblo

Date of Public Defence: _____

Date of Receipt of Certificates: _____

Table of Contents

1	List of already published content	1
2	Abstract	2
3	Zusammenfassung	4
4	Introduction	6
4.1	Diabetes mellitus – a pandemic disease	6
4.2	Anatomy and function of the human pancreas	6
4.3	Regulation of blood glucose levels by the pancreatic islet hormones	8
4.4	Development of diabetes mellitus	9
4.5	Current treatment options for diabetes mellitus – Technical vs. biological approaches	11
4.6	Types of stem cells – which is the best for the generation of β -cells?	14
4.7	Embryonic pancreatic development – The blueprint for the in vitro generation of β -cells	15
4.8	Mimicking pancreatic organogenesis for the in vitro differentiation of pancreatic β -cells	18
4.9	The extracellular matrix – a dynamic signaling hub regulating cellular function	21
4.10	The role of the extracellular matrix in the islet niche	24
4.11	Aim of the study	26
5	Methods	27
5.1	Animal housing and euthanasia	27
5.2	Generation of pancreas-specific extracellular matrix scaffolds (PanMa)	27
5.3	Generation of small intestinal submucosa serosa matrix (SISser)	28
5.4	Generation of lung-specific extracellular matrix scaffolds (LungMa)	28
5.5	Sterilization of ECM scaffolds	28
5.6	Sample preparation for histological analysis	28
5.7	Histological analyses	29
5.8	Immunohistochemical staining	30
5.9	Quantification of bile acid	30
5.10	Evaluation using the PancScore	30
5.11	Surface electron microscopy (SEM)	31
5.12	Rheology	31
5.13	Passive permeability assay	31
5.14	Determination of water storage capacity	32
5.15	Standard cell culture procedures	32
5.16	Culture of endothelial cell lines	33

5.17	Recellularization of the PanMas arterial system _____	33
5.18	hiPSC maintenance culture _____	33
5.19	hiPSC maintenance culture on ECM-TWs _____	34
5.20	Spontaneous differentiation of hiPSCs on ECM-TWs _____	34
5.21	Directed differentiation of hiPSCs towards hormone-expressing pancreatic cells (HECs) according to the 5-stage suspension culture protocol _____	35
5.22	Supplementation of liquid PanMa during the directed differentiation of hiPSCs towards HECs _____	35
5.23	Directed differentiation of hiPSCs towards β -cells (SC- β) according to the 7-stage airlift protocol _____	36
5.24	Hydrogel production _____	37
5.25	Hydrogel culture of HEC clusters _____	37
5.26	Fluorescein-Diacetate (FDA)/Propidium Iodid (PI) staining _____	37
5.27	Glucose stimulated Insulin secretion _____	38
5.28	MTT Assay _____	38
5.29	WST-1 Assay _____	39
5.30	DNA quantification _____	39
5.31	Gel electrophoresis _____	39
5.32	RNA Isolation and cDNA synthesis _____	40
5.33	Real-Time quantitative PCR (RT-qPCR) _____	40
5.34	Image acquisition, image processing and figure design _____	41
5.35	Statistical analysis _____	42
6	Results _____	44
6.1	Generation and characterization of a porcine pancreas derived ECM scaffold _____	44
6.1.1	The PanMa represents a pancreatic acellular scaffold with a largely conserved ECM architecture _____	44
6.1.2	The conserved vessel system of the PanMa allows recellularization of parts of the arterial system _____	48
6.1.3	The PancScore as a novel tool for the standardized evaluation of PanMa scaffold quality _____	50
6.2	Identification of PanMa-specific ECM properties _____	52
6.2.1	The PanMa represents a fiber-based, permeable, hygroscopic scaffold _____	52
6.2.2	The PanMa is softer compared to the SISser _____	55
6.3	Impact of the PanMa on pluripotent stem cells _____	56
6.3.1	The PanMa is suitable for hiPSC culture _____	56
6.3.2	Culture on the PanMa promotes an endoderm signature of hiPSCs during multi-lineage differentiation _____	59

6.3.3	Differentiating hiPSCs attach to the PanMa by binding to collagen fibers and bundles	65
6.4	Impact of the PanMa on pancreatic differentiation	67
6.4.1	Application of the PanMa as a liquid medium supplement does not influence the directed pancreatic differentiation of hiPSCs	67
6.4.2	Pancreatic differentiation of hiPSCs on the solid PanMa scaffold results in reduced hormone expression in S5 cells	70
6.4.3	Pancreatic differentiation of hiPSCs on the PanMa does not alter glucose stimulated insulin secretion of S5 HECs	73
6.4.4	hiPSC-derived S7 cells generated on the PanMa exhibit a reduced GCG and SST expression	74
6.4.5	Pancreatic differentiation on the PanMa does not affect GSIS of the generated S7 cells	78
6.5	Establishment of a pancreatic organ model	80
6.5.1	A PanMa-derived hydrogel allows encapsulation and prolonged culture of S5 HECs	80
6.5.2	Culture in a PanMa-derived hydrogel affects the cytomorphology of HEC clusters	82
6.5.3	Prolonged culture in the PanMa hydrogel marginally impairs the functional maturation of S5 HECs	84
7	<i>Discussion</i>	87
7.1	The generated PanMa on the test bench	87
7.2	Softer, fiber-based, hygroscopic – uncovering the PanMa’s biophysical profile	89
7.3	Culture on ECM scaffolds appears to have a minor impact on the hiPSC pluripotency network	92
7.4	The PanMa affects hiPSC differentiation – A matter of stiffness, composition, attachment or a combinatorial effect?	95
7.5	A role of the ECM as a selective factor for lineage biased cell attachment	97
7.6	Pancreatic differentiation on the PanMa does not improve β -cell function	98
7.7	Indications for an involvement of the PanMa in endocrine commitment	99
7.8	The right timing for PanMa signaling might boost endocrine development	101
7.9	Using the PanMa hydrogel as a platform for the establishment of an islet-endothelial co-culture model	104
7.10	Limitations of this study	106
8	<i>Conclusion</i>	109
9	<i>Future Perspectives</i>	110
10	<i>References</i>	111
11	<i>Tables and Figures</i>	123

12	<i>Appendix</i>	125
12.1	Suupplementary Figures	125
12.2	List of abbraviations	129
12.2.1	Protein and gene abbreviations	129
12.2.2	Other abbraviations	129
12.2.3	Units and symbols	130
13	<i>Materials</i>	132
13.1	Buffers and Solutions	132
13.2	Cell culture media composition	134
13.3	Cell lines	135
13.4	Cell culture media and solutions	135
13.5	Medium supplements	136
13.6	Cell culture surface coatings	136
13.7	Enzymes	137
13.8	Commercial kits	137
13.9	Chemicals and solutions for histology and molecular biology	137
13.10	Primary Antibodies	139
13.11	Secondary Antibodies	139
13.12	Primers	140
13.13	Expandable materials	141
13.14	Machines	142
13.15	Software	143
14	<i>Acknowledgment</i>	144
15	<i>Curriculum Vitae</i>	146
16	<i>List of Publications</i>	149
17	<i>Affidavit</i>	150
18	<i>Eidesstattliche Erklärung</i>	150

1 List of already published content

Some content of this thesis has already been published in the following scientific articles:

C. Berger*, Y. Bjørlykke*, L. Hahn, M. Mühlemann, S. Kress, H. Walles, R. Luxenhofer, H. Ræder, M. Metzger, D. Zdziebło. „Matrix decoded – A pancreatic extracellular matrix with organ specific cues guiding human iPSC differentiation.” *Biomaterials*, 2020(*shared 1st authorship)

The following chapters contain parts of the published article in a rephrased form:

5.1 – 5.18, 5.20, 5.28, 5.30 – 5.35, 6.1.1 – 6.1.3, 6.2.1, 6.2.2, 6.3.2, 6.3.3

The following figures has been modified from the published article:

Fig. 6 – 14, 16, 17, 19, 20 - S1 – S3

2 Abstract

Diabetes mellitus is an incurable, metabolic disease, which is associated with severe long-term complications. The *in vitro* generation of pancreatic β -cells from human induced pluripotent stem cells (hiPSCs) represent a promising strategy for a curative therapy of *diabetes mellitus*. However, current differentiation strategies largely fail to produce functional β -cells *in vitro* and require an additional *in vivo* transplantation to achieve terminal maturation. Previous studies demonstrated a beneficial effect of the extracellular matrix (ECM) on the survival and sustained function of adult, isolated islets of Langerhans. This raises the question whether organ-specific cell-ECM interactions might represent the missing link driving the final stage of β -cell development. In order to address this issue, this study investigated the impact of the pancreas ECM on *in vitro* β -cell differentiation and its use for the establishment of a pancreatic endocrine organ model.

To this purpose, a pancreas-specific ECM scaffolds (PanMa) was derived from porcine pancreata using whole organ decellularization with Sodium Deoxycholate. In a first step, the generated PanMa was thoroughly characterized using (immuno-) histological stainings, scanning electron microscopy and DNA quantification as well as perfusion and recellularization experiments with endothelial cells. Based on these data, a scoring system (PancScore) for a standardized PanMa generation was developed. Next, the generated PanMa was tested for the presence of tissue-specific ECM features. Therefore, the biophysical and physico-structural characteristics, such as rigidity, porosity and hygroscopy were analyzed using rheological measurements, particle diffusion analyses as well as a water evaporation assay and compared to the properties of ECM scaffolds derived from porcine small intestine (SISser) and lung (LungMa) to examine organ-specific scaffold cues. Following the thorough scaffold characterization, the impact of the PanMa on pluripotency and early development of hiPSC was studied. To this purpose, gene and protein expression of hiPSCs during maintenance culture and spontaneous differentiation on the PanMa were assessed. In a next step, the impact of the PanMa on the pancreatic endocrine differentiation of hiPSCs was tested. Therefore, the PanMa was used as a liquid media supplement or as a solid scaffold during the directed differentiation of hiPSC towards either pancreatic hormone-expressing cells (Rezania et al. 2012; Rezania et al. 2014) or maturing β -cells (Rezania et al. 2014). The impact of the PanMa on the generated cells was examined by gene expression analysis, immunohistochemical staining of important stage markers, as well as glucose stimulated insulin secretion assays. In a last part of this study, the potential of the PanMa for the prolonged culture of hiPSC derived endocrine cells for the establishment of an *in vitro* organ model of the endocrine pancreas was examined. Therefore, a PanMa-derived hydrogel was generated and used for the encapsulation and culture of hiPSC-derived hormone-expressing cells (HECs). The influence of the

PanMa-hydrogel culture was analyzed on gene, protein and functional level by gene expression analysis, immunohistochemical stainings and glucose stimulated insulin secretion.

Whole organ decellularization resulted in the generation of an acellular PanMa scaffold, with low amounts of residual DNA and a preserved ECM micro- and ultrastructure, including important ECM components, such as collagen I, III and IV. Furthermore, the PanMa maintained an intact vessel system and was verified as cytocompatible as demonstrated by the successful recellularization of the arterial system with human endothelial cells. In comparison to SISser and LungMa, the PanMa was characterized as a relative soft, hygroscopic scaffold with a collagen-fiber based structure. Furthermore, the findings indicate that the ECM-specific properties have a relevant effect on the stem cell character and early multi-lineage decisions of hiPSCs. In this regard, maintenance of hiPSCs on the PanMa resulted in a slightly changed expression of pluripotency genes (*OCT4*, *SOX2* and *NANOG*) and a weak immunohistochemical signal for NANOG protein, indicating a PanMa-dependent impact on hiPSC pluripotency. Strikingly, this presumption was corroborated by the finding that culture on the PanMa promoted an endodermal development of hiPSCs during spontaneous differentiation. In line with that, pancreatic differentiation of hiPSC on both the PanMa and SISser resulted in a significant decrease of glucagon and somatostatin gene expression as well as an unaltered insulin expression, suggesting an ECM-driven suppression of the development of non β -cell endocrine cells. However, this change did not result in an improved glucose stimulated insulin secretion of the generated HECs. Moreover, use of the PanMa as a hydrogel allowed prolonged culture of these cells in a defined culture system. HECs were viable after 21 days of culture, however already showed an altered islet morphology as well as a slightly decreased glucose stimulated insulin secretion.

Altogether, this study demonstrates a relevant biological effect of tissue specific ECM cues on the *in vitro* differentiation of hiPSCs. More specifically, the data indicate an involvement of the ECM in the endocrine commitment of hiPSC-derived pancreatic cells during directed differentiation highlighting the ECM as an important regulator of pancreatic development. Collectively, these findings emphasize the relevance of the ECM for the fabrication of functional hiPSC-derived cell types and suggest a much stronger consideration of organ specific ECM cues for tissue engineering approaches as well as clinical translation in regenerative medicine.

3 Zusammenfassung

Der *Diabetes mellitus* bezeichnet eine bislang unheilbare, metabolische Erkrankung, die mit schwerwiegenden Folgeerkrankungen einhergeht. Unter den potentiellen Strategien zur Heilung von *Diabetes mellitus* stellt die *in vitro* Generierung adulter β -Zellen des endokrinen Pankreas aus humanen induziert pluripotenten Stammzellen (hiPS) einen vielversprechenden Ansatz dar. Zwar ermöglichen bisherige Protokolle die Herstellung von Zellen mit einem β -Zell-ähnlichen Charakter, jedoch zeigen diese eine zunächst eingeschränkte Funktion, die sich erst im Verlauf einer vollständigen, durch Transplantation induzierten, Reifung der Zellen, normalisiert. Vorangegangene Studien zeigen, dass sich die Extrazellulärmatrix (EZM) von Geweben positiv auf das Überleben und die Funktion adulter, isolierter Langerhans-Inseln des Pankreas auswirkt. Vor diesem Hintergrund stellt sich die Frage, ob Einflüsse der organspezifischen EZM die finale Reifung *in vitro* hergestellter β -Zellen herbeiführen können. Um diese Hypothese zu testen, wurde im Rahmen der vorliegenden Studie die Wirkung der pankreatischen EZM auf die *in vitro* Differenzierung von hiPS zu endokrinen Zellen des Pankreas untersucht sowie die Eignung der pankreatischen EZM zur Etablierung eines Organmodells des endokrinen Pankreas erprobt.

Hierzu wurde zunächst eine pankreasspezifische EZM-Trägerstruktur (PanMa) durch Dezellularisierung von Pankreaten des Schweins mittels Natriumdesoxycholat hergestellt. Die generierte PanMa wurde anhand (immun-) histologischer Färbungen, Rasterelektronenmikroskopie, Feststellung des DNA-Gehalts sowie durch Versuche zur Perfusion und Wiederbesiedelung mit Endothelzellen eingehend charakterisiert. Zudem wurde auf Basis der ermittelten Daten ein Bewertungssystem (PancScore) zur standardisierten Herstellung der PanMa entwickelt. Als Nächstes wurde untersucht, ob die PanMa über gewebespezifische EZM-Merkmale verfügt. Zu diesem Zweck wurden biophysikalische und strukturelle Eigenschaften wie Festigkeit, Porosität und Hygroskopie mittels rheologischer Messungen sowie Versuchen zur Teilchendiffusion und zum Wasserbindungsverhalten bestimmt und mit azellulären EZMs des Dünndarms (SISser) und der Lunge (LungMa) verglichen. Nach der eingehenden Analyse der PanMa wurde deren Effekt auf die Eigenschaften von Stammzellen sowie auf frühe Stadien der Stammzellentwicklung untersucht. Hierzu wurde die PanMa als Trägerstruktur während der Erhaltung sowie der spontanen Differenzierung von hiPS verwendet und der Einfluss der PanMa anhand von Genexpressionsanalysen und immunhistochemischer Färbungen analysiert. In einem nächsten Schritt wurde die Wirkung der PanMa auf die Differenzierung von hiPS zu endokrinen Zellen des Pankreas untersucht. Hierfür wurde die PanMa zum einen in flüssiger Form als Mediumzusatz sowie als solide Trägerstruktur während der Differenzierung von hiPS zu hormonexpmierenden Zellen (Rezania et al. 2012; Rezania et al. 2014) oder maturierenden β -Zellen verwendet (Rezania et al. 2014). Der Effekt der PanMa wurde anhand von Genexpressions-

analysen, immunhistochemischer Färbungen und Analysen zur Glukose-abhängigen Insulinsekretion untersucht. In einem letzten Teil der Studie wurde die Eignung der PanMa zur verlängerten Kultivierung von hiPS-abgeleiteten endokrinen Zellen des Pankreas im Hinblick auf die Etablierung eines Organmodells des endokrinen Pankreas getestet. Hierzu wurde die PanMa zu einem Hydrogel weiterverarbeitet, welches zur Einkapselung und Kultivierung von hiPS-abgeleiteten hormonexprimierenden Zellen eingesetzt wurde. Um die Auswirkungen der Hydrogel-Kultur nachzuvollziehen, wurden die kultivierten Zellen mittels Genexpression, immunhistochemischer Färbungen und Analysen zur Glukose-abhängigen Insulinsekretion untersucht.

Mittels Dezellularisierung porziner Pankreaten konnte eine zellfreie, pankreasspezifische EZM-Trägerstruktur mit geringen Restbeständen an DNA sowie einer weitgehend erhaltenen Mikro- und Ultrastruktur mit typischen EZM-Komponenten wie Kollagen I, III und IV hergestellt werden. Im Rahmen der Besiedelung arterieller Gefäße mit humanen Endothelzellen wurde die Zellkompatibilität der hergestellten PanMa sowie eine weitgehende Unversehrtheit der Gefäßstrukturen nachgewiesen. Verglichen zu SISser und LungMa zeichnete sich die PanMa als eine relativ weiche, stark wasserbindende, faserbasierte Struktur aus. Weiterhin konnten Hinweise für einen Effekt der PanMa auf den Stammzellcharakter und die frühe Entwicklung von hiPS beobachtet werden. Hierbei führte die Erhaltung von hiPS auf der PanMa zu einer leicht veränderten Expression von Genen des Kernpluripotenznetzwerks sowie zu einem reduziertem NANOG-Proteinsignal. Einhergehend mit diesen Beobachtungen zeigten hiPS während spontaner Differenzierung auf der PanMa eine verstärkte endodermale Entwicklung. Im Verlauf der pankreatischen Differenzierung führte die Kultivierung auf der PanMa zu einer signifikant verringerten Expression von Glukagon und Somatostatin, während die Expression von Insulin unverändert blieb, was auf eine Verminderung endokriner α - und δ -Zellen hinweist. Diese Veränderung äußerte sich jedoch nicht in einer verbesserten Glukose-abhängigen Insulinsekretion der generierten hormonexprimierenden Zellen. Unter Anwendung der PanMa als Hydrogel konnten hormonexprimierenden Zellen über einen verlängerten Zeitraum kultiviert werden. Nach 21 Tagen in Kultur zeigten die eingekapselten hormonexprimierenden Zellen eine unverändert hohe Viabilität, wiesen allerdings bereits eine erste veränderte Zellanordnung sowie eine leicht verminderte Glukose-abhängige Insulinsekretion auf.

Zusammengefasst konnte in dieser Studie ein biologischer Effekt gewebespezifischer EZM-Merkmale auf die Differenzierung von hiPS nachgewiesen werden. Darüber hinaus weisen die Daten auf eine relevante Funktion der EZM im Rahmen der endokrinen Spezifizierung von hiPS während der pankreatischen Differenzierung hin. Diese Beobachtungen verdeutlichen die eminente Rolle der EZM in der Herstellung von funktionalen hiPS-abgeleiteten Zellen und plädieren für eine stärkere Einbindung organspezifischer EZMs im Bereich des Tissue Engineering und der klinischen Translation in der Regenerativen Medizin.

4 Introduction

4.1 *Diabetes mellitus – a pandemic disease*

Diabetes mellitus, commonly known as diabetes, is a global, life-threatening disease. In 2019, diabetes affected 463 million people worldwide, and 4.2 million cases of death were related to diabetes and its associated long-term consequences (International Diabetes Federation 2019). According to the sharply increasing prevalence of the disease over the last decades especially due to altered life style, studies estimate that in 2030 every 10th adult person worldwide will be affected by diabetes (Saeedi et al. 2019). Given these numbers, diabetes can undisputedly be termed as one of the major challenges of the 21th century.

Clinically, diabetes manifests as a chronic elevation of blood sugar levels in consequence of impaired glucose regulation of the body. In 90% of the cases, diabetes occurs with advanced age caused by multiple factors, including genetic predisposition and an unhealthy life-style, which is described as type 2 *diabetes mellitus*. In contrast, type 1 *diabetes mellitus*, which accounts for 5 – 10% of all diabetes cases, is defined by an autoimmune-mediated destruction of the glucose-regulating cells early in life. Vascular damages caused by the increased plasma glucose concentration lead to severe complications, which present a huge burden for patients as well as for global health care systems. So far, treatment of diabetes is limited to an amelioration of the hyperglycemic symptoms. In search of curative treatment strategies, a special focus lays on pancreatic tissue engineering and cell-based regenerative strategies to restore the body's ability to govern blood glucose homeostasis. The key for this striven aim is a profound understanding of the disease-related tissue, which predominantly renders this function: the endocrine pancreas.

4.2 *Anatomy and function of the human pancreas*

The pancreas is a glandular organ located behind the stomach in the abdomen and part of the digestive system and endocrine system of vertebrates (Fig. 1a) (Beger 2018). Anatomically, the pancreas segregates into a head, a corpus and a tail (Fig. 1b) and fulfills multiple roles in human physiology. Besides the aforementioned endocrine compartment, which primarily plays a role in controlling plasma-glucose levels, the pancreas harbors exocrine cells that are specialized in the production and secretion of the pancreatic juice for supporting nutrient digestion in the small intestine. The exocrine pancreas accounts for 98% of the pancreatic cell mass and mainly consists of acinar cells that synthesize and secrete the components of the pancreatic juice as well as duct cells lining the vessels of the excretory duct system (Fig. 1c). The comparatively small amount of endocrine tissue is represented by the Islets of Langerhans; demarcated cell clusters that are

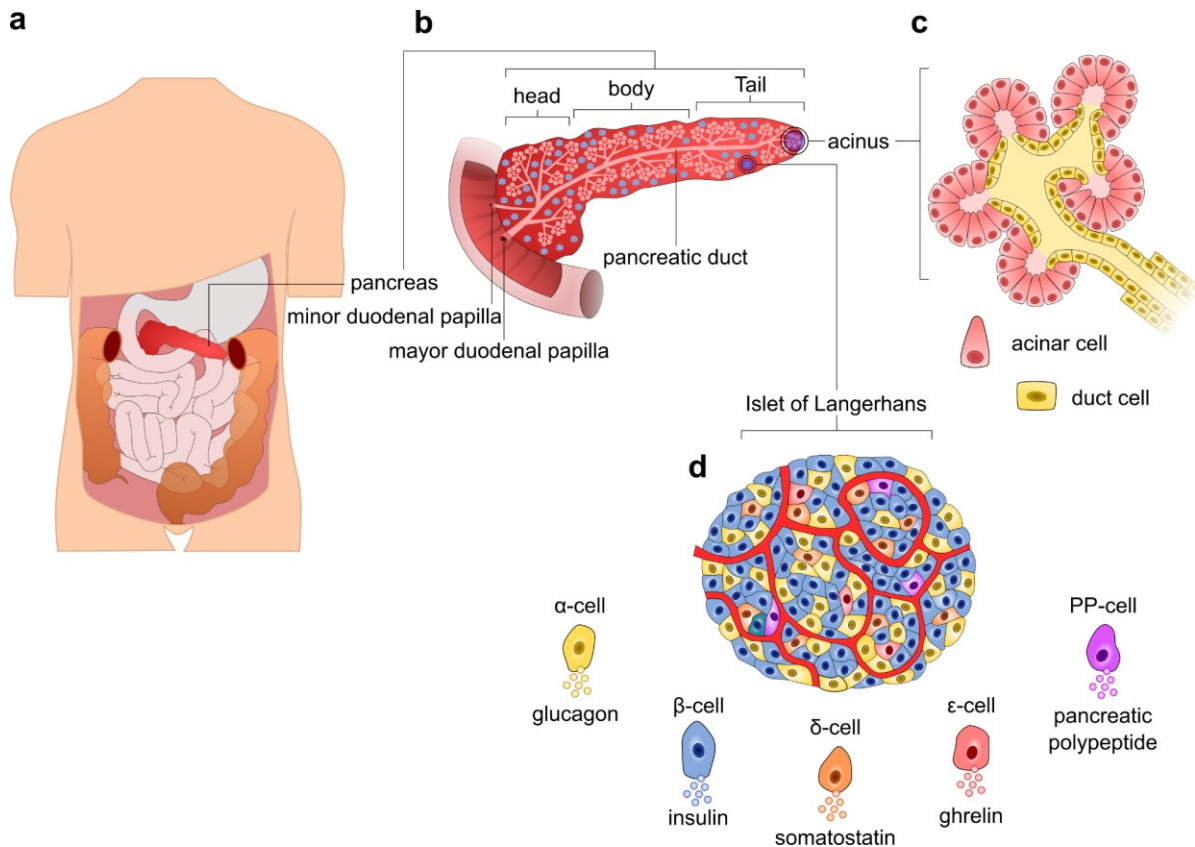


Figure 1 Anatomy of the human pancreas. **a** Location of the pancreas in the abdominal cavity. **b** Macroscopically, the pancreas is segregated into a head, body and tail. It mostly consists of exocrine tissue, which comprises acinar structures located around the duct system. The main duct is connected to the duodenum via the major and/or minor duodenal papilla. Furthermore, the pancreas contains an endocrine compartment, which is represented by cell clusters called Islets of Langerhans, which are distributed throughout the exocrine tissue. **c** Structure of an acinus with acinar cells located around a central lumen that segues into a duct which is lined by duct cells. **d** Scheme of an islets of Langerhans. The islet contains five hormone-secreting cell types: glucagon-secreting α -cells, insulin-secreting β -cells, somatostatin-secreting δ -cells, ghrelin-secreting ϵ -cells and pancreatic polypeptide-secreting PP-cells. **Sources of information:** Beger 2018.

distributed throughout the entire pancreas (Fig 1d). At the cellular level, the pancreatic islets comprise five endocrine cell types: glucagon-secreting α -cells, insulin-secreting β -cells, somatostatin-secreting δ -cells, ghrelin-secreting ϵ -cells and pancreatic-polypeptide-secreting PP-cells. Islets represent a specialized, highly vascularized and innervated microcompartment, whereas islet size, cellular composition and cytoarchitecture vary widely across species (Kim et al. 2009; Steiner et al. 2010). In this context, human islets generally consist of $\approx 55\%$ β -cells, $\approx 35\%$ α -cells, $\approx 10\%$ δ -cells and $< 5\%$ ϵ - and PP-cells (Brissova et al. 2005). However, recent studies demonstrate a large interindividual and intraindividual islet heterogeneity, suggesting that there is no human islet stereotype (Dybala and Hara 2019), which is of high interest to understand the pathophysiology of islet-related disorders.

4.3 Regulation of blood glucose levels by the pancreatic islet hormones

The ability of pancreatic islets to maintain plasma glucose levels in a physiological range (3 – 9 mmol/l) (Bertau et al. 2007; Freckmann et al. 2007) is rendered mostly, but not exclusively, by the antagonistic interplay of α - and β -cells (Fig. 2). Both cell types secrete hormones with contradictory effects on glucose homeostasis of the body (Habegger et al. 2010; Petersen and Shulman 2018). The release of hormones from α - and β -cells is dependent on the organism's nutrient state, which is reflected predominantly by the blood glucose level. β -cells exhibit a basal insulin secretion already at low glucose concentrations (\approx 3 mM) and respond to an increase in plasma glucose levels, with the elevated secretion of insulin (Alcazar and Buchwald 2019). By binding to the insulin receptor, insulin mediates pleiotropic effects in fat, brain, muscle and liver cells by regulating a variety of metabolic functions. The most relevant actions regarding glucose homeostasis are the elevation of glucose uptake in muscle and fat cells as well as the activation of anabolic pathways for an increased glucose consumption (glycolysis) and glucose deposition (glycogenesis) in the liver as well as fat synthesis (lipogenesis) and protein synthesis in skeletal muscle cells, adipocytes and hepatocytes (Petersen and Shulman 2018). Eventually, insulin triggered actions lead to a decrease of the plasma glucose concentration resulting in the normalization of high blood glucose levels. In contrast to β -cells, glucagon secretion from α -cells is suppressed at 5 – 7 mM extracellular glucose and progressively increased at lower plasma-glucose concentrations (Gylfe 2016). Glucagon antagonizes the actions of insulin and promotes glycogen breakdown (glycogenolysis) and glucose production in the liver (gluconeogenesis) as well as fat (lipolysis) and protein breakdown (proteolysis) (Habegger et al. 2010). The enhanced glucose mobilization results in increased plasma glucose levels and restoration of normoglycemia at hypoglycemic states.

The direct coupling of insulin and glucagon secretion to the amount of circulating glucose allows for a fast restoration of deviating glucose concentrations, which is of utmost importance to ensure a steady supply of energy to all cells of the body. However, glycemic control does not solely rely on glucose but comprises other factors that can trigger or alter hormone secretion from pancreatic endocrine cells. For instance, amino acids and fatty acids (Henquin et al. 2003), as well as non-nutrient secretagogues such as the neurotransmitter acetylcholine (Skelin Klemen et al. 2017) can induce insulin secretion from β -cells. Furthermore, the incretin hormones GIP and GLP-1, which are released from K- (GIP) and L-cells (GLP-1) in the intestine in the presence of dietary fats and carbohydrates along with nutrient digestion and transport, stimulate insulin secretion, thereby enhancing the glucose-lowering actions of insulin (Baggio and Drucker 2007). On the other hand, both hormones also affect glucagon release from α -cells, whereas GLP-1 inhibits (Ramracheya et al. 2018) and GIP stimulates the exocytosis of glucagon in a glucose-dependent manner (El and Campbell 2020). Another pancreatic hormone, somatostatin, has a neutralizing

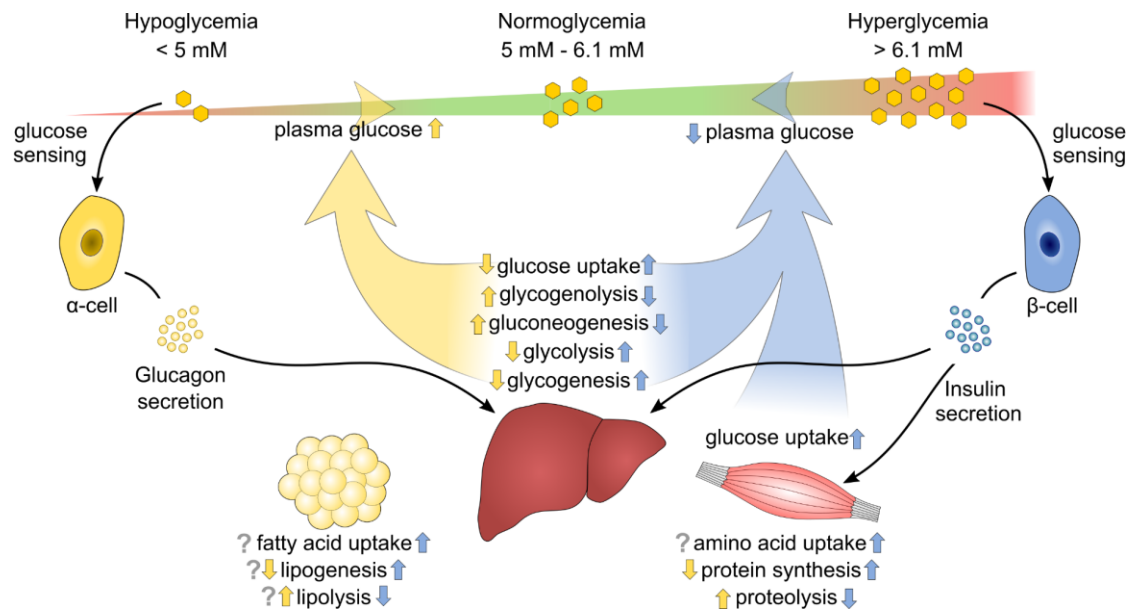


Figure 2 Glucose homeostasis of the human body. Overview of the effect of insulin and glucagon in selected tissues of the human body. Glucose plasma levels (upper panel) trigger the secretion of glucagon from α -cells (yellow, at low glucose concentrations) or insulin from β -cells (blue, at high glucose concentration). By binding to their respective receptors on the surface of effector cells, glucagon and insulin mediate antagonistic actions by up- or downregulating metabolic pathways. The effects of glucagon (yellow arrows) promote the mobilization of glucose leading to an increase of plasma glucose levels. Conversely, insulin signaling (blue arrows) induces glucose storage and results in a decrease of circulating blood glucose. In consequence, the glucagon- and insulin-mediated processes result in the restoration of normal blood glucose levels. **Sources of information:** Dimitriadis et al. 2011; Ramnanan et al. 2011; Petersen and Shulman 2018; Adeva-Andany et al. 2019.

effect on islet hormone release by inhibiting both, insulin and glucagon secretion (Hauge-Evans et al. 2009; Rutter 2009). Moreover, the crosstalk between the endocrine cells is mediated by the paracrine effect of insulin and glucagon. While insulin inhibits glucagon secretion by stimulation of somatostatin from δ -cells (Vergari et al. 2019), glucagon, in turn, promotes insulin secretion (Huypens et al. 2000).

Altogether, glucose homeostasis represents a highly balanced regulatory circuit. Despite the high interconnectivity of the involved players, especially the β -cell is of outstanding clinical importance as their failure is associated with the development of diabetes.

4.4 Development of diabetes mellitus

The ability of the body to maintain glucose levels in a physiological range depends on a sophisticated interplay of several factors and regulatory mechanisms. Important key elements are the capacity of insulin secretion, the insulin mediated actions in peripheral tissues as well as insulin-opposing factors, such as glucagon and somatostatin. Loss or malfunction of one or several components disrupts the glycemic control circuit and eventually causes chronic hyper- or hypoglycemia. The symptoms of low blood sugar levels (fasting glucose $< 3 \text{ mmol/l}$) (Bansal and

Weinstock 2020) result from a glucose shortage in the brain and ranges from fatigue to faintness or even death under (chronic) severe hypoglycemia. Instead, chronic hyperglycemia (fasting glucose > 7.8 mmol/l) is associated with vascular damages and is a major symptom of *diabetes mellitus*. Dependent on the underlying cause of the hyperglycemia, two forms of *diabetes mellitus* are distinguished. Patients with Type 1 *diabetes mellitus* (T1DM) suffer from an absolute lack of insulin due to an autoimmune-driven depletion of β -cells (Lehuen et al. 2010). T1DM usually occurs early in life and accounts for roughly 5 – 10% of all diabetes cases with an increasing prevalence worldwide (Daneman 2006). T1DM patients exhibit hyperglycemia as well as hypoinsulinemia and require a lifelong exogenous insulin administration therapy in combination with a strict diet to maintain glycemic control. In contrast to T1DM, which is caused by a deficient insulin secretion, the pathogenesis of type 2 *diabetes mellitus* (T2DM) is traced back to an impeded insulin response of the effector cells (Kahn et al. 2014). At early phases, the initial insulin insensitivity causes an elevated insulin secretion from β -cells due to missing regulatory feedback from the insulin-resistant tissue (Kahn et al. 1993; Kahn et al. 2014). Consequently, individuals exhibit basal hyperinsulinemia, while remaining under glycemic control at an early stage of insulin resistance (Shanik et al. 2008). This clinically unremarkable state can sustain as long as the increased insulin secretion compensates for the manifested insulin resistance. However, as soon as β -cell function deteriorates or insulin resistance worsens, a relative lack of insulin emerges leading to a gradual progression of hyperglycemia and the onset of T2DM (Kahn et al. 2014). With ongoing disease progression, a loss of β -cells is observed due to oxidative and endoplasmic reticulum stress in consequence of increased amounts of glucose and lipids (glucolipotoxicity) as well as amyloid deposition in β -cells (Poitout and Robertson 2008; Jurgens et al. 2011). In severe cases of T2DM, this leads to an absolute lack of insulin, which requires an insulin replacement therapy. The development of T2DM comprises multiple factors, including genetic predisposition as well as environmental influences. Currently, more than 50 genes have been linked to T2DM, whose defect either leads to a decreased β -cell function or elevates the risk of insulin resistance (Morris et al. 2012). Environmental factors including an unhealthy diet, reduced activity, overweight and age increase the risk for an impaired β -cell function or insulin resistance and thereby promote the onset of T2DM (Wu et al. 2014).

A serious consequence of chronic hyperglycemia consists in the damage of vascular structures that can lead to severe complications such as retinopathy, nephropathy, neuropathy, stroke and myocardial infarction (Papatheodorou et al. 2018). Moreover, patients with an absolute lack of insulin face the risk of acute ketoacidosis, caused by the uncontrolled production of ketone bodies in consequence of hypoinsulinemia that in worse cases may lead to death (Duca et al. 2019). To prevent acute complications as well as severe sequelae, restoring glycemic control of T1DM and T2DM patients is of utmost importance.

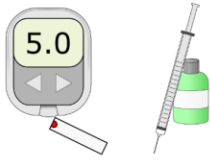
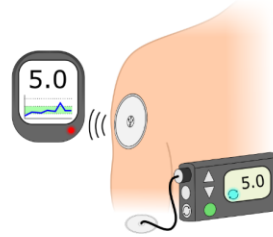
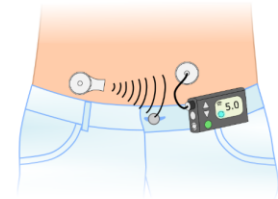
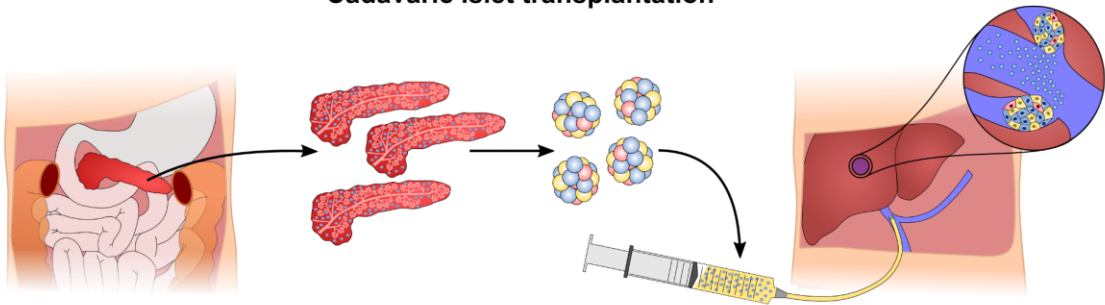
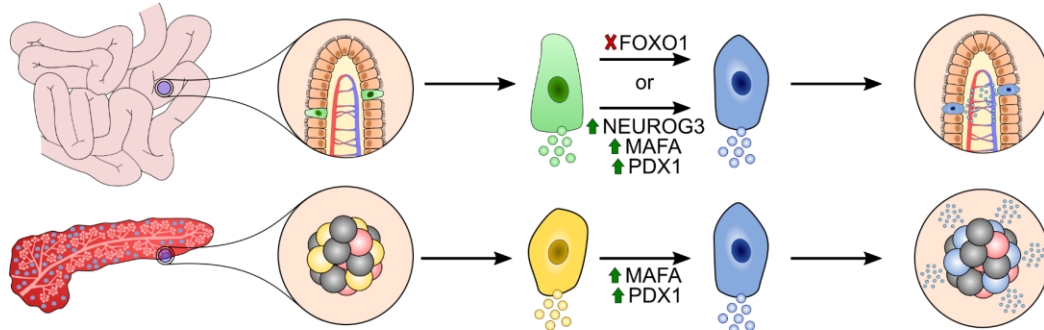
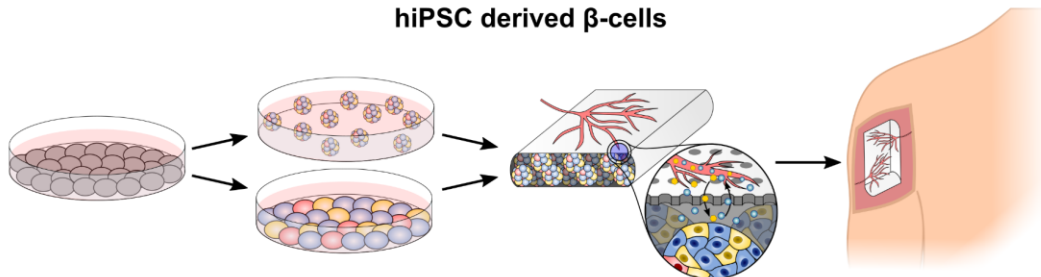
4.5 Current treatment options for diabetes mellitus – Technical vs. biological approaches

A curative treatment for any type of *diabetes mellitus* is not available yet. Available therapeutic strategies aim to ameliorate diabetic symptoms by improving glycemic control. In the case of T2DM, treatment concepts comprise lifestyle modifications, including diet, physical exercise and reduction of stress as well as pharmacological treatment (Marín-Peñalver et al. 2016). However, loss of insulin secretion, as this is the case in T1DM and advanced T2DM, always requires an insulin substitution. The development of integrated glucose sensors and insulin pumps to replace old-fashioned glucometers and insulin pens have improved the quality of life of diabetes patients (Fig. 3a, b) (Umpierrez and Klonoff 2018). Next-generation closed-loop systems promise a further improvement and close in on the realization of an artificial pancreas (Fig. 3c). A major obstacle remains the algorithm, which converts the measured glucose signal into an adapted insulin injection and which must be able to make a precise prediction about the required amount of insulin (Hovorka 2011). This prerequisite discloses the downside of all artificial solutions for insulin substitution: they solely rely on glucose measurements. However, as outlined previously, an adjustment of insulin secretion according to the nutrient status of the body requires coupling with other metabolic, neuronal and hormonal signals.

So far, this complex task can only be rendered by endogenous biological systems, demonstrating the demand for cell-based therapy approaches. Transplantation of pancreatic islets represents one branch of cell replacement strategies, which is currently used to treat T1DM with severe hypoglycemic events (Fig. 3d) (Anazawa et al. 2019). At this, islets are isolated from donor pancreata via enzymatic digestion followed by a purification step and injection into the recipient via the portal vein (Ricordi et al. 1990; Scharp et al. 1990; Shapiro et al. 2000). The establishment of the Edmonton protocol largely improved the success rate of islet transplantation and allowed T1DM patients to regain metabolic control, which however, was not sustainable for more than one year (Shapiro et al. 2000; Shapiro et al. 2006). Refinements of isolation and purification techniques as well as the combination with immunosuppression therapy resulted in an improved glucose control, a reduced need of exogenous insulin and a marked decrease in severe hypoglycemic episodes in three-quarters of T1DM patients for 10 years (Vantyghem et al. 2019). However, a large portion of islets is still lost during and after engraftment which is assigned to instant blood mediated inflammatory reaction (IBMIR), mechanical stress, hypoxia and, notably, a destruction of the islet-extracellular matrix during the isolation process (Bennet et al. 2000; Kanak et al. 2014; Cross et al. 2017). Furthermore, insulin independence by islet transplantation comes at the cost of an immunosuppression therapy, which has severe side effects. In order to circumvent the need for immunosuppressive drugs while simultaneously preventing an immunoreactive destruction of the transplants, human islets can be encapsulated in semipermeable containers or devices, which on one hand allow gas, nutrient and protein

exchange, while simultaneously shielding the islet from immune cells (Jacobs-Tulleneers-Thevissen et al. 2013; Weir 2013). A commonly used substrate for islet encapsulation are hydrogels, water-containing networks of cross-linked polymers that can be obtained from biological sources, for instance seaweed-derived alginate (Lee and Mooney 2012), or manufactured synthetically, like polyethylene glycol hydrogels (Lin and Anseth 2009). Modification of the hydrogel crosslinking as well as the combination with other materials opening up new the possibilities for islet transplantation, such as other transplantation sites (Jacobs-Tulleneers-Thevissen et al. 2013; An et al. 2018). Apart from hydrogel microencapsulation, synthetic devices are used for the macroencapsulation of islets (Agulnick et al. 2015; Magisson et al. 2020). Following the same principles as the smaller-sized variants, the macro-devices allow a precise placement of the cells. Currently, macrocapsule devices containing insulin-producing cells are tested in clinical trials highlighting their potential for future cell replacement approaches (Agulnick et al. 2015; Cooper-Jones and Ford 2017). Moreover, current focus is put on a prevascularization of islets or of the encapsulating devices with the aim to accelerate connection to the host vasculature after transplantation and thereby improve the oxygen supply of islets (Magisson et al. 2020; Nalbach et al. 2020).

Besides tremendous progress in the last two decades, the low transplantation efficacy (2 – 3 pancreata are required for one islet transplantation) in combination with a shortage in suitable donor material still greatly limits the potential of islet transplantation. To circumvent the restriction in cell material, other approaches pursue the *de novo* generation of β -cells *in vitro* or *in vivo*. Rodent studies have highlighted the stimulation of β -cell replication as a promising approach to replenish β -cell mass (Nir et al. 2007). Translation of this concept to humans fails, as human β -cells seem to lose their replicative ability within the first three decades of life (Perl et al. 2010). Likewise, β -cell neogenesis from endocrine progenitor cells is not realized so far, as such organ-specific multipotent stem cells are currently considered inexistent in the adult human pancreas (Dor et al. 2004). In contrast, transdifferentiation, which describes the conversion of a somatic cell into another cell type by targeting the activation of genetic programs, represents a valid concept for β -cell replacement *in vivo* (Fig. 3e) (Eguchi and Kodama 1993). Conversion into insulin-producing β -cells has been demonstrated for human hepatic cells, pancreatic α -cells and gallbladder cells (Gefen-Halevi et al. 2010; Bouchi et al. 2014; Galivo et al. 2017; Furuyama et al. 2019). In the mentioned approaches, a β -cell phenotype could be induced by the activation of certain transcription factors that are essential for regulating the β -cell fate. Although this concept renders immunosuppression obsolete, as the transdifferentiation takes place *in vivo* and has the advantage that β -cells are generated in an intact environment that is readily vascularized, there are several open questions. For example, it is not clear, how the extrapancreatic location affects β -cell function, to which extent cell conversion takes place, how possible hybrid genotypes affect

Technical solutions**a** manual handling**b** automated systems**c** closed loop systems**Biological solutions****d****Cadaveric islet transplantation****e****Transdifferentiation****f****hiPSC derived β -cells**

long-term function and stability of the generated cells and whether the body can compensate for the loss of another cell type in favor of β -cells. Moreover, the amount of generated β -cells is still limited by the number of cells exhibiting a (epi-) genetic predisposition suitable for conversion.

Production of larger cell numbers requires the generation of β -cells from a replicative cell type. Pluripotent stem cells (PSCs) fulfill key requirements as a cell source for cell replacement strategies, as they allow an initial, nearly unlimited expansion *in vitro* before they can be differentiated towards the desired β -cell phenotype (Fig. 3f) (Atala et al. 2019). Encapsulation of the generated cells further allows for immune evasion of the transplanted β -cells in T1DM patients, which prevents a repeated β -cell-directed autoimmune response as well as a general graft versus host reaction (Agulnick et al. 2015). However, the differentiation of PSCs towards β -cells represents a complex process that requires a profound knowledge of the underlying developmental programs and regulatory mechanisms that are by far not fully understood yet.

4.6 Types of stem cells – which is the best for the generation of β -cells?

Stem cell (SC) is a collective term applicable to cells that have the ability to self-renew and to give rise to other cell types (Atala et al. 2019). SCs are subdivided into different classes, according to their developmental potency. Totipotent stem cells can give rise to any embryonic cell as well as extraembryonic tissues such as the placenta (Seydoux and Braun 2006). *In vivo*, this ability is restricted to cells of the early phase of embryogenesis, including the zygote and cells of the 2-cell stage (Baker and Pera 2018). Ongoing cell division accompanies with a loss of differentiation capacity, resulting in cell types with more limited lineage potential. PSCs, such as the cells of the inner cell mass at the blastocyst stage of mammalian development, can give rise to cells of the three germ layers ecto-, meso- and endoderm, but have lost the ability to form extraembryonic tissue (Romito and Cobellis 2016). Cells of a single germ layer are considered as multipotent, as they are limited to only develop in multiple specialized cells types of the same germ layer (Mirzaei

Figure 3 Therapeutic strategies for the treatment of diabetes mellitus. **a – c** Technical solutions for the treatment of diabetes mellitus rest upon the measurement of glucose and the application of an appropriated amount of insulin. Besides glucometer and insulin syringe/pen (a), novel methods for the insulin application comprise glucose sensor devices and semi-automatic pumps (b). Wireless connection of glucose sensor and insulin pump aim to create an automated system for the exogenous control of plasma glucose (c). **d – f** Biological solutions not only measure glucose but are able to integrate a number of information about the metabolic state of the body into a concerted insulin response. Cadaveric islet transplantation (d) presents a well-established strategy for replacing endocrine function in type 1 diabetes patients. Thereby, islets are isolated from donor pancreata, purified and injected into the portal vein of the host. Another hypothetical strategy is the transdifferentiation of β -cell from other cells of the body, exemplarily shown for enteroendocrine and α -cells (e). At this, the cell type switch is induced by the transcriptional reprogramming induced by exogenous factors. β -cells can also be generated *in vitro* by the directed differentiation of hPSCs (f). Encapsulated, these cells can be transplanted to a patient and act as a surrogate for the endocrine pancreas. **Sources of information:** Bouchi et al. 2014; Agulnick et al. 2015; Galivo et al. 2017; Umpierrez and Klonoff 2018; Furuyama et al. 2019.

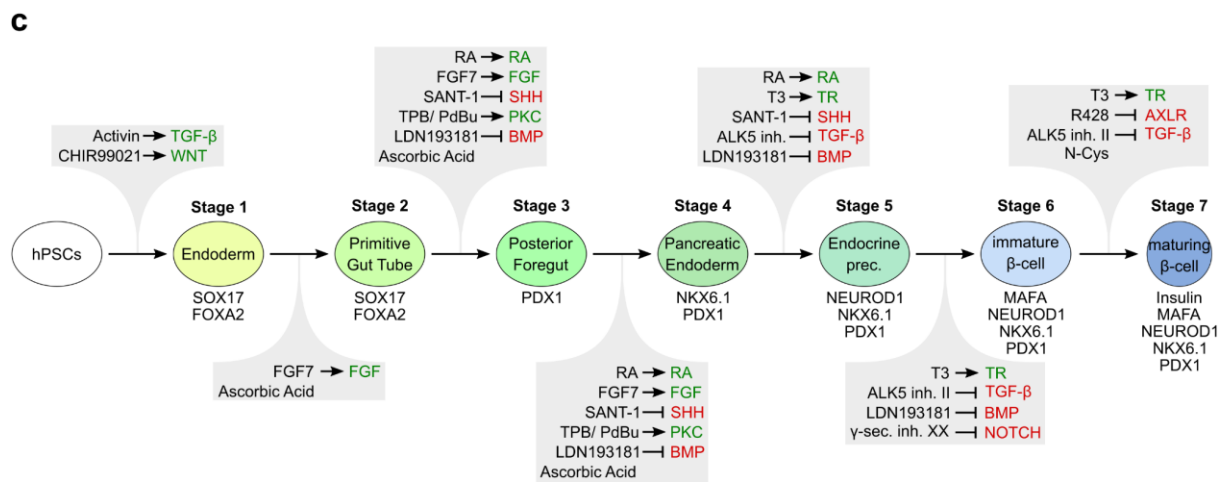
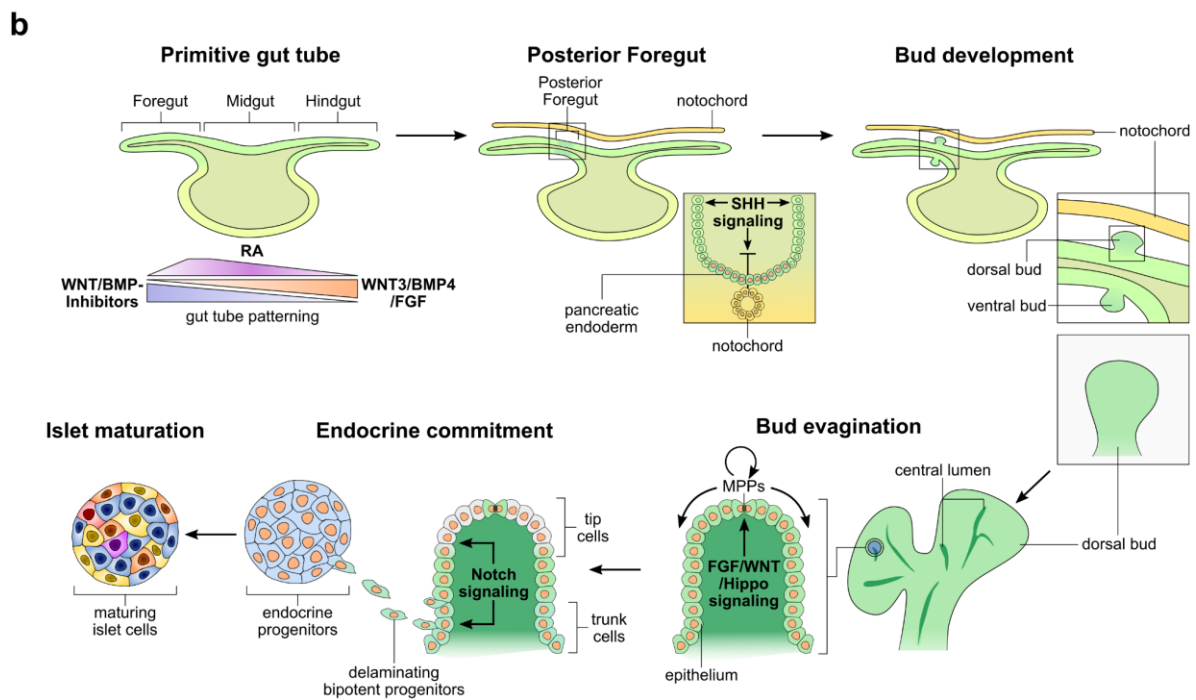
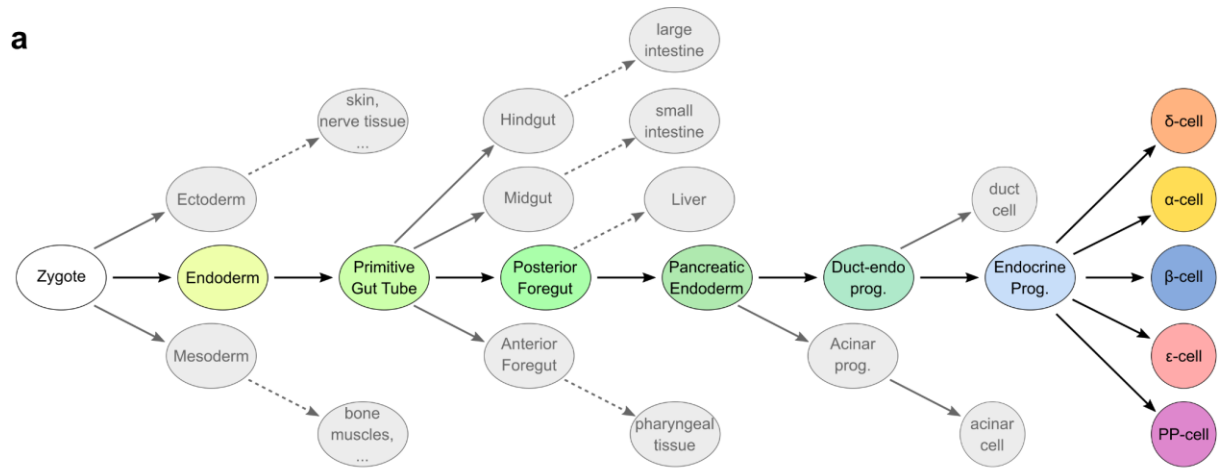
et al. 2018). The further differentiation of cells results in the appearance of oligopotent and eventually unipotent precursor cells that still have the ability to self-renew, but can give rise to only one specified cell type (Zakrzewski et al. 2019).

Whereas totipotent SCs and PSCs are only present during embryogenesis, SCs with a more restricted lineage potential are also existent in the human organism, postnatally. Such adult stem cells exhibit a multi-, oligo- or unipotent character and play a crucial role for the cell replenishment in distinct organs, such as the intestine or the hematopoietic system. In the adult pancreas, no cells with adult SC-like capacities have been identified so far, which also explains its restricted regenerative potential (Zhou and Melton 2018). Therefore, PSCs appear as a favored source for β -cell generation in the context of tissue engineering and cell replacement strategies. In general, PSCs can be obtained either by extraction of human embryonic stem cells (hESCs) (Thomson et al. 1998) or by the generation of induced pluripotent stem cells (iPSCs) from human somatic cells (Takahashi et al. 2007). In the first case, hESCs are isolated from the inner cell mass of the blastocyst and have been used for the *in vitro* generation of several cell types (Thomson et al. 1998; Liu et al. 2020). However, access to these cells is harshly restricted in some countries, including Germany (regulated by the “Embryonenschutzgesetz; legislated at 13.12.1990 (BGBl. I S. 2746), last amended at: 21.11.2011 (BGBl. I S. 2228)”), as the ethical justifiability of their extraction is controversially debated. Human iPSCs (hiPSCs) represent an attractive alternative to hESCs as they share important features, including the capacity for self-renewal and differentiation but are not tainted with ethical concerns. The generation of hiPSCs from somatic cells is achieved by the ectopic expression of the transcription factors octamer-binding transcription factor (OCT) 4, sex determining region Y-box (SOX) 2, avian myelocytomatosis virus oncogene cellular homolog (C-MYC) and Kruppel-like Factor (KLF) 4 within somatic cell types such as fibroblasts or blood cells. This results in the shut-down of the somatic program and the reactivation of the endogenous pluripotency network, comprising transcription factors that are essential for the induction and maintenance of stemness such as the core pluripotency factors OCT4, SOX2, and NANOG (Takahashi et al. 2007). Given their many advantages, hiPSCs present an ideal source for the generation of β -cells and a great opportunity for pancreatic tissue engineering approaches.

4.7 Embryonic pancreatic development – The blueprint for the *in vitro* generation of β -cells

Directed differentiation of hPSCs towards pancreatic endocrine cells represents a multistep process that is tailored to closely mimic the developmental processes *in vivo* (Petersen et al. 2018). Human pancreas development is hallmarked by important specification steps, starting with the formation of the endoderm germ layer initiated by Nodal-mediated transforming growth factor

(TGF)- β signaling during gastrulation (Fig. 4a, b) (Brown et al. 2011). Afterwards, the flat endoderm sheet folds into the primitive gut tube (PGT) which is then patterned along the anterior-posterior axis. At this, concentration gradients of bone morphogenetic protein (BMP)-4, wingless/Int-1 (WNT) and retinoic acid (RA) segregate the PGT into a foregut, a midgut and a hindgut segment, each of which with a distinct developmental fate (Davenport et al. 2016). PGT cells with the potential to form pancreatic tissue arise from the posterior foregut (PF) in consequence of high RA concentrations in the designated PF region (Davenport et al. 2016). In the next step, the pancreatic commitment of distinct cell populations of the ventral and dorsal endoderm is achieved by two different events. Inhibition of sonic hedgehog (SHH) signaling, which in mice is mediated by fibroblast growth factor (FGF) 2 and Activin released from the adjacent notochord and which is probably similarly regulated in humans, induces the formation of pancreatic endoderm (PE) from dorsal PF cells (Jennings et al. 2013). Almost simultaneously, cells from the ventral PF undergo a similar pancreatic specification, which is induced by signals from the lateral plate mesoderm, presumably BMP family members as well as Activin (Kumar 2003; Jennings et al. 2013). Both events result in the formation of a dorsal and a ventral bud, that contain multipotent pancreatic progenitors (MPPs), the first cells with a determined pancreatic fate which is manifested by the expression of pancreatic and duodenal homeobox (PDX) 1, a master regulator of pancreatic lineage development (Piper et al. 2004; Jennings et al. 2013). Accordingly, MPPs are capable of giving rise to all pancreatic cell types, including acinar, ductal and endocrine cells (Castaing et al. 2005). Signals of the FGF-, Hippo- and WNT-pathway mediate the expansion of the MPPs and drive the evagination of the buds which accompanies the formation of an outer pancreatic epithelium and the emergence of central microlumens (Ye et al. 2005; Jennings et al. 2013; Bonfanti et al. 2015; Cebola et al. 2015). In the following, gut rotation brings the dorsal and ventral bud in close proximity and thereby facilitates fusion into a single pancreas bud (Jennings et al. 2013). During this time, MPPs located in the epithelium express carboxypeptidase A1 (CPA1)/GATA binding protein (GATA) 4/homeobox protein NK-6 homolog A (NKX6.1)/SOX9. In a Notch-signaling dependent event, MPPs start to segregate into two distinct populations (Hald et al. 2003; Jennings et al. 2013). Cells at the tip of the epithelium continuously express CPA1 and GATA4 but lose NKX6.1 and SOX9 expression, which activates a genetic program for the conversion into acinar progenitors (Solar et al. 2009; Jennings et al. 2013). Slightly later, expression of NKX6.1 and SOX9 becomes restricted to cells of the epithelial trunk marking bipotent ductal-endocrine progenitors (Kopp et al. 2011; Jennings et al. 2013). In a next step, the ductal-endocrine progenitors commit to the endocrine lineage which is hallmarked by the expression of neurogenin (NGN) 3 and leads to a proliferation stop as well as the delamination of endocrine progenitors from the epithelium (Gouzi et al. 2011; Miyatsuka et al. 2011; Salisbury et al. 2014). These migrating endocrine progenitors form immature islets of Langerhans that further differentiate towards mature islets containing the five individual endocrine subtypes.



Thereby, cell specification is driven by the controlled expression of cell type-specific transcription factors (Piper et al. 2004). The development of α -cells is mainly determined by the transcription factor *aristaless* related homeobox (ARX), while its direct counterpart paired box (PAX) 4 is decisive for the β -cell fate and loss of both triggers δ -cell differentiation (Collombat et al. 2003; Collombat et al. 2005). Moreover, β -cell specification and maturation comprise PDX1, NKX6.1, and the β -cell maturation marker V-Maf avian musculoaponeurotic fibrosarcoma oncogene homolog (MAFA) (Itoh et al. 2010; Schaffer et al. 2013). Further islet maturation encompasses vascularization and neuronal innervation as well as a rearrangement of the cytoarchitecture, all of which are essential for final islet function (Jennings et al. 2013).

4.8 Mimicking pancreatic organogenesis for the *in vitro* differentiation of pancreatic β -cells

In vitro differentiation protocols for the generation of β -cells aim to simulate *in vivo* pancreatic organogenesis by the time-dependent application of signaling molecules (Fig. 4c). Essentially, the improvement and refinement of the differentiation protocols led to three milestones, the first of them being the generation of pancreatic progenitors (PPs) (D'Amour et al. 2006; Kroon et al. 2008; Rezanian et al. 2012), followed by the production of fetal-like β -cells (Pagliuca et al. 2014; Rezanian et al. 2014) and recent efforts to improve β -cell maturation *in vitro* (Russ et al. 2015; Nair et al. 2019; Velazco-Cruz et al. 2019; Hoglebe et al. 2020).

Similar to the pancreatic development *in vivo*, the *in vitro* generation of β -cells starts with the endoderm induction of PSCs. Therefore, expression of the definitive endoderm (DE) markers SOX17 and forkhead box protein (FOX) A2 is triggered by activation of the TGF- β and the WNT-signaling pathway (D'Amour et al. 2005; Bone et al. 2011). This is achieved by the application of Nodal-surrogates, like Activin A, for inducing TGF- β signaling, as well as activation of the WNT signaling pathway by supplementation of either WNT3a or, more effectively, downstream inhibition of WNT signaling repressors by the small molecule CHIR-99021. Subsequently, the PGT

Figure 4 Development of the human pancreas and derived protocols for the directed *in vitro* differentiation of hiPSC towards insulin producing cells. **a** The different cell lineages of human development starting from the zygote. Colored stages highlight the developmental branch of pancreatic endocrine cells. Stages connected with dotted lines display abbreviated lineages, in which intermediate stages are not shown. **b** Summary of the human pancreas development. Patterning of the Primitive Gut Tube results in the formation of the Posterior Foregut. SHH inhibition by signals from the notochord results in pancreatic endoderm formation located in the dorsal and ventral bud. Proliferation of MPPs in the pancreatic epithelium drives the bud evagination. Notch signaling leads to the segregation of MPPs into acinar progenitors (epithelial tip) and bipotent ductal-endocrine progenitors (epithelial trunk). Bipotent ductal-endocrine that commit to the endocrine lineage delaminate from the epithelium and form endocrine clusters, which eventually mature to islets of Langerhans. **c** Scheme of the differentiation protocol for the *in vitro* generation of hPSC-derived insulin producing cells by Rezanian et al. The scheme shows the developmental stages from hPSCs to maturing β -cells (colored circles) and important protein marker of each stage. Grey boxes contain the factors used for induction of the single stages as well as their effect on intracellular signaling pathway (green: activation, red: inhibition). **Sources of information:** Jennings et al. 2013; Rezanian et al. 2014; Mühlemann 2018.

stage is initiated by activation of the FGF-receptor-2b by application of FGF7 and further refined by the addition of ascorbic acid (AA, vitamin C) for enhanced cell survival (Rezania et al. 2014). In a next step, the patterning of the PGT is triggered similar to the *in vivo* situation by RA signaling. In combination with continued FGF7 supplementation and inhibition of BMP signaling using the small molecule inhibitor LDN193181 or Noggin, this results in the development of cells with a determined PGT fate. After cells reached the PGT stage, the commitment to the pancreatic lineage is initiated. A key event during this process is the occurrence of the transcription factor PDX1 which functions as a master regulator for pancreatic cell fate by controlling the expression of important pancreatic genes (Oliver-Krasinski et al. 2009). To induce PDX1 expression and thus achieve pancreatic commitment, cells are exposed to the SHH-inhibitors SANT-1 or cycloppamin-KAAD, which fulfill the function of the SHH-suppressing factors released from the notochord *in vivo* (D'Amour et al. 2006; Rezania et al. 2012). In addition, protein kinase C (PKC) activation by α -Amyloid Precursor Protein Modulator (TPB) or Phorbol 12,13-dibutyrate (PDBu) is supplemented to improve pancreatic specification by an enhanced PDX1 expression (Rezania et al. 2012; Pagliuca et al. 2014). At this stage, the generated cells are comparable to dorsal bud cells and correspond to cells of the PF stage. Prolonged exposure of these cells to SHH inhibiting molecules consolidates PDX1 expression and promotes the transcription of NKX6.1. NKX6.1 is a downstream target of PDX1 and hallmarks the induction of PE *in vivo* and *in vitro* (Jennings et al. 2013; Schaffer et al. 2013). Sustained expression of NKX6.1 is further important for the generation of functional β -cells (Schaffer et al. 2013). However, the exact time point, at which NKX6.1 needs to be switched on to ensure proper β -cell maturation is highly debated (Rezania et al. 2014; Petersen et al. 2017). Co-expression of PDX1 and NKX6.1 is required for the establishment of PPs derived from PE (Rezania et al. 2014). Early differentiation protocols generated PPs or PE cells with a polyhormonal phenotype characterized by the simultaneous expression of insulin, glucagon and/or somatostatin (D'Amour et al. 2006; Kroon et al. 2008; Rezania et al. 2012). However, these cells were unable to secrete insulin in response to glucose stimulation (D'Amour et al. 2006; Kroon et al. 2008; Rezania et al. 2012). In contrast, transplantation of these PP and PE cells into an *in vivo* environment triggered maturation into insulin-secreting β -cells capable to reverse diabetes in mice (Kroon et al. 2008; Rezania et al. 2012).

Based on the generated PPs and PE cells, the following protocols aimed for the addition of differentiation stages recapitulating β -cell development. Thereby, commitment to the endocrine lineage, induced by the expression of NGN3, covers a pivotal role (Gu et al. 2002). In the developing pancreas, NGN3 is transiently expressed and followed by the expression of its downstream targets, such as neuronal differentiation 1 (NEUROD1) and homeobox protein NK-2 homolog B (NKX2.2) that are essential for the consolidation of an endocrine phenotype (Rukstalis and Habener 2009). Reinforcement of NGN3 expression can be achieved by inhibition of TGF- β

signaling, for example by the addition of activin receptor-like kinase (ALK) 5 inhibitor, with simultaneous suppression of BMP signals (Pagliuca et al. 2014; Rezanian et al. 2014; Spagnoli 2015). Besides these chemical stimuli, NGN3 expression can also be promoted by the establishment of an air-liquid culture (Rezanian et al. 2014), as well as by the modulation of the polymerization state of the actin-cytoskeleton (Mamidi et al. 2018; Högberg et al. 2020). Furthermore, inhibition of Notch signaling, which is involved in the tip-trunk decision in the pancreatic epithelium and the segregation of MPPs into bipotent ductal-endocrine progenitors (NKX6.1⁺/SOX9⁺) and acinar progenitors (CPA1⁺/GATA4⁺) *in vivo*, by supplementation of γ -secretase inhibitor, enhances the proportion of NKX6.1⁺ cells *in vitro* (Hald et al. 2003; Jennings et al. 2013). Thereby the PE cells can be converted into pancreatic endocrine precursors (PEP) expressing NKX6.1, NGN3, NKX2.2 and NEUROD1 (Rezanian et al. 2014; Högberg et al. 2020), which are comparable to *in vivo* PE cells that delaminate from the epithelium to form immature islets. Further specification into β -cells requires MAFA which is only expressed in adult β -cells and is therefore assumed to be an essential player for establishing β -cell function (Matsuoka et al. 2004). Expression of MAFA can be enhanced by inhibition of the AXL receptor tyrosine kinase using the small molecule Bemcentinib (R428) in combination with the thyroid hormone Triiodo-L-Thyronine (T3) and acetylcysteine. Collectively, the application of these factors improves the generation of β -like cells (Rezanian et al. 2014). Although the yielded cells reveal key factors of mature β -cells, including PDX1, NKX6.1, MAFA and insulin and a reduced number of polyhormonal cells, they still exhibit an inappropriate glucose stimulated insulin secretion capacity compared to *bona fide* β -cells (Pagliuca et al. 2014; Rezanian et al. 2014). However, when transplanted into an *in vivo* environment, the cells mature and reverse diabetes in diabetic mice more rapidly than transplanted polyhormonal PPs (Pagliuca et al. 2014; Rezanian et al. 2014).

Given the still incomplete function of hiPSC-derived β -cells, researchers refined differentiation protocols once more and found that the chronology of fate-determining transcription factors, especially the timing of endocrine specification is of paramount importance for the later β -cell maturation and functionality. Studies report that an NGN3-driven endocrine induction that precedes NKX6.1 expression results in primarily polyhormonal cells with an α -cell favored fate (Russ et al. 2015), while NGN3 expression at later stages consolidates a β -cell development (Johansson et al. 2007; Russ et al. 2015). However, cells generated according to these refined protocols still exhibit deficits in glucose-stimulated insulin secretion and achieve final maturation only upon *in vivo* transplantation (Russ et al. 2015; Nair et al. 2019).

Thus, it appears that the *in vivo* environment provide information, which is required for the terminal β -cell maturation, but is so far not addressed by the current differentiation protocols. Of the many possible factors – circulating signal molecules, cell-cell interactions, neuronal signaling and interactions with the vascular interface – one has been already proven to affect many cellular

processes and therefore emerges as a particularly promising candidate for contributing to β -cell maturation: the extracellular matrix (ECM).

4.9 *The extracellular matrix – a dynamic signaling hub regulating cellular function*

The ECM is often described as a non-cellular meshwork of secreted proteins that provide physical support of the embedded cells. Although this statement is certainly true, the functional scope of the ECM comprises far more than passive scaffolding actions. By storage and release of cytokines, growth factors and vesicles as well as by binding to cell surface receptors, the ECM provides a plethora of chemical and mechanical signals that have been shown to regulate cellular processes such as survival (Carlo 2009), proliferation (Musah et al. 2012) and differentiation (Engler et al. 2006).

In general, the ECM composes of protein and non-protein constituents that assemble into a highly organized meshwork (Fig. 5a, b). Collagens represent the most abundant component of the ECM. Up to now, 28 different collagen types have been identified, each of which representing homo- or heterotrimers composed of three α -chains (Ricard-Blum and Ruggiero 2005). According to their supramolecular organization, collagens are classified into fibrillar and non-fibrillar collagens. Fibrillar collagens (I, II, III, V, XI) assemble into elongated, string-like structures that provide a high degree of stability (Bella and Hulmes 2017). In contrast, non-fibrillar collagens form various supramolecular structures, such as networks (IV, VIII, X), beaded filaments (VI) or anchoring fibrils (VII) (Bella and Hulmes 2017). Both types of collagen interact with cells, other proteins and glycosaminoglycans (GAGs) (Mouw et al. 2014). GAGs are linear polysaccharides of repeating sugar- and amino-sugar-molecules that bind water (hygroscopic) due to their polar structure (Mouw et al. 2014). Linked to a protein core, GAGs form proteoglycans, a major component of the ECM. Thereby, the function of different proteoglycans is predominantly defined by the composition and density of the attached GAGs (Mouw et al. 2014). Another essential component of the ECM are laminins that are large glycoproteins composed of one α -, β - and γ -chain. Different combinations of α -, β - and γ -chain subtypes result in various forms of laminins with a distinct molecular shape and binding properties, which defines laminin assembly as well as the interaction with other ECM components and cell surface receptors (Miner and Yurchenco 2004). Moreover, the ECM comprises several other ECM components including elastin, vitronectin and fibronectin. While elastin provides elastic mechanical properties and contributes to the architecture of arterial vessel walls, lung and bladder, the glycoproteins vitronectin and fibronectin both mediate cell-ECM interactions (Leavesley et al. 2013; Halper and Kjaer 2014).

All the single components exhibit individual structures and properties that determine the overall characteristics of the entirely assembled ECM. These tissue-specific ECM parameters are essential

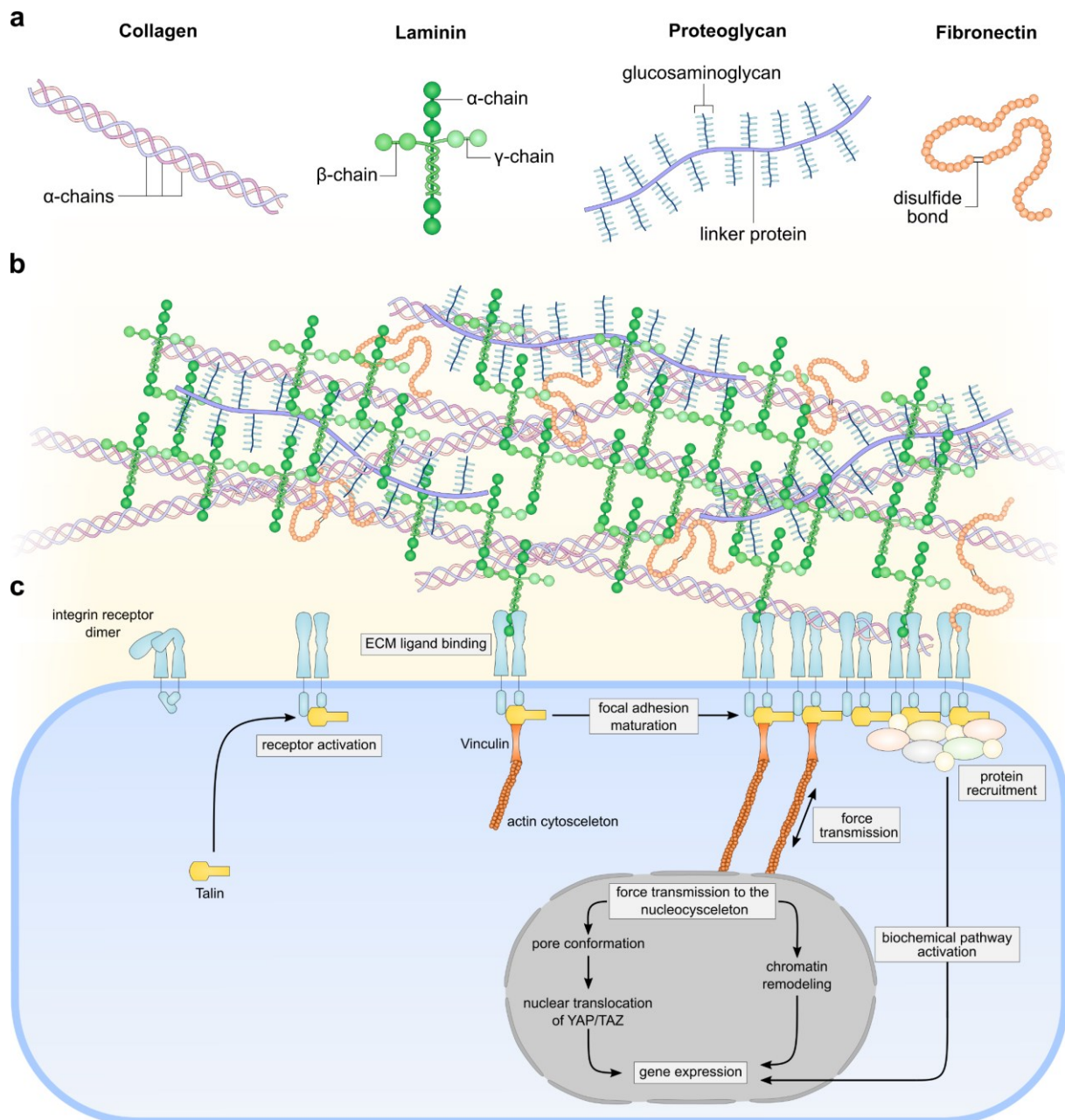


Figure 5 Extracellular matrix assembly and integrin signaling. **a** Structure of the main components of the ECM. Shown are collagens, which are helical, elongated proteins that assemble of three different α -chain, cross-shaped laminins, which consist of an α -, β - and γ -chain, proteoglycans that compose of glycosaminoglycans connected to a linker protein and fibronectin, which is a protein dimer formed by two polypeptide chains that are linked by a disulfide bonds. **b** Example for an ECM assembly. Collagens form an underlying network, which supports the formation of laminin-based sheet-like structures. Proteoglycans and fibronectins are bound to collagens and laminins. **c** Integrin receptors usually exist in an inactive state and are activated upon intracellular binding of talin. The activated integrin receptor can then bind to ECM ligands, which leads to the exposure of intracellular recognition sites for adaptor proteins. Vinculin links the integrin receptor to the actin cytoskeleton thereby establishing a mechanosensory signaling system. Applied force leads to a maturation of the focal adhesion. Integrin signaling is on one hand mediated by recruited proteins triggering intracellular signaling pathways. On the other hand, force is transmitted from the integrin receptor via the cytoskeleton to the nucleus leading to an alteration of the nucleoskeleton. This can lead to chromatin remodeling or nuclear translocation of mechanosensitive transcription factors such as YAP/TAZ and result in gene expression changes. **Sources of information:** Miner and Yurchenco 2004; Harburger and Calderwood 2009; Mouw et al. 2014; Kechagia et al. 2019.

for cell-ECM signaling. One important property is the rigidity of the ECM, which describes the resistance of a material to mechanical deformation. In biological scaffolds, the rigidity is largely defined by the type of collagen fibers, the extent of crosslinking and fiber density and has been shown to affect cell development (Engler et al. 2006; Bonnans et al. 2014). Within the body, organs display different ECM rigidities, ranging from stiff tissues (1 – 2 GPa) such as bone to soft tissues (0.1 – 10 kPa), like the brain and the pancreas (Smith et al. 2018; Galli et al. 2020). The assembly of various ECM components further results in different surface properties, compromising roughness and porosity. Regarding the topographical characteristics, one can distinguish between microscale features, for example, the direction of collagen fibers, or nanoscale effects, such as the signaling of individual ECM constituents (Nguyen et al. 2016). The effects of stiffness and topography are largely altered by the geometry of a scaffold. Mechanical stiffness, for example, is differentially transduced on a flat, two-dimensional (2D) surface compared to three-dimensional (3D) environments (Doyle and Yamada 2016). The latter enables the establishment of stiffness and topographical gradients as well as orientation marks and thereby affects the spatial arrangement of cells (Galli et al. 2020).

The ECM must not be seen as a static, immutable system, but rather represents a dynamic environment that is subject to a constant remodeling process regulated by the secretion of newly sequestered components and ECM-degrading proteases from resident cells (Bonnans et al. 2014). This flexibility allows the adaption of the ECM in response to environmental stimuli, such as mechanical strain, inflammation or injuries. As the ECM organization is largely under the control of resident, tissue-specific cells, the composition and, thus, its properties, differ among tissues (Travascio 2016). In most cases, the ECM of a tissue is likewise not a homogenous entity, but exhibits specific compartments with specialized functions that result from local accumulations of certain ECM components. One example is the basement membrane, a sheet like structure that is found, for instance, as a supporting layer beneath epithelial and endothelial cell layers (Kruegel and Miosge 2010). Usually, the basement membrane composes of laminin sheets that are linked to a supporting collagen IV network as well as to different proteoglycans. The basement membrane serves as an anchor for adjacent cells and provides spatial information that contributes substantially to cell polarization and the maintenance of cell function (Pozzi et al. 2017).

Collectively, the tissue-specific compositions, different mechanical parameters and local specifications of the ECM are important cues for resident cells. Thus, the ECM can be seen as a signaling hub, which can affect important cellular functions. The informational exchange between cells and the surrounding ECM is mediated by the binding of ECM components to cell-surface-adhesion receptors, mostly integrins (Fig. 5c). Apart from a direct signaling by the activation of intracellular biochemical pathways (Hamidi and Ivaska 2018), integrins are essential for linking the cellular cytoskeleton to the ECM and for the establishment of a mechanosensory signaling

system (del Rio et al. 2009). At this, the force which is applied to an integrin receptor is directly transmitted to the actin cyto- and nucleoskeleton, thereby governing the nuclear translocation of mechanosensitive transcription factors, for instance, yes1 associated transcriptional regulator (YAP)/tafazzin (TAZ) (Elosegui-Artola et al. 2017; Chang et al. 2018) as well as chromatin remodeling (Tajik et al. 2016). Two factors that decisively affect force transmission and thereby the integrin response, are the ECM rigidity and the number of adhesion spots. When force is applied to the ECM, the amount of energy that is transmitted to the integrin receptors of the cell is higher on stiff scaffolds compared to soft materials. Hence, the integrin downstream effects, including biochemical signaling and the connection to the cytoskeleton are more pronounced on stiff materials (Kechagia et al. 2019). In contrast, a large number of adhesion spots, which is the binding of one integrin to an ECM ligand, reduces the force that is transmitted to a single integrin molecule and thereby dampens the strength of downstream signaling effects (Oria et al. 2017). Consequently, different ECM rigidities as well as binding spot densities are decisive for ECM-mediated signaling and influence cell functions, such as migration and differentiation (Engler et al. 2006).

Thus, integrins are responsible for the integration of mechanical information into the cellular decision processes and can induce certain cellular responses. Thereby, the scope of processes regulated by the ECM is not limited to regulate cellular homeostasis, but also comprises crucial processes that are decisive for the fate of a cell and entire tissue compartments.

4.10 The role of the extracellular matrix in the islet niche

The perception of biophysical and biochemical stimuli provided by the ECM is a prerequisite for fundamental processes throughout the human body. Concerning this matter, the pancreatic islet is no exception.

Adult human islets represent a specified niche tailored to the demands of endocrine cells (Stendahl et al. 2009; Galli et al. 2020). Islets are surrounded by a peri-insular basement membrane that demarcates the endocrine cells from the pancreatic exocrine tissue. According to the general structure of basement membranes, it is mainly composed of laminin and collagen IV, but also exhibits amounts of collagen I, III, V and VI (van Deijnen et al. 1994). A second basement membrane, the perivascular membrane, pervades the islets as part of the microvasculature and mainly consists of laminins and collagen IV (van Deijnen et al. 1994). In humans, in contrast to rodents, the perivascular membrane is covered by a second basement membrane, which separates the endocrine cells from the perivascular membrane (Virtanen et al. 2008). The laminin content of human islets is traced to the presence of the laminin isoforms laminin-411 (composed of an $\alpha 4$, $\beta 1$ and $\gamma 1$ chain), laminin-332 and laminin-511/521. While laminin-511/521 is present

in both, the perivascular and the periinsular membrane, laminin-411 is located only in blood vessels and laminin-332 in close proximity to α -cells (Parnaud et al. 2006; Virtanen et al. 2008).

Several studies consistently show an effect of ECM molecules on a number of islet and β -cell specific functions (Cheng et al. 2011). Disruption of the native islet ECM increases apoptosis of endocrine cells, as seen after isolation of human islets (Thomas et al. 1999), where the partial reestablishment of the pancreatic microenvironment by a pancreas ECM substrate promotes the survival of islet cells (Carlo 2009). ECM-mediated effects further influence survival (Lucas-Clerc et al. 1993; Ris et al. 2002), glucose-stimulated insulin secretion (Lucas-Clerc et al. 1993; Kaido et al. 2006) and the gene expression profile (Kaido et al. 2006) of islets and β -cells. Attempts to deconstruct the signaling of the ECM to clarify the role of individual factors on islet function revealed a link between substrate stiffness and the insulin expression of murine islets and cell of the mouse insulinoma 6 (MIN6) line. Thereby, cells cultured on soft substrates (Young's modulus $E = 0.1$ kPa) exhibited an increase in INS expression compared to cells cultured in an environment with higher rigidity ($E = 10$ kPa) (Nyitray et al. 2014). Besides mechanical stimuli, single ECM components contribute differently to islet function. While fibronectin improves the glucose stimulated insulin secretion of rat insulinoma (INS-1) cells (Kuehn et al. 2012), vitronectin and collagen IV cause a major reduction of insulin content and insulin production of human β -cells with ongoing culture (Kaido et al. 2006). Moreover, integrin interactions with the perivascular basement membrane contributes to β -cell polarization by the relocation of intracellular insulin granules to integrin activation sites and thereby ensures a targeted secretion of insulin at cell-vasculature interfaces (Gan et al. 2018). This last example impressively highlights the importance of the interaction between adult islet cells and their natural ECM environment.

Although general concepts describing the interplay between islet ECM and endocrine cell function are largely missing, there is a common consensus about the elementary role of the ECM for islet physiology. The involvement of the ECM in endocrine functions of mature islets and islet cells suggests a possible role of the ECM also during endocrine development. This assumption eventually leads to the question of whether the ECM might represent the missing link for the terminal differentiation of *in vitro* generated β -cells.

4.11 Aim of the study

Pancreatic tissue engineering pursues the generation of β -cells for transplantation as well as for *in vitro* test models. However, both approaches suffer from the current limitation in the generation of mature β -cells *in vitro*. Given the elementary role of the ECM for adult islet function as well as the ECM tissue specificity, the question arises whether biochemical or biophysical features of the pancreas ECM are involved in the terminal maturation of *in vitro* generated β -cells.

The overall aim of this thesis was to investigate whether the application of a pancreas derived ECM scaffold promotes the differentiation of hiPSCs to β -cells and allows the establishment of improved *in vitro* organ models.

To this purpose, the present study aimed for the generation of a biomimetic pancreas-specific ECM scaffold (PanMa) that retains elementary structures and ECM properties of the native pancreas by whole organ decellularization of porcine pancreata. Given the fact that the ECM differs among native organs, it was further hypothesized that the PanMa exhibits specific biophysical and physico-structural features compared to ECMs derived from the small intestine and the lung. To address this question, a comparative analysis of ECM scaffold topography, rigidity, water content and porosity was conducted. Furthermore, it was assumed that the postulated ECM-specific properties have an influence on the maintenance culture and differentiation capacity of hiPSCs. For testing this hypothesis, it was investigated whether the differences of the generated ECM scaffolds have a relevant effect on the multi-lineage differentiation of hiPSCs.

In view of the essential role of the ECM for the sustained function of pancreatic islets *in vivo*, it was also hypothesized that the PanMa improves the generation of hiPSC-derived insulin producing cells. Thereby, one main assumption was that the PanMa particularly promotes the terminal differentiation of hiPSC-derived insulin producing cells towards β -cells. To address this question, the impact of the PanMa on the generation of endocrine cells was examined by applying the PanMa in different scenarios of the directed pancreatic differentiation of hiPSCs.

Another aim of this study was the generation of a PanMa derived hydrogel for the establishment of an *in vivo*-like ECM-based *in vitro* culture system for hiPSC-derived insulin producing cells. In this regard the hypothesis was tested whether a tissue-specific hydrogel improves the survival and function of hiPSC-derived endocrine cells by assessing the impact of the hydrogel on the morphology and endocrine signature of hiPSC-derived HECs.

5 Methods

5.1 Animal housing and euthanasia

Pigs were born and raised at a state-approved external breeding facility (Niedermayer, Dettelbach, Germany). The animals received proper attention and humane care in compliance with the Guide for Care and Use of Laboratory Animals published by the National Institute of Health (NIH publication no. 85e23, revised 1996) and as approved by the institutional board of animal protection. Animal Euthanasia and organ explantation was conducted at the local animal facility of the Centre for Experimental Molecular Medicine (ZEMM, University Hospital Würzburg) by a veterinarian in compliance with the German Animal Protection Law (§4 Abs.3) and with the approval of the Ethics Committee of the District of Unterfranken, Würzburg, Germany (approval number: 55.2-2532-2-256).

For organ explantation, 6 – 10 week old pigs were anaesthetized by application of 3 mg Stresnil® and 14 mg Ursotamin® per kg body weight. Blood coagulation was prevented by injection of heparin. Subsequently, euthanization was executed using 0.5 ml T61® per kg body weight.

5.2 Generation of pancreas-specific extracellular matrix scaffolds (PanMa)

Generation of the PanMa was carried out as described before (Berger et al. 2020). The pancreas was explanted *en bloc* along with the spleen and the duodenum to preserve connected vessel structures. The organ was released from connective tissue and vessel accesses established via the *arteria* and *vena mesenterica cranialis* as well as the *ductus pancreaticus* using 18, 20 or 22 G catheters, respectively. Upon connection to a fluidic system, the organ was perfused anterograde *via the arteria cranialis* and retrograde through the *ductus pancreaticus* at a constant flow rate of 3.9 ml/min. For decellularization, the pancreas was flushed with Milli-Q® H₂O for 1 h to remove residual blood and subsequently perfused with 3.4% (w/v) Sodium Deoxycholate (SDC) for 40 – 60 h, Phosphate Buffered Saline without Ca²⁺ and Mg²⁺ pH 7.4 (PBS⁻) for 8 h and PBS⁻ containing 1% Penicillin/Streptomycin (P/S) for 48 h. The decellularized pancreas was placed in PBS⁻ with 1% P/S for 72 h on a rocking shaker. For DNA digest, the pancreas scaffold was incubated in PBS⁻ with Ca²⁺ and Mg²⁺ pH 7.4 (PBS⁺) containing 1% P/S and 1 mg/ml DNase I at 37 °C for 16 h. The decellularized pancreas was washed with PBS⁻ containing 1% P/S for at least 24 h on a rocking shaker. The washing solution was changed at least three times for the first 24 h. Integrity of the duct and the arterial vessel system was checked by perfusion with 0.1% Phenol red diluted in PBS⁻ between the washing steps.

5.3 *Generation of small intestinal submucosa serosa matrix (SISser)*

Production of the SISser was performed as described before (Linke et al. 2007). In brief, parts of the jejunum were explanted, thoroughly washed with Milli-Q® H₂O and cut into pieces of 10 cm length. The tubes were inverted and the mucosa removed by scraping. Tissue tubes were washed with PBS⁻, filled with 3.4% (w/v) SDC and incubated for 1.5 h at 4 °C on a rocking shaker. Subsequently, SDC was removed and tubes were filled with PBS⁻ followed by incubation for 1 h at 4 °C on a rocking shaker. The tissue pieces were five times washed with PBS⁻ for 1 h and stored overnight in PBS⁻ containing 1% P/S. Next, the SISser scaffolds were incubated in PBS⁺ supplemented with 1% P/S and 0.167 mg/ml DNase I at 37 °C for 2 h. Subsequently, SISser segments were washed with PBS⁻ and stored in PBS⁻ with 1% P/S at 4 °C.

5.4 *Generation of lung-specific extracellular matrix scaffolds (LungMa)*

Lung explantation and decellularization was performed as described previously (Berger et al. 2020). In brief, blood and pulmonary surfactant was removed by flushing the explanted lung with Milli-Q® H₂O through the *trachea* and the *arteria pulmonalis*. The lung was connected to peristaltic pumps via the *arteria pulmonalis* and perfused at a constant flow rate of 23.4 ml/min. Decellularization was achieved by perfusion with 3.4% (w/v) SDC for 72 – 120 h and an intermediate washing step with PBS⁻. Subsequently, the lung was perfused with PBS⁻ for 8 h and with PBS⁻ containing 1% P/S for 72 – 120 h. For DNA digest, the lung scaffold was incubated in PBS⁺ containing 0.5 mg/ml DNase I at 37 °C for 16 h. Next, the lung scaffold was washed with PBS⁻ containing 1% P/S for at least 24 h at 4 °C. The washing solution was changed at least three times for the first 24 h.

5.5 *Sterilization of ECM scaffolds*

ECM scaffolds were sterilized by γ -irradiation at a dosage of >25 kG by an external sterilization service (BBF steriXpert, Kernren-Rommelshausen, Germany). Scaffolds were transferred to fresh PBS⁻ and stored at 4 °C until further use.

5.6 *Sample preparation for histological analysis*

Native and decellularized matrices were cut in small pieces (1 x 1 cm) and fixed with 4% Histofix for 2 h at RT. For fixation of reseeded scaffolds, cell crowns were placed in 24-well tissue culture plates containing 4% Histofix, incubated for 2 h at RT and washed twice with PBS⁻. Cell crowns were disassembled and seeded matrices were transferred to embedding containers. HEC clusters

and embryoid bodies were collected in Eppendorf tubes and fixed with 4% Histofix for 1 h at RT. Samples were washed twice with PBS and embedded in Histogel™. The Histogel™ droplets were placed in a humidified chamber at RT for 15 – 45 min until solid drops had formed and subsequently transferred to an embedding container. Samples were embedded in Paraffin using an automated embedding machine, cut into 5 – 10 µm thick sections and mounted on superfrost or poly-l-lysine-coated glass slides.

5.7 *Histological analyses*

For histological analyses, paraffin-embedded samples were dewaxed at 60 °C for 1 h followed by incubation in Xylene twice, for 10 min each. Samples were rehydrated in a descending EtOH series (dipping three times in: 96% EtOH I, 96% EtOH II, 70% EtOH, 50% EtOH, aq. dest). Afterwards, samples were processed according to different staining protocols:

Hematoxylin & Eosin: Hematoxylin (6 min), aq. dest. (rinsing), aq. nondest. (5 min), Eosin (6 min), aq. dest. (rinsing).

Movat's Pentachrom: 1% Alcian blue (12 min), alkaline alcohol (1 h), aq. nondest. (10 min), Weigert's iron Hematoxylin (10 min), aq. nondest. (15 min), Brilliant Crocein-Acid Fuchsine (10 min), 1% acetic acid (30 s), 5% phosphotungstic acid (20 min), acetic acid (2 min), 99% EtOH (1 min), 99% EtOH (6 min), Safron du Gatinais (1 h).

Feulgen: aq. nondest. (10 min), hydrochloric acid (50 min), aq. dest. (2 min), aq. dest. (2 min), Schiff's reagent (60 min), sodium metabisulfite (3 min), sodium metabisulfite (3 min), aq. dest. (2 min), aq. dest. (2 min).

Elastica/Van Gieson: Resorcin-Fuchsine (15 min), aq. nondest. (1 min), Weigert's iron Hematoxylin (5 min), aq. nondest. (1 min), acidified EtOH with 1% hydrochloric acid (10 s), aq. dest. (rinsing), Van Gieson's Picrofuchsin (2 min), aq. dest. (rinsing).

Masson Goldner Trichrome: Weigert's iron Hematoxylin (5 min), aq. dest (10 s), aq. nondest. (8 min), Ponceau Acid Fuchsine (4 min), 1% acetic acid (10 s), Phosphomolybdic Acid-Orange G (5 min), 1% acetic acid (10 s), Light Green Goldner III (6 min), 1% acetic acid (10 s), aq. nondest. (tepid, 1 min).

Stained samples were dehydrated in an ascending EtOH series (dipping twice in 70% EtOH, 2 min 96% EtOH, 5 min 2-propanol I, 5 min 2-propanol II, 5 min Xylene I, 5 min Xylene II.) and mounted with Entellan.

5.8 *Immunohistochemical staining*

Prior to staining, paraffin sections were dewaxed and rehydrated as described in section 5.7. Heat-mediated antigen retrieval was performed by incubation of the sections at 95 °C for 20 min in citrate buffer (pH 6.0) or TE buffer (pH 9.0). Slides were transferred to aq. dest, samples encircled with a PAP pen and specimens incubated in PBS⁻ containing 0.5% Tween 20 (PBST). Blocking was performed with PBS⁻ containing 5% (w/v) Bovine serum albumin and 5% (v/v) donkey serum for 1 h at RT prior to treatment with primary antibodies at 4 °C overnight. Samples were washed with PBST three times for 5 min and incubated with secondary antibodies diluted in antibody dilution solution for 2 h at RT. After three times washing with PBST for 5 min each, samples were mounted with Fluoromount G containing DAPI.

5.9 *Quantification of bile acid*

To verify the removal of the decellularization agent SDC, the amount of remaining bile acid was quantified using the total bile acid kit. Samples for analysis were taken from the storage Buffer (PBS⁻, approximately 100 ml) at earliest 24 h after γ -irradiation and processed following the manufacturer's guidelines. Standard control and samples were measured in triplicates 0 s (E0), 60 s (E1) and 120 s (E2) after reaction start. Bile acid concentration was determined for $\Delta E = E2 - E1$ using a given calibrator (50 $\mu\text{mol/l}$).

5.10 *Evaluation using the PancScore*

In order to standardize the production of pancreas derived whole organ ECM scaffolds, a quality control system for the generated PanMas was established (Berger et al. 2020). Therefore, scoring criteria for the assessment of decellularization efficacy, integrity of the duct and vascular vessel system, DNA removal and elimination of remaining SDC in terms of bile acid content were defined (Table 3). Evaluation criteria for decellularization efficacy and vessel integrity were determined based on previous decellularization experiments of this study. Standard values for the residual DNA content were partially adopted from the literature (Londono and Badylak 2015). Values for the remaining bile acid were defined according to the standard operating procedure for bile acid quantification from the Chair of Tissue Engineering and Regenerative Medicine at the University Hospital Würzburg. PanMas were rated according to the criteria with either 0 (unsuitable), 1 (low quality), 2 (moderate quality) or 3 (high quality) points as described before (Berger et al. 2020). For categories with measurable values (bile acid content and DNA quantification), scoring was performed according to the defined thresholds. Scores for categories that required qualitative

assessment were determined by three independent evaluators. The final score was calculated by the mode (D = most occurring value) of the assigned points (e.g. 1, 1, 3; D = 1).

5.11 *Surface electron microscopy (SEM)*

Samples for SEM were fixed in SEM fixation buffer at 4 °C overnight. After fixation, samples were washed five times with 0.1 M Sorensen Phosphate buffer at RT for 10 min each. Consecutive sample preparation and imaging was carried out at the Biocenter Imaging Core facility, University of Würzburg, in collaboration with Prof. Krohne and Prof. Stigloher. In brief, the fixed samples were coated with 10 – 20 nm gold/palladium (80/20) particles in an argon bath using a BAL-TEC SCD 005 Sputter Coater. Samples were imaged using a JEOL JSM 7500F scanning electron microscope at 5 kV (Markert et al. 2016).

5.12 *Rheology*

Rheology measurements were conducted in cooperation with Lukas Hahn (Research group Prof. Luxenhofer, Department of Chemistry and Pharmacy, Julius-Maximilians University Würzburg) using an Anton Paar Physica MCR 301 system with a plate-plate geometry (25 mm diameter) equipped with a solvent trap and a Peltier element. Measurements were carried out with PBS-soaked samples at 37 °C. The optimal gap width for each scaffold was determined before the successive measurement steps were conducted. First, amplitude sweeps with a strain deformation ranging from 0.01% to 100% and a fixed angular frequency of 10 rad/s were performed to obtain the linear viscoelastic region (LVR) and assess the viscoelastic properties of the scaffolds. Next, the frequency sweeps from 0.1 to 100 rad/s were measured at 0.5% strain deformation. Subsequently, steady shear experiments were performed with a control shear rate from 0.1 to 0.001 1/s. The obtained viscosity η and shear stress τ were plotted against the applied shear rate $\dot{\gamma}$.

5.13 *Passive permeability assay*

For measuring the passive permeability, FITC Dextran particles with an average molecular weight of 4 or 40 kD were dissolved in PBS⁻ at a concentration of 10 μ M. Molecular fragments were removed using Amicon® Ultra Centrifugal filters with a threshold of 3kD or 30 kD, respectively. Upon centrifugation according to the manufacturer's guidelines, the supernatant was collected and refilled with PBS⁻ to the initial volume. The generated scaffolds were mounted in cell crowns to obtain an ECM-Transwell®-like culture systems (ECM-TWs) set up and placed in a 24-well plate.

ECM-TWs were filled with PBS⁻ and incubated for 1 h at 37 °C, 95% humidity, 5% CO₂ prior to the experiment start. Subsequently, 900 µl fresh PBS⁻ were applied to the basal compartment and 200 µl of the FITC Dextran solution to the apical compartment of the ECM-TW. Scaffolds were incubated at 37 °C, 95% humidity, 5% CO₂. Samples of 50 µl were taken from the basal compartment at different time points and the volume replenished with pre-warmed PBS⁻. Collected samples were transferred to a 96-well plate with black bottom, filled up with PBS⁻ to a total volume of 200 µl and the fluorescent intensity measured at an excitation wavelength of 495 nm and an emission at 520 nm using an Infinite M200 Plate Reader. The total amount of substance was calculated from a prepared standard curve. The passive permeability of the substance per area over time, given as permeability coefficient (P_{app}), was determined as previously described (Hellinger et al. 2012).

5.14 *Determination of water storage capacity*

Analysis of water storage capacity was carried out as described previously (Berger et al. 2020). Pieces with a defined size were prepared using 8 mm diameter biopsy punches. Scaffolds were soaked with PBS⁻ and placed on a weighed cover slip. The remaining liquid was removed with a filter paper. Wet scaffolds were weighed and subsequently placed at 37 °C in a non-humidified chamber. Scaffold weight was documented at different time points and the amount of evaporated water determined by calculating the difference of the initial scaffold weight and the scaffold weight at each time point. The experiment was terminated after 5 h when scaffolds were entirely dried. Dried scaffolds were weighed in order to determine the water storage capacity given by the amount of water per mg dry weight.

5.15 *Standard cell culture procedures*

All cells were routinely cultured at 37 °C, 95% humidity, 5% CO₂. If not stated otherwise, centrifugation steps were carried out with 350 x g for 5 min at RT. Cryopreserved cells were thawed in a 37 °C waterbath, transferred to Dulbecco's modified Eagle's medium (DMEM)/F12 medium and centrifuged. Cells were resuspended in the respective cell culture medium and cultured in accordance to their maintenance culture conditions. Medium of iMR 90-4 cells was additionally supplemented with 10 µM ROCK inhibitor for plating. For freezing, cells were detached according to the respective passaging protocols and centrifuged. Endothelial cells were resuspended in DMEM/F12 medium containing 10% dimethyl sulfoxide (DMSO). iMR 90-4 cells were resuspended in Knockout™ serum replacement supplemented with 10% DMSO. Cells were transferred to Cryovials and cooled at -80 °C using freezing containers. Cells were long-time

stored in liquid nitrogen at -183 °C. For cell counting, cell suspensions were diluted with Trypan blue at a ratio of 1:1 to 1:4 and cells counted manually with an improved Neubauer counting chamber.

5.16 *Culture of endothelial cell lines*

Red fluorescent protein (RFP) expressing primary human dermal microvascular endothelial cells (ECs) were a generous gift from Dr. Sebastian Kress (Research Group Dr. Joachim Nickel, Chair of Tissue Engineering and Regenerative Medicine, University Hospital Würzburg). ECs were cultured in VascuLife® medium and medium changed every other day. ECs were passaged at 80% confluency as single cells at a ratio of 1:2 to 1:30. Therefore, ECs were rinsed with PBS and incubated with 0.5% Trypsin/EDTA at 37 °C, 95% humidity, 5% CO₂ for 2 – 5 min. Trypsin digest was stopped by addition of 1/10 (v/v) FCS, cells were collected and centrifuged followed by resuspension of the cell pellet in fresh cell culture medium and plating of cells on new tissue culture flasks.

5.17 *Recellularization of the PanMas arterial system*

Recellularization of the PanMa's arterial system was performed with RFP tagged ECs cultured in VascuLife® medium as described before (Kress et al. 2018) with slight modifications (Berger et al. 2020). The PanMa scaffold was incubated in VascuLife® medium at 37 °C, 95% humidity, 5% CO₂ overnight. The next day, cells were harvested according to the appropriate detachment protocol in section 5.16 and resuspended in fresh medium. 10⁷ cells were suspended in 2 ml medium and injected into the arterial system via the established access using a 2 ml syringe, followed by 500 ml medium. The injection was repeated after 2 h incubation at 37 °C, 95% humidity, 5% CO₂ for a total of three times. The recellularized PanMa was cultured under static conditions in a 145 mm petridish. 5 ml VascuLife® medium were applied to the arterial system every other day. The entire medium was changed weekly.

5.18 *hiPSC maintenance culture*

For all hiPSC-based experiments iMR 90-4 cells were used. iMR 90-4 cells were routinely cultured in mTeSR™1 maintenance medium on Matrigel®-coated plates with daily medium change. Cells were passaged every 2 – 5 days according to colony morphology and confluence at ratios from 1:3 to 1:18. For passaging, cells were incubated with 2 mg/ml dispase diluted in DMEM/F12 medium for 5 – 7 min at 37 °C, 95% humidity, 5% CO₂. Cells were rinsed twice with DMEM/F12 medium,

detached in mTeSR™1 medium, fragmented by pipetting 7 – 12 times up and down and subsequently plated in mTeSR™1 medium supplemented with 10 µM Y-27632.

To achieve single cell suspensions, iMR 90-4 cells were detached by treatment with Accutase® for 5 – 7 min at 37 °C, 95% humidity, 5% CO₂. Cells were detached, singled by pipetting and collected. One volume of DMEM/F12 medium was added to inhibit Accutase® activity. Cells were centrifuged and the pellet resuspended in mTeSR™1 medium supplemented with 10 µM Y-27632.

5.19 *hiPSC maintenance culture on ECM-TWs*

In order to culture cells directly on ECM surfaces, decellularized tissue scaffolds were mounted in cell crowns to obtain an ECM-TW system with an inner and an outer medium compartment. For seeding, hiPSCs were detached using Accutase®. Single cells were seeded at a density of 4.97×10^5 cells/cm² ($\cong 2.5 \times 10^5$ cells/ECM-TW) in 50 – 100 µl mTeSR™1 medium including 10 µM Y-27632 on the ECM scaffold. Seeded ECM-TWs were incubated for 1 h to ensure proper cell distribution across the scaffold before medium level of the inner compartment was brought to its final volume of 200 µl. Cells were cultured in mTeSR™1 medium with daily medium change using 200 µl of medium in the inner and 1 ml of medium in the outer compartment.

5.20 *Spontaneous differentiation of hiPSCs on ECM-TWs*

Spontaneous differentiation was performed according to a protocol from Takahashi et al. with slight modifications (Takahashi et al. 2007; Berger et al. 2020). Briefly, iMR 90-4 cells were harvested as single cells using Accutase® and resuspended in mTeSR™1 medium supplemented with 10 µM Y-27632. For the formation of embryoid bodies (EBs), 3×10^3 cells were seeded in 30 µl medium and cultured as hanging drops for 2 days. EBs were collected in DMEM/F12 medium and transferred to suspension culture in SD medium. Medium was changed every other day. After 4 days, EBs were collected and 30 – 50 EBs plated on ECM-TWs or on 0.1% gelatin-coated tissue culture plates (48-well format). ECM-TWs were placed in wells of a 24-well plate and filled with SD medium (inner compartment: 200 µl, outer compartment: 1 ml). Cells were cultured for 20 days in SD medium and medium changed every other day. During the first 6 days, only half medium change was performed to prevent detachment of the EBs.

5.21 *Directed differentiation of hiPSCs towards hormone-expressing pancreatic cells (HECs) according to the 5-stage suspension culture protocol*

Differentiation of hiPSCs towards HECs was achieved following the 4-stage protocol by Rezania et al. with small adaptations and subsequent 7-day suspension culture (Rezania et al. 2012; Rezania et al. 2014). iMR 90-4 cells were harvested as single cells using Accutase®. $9.38 \times 10^4 - 1.04 \times 10^5$ cells/cm² ($\approx 9 \times 10^5 - 10^6$ cells/well) were plated in mTeSR™1 medium supplemented with 10 µM Y-27632 on Matrigel®-coated plates. For DE induction, cells were exposed to R-S1a medium 24 h after seeding. Further differentiation was achieved by daily medium change with the following media: R-S1b medium (day 1, 2), R-S2 medium (day 3 – 5), R-S3 medium (6 – 9), R-S4 medium (day 10 – 13). At day 14 cells were incubated with 5 mg/ml Dispase dissolved in DMEM high glucose at 37 °C for 5 min to induce cell detachment. Cells were rinsed twice with DMEM high glucose suspended in R-S5 medium. The detaching cell layers were carefully pipetted up and down with a 1 ml pipette (3 – 5 times) to achieve cell fragments of 100 – 300 µm. The resulting cell clumps were subsequently transferred to Costar® 6-well ultra-low attachment plates or Nunc® 6-well plates pre-treated with anti-adherens solution. Cell clusters were cultured in suspension culture until day 21 of differentiation with daily medium change. Therefore, clusters were collected in a 15 ml falcon tube, incubated for 5 – 10 min at RT until clusters settled by gravitation and the medium was aspirated. Clusters were resuspended in fresh R-S5 medium and transferred back to the same wells.

For pancreatic differentiation of hiPSCs on ECM-TWs, single cells were seeded at a density of 4.97×10^5 cells/cm² ($\approx 2.5 \times 10^5$ /ECM-TWs) with mTeSR™1 medium supplemented with 10 µM Y-27632. Cells were initially incubated for 1 h in 50 – 100 µl medium per ECM-TWs to facilitate cell attachment to the surface. Subsequently, mTeSR™1 medium with 10 µM Y-27632 were applied to the inner compartment to obtain a total volume of 200 µl. Cells were cultured on ECM-TWs during the entire differentiation experiment. The medium succession was the same as described for the suspension control.

5.22 *Supplementation of liquid PanMa during the directed differentiation of hiPSCs towards HECs*

For the application of liquid PanMa as a medium supplement, HECs were generated according to the 5-stage differentiation protocol by Rezania et al. (Rezania et al. 2012; Rezania et al. 2014). The liquid PanMa was added to the differentiation medium during stage 5 of suspension culture (day 14 to 21) at different concentration (in ng/ml: 100, 200, 400, 800). For generating a liquid PanMa supplement, the ECM was frozen at -80 °C overnight and subsequently lyophilized using an Alpha 1-2 LO Plus Lyophilizer. The freeze-dried PanMa was chopped with a scissor and crushed into a powder using a tissue rupture equipped with a metal rotor unit. Next, the PanMa powder was

dissolved in Matrix solubilization buffer and sonicated on ice at 50% energy for three times 30 s with a 30 s break using a Branson sonicator equipped with a 3/16 Micro Tip. The protein content of the liquid PanMa was determined using the BCA Protein Assay Kit according to the manufacturer's guidelines. The liquid PanMa was further diluted to an appropriate concentration with DMEM high glucose medium and sterile filtered before use.

5.23 *Directed differentiation of hiPSCs towards β -cells (SC- β) according to the 7-stage airlift protocol*

For generation of maturing SC- β cells, the 7-stage protocol by Rezanian et al. with minor adaptations was used (further referred to as "Bergen-Airlift-Protocol") (Rezanian et al. 2014). Therefore, iMR 90-4 hiPSCs cultured in mTeSR™1 medium were collected as single cells using Accutase® and $9.38 \times 10^4 - 1.04 \times 10^5$ cells/cm² ($\cong 9 \times 10^5 - 10^6$ cells/well) seeded on Matrigel®-coated plates in fresh mTeSR™1 medium supplemented with 10 μ M Y-27632. 24 h after seeding, medium was changed to B-S1a medium for DE induction (d0). For the first 10 days, cells were cultured submerge with daily medium change using the following media: B-S1b (day 1), B-S1c (day 2), B-S2 (day 3, 4), B-S3 (day 5, 6), B-S4 (day 7 – 9). At day 10, S4 cells were treated with 10 μ M Y-27632 for 4 h and subsequently detached by incubation with Accutase® for 7 – 10 min. The collected cells were centrifuged and resuspended in B-S5 medium at a concentration of 5×10^4 cells/ μ l. Four droplets of a 5 μ l cell suspension with 2.5×10^5 cells each were seeded on 12-well filter inserts. Seeded cell clusters were cultured at an air-liquid interface (ALI) for the remaining differentiation experiment. Therefore, the outer compartment of the 12-well inserts was filled with 800 μ l using the following media: B-S5 (day 10 – 12), B-S6 (day 13 – 19), B-S7 (day 20 – 26).

For differentiation of hiPSCs on Matrigel®-coated PET membranes and ECM-TWs, cells were seeded at a density of 4.97×10^5 cells/cm² (\cong PET-Insert: 1.67×10^5 cells/PET-Insert, ECM-TW: 2.5×10^6 /ECM-TW) in 50 – 100 μ l mTeSR™1 medium supplemented with 10 μ M Y-27632. After 1 h incubation, PET-Inserts and ECM-TWs were filled with mTeSR™1 medium supplemented with 10 μ M Y-27632 to a total volume of 150 μ l or 200 μ l, respectively. Further cell culture on PET-Inserts was performed with 850 μ l medium in the outer and 200 μ l medium in the inner compartment. Inner and outer compartments of ECM-TWs were filled with 900 μ l and 200 μ l, respectively. Differentiation was conducted with the same media as described above. Cells were cultured on the PET-Inserts or ECM-TWs during the whole differentiation experiment and were not detached at stage 4. At day 10, cultures were changed to ALI. Therefore, the outer compartment of PET-Inserts and was filled with 550 μ l medium. For ECM-TWs, 700 μ l were used.

5.24 Hydrogel production

Pancreas-specific ECM hydrogels were generated according to protocols for ECM hydrogels for other organs (Wolf et al. 2012) with minor adaptations to the PanMa scaffold as described previously in a supervised bachelor thesis from Anna Lena Ziegler (Ziegler 2019). In brief, PanMas were frozen at -80 °C for at least 24 h and freeze-dried using an Alpha 1-2 LO Plus Lyophilizer. Lyophilized samples were chopped in pieces using a scissor and subsequently crushed into powder with a Tissue Rupture equipped with a metal rotor. The PanMa powder was strained through a 500 µm nylon mesh to remove large tissue pieces. Next, the PanMa powder was sterilized by tyndalization. Therefore, the ECM powder was transferred to Falcon tubes, incubated for 60 min in a 95 °C waterbath and subsequently cooled down to RT. This cycle was repeated for three times. Subsequently, 10 mg of tyndalized PanMa powder were incubated with 1 ml ECM digest buffer for 72 h at RT under constant stirring. The resulting pregels were centrifuged at maximum speed and 4 °C for 15 min to insoluble ECM components and aliquoted in Eppendorf tubes. For neutralization, pregels were mixed with precooled 1/9 (v/v) 10x PBS⁻ as well as 1/10 (v/v) 0.1 N NaOH. Neutralized hydrogels retained soluble when placed on ice. For gelation, neutralized hydrogels were incubated at 37 °C, 95% humidity, 5% CO₂. Pregels could be stored at -20 °C for more than 2 years without recognizable impact on gelation.

5.25 Hydrogel culture of HEC clusters

HEC clusters were cultured in PanMa-hydrogels diluted 3:1 (v/v) in cell culture medium. For encapsulation, clusters were collected and resuspended in a small volume of fresh R-S5 medium. After determining the number of clusters by counting a sample of the cell suspension, HEC concentration was adjusted to 600 clusters/100 µl. Subsequently, 300 µl of neutralized hydrogel were added and the cell suspension mixed thoroughly by careful pipetting. Three droplets of 10 µl hydrogel cell suspension, each containing approximately 15 HEC clusters, were plated in wells of 24-well plates. To accelerate the gelation process, plates were placed on a heating device prewarmed to 37 °C during cell seeding. Plated droplets were incubated for 15 – 20 min at 37 °C, 95% humidity, 5% CO₂ until the hydrogel had solidified. Subsequently, 400 µl of prewarmed R-S5 medium were added to each well. For daily medium change, it was necessary to use prewarmed R-S5 medium (37 °C) to prevent liquefaction of the hydrogels.

5.26 Fluorescein-Diacetate (FDA)/Propidium Iodid (PI) staining

For FDA/PI-based live/dead staining, hydrogel-encapsulated HEC clusters were washed with PBS⁻ and subsequently incubated with PBS⁻ containing 0.5 µg/ml FDA and 0.5 µg/ml PI for 10 – 20 s.

After removal of FDA/PI solution, hydrogel drops were washed with PBS and HECs imaged instantly using a BZ-9000 fluorescent microscope equipped with filter sets for GFP (FDA) and Texas Red (PI).

5.27 *Glucose stimulated Insulin secretion*

For glucose-stimulated Insulin secretion (GSIS), 40 – 50 HEC clusters were picked and transferred to 40 µm cell strainers mounted in cell crowns placed in a 24-well plate. In case of cells cultured on ECM-TWs, filter-inserts, PET membranes, or cells encapsulated in hydrogels, GSIS was performed directly on the wells containing the inserts, ECM-TWs or the hydrogels. All incubation steps were performed with a total volume of 1 ml on a rocking shaker (100 rpm) at 37 °C, 95% humidity, 5% CO₂. For GSIS, samples were initially washed with KRB and incubated with KRB for 40 min. Subsequently, KRB was removed and cells were incubated for 60 min with KRB spiked with 3 mM glucose. The supernatant was collected and samples were incubated with KRB containing 15 mM glucose for another 60 min. After buffer collection, membranes or ECM scaffolds were dismantled and the seeded matrices were stored in 1 ml TE buffer. Clusters cultured in PanMa hydrogel were released by suspending the hydrogels in 1 ml TE buffer and the clusters were transferred to Eppendorf tubes.

Insulin content of the collected samples was determined using the Mercodia ELISA Kit for human Insulin according to the manufacturer's guidelines. Concentration of insulin was calculated from a standard curve of calibrators provided in the kit. If necessary, samples were diluted in KRB buffer to fit the range of the standard curve. Insulin secretion was normalized to the DNA content of the cell lysates. Therefore, cells or matrices containing cells were sonicated on ice with 12 pulses of 2 s at 80% energy and 8 s break between each pulse using a Sonopuls HD 4100 equipped with TS103 sonotrode. Sonicated samples were centrifuged at 14.000 rpm for 10 min at 4 °C to remove cellular debris and lysates were stored at -80 °C until analysis. DNA was quantified using the Quant-iT™ PicoGreen™ dsDNA Assay Kit as described in section 5.30. For calculation of the stimulation index for insulin, insulin secretion at 15 mM glucose was normalized to insulin secretion at 3 mM glucose.

5.28 *MTT Assay*

The MTT assay was used for qualitative and quantitative evaluation of cell metabolism. Therefore, MTT stocks were diluted in appropriate cell culture medium to working solutions of 1 mg/ml. For qualitative analysis, cell culture models (dish-cultures, ECM-TWs or recellularized pancreases) were incubated with MTT working solutions for 2 h at 37 °C. Subsequently samples were washed

briefly with PBS⁻ and the liquid was aspirated. Photo-documentation of MTT-stained samples was performed using a petri dish and a light source placed underneath to increase the contrast.

5.29 WST-1 Assay

WST Assay was performed with the Cell Proliferation Reagent WST-1 to non-invasively determine the amount of metabolic active cells. Therefore, ECM-TWs were dismounted and seeded scaffolds were transferred to 48-wells containing 250 μ l of WST-1 solution diluted 1:10 in PBS⁺. Samples were incubated at 37 °C, 95% humidity, 5% CO₂ and 100 μ l of supernatant were taken after 30 and 70 min, respectively. Optic density (OD) of the collected samples was measured at 450 nm with 10 flashes and a reference OD at 620 nm. Determined values were normalized to PanMa day 2 and presented as the fold change of metabolic activity.

5.30 DNA quantification

For quantification of the DNA content, samples from native tissue and decellularized scaffolds were lyophilized and chopped in pieces using a scissor. Approximately 3 mg tissue were transferred to an Eppendorf tube and digested with proteinase K solution (provided in the kit) at a 1:9 dilution (v/v) at 56 °C overnight. DNA was isolated using the DNEasy Blood and Tissue Kit according to the manufacturer's instructions. The DNA content was roughly estimated using a NanoQuant plate and an Infinite 200 PRO microplate reader. An exact measurement of sample DNA content was achieved using the Quant-iT™ PicoGreen™ dsDNA Assay Kit. DNA samples were diluted with TE-buffer to fit the standard range according to the results obtained from the Nanodrop measurements. Fluorescent analysis was performed at an excitation wavelength of 480 nm and a detection wavelength of 525 nm using an Infinite M200 Plate Reader. The total amount of sample DNA was determined from a Lambda-DNA Standard curve.

5.31 Gel electrophoresis

For size-based separation of DNA fragments, DNA samples were mixed 1/6 (v/v) with loading dye and applied to 0.5 – 2% agarose gels spiked with Gel Red. Gels were run in 1x TAE buffer at 150 V and maximum current. DNA gels were analyzed under UV light in a gel imaging device.

5.32 RNA Isolation and cDNA synthesis

Total RNA was isolated from cultured cells using the RNeasy Mini Kit for large amount of cells ($> 2 \times 10^5$) or the RNeasy Micro Kit for small amount of cells ($< 2 \times 10^5$) as well as for cells seeded on ECM-TWs. Cells grown in tissue culture plates were lysed in RLT buffer containing 143 mM β -Mercaptoethanol and homogenized using a QIAshredder spin column. ECM-TWs were dismounted and entire scaffolds transferred to RLT buffer containing 143 mM β -Mercaptoethanol. Scaffold samples were homogenized with metal beads and a Tissue Lyser (2x 3 min, 50 Hz). Filter- and PET-Inserts were dismounted, rinsed with RLT buffer containing 143 mM β -Mercaptoethanol and the supernatant collected. Hydrogel-cultured HECs were released by pipetting in PBS, picked and transferred to tubes containing RLT buffer with 143 mM β -Mercaptoethanol.

Homogenized samples were further processed according to the manufacturer's guidelines including DNA digest. Concentration and purity of isolated RNA were determined using a NanoQuant plate and an Infinite 200 PRO microplate reader. RNA was stored at -80°C .

cDNA was generated from 400 – 1000 ng of isolated RNA using the iScript™ cDNA Synthesis Kit according to the manufacturer's guidelines. The cycling program (Table 1) was performed on a LabCycler 48. Synthesized cDNA was stored at -20°C for no longer than 4 weeks.

Table 1 Protocol for cDNA synthesis

Step	Process	Temperature [$^\circ\text{C}$]	Time [min]	Cycles
1	Warming	25	5	1
2	Transcription	42	30	1
3	Enzyme inactivation	85	5	1
4	Cooling	12	∞	1

5.33 Real-Time quantitative PCR (RT-qPCR)

RT-qPCR was performed with the SsoFast™ EvaGreen® Supermix (Bio-Rad) and a CFX 96 Touch™ Real-Time PCR Detection System (Bio-Rad) according to the manufacturer's instructions. For each reaction, 1 – 2 μl of undiluted or diluted (up to 1:3) cDNA was used (≈ 5 – 50 ng cDNA). Reactions were performed in technical duplicates using a two-step protocol with subsequent melt curve analysis:

Table 2 Protocol for RT-qPCR

Step	Process	Temperature [$^\circ\text{C}$]	Time [s]	Cycles
1	Enzyme activation	95	30	1
2	Denaturation	95	5	39
3	Annealing and elongation	60 – 62	10	back to step 2
4	Strand annealing	55	30	1
5	Melt curve	55 – 95 (in 0.5 steps)	0.5 per step	1

The annealing temperature was adjusted to the primer-specific melting temperatures. When possible, runs were designed according to the sample maximization method (Hellemans et al. 2007). For a list of primers and used conditions, see table 2. RT-qPCR data were analyzed using the $\Delta\Delta\text{CT}$ -method assuming an amplification efficiency of 100%, equaling a template doubling per run. If not stated otherwise *RPL4* and *RPL6* were used as housekeeping genes. Gene expression is given as a fold change of hiPSC expression:

$$E_r(SOI) = \frac{E_a(SOI)}{\frac{1}{n} \sum_{i=1}^n \frac{E_a(\text{hiPSC}_1) + E_a(\text{hiPSC}_2) + \dots + E_a(\text{hiPSC}_n)}{n}}, \quad [1]$$

where $E_r(SOI)$ is the relative expression of the sample of interest, $E_a(SOI)$ is the absolute expression of the sample of interest and $E_a(\text{hiPSC}_n)$ is the absolute expression of the hiPSC samples (reference samples) of all biological replicates.

For the expression analysis of spontaneous differentiating EBs on ECM scaffolds *RPL4*, *RPL6* and *RPS29* were used as housekeeping genes. Gene expression was determined according to the calculation model by D'Antonio et al. (D'Antonio et al. 2017). Therefore, gene expression of each gene was normalized to the range between the maximum absolute expression and minimum absolute expression across all analyzed samples (max = 1; min = 0):

$$S_g(SOI) = \frac{E_a(SOI) - E_a(\min)}{E_a(\max) - E_a(\min)}, \quad [2]$$

where $S_g(SOI)$ is the gene expression score of the sample of interest, $E_a(\max)$ is the maximum absolute expression among all samples for this gene and $E_a(\min)$ is the minimum absolute expression among all samples for this gene.

For the determination of the germ layer score, as introduced by D'Antonio et al. (D'Antonio et al. 2017), normalized expression of genes associated with a certain germ layer were averaged:

$$S_{gl}(SOI) = \frac{1}{n} \sum_{i=1}^n \frac{S_{g1} + S_{g2} + \dots + S_{g3}}{n}, \quad [3]$$

where $S_{gl}(SOI)$ is the germ layer score for a sample of interest and $S_{g(\text{GOIn})}$ is the gene expression of the germ layer associated genes.

5.34 Image acquisition, image processing and figure design

Pictures showing the surgical procedure, native and decellularized samples as well as results from MTT-assays were taken with a Digital camera model DS126191. Images of cell cultures were acquired using an EVOS XL microscope with standard settings at 4x and 10x magnification.

For Light- and fluorescent microscopy, a BZ-9000 light microscope equipped with 2x, 4x, 10x, 20x, or 40x magnification objectives was used. Histological sections were imaged in Brightfield acquisition mode with default settings and white balance correction. Images of fluorescently labelled samples were acquired using the fluorescence mode of the BZ-9000 microscope equipped with filters for GFP (excitation: 470/40 nm), TRITC (excitation: 545/25 nm), and Cy5 (excitation: 620/60 nm) and the following settings: gain +12 db, adjusted black balance, adjusted exposure time. If required, images were taken as z-stacks. For the acquisition of stitched images, the merge mode was used. Images taken as z-stacks or with the merge mode were assembled with the BZ-II Analyzer software.

Confocal imaging of fluorescently labelled samples was performed using a TCS SP8. Images were captured with 20x, 40x (water), 63x (glycerin) objectives, using a PMT detector for lower magnifications (20x) and the HyD detector for high magnifications (40x and 63x). Images were acquired using the sequential mode with the following settings: Laser power 0.1% - 30%, magnification 1 - 2x, PMT gain 800 - 1200 V, HyD gain 10 - 50%, resolution 512 x 512 and 1024 x 1024 px, camera speed 200, averaging 1 - 3 times between frames, z-stack 0.48 - 1 μ m, airy unit 1.0. Stitched images were acquired using the Tilescan mode.

Acquired images were further processed using the open source program Fiji (BioVoxel version). The following commands were used: Z-project (Merging of z-stack) with average or maximum projection, subtract background (rolling ball diameter), change image type, assign LUT, adjust brightness and contrast, cropping, split channels, merge channels, stack to RGB, insert scale bar. For manual cell counting, the Fiji Cell Counter Tool was used.

Graphs were designed with OriginPro 2020 and GraphPad PRISM. For production of line arts and figure arrangements, the open source software Inkscape was used.

5.35 *Statistical analysis*

Statistical analyses were performed with the GraphPad PRISM software. Data were not tested for normality due to low sample size. Nevertheless, normality was assumed for biological samples and data sets were analyzed with parametric tests. For the comparison of two independent data sets, the student's t-test was used. When more than two independent data-sets were compared, One-way Anova with Tukey's multiple comparisons, Sidak's multiple comparisons or Dunnet's multiple comparisons test was used, depending on the sets of data that were compared. For the comparison of samples of two different groups, Two-way Anova with Tukey's multiple comparisons was used. All statistical tests were performed with a 95% confidence interval. P-values < 0.05 were considered as significant, whereas P-values > 0.5 and < 1 were considered as

a trend. Significances are indicated as asterisks in the figures with the following nomenclature: ns (not significant), $P > 0.05$, * $P < 0.05$, ** $P < 0.01$, *** $P < 0.001$, **** $P < 0.0001$. All data in this study are shown as the mean of the given number of biological replicates \pm SD.

6 Results

6.1 Generation and characterization of a porcine pancreas derived ECM scaffold

6.1.1 The PanMa represents a pancreatic acellular scaffold with a largely conserved ECM architecture

The choice of a proper decellularization technique strongly depends on the organ properties and the desired use of the produced scaffold. To generate a pancreas-specific ECM (PanMa) scaffold for studying the effects of the pancreas-specific ECM on pancreatic cell development and function, the conservation of matrix components and structure are of high importance. To this purpose, SDC, which is described as an efficient decellularization agent for tissues of various thicknesses, was used for perfusion-based whole-organ decellularization geared towards the preservation of macrostructural features.

Initially, the porcine pancreas (Fig. 6a) was explanted *en bloc* with the spleen and a duodenal segment (Fig. 6b). Vessel accesses were established via the spleen artery and vein for perfusion of the splenic lobe, as well as to the pancreatic duct for agent delivery to the duodenal and connective lobe (Fig. 6c). Pump-based SDC perfusion via the duct and spleen artery (Fig. 6d) induced a venous outflow, demonstrating the establishment of an, at least partially, closed vascular circuitry in the splenic lobe (Fig. 6e). Completed decellularization resulted in a cleared ECM scaffold with visible vessel structures (Fig. 6f).

Qualitative analyses of the generated scaffold using different histological stainings demonstrated an efficient cell removal and a largely preserved ECM structure (Fig. 7a – d). The generated PanMa exhibited blood (black arrowheads) and duct vessels (black arrows) embedded in a loosely packed ECM network resembling the native state. Histological stainings identified collagens (yellow staining in Fig. 7b) as the main remaining ECM component as well as elastin (black lining in Fig. 7c) in the wall of larger vessels. Efficient removal of cellular components was demonstrated by negative Feulgen staining (Fig. 7e). In line with that, DNA content was significantly reduced in the PanMa (306 ± 204 ng DNA/mg dry weight) compared to the native pancreas (4238 ± 1494 ng DNA/mg dry weight) (Fig. 7f). Accordingly, no DNA bands were visible for PanMa samples on agarose gels after electrophoretic DNA separation (Fig. 7g).

Microstructural analyses revealed a partial preservation of constituent ECM components and their spatial arrangement (Fig. 8a – d). In the native pancreatic tissue, collagen (COL) I was detected mainly in large vessels and lobular interstices (Fig. 8a), while COLIII (Fig. 8b), COLIV (Fig. 8c), and Laminin (LAM) (Fig. 8d) were observed as components of a fine network permeating the acinar tissue and islets of Langerhans. Likewise, COLI, COLIII, and COLIV were present in the

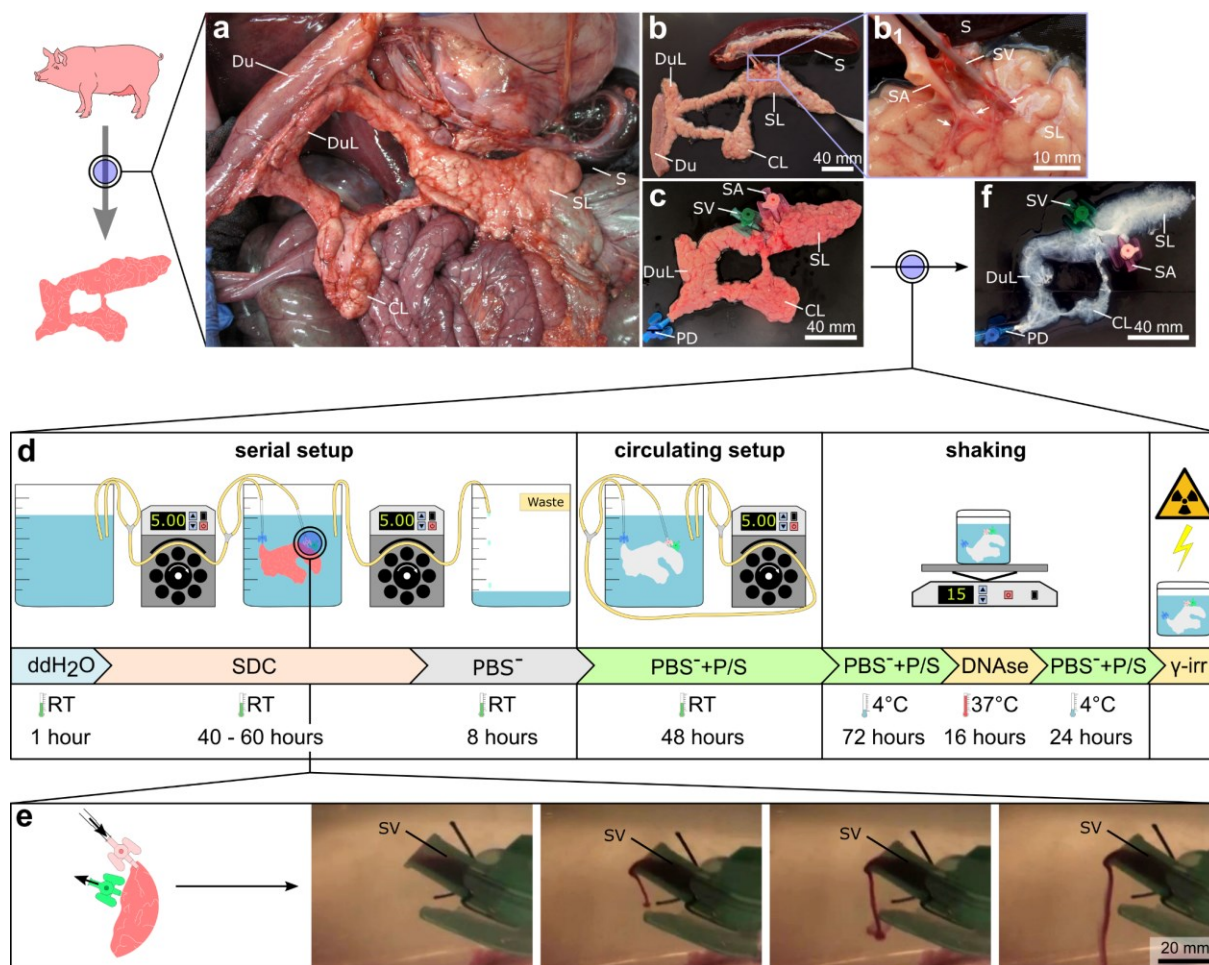


Figure 6 Generation of the PanMa by whole organ perfusion decellularization. **a** Exposed pancreas in the peritoneal cave of a pig connected to Du and S. **b** Explanted pancreas freed from connective tissue. Vascular branches of the SA and SV penetrating the SL are exposed (b1, white arrows). **c** Pancreas with established accesses to the PD (blue cannula), SA (pink cannula) and SV (green cannula). **d** Schematic representation of the decellularization procedure. The upper row illustrates the set ups used during decellularization. The pancreas was connected to peristaltic pumps arranged in a serial set up for removal of cellular debris and a circulating set up for washing. A shaker was used for the remaining steps. The bottom row depicts the succession of the applied solutions as well as temperature and duration of the single steps. **e** Images series of the access to the SV showing outflow of blood shortly after anterograde perfusion of the SL's vascular system through the SA. **f** Pancreas after decellularization with vessel accesses to the duct pervading DL and CL and the vasculature of the SL. **Abbreviations:** CL: connecting lobe, DNase: DNase I digest, Du: duodenum, DuL: duodenal lobe, PBS⁻: phosphate buffered solution without calcium and magnesium, P/S: penicillin/streptomycin, PD: pancreatic duct, SA: splenic artery, SDC: Sodium deoxycholate, SL: splenic lobe, S: spleen, SV: splenic vein, γ -irr: γ -irradiation. Figure modified from Berger et al. 2020.

PanMa exhibiting a spatial distribution similar to the native pancreatic tissue, although the ECM architecture appeared slightly degraded. In contrast to the analyzed collagens, LAM was only faintly detectable in the wall of larger vessels indicating a substantial loss of LAM during the decellularization process. The absence of INS and DAPI signals in the IHC-stained PanMa sections compared to the native pancreas underlined the efficient removal of cellular components.

Ultrastructural analyses of the PanMa further underscored the retention of the tissue-specific ECM architecture (Fig. 9a – c). In correspondence with the native tissue structure (Fig. 9a – b), the PanMa exhibited a comb-like ECM shape (Fig. 9c1, c2) as well as differently-sized vessels of the

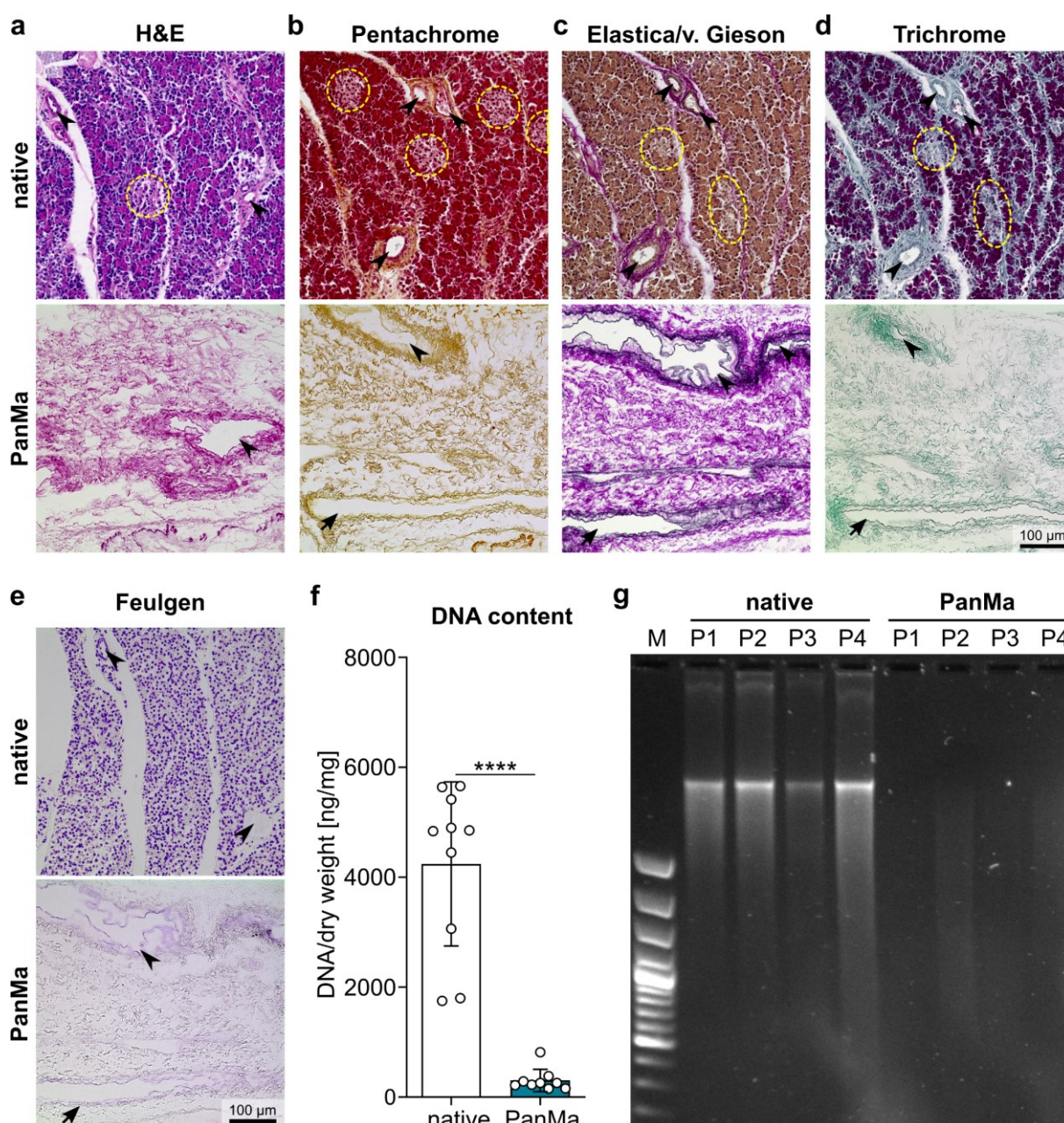


Figure 7 The PanMa represents an acellular scaffold with a largely preserved ECM structure. **a – d** Representative images of Hematoxylin & Eosin (a), Pentachrome (b), Elastica/v. Gieson (c) and Trichrome (d) stained sections of the native pancreas (upper panel) and the PanMa (lower panel) ($n = 3$). Vessels of the duct (arrowheads) and the vasculature (arrowheads) as well as pancreatic islets (circles) are annotated. **e** Representative Feulgen stainings of sections of the native porcine pancreas and the PanMa ($n = 3$). **f** DNA content of native porcine pancreas ($n = 9$) and PanMa ($n = 10$) given as ng DNA/mg dry weight. **g** Electrophoretic analysis of 4 representative pancreas samples before and after decellularization for evaluation of DNA separated on an agarose gel ($n = 14$). **Statistics:** Data represent mean \pm SD. **** $P < 0.0001$, unpaired two-tailed t-Test. **Scale bars:** If not annotated in the picture, the image size refers to the scale bar displayed in the picture at the right bottom corner in the same figure part. Figure modified from Berger et al. 2020.

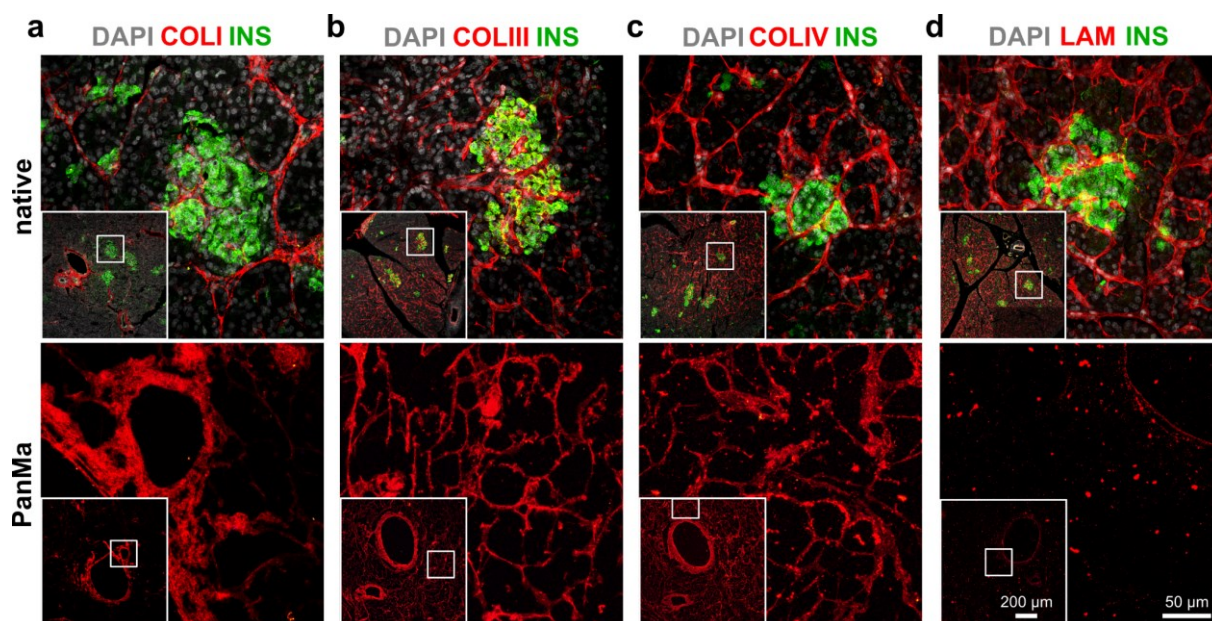


Figure 8 Collagens are preserved in the PanMa while laminins are lost. **a – d** Representative immunofluorescent stainings of histological sections from the native porcine pancreas (upper panel) and the PanMa (lower panel). Sections were stained for INS (green) and the ECM components (red) COLI (a), COLIII (b), COLIV (c) and LAM (d) and counterstained with DAPI (grey). Inlets show a magnified part of the sections. (n = 5). **Scale bars:** If not annotated in the picture, the image size refers to the scale bar displayed in the picture at the right bottom corner in the same figure part. Figure modified from Berger et al. 2020.

pancreatic duct (white arrows in Fig. 9c) and the vascular system (white arrowheads in Fig. 9c, c1). Large vessels showed an intact vessel wall with diametrically orientated collagen bundles (Fig. 9c3, c4). Single collagen fibers appeared highly conserved (Fig. 9c5), corroborating the high degree of ECM preservation of the PanMa. Taken together, the findings prove the generation of an acellular pancreatic ECM scaffold that resembles major parts of the native pancreatic micro- and ultrastructural ECM.

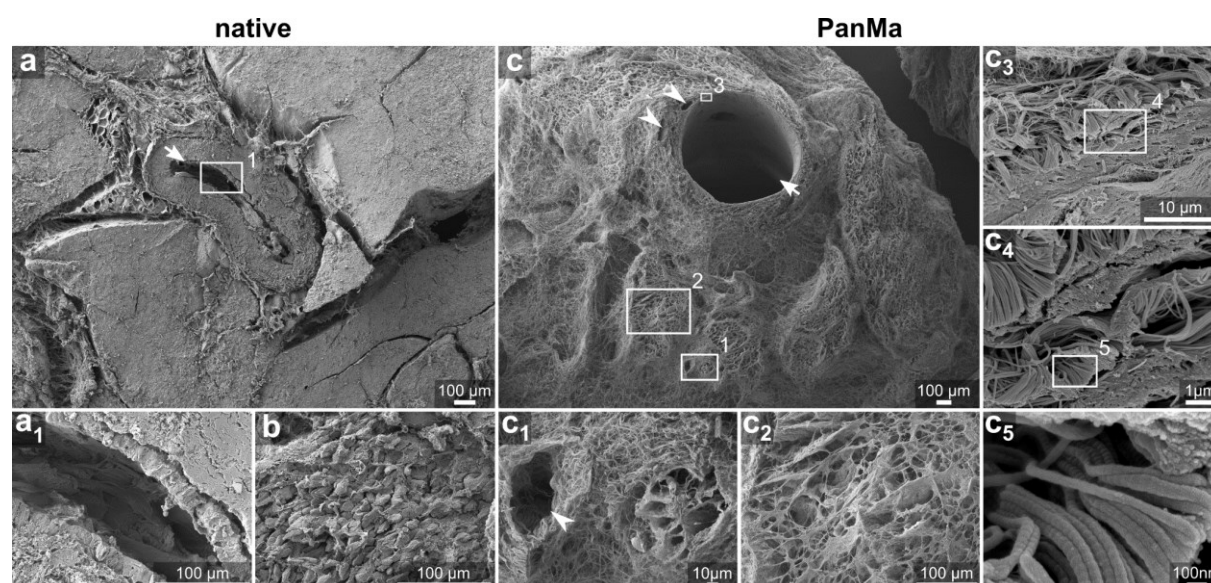


Figure 9 The PanMa exhibits a well-preserved ultrastructure. **a – c** Representative SEM pictures of the native porcine pancreas (a – b) and the PanMa (c). Vessels of the duct (arrowhead) and vasculature are annotated (n = 4). Boxed areas are shown at higher magnification in the pictures with the corresponding number. Figure modified from Berger et al. 2020.

6.1.2 *The conserved vessel system of the PanMa allows recellularization of parts of the arterial system*

After confirming the PanMa as an acellular scaffold with well-preserved ECM structure, the suitability of the PanMa for cell culture purposes was investigated next. Moreover, vessel integrity as well as the possibility for revascularization was explored. As shown in figure 10, Phenol red perfusion through the spleen artery (Fig. 10a) or pancreatic duct (Fig. 10b) confirmed the integrity of major vessels and smaller branches of the pancreatic duct and the arterial vessel system. Phenol red injection through the spleen artery resulted in an extensive perfusion of the splenic lobe (Fig. 10a), while perfusion of the ductal system comprised most, but not all ductal branches as well as single acinar structures (Fig. 10b). Small leakage at different sites of the PanMa was observed, which however, did not affect vessel perfusion.

To test whether revascularization of the PanMa is feasible, RFP-expressing human microvascular endothelial cells (ECs) were injected into the arterial system of the splenic lobe and cultured for 15 days under static conditions (Fig. 10c). RFP-expression allowed live monitoring of recellularized structures. Three days after injection, ECs covered large parts of the PanMa's vasculature (Fig. 10d). Recellularized branches were sharply delineated, underlining vessel integrity. Intense RFP signals were detectable especially in small branches, whereas larger vessels were not discernable. At day 15, signal intensity as well as the number of spots with sharply delineated signals were slightly decreased compared to day 3 (Fig. 10e). Nevertheless, most recellularized branches showed a nearly unaltered RFP signal suggesting vitality of the ECs. This assumption was confirmed by MTT analysis proving metabolic activity of the injected cells at day 15 of culture (Fig. 10f). Interestingly, the MTT signal was restricted to arterial vessels (Fig. 10f1), further proving vessel integrity as ECs were evidently unable to pass microcapillaries during recellularization. H&E stainings further revealed adherence of injected ECs to the vessel wall and the formation of a circular lining with a central lumen (Fig. 10g). Of note, in vessels with a small diameter, increased clogging of the luminal space was observed. IHC analysis for the endothelial marker van-Willebrand (VWF) factor demonstrated the maintenance of cell type-specific attributes after 15 days of culture (Fig. 10h).

Altogether, these findings show that the generated PanMa represents a cytocompatible scaffold with a preserved vessel system suitable for recellularization and supportive of cell attachment, cell survival and maintenance of EC-characteristics.

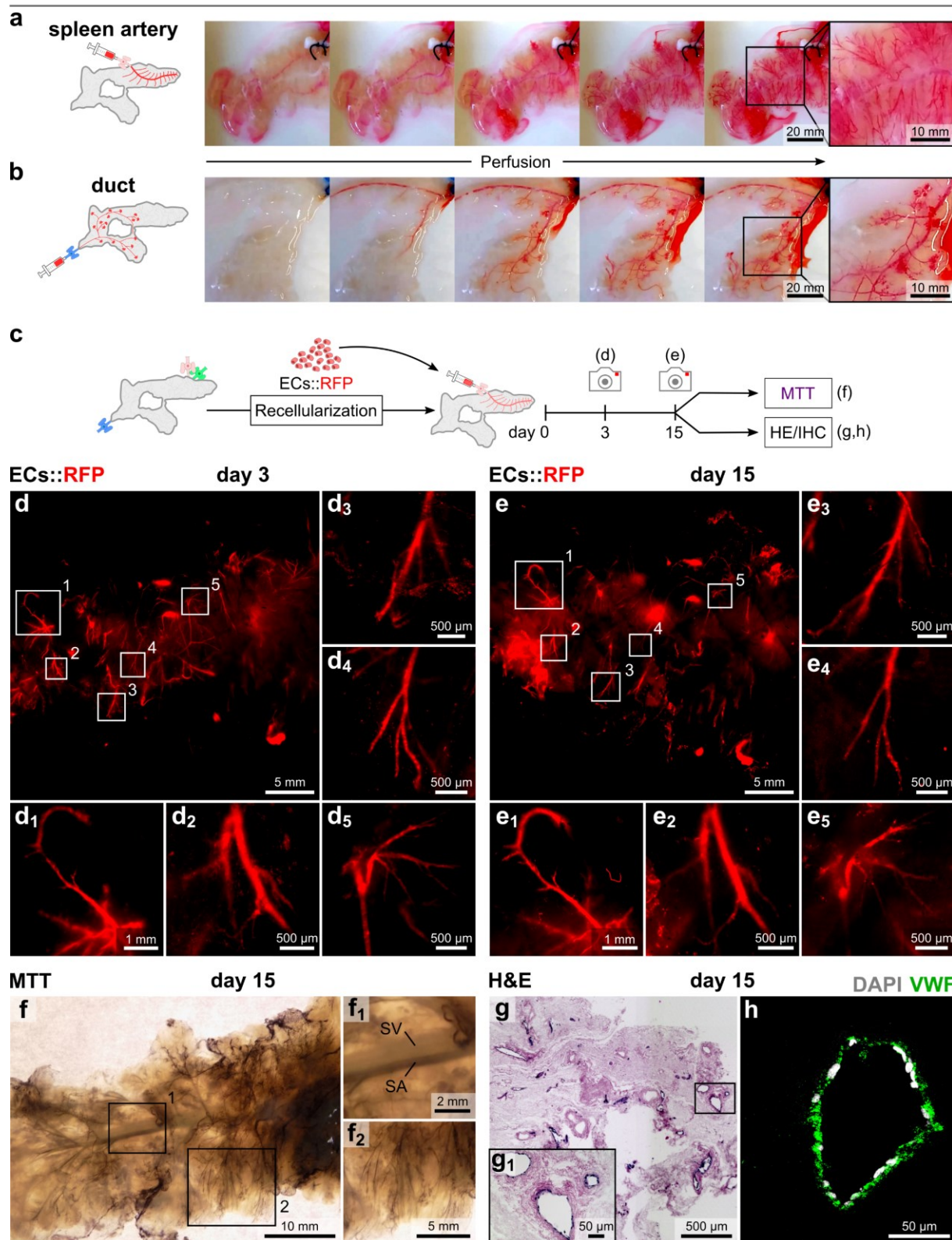


Figure 10 Preservation of the PanMa's vessel system allows recellularization of the splenic lobe arterial vasculature with human ECs. **a, b** Picture series showing the perfusion of the SL vascular system with Phenol red by injection through the SA as well as perfusion of the duct system by injection into the PD. **c** Schematic representation of the recellularization procedure. RFP-expressing ECs were injected into the arterial system of the SL via the SA. **d, e** Non-invasive fluorescent microscopy images of the SL arterial system 3 days (b) and 15 days (c) after injection of the ECs. Boxed areas are enlarged in the corresponding pictures and show the same spot of the sample at day 3 (b1 – b5) and day 15 (c1 – c5) (n = 3). **f** MTT-Assay at day 15 after EC injection. Violet stain shows areas with metabolic activity (n = 3). **e** Hematoxylin & Eosin stained cross-section of the recellularized SL 15 days after EC injection. **f** Fluorescent staining of the EC marker VWF (green) in cross-sections of the SL 15 days after recellularization counterstained with DAPI (grey) (n = 3). **Abbreviations:** PD: pancreatic duct, SA: splenic artery, SL: splenic lobe, SV: splenic vein. Figure modified from Berger et al. 2020.

6.1.3 The PancScore as a novel tool for the standardized evaluation of PanMa scaffold quality

For the reliable use of decellularized ECMs in tissue engineering approaches, a consistent scaffold quality is required to assure standardized experimental conditions.

To this purpose, a novel scoring system (PancScore) was developed enabling the evaluation of the generated PanMas in terms of decellularization efficiency, preservation of the ductal and arterial system, DNA removal and elimination of decellularization agent by quantification of remaining bile acid along defined criteria (Fig. 11a). Scaffolds are rated with 0 points (unsuitable), 1 point (low quality), 2 points (moderate quality) or 3 points (high quality) in each category (Table 3).

Table 3 Criteria of the PancScore.

Category	Criteria	3 points	2 points	1 point	0 points
1	Decellularization	No visible impurities.	Minimal impurities visible. Limited to single acini.	Larger regions with impurities are visible.	Entire lobes (spleen, duodenal, Connective) are non-decellularized.
2	Duct Perfusion	Both ductal branches are perfused. Perfusion reaches the single acini and is evenly distributed.	Both ductal branches are perfused. Perfusion is restricted to few acini.	Only one ductal branch is perfused.	No perfusion.
3	Vascular Perfusion	Splenic lobe is completely perfused (>90%).	50 – 90% of the splenic lobe are perfused.	<50% of the splenic lobe are perfused.	No perfusion.
4	DNA content	<50 ng DNA/mg dry weight	50 – 250 ng DNA/mg dry weight	250 – 500 ng DNA/mg dry weight	>500 ng DNA/mg dry weight
5	Bile acid	<25 (µmol/l)	25 – 50 (µmol/l)	50 – 150 (µmol/l)	>150 (µmol/l)

The PancScore was used to evaluate the applied decellularization protocol based on nine PanMas generated from ten consecutive experiments. One pancreas was excluded from analysis because of failed cannulation. Scores for qualitative assessment criteria (category 1, 2 and 3) were

assigned by three independent evaluators. The underlying data for the evaluations are summarized in supplementary figure 1.

In general, the PancScore showed a good practicability as suggested by a high correspondence between the scores of the three evaluators (Table 4). Assessment of the decellularization efficiency based on scaffold purity resulted in a mean score of 2.3 (Fig. 11b), while perfusion of the pancreatic duct (Fig. 11c) and splenic artery (Fig. 11d) were rated with a mean score of 2.4 and 2.3 respectively. For DNA removal, PanMas achieved a score of 1.3 (Fig. 11e), whereas elimination of bile acid was evaluated with a mean score of 2.9 (Fig. 11f). In total, PanMas received a mean score of 11.3 out of 15 points (Fig. 11g), suggesting a good average quality of the scaffolds according to the PancScore.

Table 4 Scoring of the single PanMas.

	<i>Category</i>	<i>Evaluator</i>	<i>PanMas</i>								
			P1	P2	P3	P4	P5	P7	P8	P9	P10
qualitative	optic purity	#1	1	1	3	3	2	2	2	1	2
		#2	2	2	3	3	3	3	3	2	2
		#3	1	1	2	2	3	3	3	2	3
		Mode (D)	1	1	3	3	3	3	3	2	2
	duct perfusion	#1	1	3	3	2	2	2	3	2	2
		#2	2	3	3	3	2	2	3	2	3
		#3	2	2	2	2	3	2	2	3	2
		Mode (D)	2	3	3	2	2	2	3	2	2
	vascular perfusion	#1	3	2	3	3	2	2	3	1	2
		#2	2	2	2	3	2	2	2	1	3
		#3	3	2	3	3	3	3	3	0	3
		Mode (D)	3	2	3	3	2	2	3	1	3
	quant.	DNA content		2	2	2	1	0	1	1	2
Bile acid			3	3	3	3	3	2	3	3	3

Summarized, the standardized evaluation of the generated PanMas using the PancScore indicated a good and robust performance of the applied decellularization protocol and identified DNA removal as a step with potential for improvement.

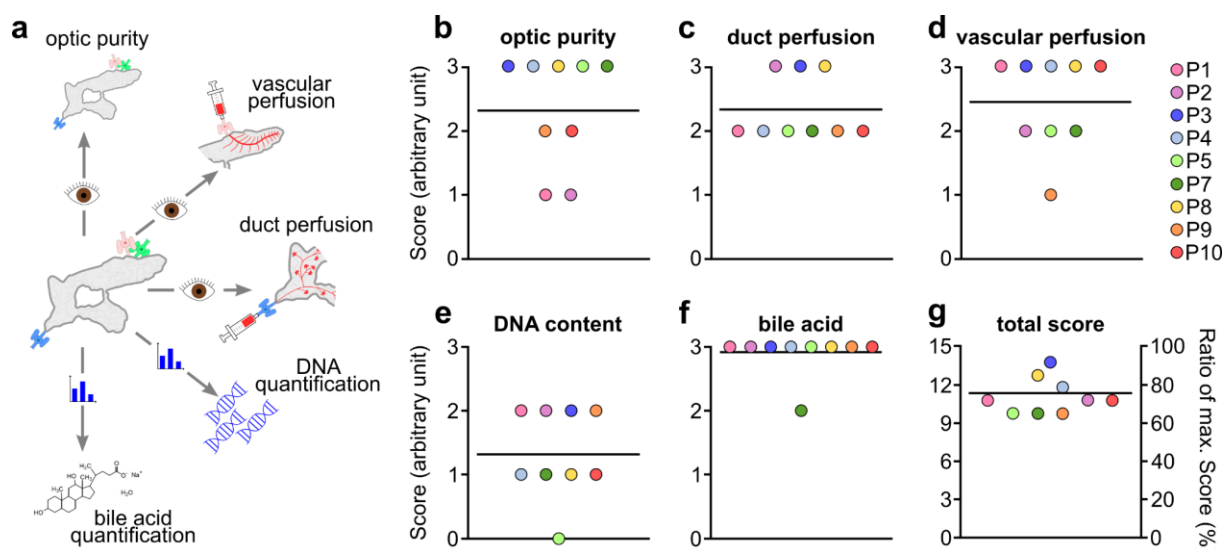


Figure 11 Application of the newly established PancScore for the evaluation of generated PanMas. **a** Schematic illustration of the PancScore quality assessment. **b – f** Scatter plots showing the single scores of nine PanMas generated from ten consecutive decellularization experiments. PanMas were evaluated for optic purity (**b**), extent of duct (**c**) and vascular (**d**) perfusion, residual DNA (**e**) and bile acid (**f**) content by three independent evaluators. Single values represent the mode (most occurring value) calculated from the scores of the evaluators. **g** PancScore for each PanMa shown as the total score and the percentage of the maximum score. The black line displays the mean of all samples. Figure modified from Berger et al. 2020.

6.2 Identification of PanMa-specific ECM properties

6.2.1 The PanMa represents a fiber-based, permeable, hygroscopic scaffold

In the first part of this study, a cytocompatible PanMa scaffold was generated which retains many characteristics of the native pancreas ECM. From other studies, it is known that ECM compositions, and thus biophysical properties, differ among organs (Travascio 2016). Therefore, the hypothesis was tested, whether specific ECM characteristics are conserved in the PanMa. To address this issue, the biophysical and physicostructural properties of the PanMa were analyzed and compared to ECM scaffolds derived from intestine (SISser) and lung (LungMa). Generation and basal characterization of the SISser and LungMa are shown in supplementary figure 2 (SISser) and supplementary figure 3 (LungMa). Ultrastructural analysis revealed a smooth surface of PanMa (Fig. 12a), which was similar to SISser (Fig. 12b), but in sharp contrast to the rough topography of the LungMa (Fig. 12c). A basal lamina, discernable as sheet-like structures, was not found in the PanMa, but predominantly on the surface of the SISser (Fig. 12b, b1) and to a fewer extent in the LungMa (Fig. 12c1). Collagen bundles of the PanMa appeared larger (Fig. 12a1) compared to those of the SISser (Fig. 14b1), while the diameter of single fibers was comparable between all scaffolds. The porosity of the PanMa meshwork (Fig. 12a2) seemed similar to that of the SISser (Fig. 12b2), whereas fibers of the LungMa appeared more densely packed (Fig. 12a2), suggesting a lower porosity.

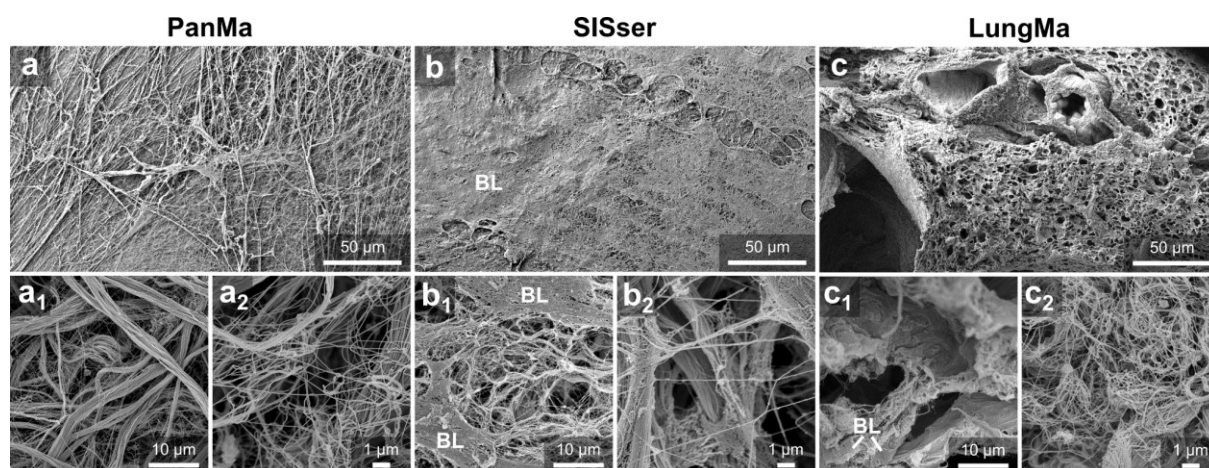


Figure 12 The microscale topography of the PanMa is characterized by a homogenous fiber-based network.

a – c Representative scanning electron microscopy images of the PanMa (a), SISser (b) and LungMa (c) surface.

Abbreviations: BL: Basal Lamina. Figure modified from Berger et al. 2020.

To gain more information about scaffold porosity, permeability of the ECMs for low and high weight molecules was analyzed by measuring the diffusion rate of 4 kD and 40 kD FITC dextran through the ECM scaffolds. All three scaffolds were permeable for both 4 kD (Fig. 13a, b) and 40 kD (Fig. 13c, d) FITC Dextran. Diffusion of 4 kD FITC Dextran appeared in general slower through PanMa and LungMa than through SISser, although this was not statistically significant (Fig. 13a). Determination of the apparent permeability coefficient (P_{app} -value), representing a measure for the passive permeability of a substance, revealed a slightly slower diffusion of 4 kD FITC Dextran through the PanMa ($4.4 \times 10^{-5} \pm 1.3 \times 10^{-5}$ cm/s) and the LungMa ($4.1 \times 10^{-5} \pm 0.5 \times 10^{-5}$ cm/s) compared to the SISser ($6.4 \times 10^{-5} \pm 0.9 \times 10^{-5}$ cm/s) within the first 60 min after application (Fig. 13b), which was probably due to a larger scaffold thickness. At later time points (360 – 1440 min), diffusion through the PanMa ($1 \times 10^{-6} \pm 0.4 \times 10^{-6}$ cm/s) and the LungMa ($1 \times 10^{-6} \pm 0.4 \times 10^{-6}$ cm/s) appeared slightly enhanced than through SISser ($0.4 \times 10^{-6} \pm 0.2 \times 10^{-6}$ cm/s). Diffusion of high weight 40 kD FITC Dextran in contrast appeared to be faster through the PanMa ($5.3 \times 10^{-5} \pm 0.4 \times 10^{-5}$ cm/s) than through the LungMa ($4.7 \times 10^{-5} \pm 0.6 \times 10^{-5}$ cm/s) within the first 60 min (Fig. 13c, d). The total amount of substance diffused through the scaffold after 24 h (Fig. 13 a, c) was slightly decreased for PanMa (4 kD: 21%, 40 kD: 23%) and LungMa (4 kD: 19%, 40 kD: 20%) compared to SISser (4 kD: 22%, 40 kD: 24%).

In summary, the diffusion of the 4 and 40 kD FITC Dextran through the scaffold resulted in marginal different diffusion rates. As none of these data were statistically significant, no final statement can be drawn from these findings. However, the made observation indicate that the PanMa and the LungMa might bind a greater amount of water and dissolved FITC Dextran compared to the SISser.

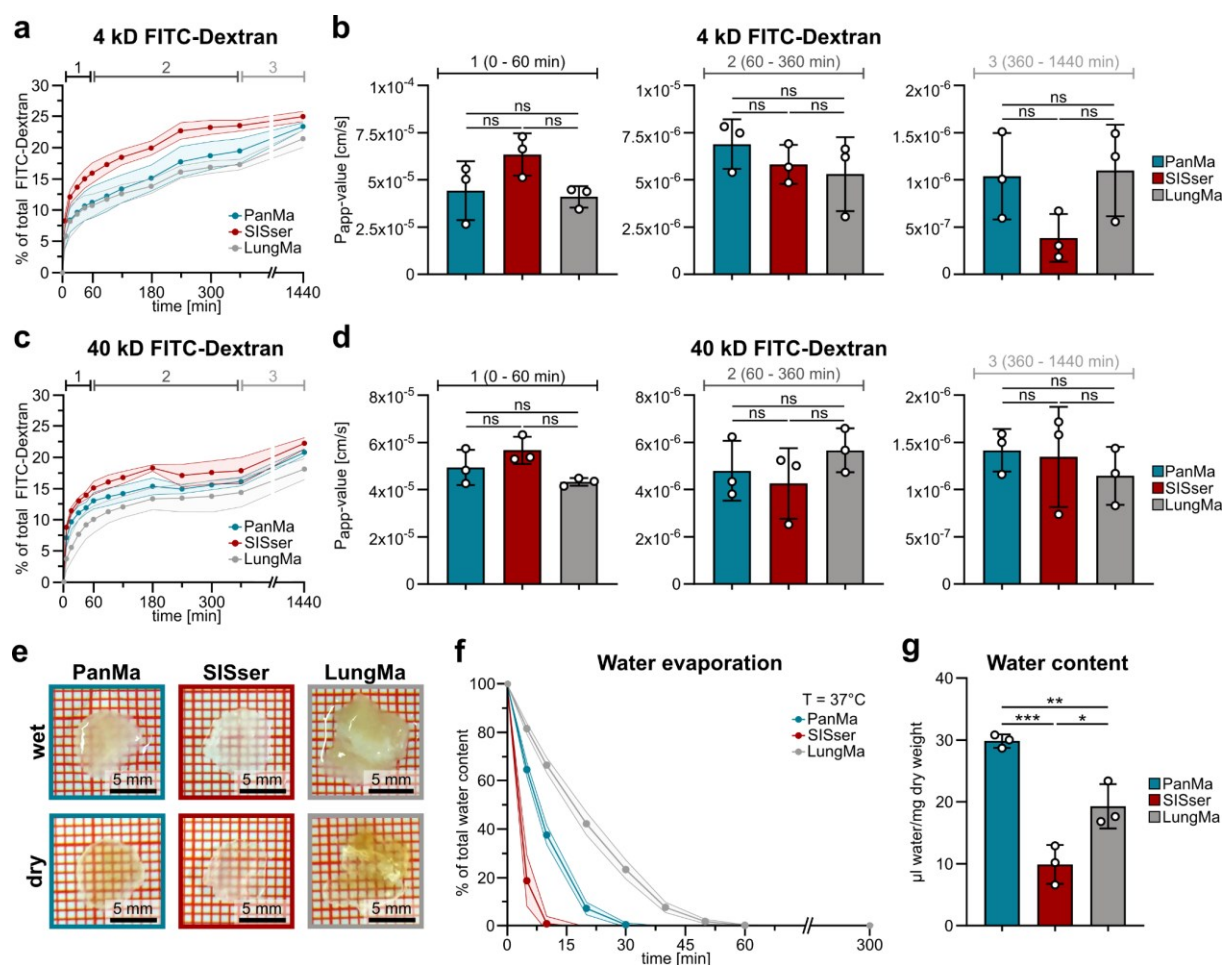


Figure 13 The PanMa represents a hygroscopic scaffold permeable for low and high weight molecules. **a – d** Diffusion of 4 kD (**a**, **b**) and 40 kD (**c**, **d**) FITC Dextran through PanMa, SISser and LungMa mounted in a Transwell®-like, ECM-based cell crown system. The line charts (**a**, **c**) show the ratio of FITC Dextran that passed the ECM scaffold over time. P_{app} -values (**b**, **d**) were calculated for an early (0 – 60 min), an intermediate (60 – 360 min) and a late (360 – 1440 min) period ($n = 3$). **e** Representative images of biopsy punches of the PanMa, SISser and LungMa soaked with PBS (upper panel) and after drying (lower panel) ($n = 3$). **f** Water content of scaffold pieces from PanMa, SISser and LungMa when incubated at 37°C . Water content was measured over time by determining the scaffold weight ($n = 3$). **g** Water content of PanMa, SISser and LungMa per mg dry weight ($n = 3$). **Statistics:** Data represent mean \pm SD (in the line charts SD is shown as error shadows). ns (not significant) $P > 0.05$, * $P < 0.05$, ** $P < 0.01$, *** $P < 0.001$, one-way Anova with Tukey's multiple comparisons test. Figure modified from Berger et al. 2020.

To confirm this assumption, the water storage capacity of the ECMs was determined. Indeed, analysis of the water content confirmed the hygroscopic properties of the PanMa (Fig. 13e – g). At 37°C water evaporated slower from the PanMa (dried after 40 min) scaffold than from SISser (dried after 10 min) and faster compared to LungMa (dried after 60 min) (Fig. 13f). Similarly, the PanMa exhibited a significantly higher water content per ECM dry mass ($30 \pm 0.9 \mu\text{l/mg}$) compared to SISser ($10 \pm 2.6 \mu\text{l/mg}$) and LungMa ($19 \pm 3 \mu\text{l/mg}$) (Fig. 13g).

Taken together, the PanMa represents a hygroscopic, collagen-fiber-based scaffold permeable for low and high weight molecules with a potential function as a reservoir for water and dissolved molecules.

6.2.2 The PanMa is softer compared to the SISser

Apart from composition and structure, the material stiffness represents an important characteristic of a biological scaffold. For unraveling the mechanical properties of the PanMa, oscillatory and rotational rheological measurements were performed in comparison to SISser and LungMa. Test series were executed with PBS-soaked scaffolds to resemble cell culture conditions and with a gap width optimized to the thickness of each scaffold (Fig. 14a).

Storage and loss modulus (G' and G'') are measures for the energy that can be stored in the structure of a material (storage modulus, elastic behavior) or that dissipates through heat (loss modulus, viscous behavior). Both parameters were significantly lower for the PanMa (0.089 ± 0.027 kPa and 0.033 ± 0.04 kPa) than for SISser (1.10 ± 0.12 kPa and 177 ± 42 Pa), suggesting a reduced viscoelastic strength of the PanMa (Fig. 14b, e, f). The linear viscoelastic region, defined as the range in which the applied strain does not affect the shear modulus, was similar for all scaffolds (Fig. 14b). The structure of the PanMa showed to be less resilient to strain compared to SISser and LungMa, as indicated by an earlier flow point, represented by the intersection point of both graphs ($G' = G''$) (Fig. 14b). PanMa, SISser and LungMa, exhibited damping factors ($\tan \delta = G''/G'$) of $\tan \delta < 1$, demonstrating a viscoelastic behavior of all scaffolds

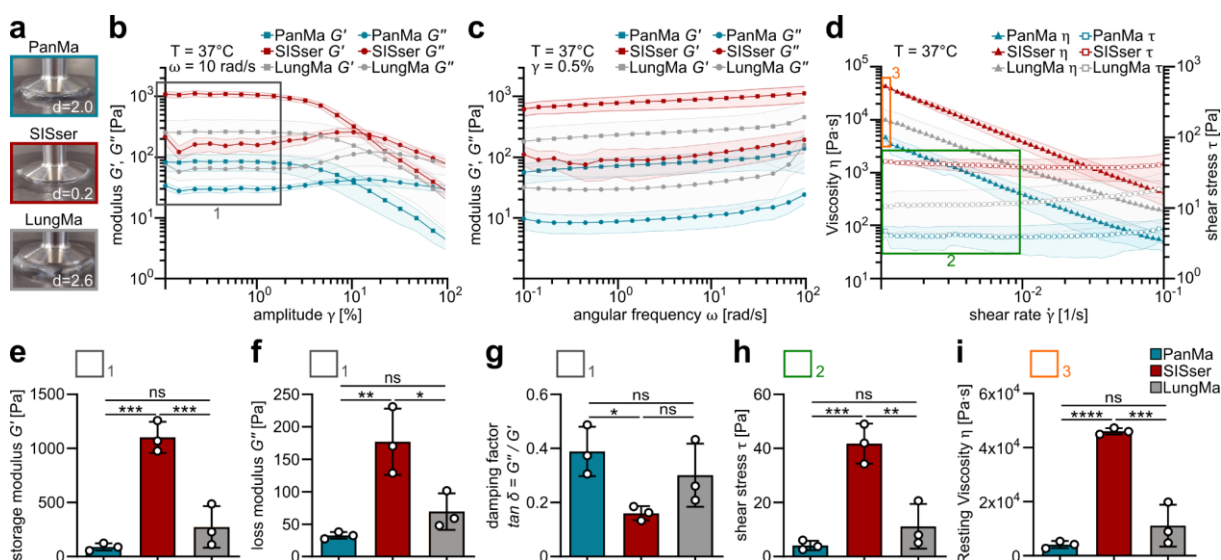


Figure 14 Rheological measurements highlight the PanMa as a soft scaffold. **a** Images of the PanMa (blue), SISser (red) and LungMa (grey) mounted in the plate-to-plate rotational rheometer with optimized gap width d (in mm). **b – d** Line-charts showing oscillatory (b, c) and rotational (d) measurements. Storage modulus G' (squares) and loss modulus G'' (dots) are given in dependency on strain deformation γ (b; $\omega = 10$ rad/s) and angular frequency ω (c; $\gamma = 0.5\%$) at 37°C . Steady shear measurements (d) show the viscosity η (triangle) and the shear stress τ (blank squares) with changing shear rates $\dot{\gamma}$ at 37°C . **e – i** Bar graphs presenting the mean values of the measurements shown in b – d. Average storage and loss modulus as well as the average damping factor were calculated from the linear viscoelastic region (grey box in a). To determine the mean shear stress data points showing a linear progression at low shear rates were taken (green box). Resting viscosity was calculated from viscosity values at low shear rates 0.001 1/s (orange box). **Statistics:** Data represent mean \pm SD (in the line charts SD is shown as error shadows). ns (not significant) $P > 0.05$, $*P < 0.05$, $**P < 0.01$, $***P < 0.001$, $****P < 0.0001$, one-way Anova with Tukey's multiple comparisons test. Figure modified from Berger et al. 2020.

(Fig. 14g). However, the damping factor of the PanMa (0.39 ± 0.07) was significantly higher than that of the SISser (0.16 ± 0.02), suggesting that the PanMa contains a higher ratio of viscous components. This finding was corroborated by shear rotational (Fig. 14d) measurements, demonstrating that the required shear stress τ for inducing a viscous behavior was lower for PanMa (4 ± 1 Pa) than for LungMa (11 ± 7 Pa) and SISser (42 ± 6 Pa) (Fig. 14h). Moreover, all scaffolds revealed a shear thinning behavior at low shear rates (Fig. 14d). Decreased values for the resting viscosity η were observed for the PanMa (4.1 ± 1.1 kPa·s) compared to SISser (46 ± 1.0 kPa·s) providing further evidence that the PanMa contains a greater proportion of viscous elements (Fig. 14i). Rheological measurements did not reveal significant differences between the viscoelastic properties of PanMa and LungMa, but a trend suggesting that the LungMa contains a higher proportion of elastic structures.

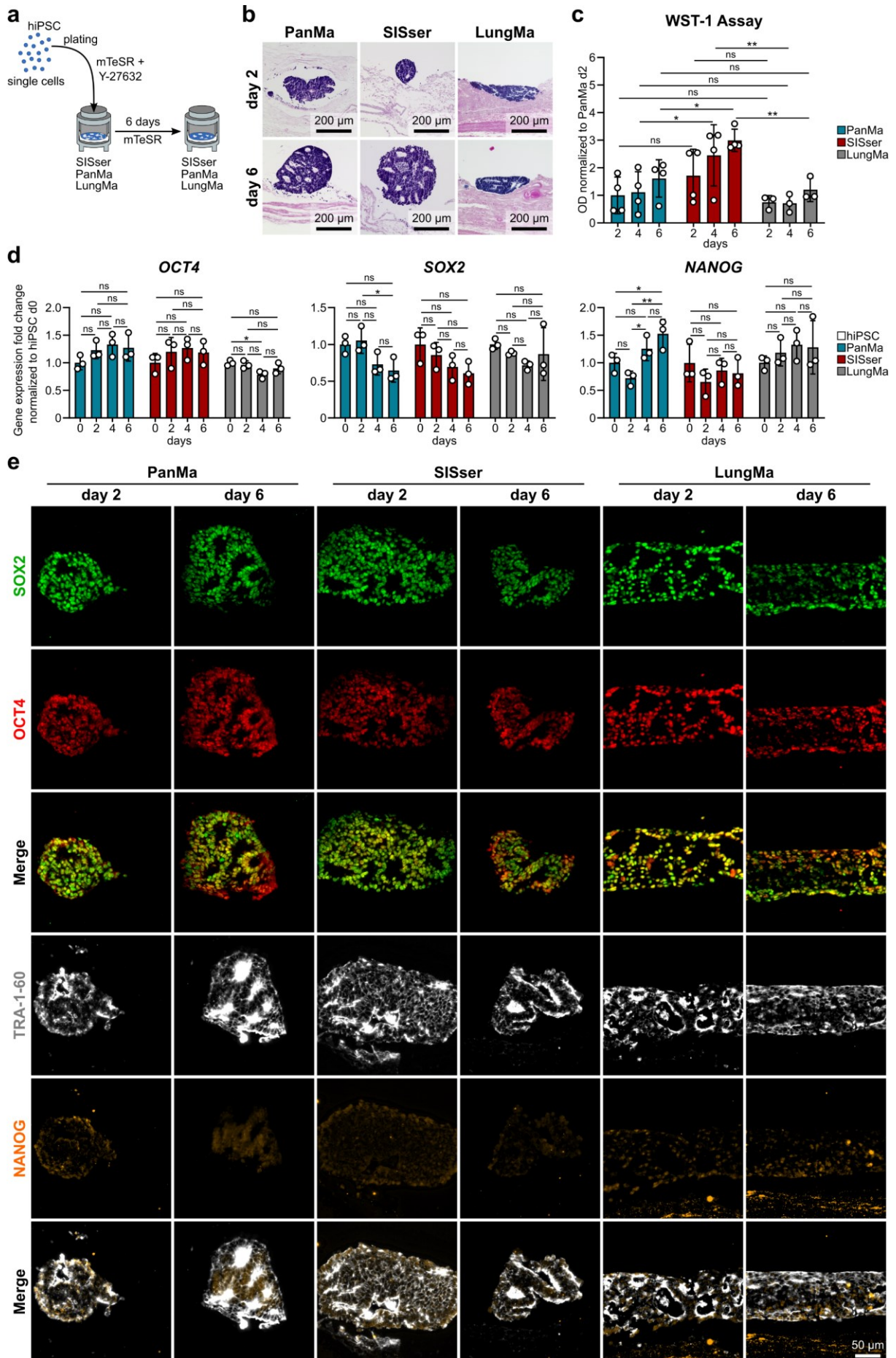
Summarized, the data show that the PanMa exhibited a lower stiffness compared to SISser due to a higher ratio of viscous components, and thus represents a slightly softer ECM scaffold than the SISser.

6.3 *Impact of the PanMa on pluripotent stem cells*

6.3.1 *The PanMa is suitable for hiPSC culture*

After the identification of unique biophysical and physicostructural characteristics of the PanMa, experiments were conducted to clarify whether these specific properties have a relevant impact on cellular physiology. Therefore, the PanMa was mounted in a cell crown and used as ECM-TWs in hiPSC maintenance culture allowing direct contact of the cells to the ECM in a 3D-like environment (Fig. 15a). SISser and LungMa were used as controls to discriminate the effect of general and tissue-specific ECM properties.

When seeded on the PanMa, hiPSCs aggregated to round cell clusters with reduced surface contact as well as elongated multilayered structures, which adhered to the ECM (Fig. 15b), as shown by representative H&E stainings. An equal clustering was observed on SISser and LungMa. Apart from the qualitative assessment of cellular attachment on the ECM, cellular viability was analyzed by quantitative WST-1 assay. As shown in figure 15c, the metabolic activity of cells cultured on the PanMa could be confirmed at 2, 4, and 6 days after seeding. However, the PanMa showed a significant lower metabolic activity (normalized to PanMa day 2) than hiPSC cultured on the SISser at day 2 (PanMa: 1 ± 0.7 , SISser: 1.8 ± 1), day 4 (PanMa: 1.1 ± 0.8 , SISser: 2.7 ± 1.1) and day 6 (PanMa: 1.8 ± 0.7 , SISser: 3.5 ± 0.4), indicating a lower seeding efficiency on the PanMa. Due to a missing positive control, no final statement to the cytocompatibility of the PanMa can be drawn



from this assay. However, a slight increase of the metabolic activity of hiPSCs on the PanMa from day 2 (1 ± 0.7) to day 6 (1.8 ± 0.7), indicate that cells proliferate on the PanMa.

Sustained stemness is the main criteria for the maintenance culture of hiPSCs and can be validated at distinct levels. One gold standard method is the determination of the gene expression profile of the core pluripotency network comprising the pluripotency markers *OCT4*, *SOX2* and *NANOG*. Gene expression analysis revealed only minor changes in the transcript abundance of *OCT4*, *SOX2* and *NANOG* in cells cultured on the PanMa (Fig. 15d). Expression of *OCT4* appeared to be slightly upregulated at day 6 (1.2-fold \pm 0.2), while *SOX2* expression seemed decreased (0.6-fold \pm 0.1). Both observations were not significant. *NANOG* expression varied over time and showed a mild, but significant increase at day 6 (1.5-fold \pm 0.2). Gene expression patterns were slightly different in cells cultured on SISser and LungMa. In contrast to hiPSCs on the PanMa, *NANOG* expression appeared to be marginally downregulated in cells on the SISser at day 6 (0.8-fold \pm 0.2) and in cells on the LungMa gene expression was nearly unchanged at day 6 (*OCT4*: 0.9-fold \pm 0.14, *SOX2*: 0.9-fold \pm 0.4 and *NANOG*: 1.3 \pm 0.5).

Analysis by immunofluorescence analysis revealed no scaffold-dependent difference in the protein marker expression. As shown in representative microscope pictures of IHC-stained sections in figure 15e, the hiPSC surface marker TRA-1-60 was ubiquitously abundant in hiPSCs cultured on the PanMa with enriched signal intensities at borders of cavities within the cell clusters. Irrespective of the used scaffold, the majority of hiPSCs showed co-expression of *OCT4* and *SOX2*, while few individual areas of cell clusters lacked either *OCT4* or *SOX2* expression. Most strikingly, in the majority of hiPSC cells *NANOG* signals were only weakly detectable or even completely absent at day 2 and day 6 on all scaffolds.

Altogether, the data indicate the suitability of the PanMa for application in stem cell culture and indicates a possible impact of the ECM on the stem cell character of hiPSCs. Especially the weak *NANOG* signal indicates an effect of the ECM culture on the stemness of hiPSCs.

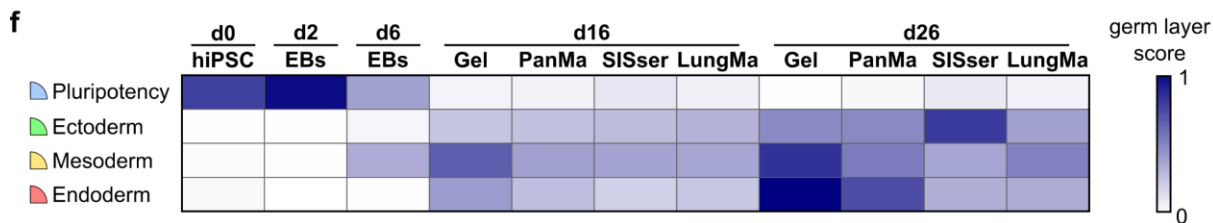
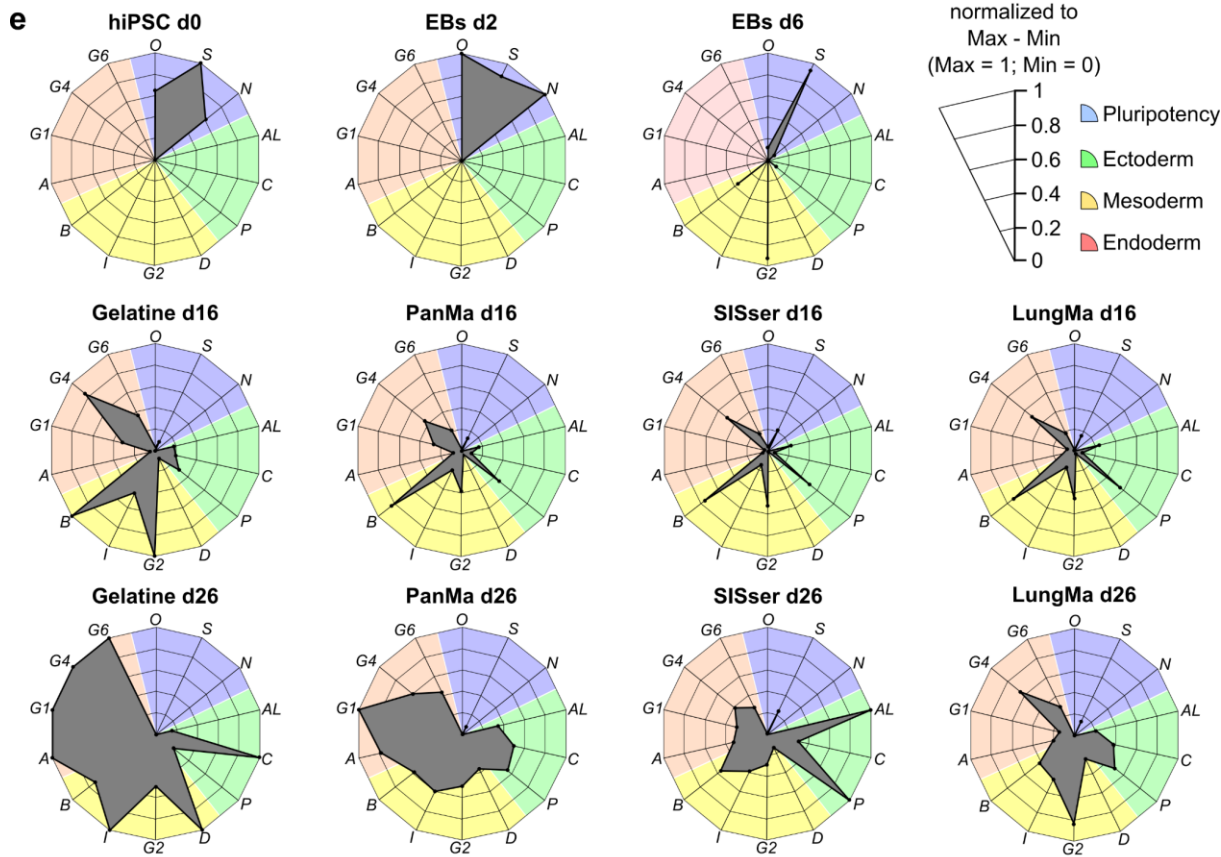
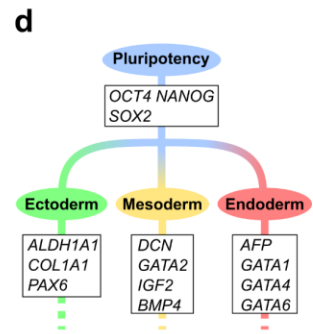
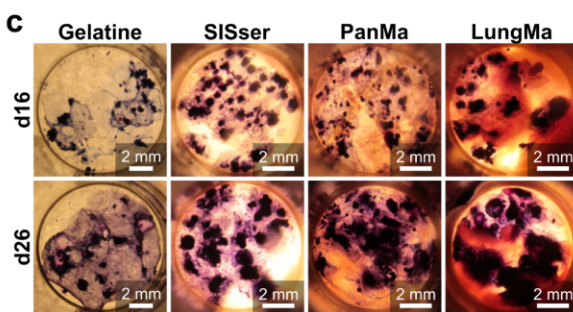
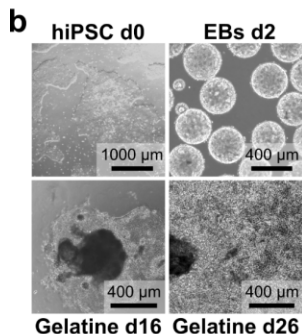
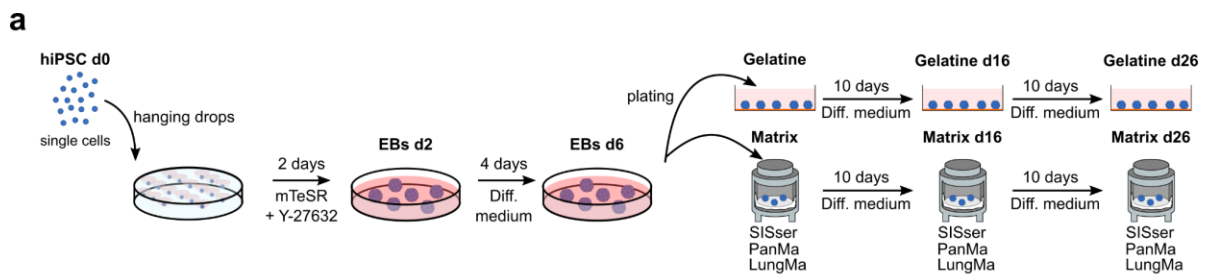
Figure 15 Marginal changes in the gene expression of pluripotency markers and weak *NANOG* signals in hiPSCs maintained on the ECM scaffolds. **a** Schematic illustration of the experimental setup. ECM scaffolds were mounted in cell crowns to obtain a Transwell®-like system. hiPSCs were detached, seeded as single cells on the ECM scaffolds and cultured for up to 6 days. **b** Representative Hematoxylin & Eosin stainings of cross-sections of the scaffolds at day 2 and day 6 of culture (n = 3). **c** Metabolic activity of the hiPSC cultured on PanMa, SISser or LungMa at day 2, day 4 and day 6 measured by WST-1 assay. Data are shown as the OD fold change compared to the OD measured for PanMa day 2 (n = 3). **d** Gene expression of the pluripotency markers *OCT4*, *SOX2* and *NANOG* in cells cultured on the ECM scaffolds at day 2, day 4 and day 6, shown as the fold change of expression at day 0 (n = 3). **e** Representative images of cross-sections of cells cultured on the ECM scaffold at day 2 and day 6 immunohistochemically stained for the pluripotency marker proteins *SOX2* (green), *OCT4* (red), TRA-1-60 (grey) and *NANOG* (orange). Panels with merged images show the overlay of the two pictures above (n = 2). **Statistics:** Data represent mean \pm SD. ns (not significant) P > 0.05, *P < 0.05, **P < 0.01, two-way Anova with Tukey's multiple comparisons test (c: test between groups) and one-way Anova with Tukey's multiple (d: test within group). **Scale bars:** If not annotated in the picture, the image size refers to the scale bar displayed in the picture at the right bottom corner in the same figure part. **Abbreviations:** OD: optic density.

6.3.2 Culture on the PanMa promotes an endoderm signature of hiPSCs during multi-lineage differentiation

Slightly diverging expression patterns of pluripotency genes and the reduced abundance of NANOG protein signals in hiPSCs cultured on the different ECM scaffolds provided evidence for a scaffold-dependent impact on stem cell pluripotency and therefore a potential effect on early lineage specification. To uncover a potential link between ECM origin and hiPSC fate decisions, the impact of the different ECM scaffolds was investigated during spontaneous multi-lineage differentiation. As illustrated in figure 16a, hiPSCs (day 0) were first cultured as hanging drops to generate embryoid bodies (EBs) (day 2). After 2 days, EBs were collected and cultured in suspension for 4 days in a spontaneous differentiation medium. At day 6, EBs were seeded on either PanMa, SISser or LungMa or on gelatin as a 2D control and exposed to spontaneous differentiation medium for 10 or 20 days (Fig. 16b).

At first, cellular viability was assessed by MTT analysis confirming vitality of the cultured cells during the experimental procedure on gelatin and all ECM scaffolds (Fig. 16c). Moreover, the MTT assay visualized the spreading of cells from the EBs, which was less on the scaffolds compared to the gelatin 2D control. Among the scaffolds, migration appeared less on the LungMa, while cell spreading on the SISser seemed to be slightly increased compared to the PanMa.

For tracking the developmental stages of the hiPSCs during differentiation, gene expression analysis of representative marker genes for the pluripotent state (*OCT4*, *SOX2*, *NANOG*) as well as the three germ layers ectoderm (*ALDH1A1*, *COL1A1*, *PAX6*), mesoderm (*DCN*, *GATA2*, *IGF2*, *BMP4*) and endoderm (*AFP*, *GATA1*, *GATA4*, *GATA6*) was performed (Fig. 16d). Expression of each gene was normalized to the range of expression of all samples (maximum = 1, minimum = 0) and visualized as network diagrams. hiPSCs at d0 showed high expression levels of the pluripotency genes *OCT4*, *SOX2* and *NANOG*, which were slightly increased after EB formation at day 2 (Fig. 16e). In contrast, with ongoing differentiation, a decline of *OCT4* and *NANOG* expression was observed at day 6. Of note, *SOX2* expression remained at high levels at this time point. Furthermore, increased transcript levels of the mesoderm-associated genes *GATA2* and *BMP4* were detectable, indicating an onset of differentiation. At d16, elevated expression of lineage-specific marker genes associated with all three germ layers was observed in cells cultured on gelatin and, to a lower extent, in cells seeded on the ECM scaffolds. Interestingly, similar expression profiles were observed in cells seeded on the different scaffolds, suggesting no impact of the ECM at this stage of differentiation. However, prolonged culture resulted in diverging expression patterns among cells cultured on the three ECM scaffolds. In detail at day 26, cells seeded on the PanMa revealed a slight upregulation of the endoderm-associated genes *AFP*, *GATA1* and *GATA4* compared to SISser and LungMa. In contrast, cells on the SISser exhibited increased

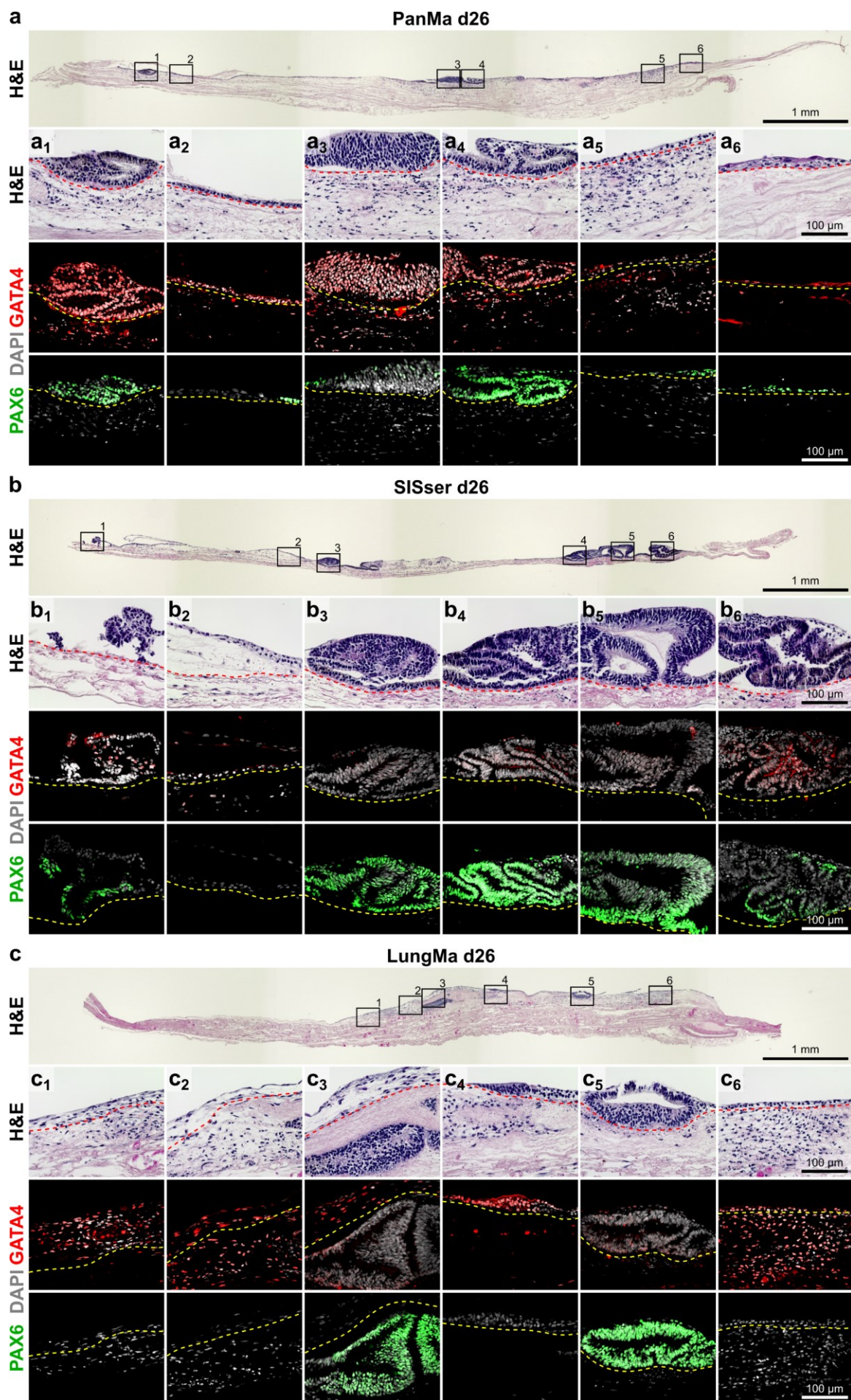


transcript levels of the ectodermal markers *ALDH1A1* and *PAX6*, which were less abundant in cells cultured on PanMa and LungMa. In order to examine the overall tendency of hiPSC differentiation towards the germ layer lineages dependent of the ECM scaffold, the germ layer score was calculated. Thereby, expression of genes associated to a certain lineage were averaged and given as a single value (Fig. 16f). Determination of the germ layer score confirmed an ECM-dependent effect on early differentiation. Culture on the PanMa led to an increased endodermal score at day 26 (PanMa: 0.70; SISser: 0.32; LungMa: 0.33), while the highest ectodermal score at day 26 was observed in cells seeded on the SISser (PanMa: 0.46; SISser: 0.77; LungMa: 0.36). However, it must be noted that gene expression differences were not statistically significant, whereas this hypothesis needs to be considered with caution.

Taken together, the data suggest that culture of hiPSC on the ECM scaffolds could affect the expression of lineage-associated genes and thus indicate a possible effect of the ECM on early fate decisions during the development of hiPSCs.

To verify the observations made on gene expression level, cell morphology and protein expression were investigated more closely. Examination of the microscopic appearance of the seeded scaffolds by H&E staining revealed a variety of diverse cell types and different cell structures (Fig. 17a – c). Apart from dense cell clusters that were predominantly found on top of the scaffolds (Fig. 17a1, a3, a4, b3 – b6, c3, c5) elongated cells infiltrating the matrix (Fig. 17a1 – a5, b2, b6, c1, c2, c6) as well as cells arranged in monolayers on the ECM surface (Fig. 17a2, a5, a6, b2, c2, c4, c6) were observed. Dense cell clusters harbored pigmented cells (Fig. 17a1, b4, b6), while some cells contributed to the formation of sheet-like structures that were shedding from the ECM surface (Fig. 17b2, c2, c3). The various cell types were found on all scaffolds and no prevalence of a certain cell type on a specific scaffold was apparent. In order to uncover the association of the differentiated cells to the endodermal and ectodermal lineage, cells were stained for the endoderm marker *GATA4* and the ectoderm-associated marker *PAX6*. Immunohistochemical analyses indicated a more pronounced expression of *GATA4* in cells on the

Figure 16 Culture of hiPSC on the PanMa slightly enhances the expression of endoderm-associated genes during spontaneous differentiation. **a** Schematic illustration of the experimental setup. hiPSC were cultured as hanging drops to form EBs, which were collected, cultured for 4 days in spontaneous differentiation medium and subsequently seeded on ECM-based cell crowns in Transwell®-like system or on gelatin coated plates as a control. **b** Brightfield images of hiPSC before detachment, EBs after collection and differentiating cells 10 and 20 days after seeding on gelatin coated plates. **c** Representative images of MTT assays of cells seeded on gelatin or the Transwell®-like system at d16 and d26 of spontaneous differentiation (n = 3). **d** Scheme of early hiPSC development into the three germ layers with representative lineage markers used for gene expression analysis. **e** Gene expression of cells at d0 (hiPSCs), d2 (EB formation), d6 (EB culture) as well as after seeding on gelatin coated plates PanMa, SISser or LungMa at d16 and d26. Gene expression of each gene was normalized to the range between minimum (= 0) and maximum (= 1) expression and displayed as network diagrams (n = 3). **f** Heat-map showing the germ layer score for each sample, representing the average normalized expression of genes associated with a certain germ layer (n = 3). **Abbreviations:** *O*: *OCT4*, *S*: *SOX2*, *N*: *NANOG*, *AL*: *ALDH1A1*, *C*: *COL1A1*, *P*: *PAX6*, *D*: *DCN*, *G2*: *GATA2*, *I*: *IGF*, *B*: *BMP4*, *A*: *AFP*, *G1*: *GATA1*, *G4*: *GATA4*, *G6*: *GATA6*, d: day, Gel: Gelatin, EB: embryoid body. Figure modified from Berger et al. 2020.



PanMa (Fig. 17a) while PAX6 appeared to be more abundant in cells on the SISser (Fig. 17b). The marker expression in cells on the LungMa were comparable to the PanMa (Fig. 17c). Furthermore, it was apparent that cells on the PanMa and LungMa increasingly infiltrated the ECM, while cells on the SISser were found predominantly above the ECM surface (red dotted line in H&E stainings, yellow dotted line in immunofluorescent pictures). In this context, it seemed that cells located within the ECM were GATA4⁺ but not PAX6⁺, irrespective of the used scaffold.

In order to confirm this impression, cell numbers of GATA4⁺ and PAX6⁺ cells were quantified by manual counting (Fig. 18). The obtained data were not statistically significant, wherefore the findings do not allow making a definitive statement. According to the data, it seemed that more cells expressing the endoderm-associated transcription factor GATA4 were found on the PanMa ($57 \pm 17\%$) than on SISser ($32 \pm 20\%$) (Fig. 18a). Similarly, the number of PAX6⁺ cells, indicating an ectodermal cell fate, was twice as high on the SISser ($60 \pm 32\%$) compared to the PanMa ($33 \pm 21\%$) (Fig. 18b). Interestingly, 34% (± 17) and 42% (± 31) of the cells cultured on the PanMa and LungMa were found inside the scaffold (Fig. 18c), respectively, while a higher ratio of cells seeded on the SISser was found on top of the ECM ($85 \pm 8\%$) (Fig. 18d). GATA4 expression was found in cells located above ($35 \pm 20\%$) and below ($22 \pm 9\%$) the PanMa ECM surface to a similar extent (Fig. 18e), which argues against a correlation of GATA4 expression and the migration behavior of cells. In contrast, PAX6⁺ cells were almost exclusively found on top of the PanMa ($42 \pm 23\%$), while cells located inside the scaffold were rarely PAX6⁺ ($4 \pm 3\%$) (Fig. 18f). Notably, this unequal distribution of PAX6⁺ cells was not found on the SISser or LungMa. This could be a hint that the microenvironment inside the PanMa could have a negative effect on PAX6 expression.

In order to gain an insight whether the ECM scaffolds also affect hiPSC development beyond germ layer commitment, expression of genes marking later stages of development were analyzed. In view of the high endodermal score of cells cultured on the PanMa (Fig. 16f), the focus was put on genes associated with early and advanced stages of the endodermal lineage (Fig. 19a). As previously, gene expression was calculated as the fold change of the range between maximum (= 1) and minimum gene expression (= 0) for each gene and shown as Heatmap (Fig. 19b).

Figure 17 Distribution of GATA4⁺ and PAX6⁺ cells after spontaneous differentiation on the ECM scaffolds. a - c Representative images of stained cross-sections of the seeded PanMa (a), SISser (b) or LungMa (c) at day 26 of spontaneous differentiation. The upper panel in each figure part shows a Hematoxylin & Eosin stained cross-section of the respective scaffold. Boxed areas are presented at a higher magnification in the panel below according to the numerical annotation. The two lower panels of each figure part show serial sections of the scaffolds stained for the endodermal marker GATA4 (red) and the ectodermal marker PAX6 (green) displaying the approximated area shown in the Hematoxylin & Eosin stainings. Immunofluorescent stainings were counterstained with DAPI (grey). Dashed lines indicated the scaffold surface (n = 3). **Scale bars:** If not annotated in the picture, the image size refers to the scale bar displayed in the picture at the right bottom corner in the same figure part. Figure modified from Berger et al. 2020.

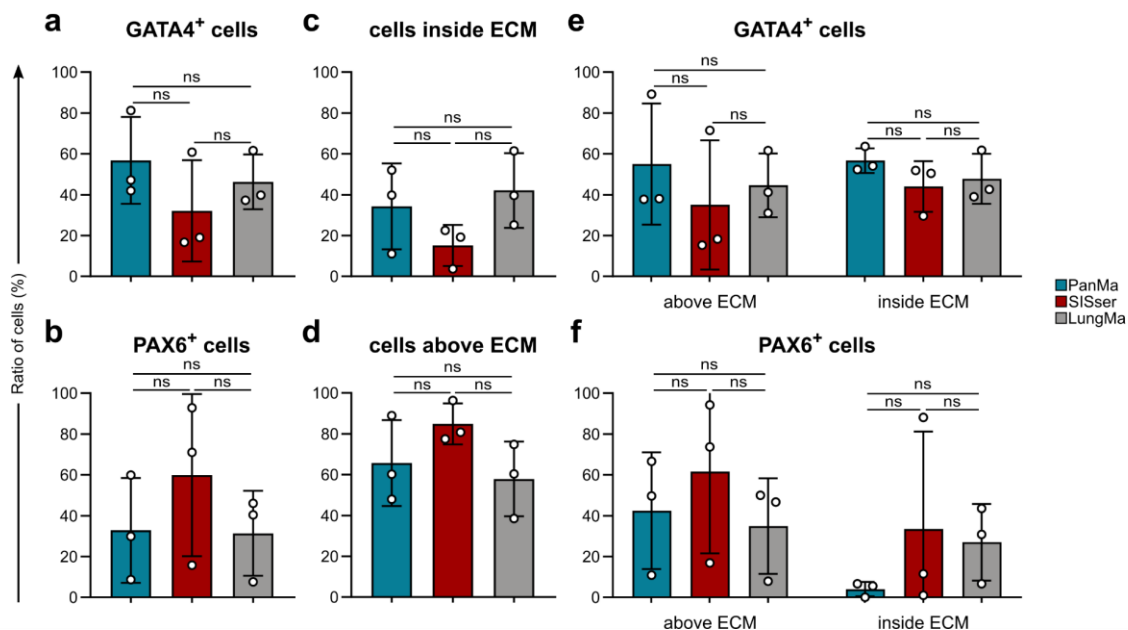


Figure 18 Spontaneous differentiation of hiPSCs on the PanMa results in an elevated number of GATA4+ cells. a - f Quantification of the immunostainings shown in Figure 12. The bar graphs display the ratio of GATA4+ (a) and PAX6+ (d) cells on the PanMa, SISser and LungMa and the proportion of cells located above (b) or below (e) the scaffold surface. Graphs on the right display the ratio of GATA4+ (c) or PAX6+ (f) determined for the cell populations located above or below the scaffold surface (n = 3). **Statistics:** Quantification of the immunohistochemical analysis was performed by manual counting of randomized samples. Data represent mean \pm SD. ns (not significant) P > 0.05, one-way Anova with Tukey's multiple comparisons test.

As shown in figure 19b, genes regulating the formation of definitive endoderm, foregut and mid-/hindgut structures were expressed in cells cultured on the different scaffolds as well as on gelatin at day 16, without an apparent expression profile. In contrast to that, diverging expression patterns became discernable at day 26. Gene expression of *SOX17* and *FOXA2* (definitive endoderm), *HNF1b* and *HNF4a* (foregut), as well as *CDX2* (mid-hindgut) was sustained in cells cultured on the PanMa in comparison to day 16, while expression of these genes appeared to be downregulated in cells on SISser and LungMa. No distinct pattern was apparent for genes associated with advanced stages of the endodermal lineage. While expression of the pancreatic genes *PDX1* and *PTF1a* appeared to be slightly enhanced in cells seeded on SISser or LungMa, respectively, *CDX2*, a regulator of intestinal development showed higher transcript levels in cells on the PanMa. Again, gene expression data were not significant for the different samples. In contrast, a significant elevated expression was found for the pharyngeal marker *PAX9* in cells cultured on the LungMa, indicating a beneficial effect of the LungMa on the regulation of *PAX9*.

Taken together, these data indicate that culture on the PanMa was associated with an enhanced expression of endodermal markers, while differentiation on the SISser seemed to promote an ectoderm phenotype. Although this observation could be verified on gene and protein level, a conclusion cannot be drawn, as data were not statistically significant.

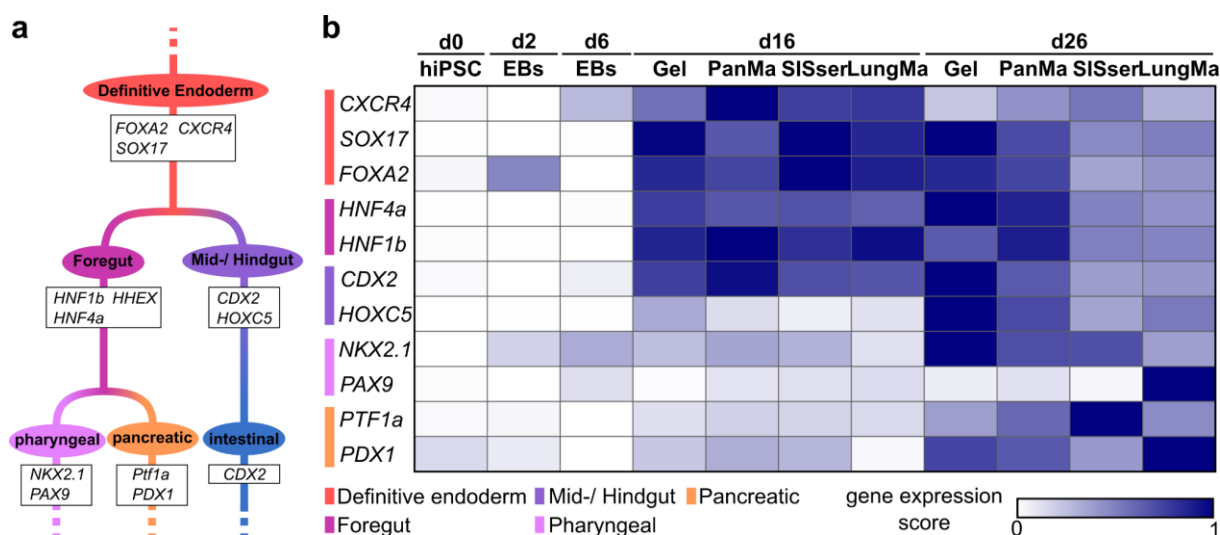


Figure 19 Spontaneous differentiation of hiPSCs on the PanMa leads to an increased expression of endoderm lineage genes. **a** Schematic illustration showing the endodermal development with representative markers for each stage that were used for gene expression analysis. **b** Heat map showing the expression pattern of cells during spontaneous differentiation before (d0, d2, d6) and after seeding on the respective scaffold (d16, d26) for genes representative for different stages of the endodermal development. The expression of each gene was normalized to the range of minimum (set to 0) and maximum expression (set to 1) among all samples for the respective gene (n = 3). **Abbreviations:** d: day, Gel: Gelatin. Figure modified from Berger et al. 2020.

6.3.3 Differentiating hiPSCs attach to the PanMa by binding to collagen fibers and bundles

ECM signaling is mostly mediated by direct cell-matrix binding. Thereby, the facets of ECM-interactions, such as number and topography of adhesion sites, play a decisive role for signal transduction and eventually the induced cellular response. In order to analyze the cellular attachment to the different ECM scaffolds on an ultrastructural level, the interactions of the spontaneously differentiating cells with the different scaffolds were analyzed by electron microscopy (Fig. 20).

2 days after seeding of EBs, hiPSC exhibited a number of microvilli, visible as short, cytoplasmic protrusions, as well as larger extensions, termed filopodia, irrespective of the used scaffold (Fig. 20a – g). ECM-attachment of cells seeded on the PanMa was mostly mediated by binding of microvilli to single collagen fibers (Fig. 20a, b) as well as larger collagen bundles (Fig. 20c). In contrast to this, cells on the SISser predominantly attached to the basal lamina by forming flat protrusions with an enlarged contact area (Fig. 20d). In addition, cells on the SISser bound to single collagen fibers (Fig. 20e) and bundles (Fig. 20f), as observed on the PanMa. On the LungMa, cells showed only few ECM-interactions sites and bound merely to single collagen fibers (Fig. 20f, g). In general, cells seeded on the SISser exhibited more contact sites to the ECM compared to cells on the PanMa and LungMa, suggesting a stronger surface adhesion on the SISser.

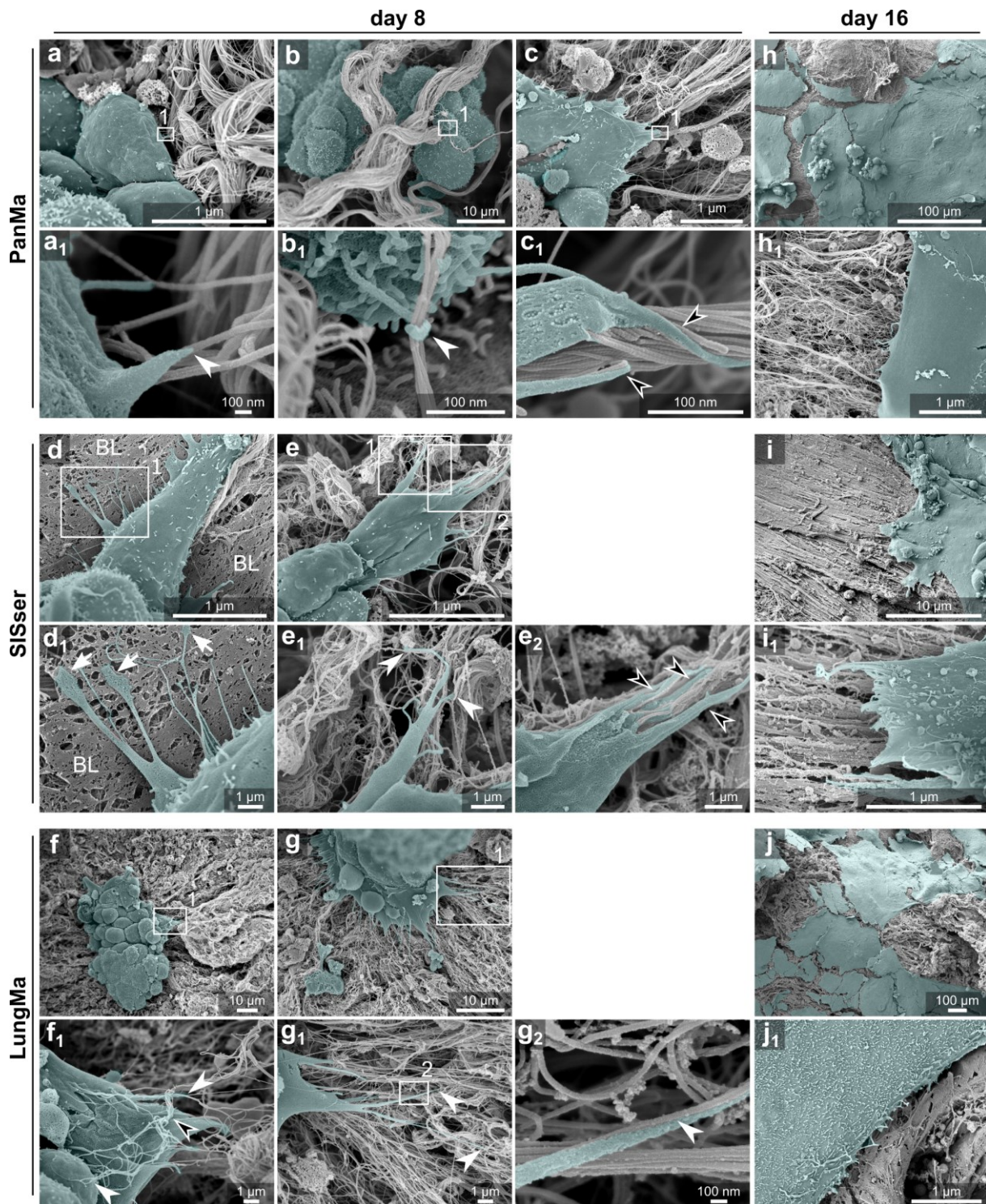


Figure 20 Attachment of hiPSCs to the PanMa is mediated by binding to collagen fibers. a – g Representative scanning electron microscopy images of hiPSC-derived EBs during spontaneous differentiation two days after seeding (day 8) on PanMa (a – c), SISser (d, e) or LungMa (f, g). Cells (cyan) show the formation of short microvilli or longer filopodia to a different extent. Binding to the ECM is scaffold dependent and takes place by cell-interaction with single collagen fibers (white arrowhead), collagen bundles (black arrowhead) or the BL (white arrows) (n = 2). **h – j** Scanning electron microscopy images of hiPSC-derived spontaneously differentiated cells at day16 of culture (n = 1). **Abbreviations:** BL: Basal Lamina. Figure modified from Berger et al. 2020.

After 10 days of culture (day 16), scaffolds were largely covered with a cell layer of morphologically distinguishable types of cells (Fig. 20h – j). Extension of the cell layer appeared to be orientated towards the fiber alignment. Interestingly, fiber alignment of the SISser (Fig. 20h) was more homogenous compared to PanMa (Fig. 20i) and LungMa (Fig. 20j).

Summarized, the SEM analysis demonstrated that the ECM interaction of differentiating hiPSCs was largely determined by the ultrastructural and compositional features of the respective scaffold, which provides one possible explanation for the scaffold-dependent influences on the early differentiation of hiPSCs.

6.4 *Impact of the PanMa on pancreatic differentiation*

6.4.1 *Application of the PanMa as a liquid medium supplement does not influence the directed pancreatic differentiation of hiPSCs*

Previous studies demonstrated a supportive effect of the ECM on survival and function of mature islets isolated from human pancreata (Cheng et al. 2011). By contrast, the contribution of the ECM to β -cell development and maturation is less understood. Considering the PanMa-specific effects on early events of hiPSC development, the next aim of this study was to examine whether the ECM cues of the PanMa are capable to improve the directed differentiation of hiPSCs towards endocrine cell types such as pancreatic β -cells. To address this issue, directed differentiation of hiPSCs towards pancreatic endoderm was conducted using a 4-stage protocol by Rezania et al. (Rezania et al. 2012). The generated stage (S) 4 cells were subsequently transferred to suspension culture for further maturation towards S5 INS⁺ cells (Fig. 21a) (Rezania et al. 2014).

In a first experimental set up, the hypothesis was tested whether the biochemical signaling of PanMa components and ECM bound factors are sufficient to alter directed pancreatic differentiation. In order to isolate the biochemical signature of the PanMa from the biophysical information of the solid scaffold, the PanMa was disrupted and solubilized, resulting in a suspension of potentially biochemical active ECM components without macrostructure. The solubilized PanMa was applied as a medium supplement at different concentrations (100 ng/ml – 800 ng/ml) during S5 suspension culture (Fig. 21a). Cells treated with only SDS at a concentration similar to the SDS concentration of cells treated with 800 ng/ml PanMa served as a solvent control.

Bright field images of the S5 cells at day 21 demonstrate that the application of the liquid PanMa had no apparent effect on cell cluster morphology (Fig. 21b). Gene expression analyses of untreated and SDS-exposed S5 cells coincided with the data of the original protocol (Fig. 21c). Thereby S5 cells of both conditions showed an elevated expression of genes encoding for the

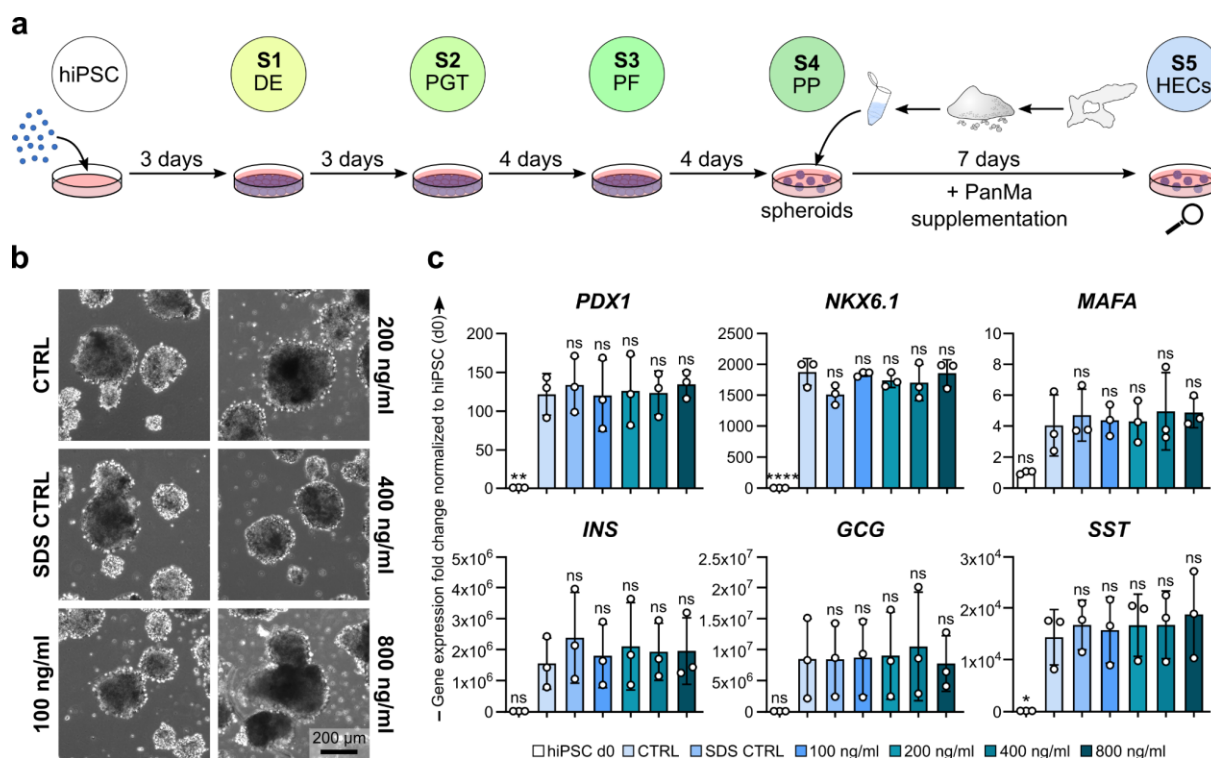


Figure 21 Supplementation of the PanMa as a liquid medium supplement has no effect on the differentiation of hiPSCs towards pancreatic HECs. **a** Schematic drawing of the experimental procedure. hiPSCs were differentiated towards HECs using a 5-stage protocol as described by Rezania et al (Rezania et al. 2012; Rezania et al. 2014). At d14 of culture, cells were detached as cell clusters, transferred to suspension culture and exposed to differentiation medium supplemented with different concentration of solubilized PanMa. **b** Brightfield images of HEC clusters at day 21 of culture after exposure to different concentrations with PanMa for seven days or with only SDS as solvent compared to non-treated control HECs ($n = 3$). **c** Gene expression analysis of differently treated HECs at day 21 of differentiation. Expression of the transcription factors *PDX1*, *NKX6.1* and *MAFA* as well as the pancreatic hormones *INS*, *GCG* and *SST* is shown as fold change compared to gene expression of hiPSCs ($n = 3$). For testing of statistical significance, samples were compared to CTRL. **Statistics:** Data represent mean \pm SD. ns (not significant), * $P < 0.05$, $P > 0.05$, ** $P < 0.01$, **** $P < 0.0001$, one-way Anova with Dunnet's multiple comparisons test (all samples versus CTRL). **Scale bars:** If not annotated in the picture, the image size refers to the scale bar displayed in the picture at the right bottom corner in the same figure part. **Abbreviations:** DE: definitive endoderm; PGT: posterior gut tube, PF: posterior foregut, PP: pancreatic progenitor, HECs: hormone-expressing cells.

pancreatic progenitor markers *PDX1* (CTRL: 120-fold \pm 27) and *NKX6.1* (CTRL: $1.8 \times 10^3 \pm 0.2 \times 10^3$), whereas expression of the β -cell maturation marker *MAFA* (CTRL: 4 ± 2) was only slightly enhanced compared to hiPSCs (Fig. 21c). In correlation with the upregulation of genes orchestrating an endocrine cell fate, transcript levels of the α -cell hormone *GCG* (CTRL: $8.5 \times 10^6 \pm 6.5 \times 10^6$), the β -cell hormone *INS* (CTRL: $1.5 \times 10^6 \pm 0.8 \times 10^6$) and the δ -cell hormone *SST* (CTRL: $1.4 \times 10^4 \pm 0.5 \times 10^4$) were largely enhanced. However, supplementation of the PanMa showed no additional effect on the gene expression compared to the control groups.

In order to assess the expression of endocrine markers on protein level, immunofluorescent analyses were conducted (Fig. 22). For the detection of insulin⁺ cells, S5 cells were stained for C-Peptide (CPEP), which is localized within insulin-containing granules as a part of the insulin-precursor protein and, thus can be used for the detection of β -cells equivalently to insulin. Most

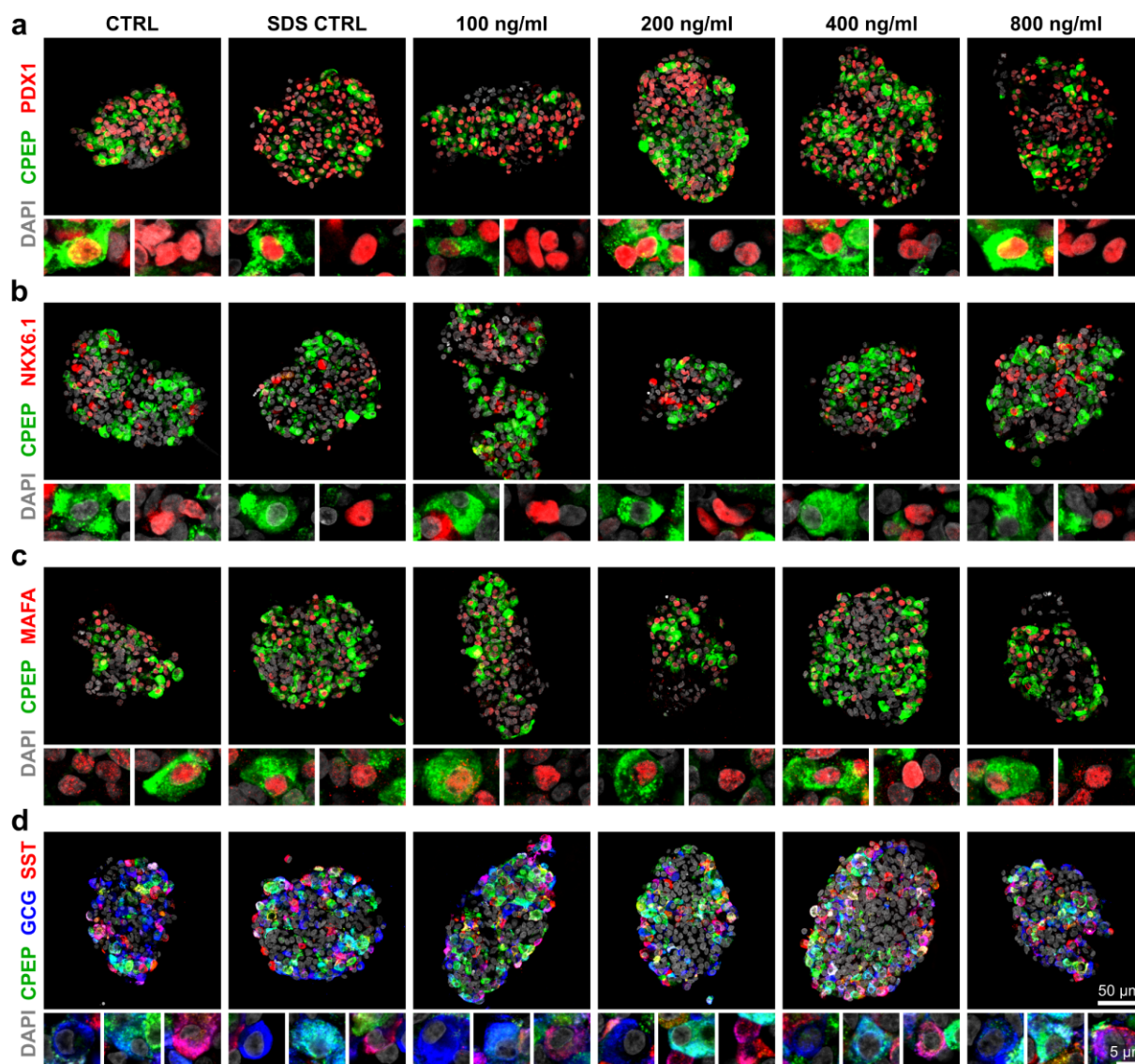


Figure 22 Supplementation of liquid PanMa during pancreatic differentiation has no influence on the phenotype of hiPSC derived HECs. **a – d** Representative images of sections of the differently treated HECs stained for the transcription factors (red) PDX1 (a), NKX6.1 (b) or MAFA (c), the β -cell marker C-PEP (green, a – d), the α -cell marker GCG (blue, d) and the δ -cell marker SST (red, d). Sections were counterstained with DAPI (grey). Higher magnification images highlight frequently observed phenotypes, according to a qualitative assessment ($n = 3$). **Scale bars:** If not annotated in the picture, the image size refers to the scale bar displayed in the picture at the right bottom corner in the same figure part.

of the differentiated S5 cells were PDX1⁺, indicating commitment to the pancreatic lineage (Fig. 22a). Moreover, expression of NKX6.1 (Fig. 22b) and the β -cell maturation marker MAFA (Fig. 22c) was restricted to a smaller cell population. Interestingly, some CPEP⁺ cells co-expressed PDX1 and MAFA, but were almost exclusively negative for NKX6.1. The presence of CPEP⁺/MAFA⁺ cells corroborated the generation of a maturing β -cell population (Fig. 22c). However, lack of NKX6.1 expression in CPEP⁺ cells (Fig. 22b), which is in contrast to the original publication (Rezania et al. 2014), suggested an incomplete β -cell development. In correlation, most S5 cells exhibited a polyhormonal phenotype, which is a further sign for endocrine immaturity (Fig. 22d). Of note, a large number of GCG⁺ cells was observed that exhibited either a monohormonal

phenotype, or showed co-expression of CPEP and/or SST. In contrast, monohormonal CPEP⁺/GCG⁻/SST⁻ cells were rarely detectable. Furthermore, monohormonal S5 cells appeared to be located at the center of the clusters, whereas polyhormonal cells were predominately located at its border. No difference was observed between control S5 cells and S5 cells cultures supplemented with the liquid PanMa.

Taken together, the findings show that the application of the PanMa-specific components at the applied concentrations alone is not sufficient to alter the small molecule-driven differentiation of hiPSC towards pancreatic endocrine cells.

6.4.2 Pancreatic differentiation of hiPSCs on the solid PanMa scaffold results in reduced hormone expression in S5 cells

As the addition of liquid PanMa alone was insufficient to amend pancreatic differentiation, it was next tested whether cellular interactions with the solid scaffold alter the differentiation outcome. Therefore, hiPSCs were seeded on PanMa-TWs and differentiated towards HECs according to the 5-stage protocol from Rezanian et al. (Rezanian et al. 2012; Rezanian et al. 2014) (Fig. 23a). In contrast to the original protocol, S4 cells cultured on the PanMa were not taken into suspension in order to provide a continuous ECM-stimulus during the entire differentiation procedure. hiPSCs were additionally differentiated on the SISser to distinguish between general ECM and PanMa-specific effects.

As shown by MTT assay displayed in figure 23b, S5 cells exhibited metabolic activity on both PanMa and SISser thereby proving cellular viability. While S5 cells on the PanMa were mostly visible as clusters that covered only small parts of the scaffold, S5 cells on the SISser showed an increased spreading and additionally formed thin cell layers that covered large parts of the scaffold. Gene expression analysis indicated a slightly decreased expression of the pancreatic markers *PDX1* and *NKX6.1* as well as the β -cell marker *MAFA* in S5 cells on the PanMa and the SISser to a similar extent (*PDX1*: 0.72-fold, *NKX6.1*: 0.76-fold, *MAFA*: 0.76-fold) compared to S5 control cells, which however was not statistically significant (Fig. 23c). Moreover, S5 cells on PanMa and SISser showed significantly reduced gene expression levels of *INS* (0.4-fold), *GCG* (0.15-fold) and *SST* (0.3-fold) in comparison to the control, proving a reduced endocrine induction. No differences in gene expression were observed between S5 cells generated on the PanMa and SISser.

Immunohistochemical analysis confirmed the formation of cell clusters on the PanMa, while S5 cells on the SISser were evenly distributed across the scaffold (Fig. 24a). Interestingly, CPEP⁺ cells on the PanMa accumulated in clusters whereas regions with thinner cell layers harbored only

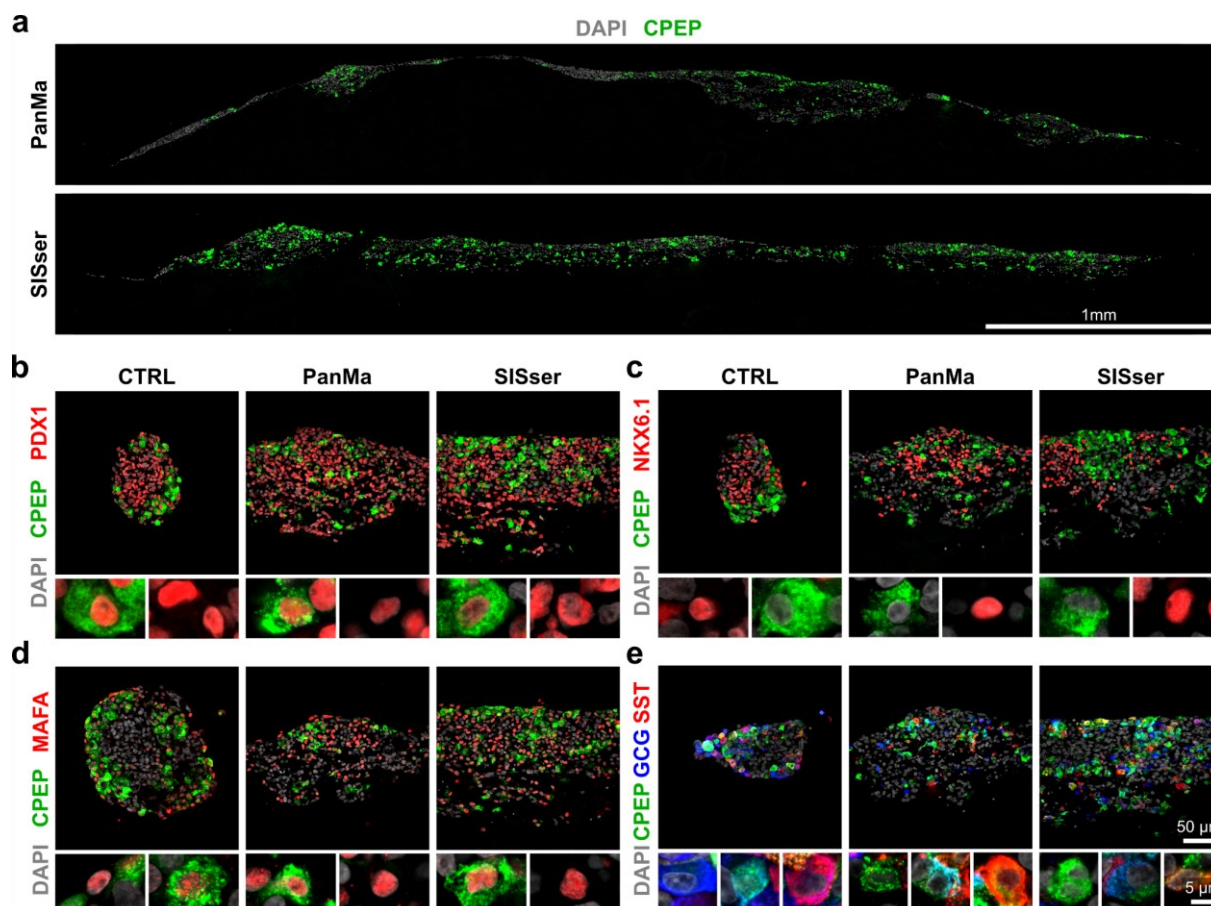


Figure 24 Fig. 19 hiPSC-derived HECs generated on the PanMa display a typical marker expression. **a**. Representative cross-sections of scaffolds showing the cellular distribution on PanMa and SISser at the end of the 5-stage differentiation protocol (day 21). Cells are stained for the β -cell marker CPEP (green) and counterstained with DAPI (grey) ($n = 2$). **b - d** Representative immunofluorescent images of HECs generated according standard 5-stage protocol and on the PanMa or the SISser stained for the transcription factors (red) PDX1 (**b**), NKX6.1 (**c**) and MAFA (**d**) as well as the pancreatic hormones GCG (blue) and SST (red) (**e**). All images are co-immunostained of the β -cell marker CPEP (green) and counterstained with DAPI. Images with higher magnifications show frequently observed cell types according to a qualitative assessment of the biological replicates ($n = 2$). **Scale bars:** If not annotated in the picture, the image size refers to the scale bar displayed in the picture in the right bottom corner in the same figure part.

(Fig. 24d). Co-staining of cells for the pancreatic hormones GCG and SST as well as CPEP as a representative for insulin, revealed a decreased number of hormone-expressing cells on PanMa and SISser compared to control S5 cells (Fig. 24e). Particularly, GCG⁺ and SST⁺ cells were less frequently observed on the PanMa and SISser compared to S5 control cells. Qualitative assessment of the stained sections suggests that S5 cells on the PanMa and SISser contained a reduced number of bihormonal compared to control S5 cells. In line with that, the proportion of hormone-expressing cells showing a monohormonal CPEP⁺ phenotype appeared to be slightly elevated in ECM-cultured S5 cells compared to S5 control cells. However, since the made observations base only on a qualitative evaluation, a higher ratio of monohormonal CPEP⁺ cells can only be assumed.

Taken together, the differentiation of S5 cells on the PanMa and SISser led to a significant decrease of hormone expression on gene and protein level on both ECM scaffolds. However, qualitative

assessment of the immunofluorescent staining suggest that the 5-stage differentiation on the ECM could lead to a shift of hormone expression in favor of Insulin.

6.4.3 Pancreatic differentiation of hiPSCs on the PanMa does not alter glucose stimulated insulin secretion of S5 HECs

A major downside of current *in vitro* β -cell differentiation protocols is the inappropriate insulin secretion of the generated cells in response to glucose stimuli. Considering the changes in the hormone expression ratios of S5 cells generated on the PanMa, it was next investigated whether the ECM-based differentiation affects β -cell function in terms of glucose stimulated insulin secretion. Therefore, the insulin secretion of S5 cells generated on PanMa was measured in response to elevating glucose levels (3 mM to 15 mM) and compared to control S5 cells as well as S5 cells differentiated on the SISser (Fig. 25).

As reported in the original publication (Rezania et al. 2012; Rezania et al. 2014), S5 control cells showed a slightly higher insulin secretion at 3 mM glucose than at 15 mM glucose (Fig. 25a), proving that S5 cells were unable to adapt insulin secretion to extracellular glucose levels. Similarly, differentiation of HECs on the PanMa and SISser did not remedy the impaired insulin

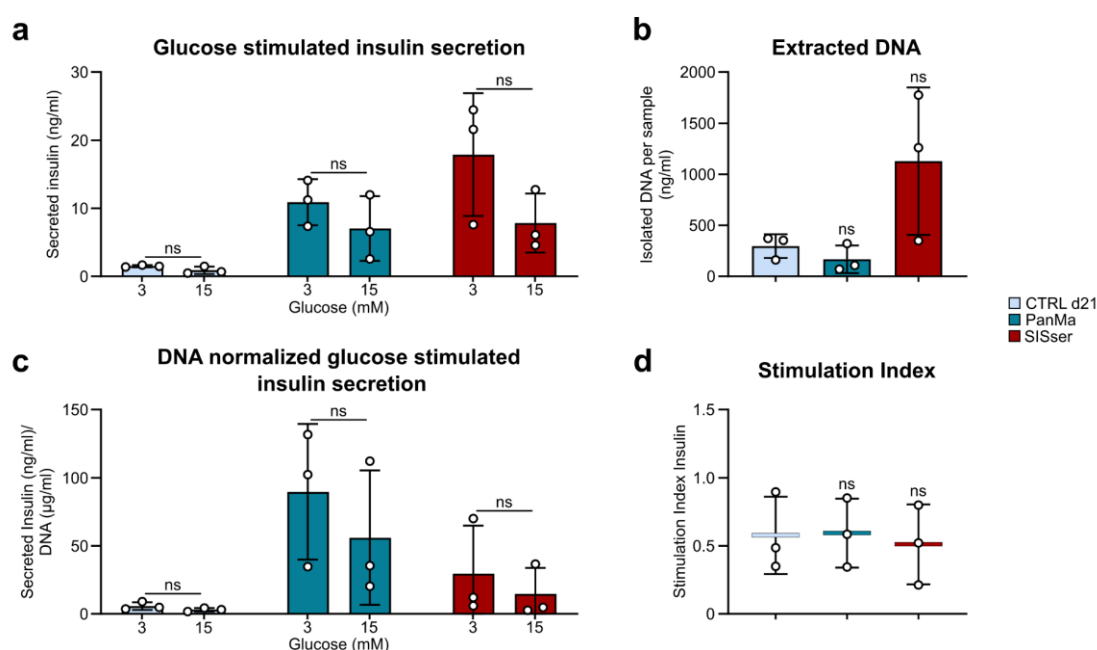


Figure 25 Analysis of the glucose stimulated insulin secretion of HECs on the PanMa and SISser delivers false measurement results. **a** Amount of recovered DNA per sample after DNA extraction from standard HECs (CTRL) as well as HECs generated on the PanMa or SISser (n = 3). **b** Secreted insulin of standard HECs (CTRL) and HECs generated on the PanMa or SISser in response to 3 mM and 15 mM glucose (n = 3). **c** Insulin secretion of standard HECs (CTRL) and HECs generated on the PanMa or SISser normalized to the DNA content (n = 3). **d** Stimulation index (insulin secretion at 15 mM glucose/ insulin secretion at 3 mM glucose), of standard HECs and HECs generated on the PanMa or SISser (n = 3). **Statistics:** Data represent mean \pm SD. ns (not significant) P > 0.05, one-way Anova with Dunnet's multiple comparisons test (a, d; all samples vs. PET) or two-way Anova with Sidak's multiple comparisons test (b, c; 3mM vs. 15mM).

secretion. However, amounts of secreted insulin at 3 and 15 mM were higher on SISser samples (18 ± 7 and 8 ± 4 ng/ml) compared to PanMa (11 ± 3 and 7 ± 4 ng/ml) and control S5 cells (1.5 ± 0.1 and 0.9 ± 0.4 ng/ml), which was probably due to a larger number of stimulated cells on the ECM scaffolds. In order to normalize the amount of secreted insulin to the number of stimulated cells, samples were analyzed for DNA content. Surprisingly little amounts of DNA were extracted from S5 cells cultured on the PanMa (167 ± 111 ng/ml) in comparison to SISser samples (1129 ± 590 ng/ml) and S5 control cells (296 ± 95 ng/ml) (Fig. 25b). In accordance with that, DNA-normalized insulin secretion at 3 mM and 15 mM for S7 cells on the PanMa (90 ± 41 and 56 ± 40 ng/ml insulin/ μ g/ml DNA) was increased 3-fold compared to SISser (29 ± 29 and 14 ± 15 ng/ml insulin/ μ g/ml DNA) and 16-fold compared to S5 control cells (6 ± 2 and 3 ± 1 ng/ml insulin/ μ g/ml DNA) (Fig. 25c). Importantly, the extent of elevated insulin secretion on the PanMa cannot be explained by a physiological effect but merely represents an artefact of the ECM, which is discussed in detail in section 7.10. In order to eliminate putative variables distorting the results for absolute insulin secretion, the stimulation index, giving the fold change of insulin secretion at high glucose levels (15 mM) compared to basal glucose levels (3 mM), was determined (Fig. 25d). S5 cells generated on the PanMa exhibited a similar stimulation index (0.59 ± 0.2) compared to S5 cells on the SISser (0.51 ± 0.23) and S5 control cells (0.58 ± 0.23), demonstrating that S5 cells harbor an equal insulin secretion mechanism independently of the differentiation condition.

Taken together, these findings demonstrated that differentiation of S5 HECs on the PanMa does not alter β -cell function in terms of glucose stimulated insulin secretion.

6.4.4 *hiPSC-derived S7 cells generated on the PanMa exhibit a reduced GCG and SST expression*

Using the 5-stage protocol for the differentiation of HECs on the PanMa revealed a minor ECM effect on the hormone expression of the generated cells. To confirm this observation as well as to test the influence of the PanMa on advanced stages of β -cell development, hiPSC differentiation on the PanMa was performed using a sophisticated 7-stage differentiation protocol for the generation of maturing β -cells. In contrast to the 5-stage protocol, cells of the 7-stage protocol are detached at S4 (PE, day 10) and cultured as clusters until S7 at an air liquid interface (Fig. 26a). For the differentiation on the PanMa, hiPSCs were seeded as single cells on the PanMa mounted in cell crowns and differentiated in static adherent culture for the entire differentiation experiment without detachment at S4. Similar to the control cells, the PanMa-TWs were transferred to an air liquid culture at S4. Differentiation was similarly performed on SISser scaffolds to discriminate potential ECM-specific effects, as well as on Matrigel[®]-coated PET membranes to assess the impact of the omitted detachment and cluster formation at S4.

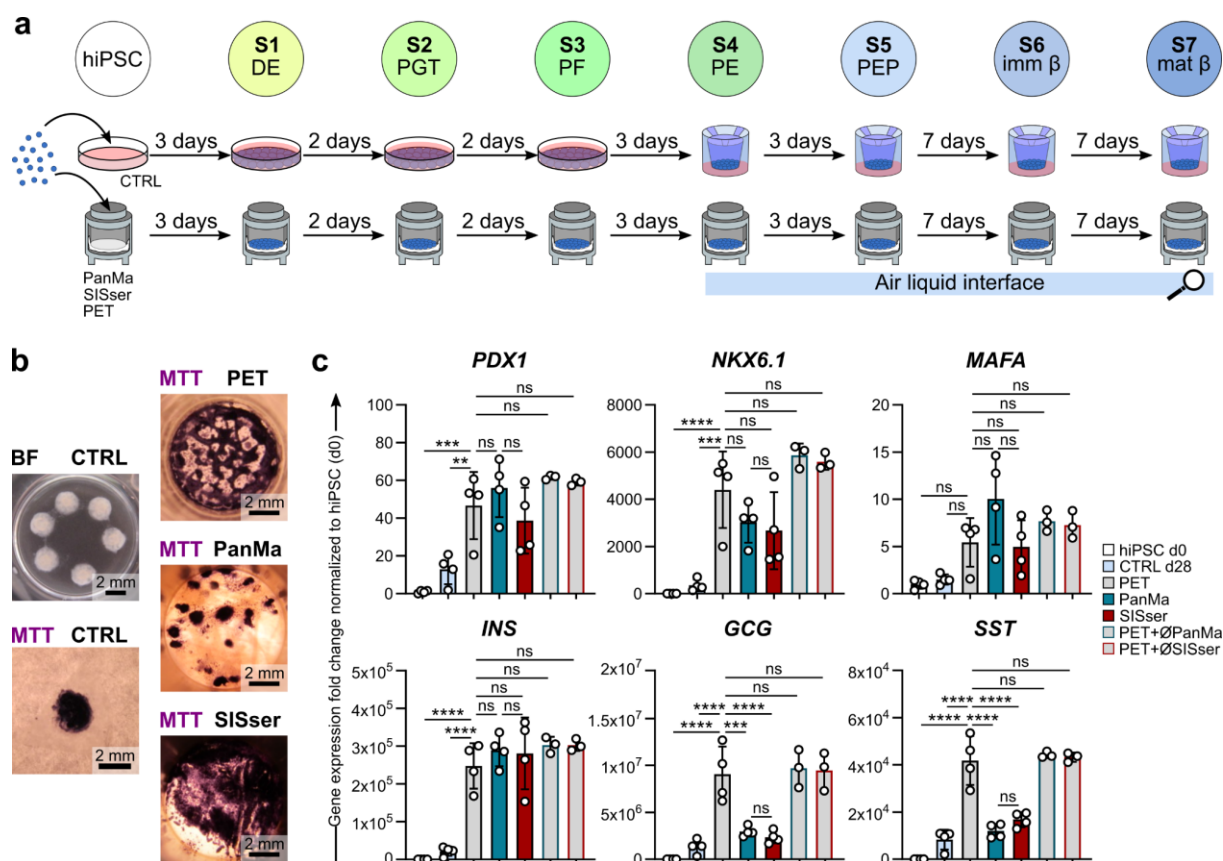
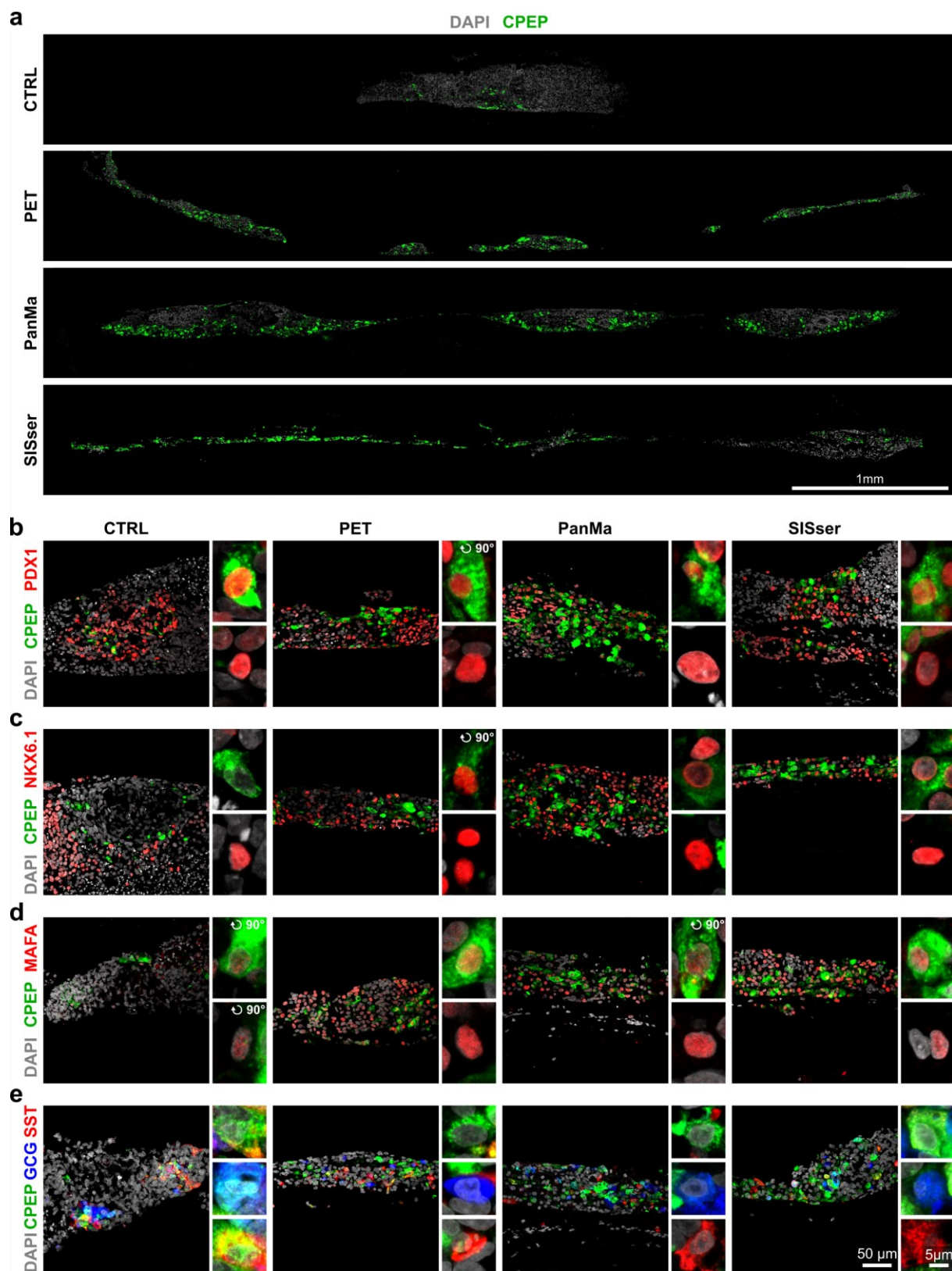


Figure 26 Differentiation of hiPSCs towards β -like cells on the PanMa reduces the expression of glucagon and somatostatin. **a** Schematic illustration of the 7-stage differentiation protocol for the generation of hiPSC-derived β -like cells (Rezania et al. 2014). hiPSCs were seeded as single cells on either Matrigel[®]-coated plates (CTRL), PET-Transwells[®] (PET) or PanMa or SISser scaffolds mounted in cell crowns. At S4 (PE, day 10) cells from Matrigel[®]-coated plates were detached and transferred to filter-inserts and cells on all scaffolds exposed to an air-liquid interface (day 10 – day 28). **b** Images of MTT assays of S7 cells generated on filter-inserts (CTRL), PET-Transwells[®] (PET), PanMa or SISser. Purple staining marks metabolic active cells ($n = 2$). **c** Gene expression analysis of S7 cells generated on filter-inserts (CTRL), PET-Transwells[®] (PET), PanMa or SISser. Expression of genes encoding for *PDX1*, *NKX6.1*, *MAFA* and the pancreatic hormones *INS*, *GCG* and *SST* is shown as the fold change of hiPSC expression. Grey bars with colored frames show the expression of S7 cells on PET with supplemented cDNA from negative controls of the empty PanMa (blue frame) and SISser (red frame) ($n = 4$, except hiPSC $n = 3$ and PET + empty scaffold $n = 3$). **Statistics:** Data represent mean \pm SD. ns (not significant) $P > 0.05$, *** $P < 0.001$, **** $P < 0.0001$, one-way Anova with Sidak's multiple comparisons test (all samples vs. PET and PanMa vs. SISser). **Abbreviations:** DE: definitive endoderm; PGT: posterior gut tube, PF: posterior foregut, PE: pancreatic endoderm, PEP: pancreatic endocrine precursors, imm β : immature β -cells, mat β : maturing β -cells.

MTT assays confirmed the viability of the generated S7 cells and further demonstrated a diverse cell spreading on the different scaffolds, as shown in figure 26b. Control cells, which were seeded as clusters at S4, remained in shape at S7, while S7 cells generated on PET membranes and the SISser formed elongated cell layers that covered large parts of the scaffolds. In contrast, S7 cells differentiated on the PanMa formed clusters that were distributed over the scaffold, as well as very thin cell layers connecting the single cell clusters. Analysis of pancreatic marker gene expression profiles revealed a significant elevation of *PDX1*, *NKX6.1*, *INS*, *GCG* and *SST* expression as well as an increased expression of *MAFA* (not statistically significant) in S7 cells generated on the PET membrane, the PanMa and the SISser compared to hiPSCs, proving a successful induction

of pancreatic and endocrine phenotypes (Fig. 26c). Surprisingly, all genes were significantly lower expressed (except for *MAFA* showing an insignificant reduction) in S7 control cells compared to S7 cells generated on the scaffolds, indicating an insufficient differentiation of hiPSCs cultivated according to the standard protocol. Interestingly, S7 cells cultured on the PanMa exhibited a slightly elevated *PDX1* (1.2 – 1.4-fold) and *MAFA* (1.8 – 2.0-fold) expression compared to S7 cells generated on PET membranes and SISser, which however was not statistically significant. In contrast, to the elevated *PDX1* transcript levels, *NKX6.1* expression appeared slightly but not significantly reduced in S7 cells differentiated on the PanMa (0.7-fold) and SISser (0.6-fold) compared to S7 cells on the PET membrane. Analysis of hormone gene expression revealed a similar *INS* expression in S7 cells on all scaffolds. Remarkably, expression of *GCG* and *SST* was significantly downregulated in S7 cells on the PanMa (both 0.3-fold) and on the SISser (0.3-fold and 0.4-fold) compared to S7 cells generated on the PET membranes suggesting a shift of hormone gene expression in favor of *INS* in ECM-based S7 cell populations. To ensure that the observed changes in gene expression do not originate from possible nucleic acid remnants of the decellularized tissues, cDNA from empty ECMs were added to cDNA samples from S7 PET cells and gene expression was analyzed. Samples spiked with the cDNA of the empty control showed no difference in gene expression of *INS*, *GCG* and *SST* compared to the PET S7 sample, verifying that the shift in hormone gene expression was due to transcriptional changes.

The marker expression of S7 cells was further investigated on protein level by immunohistochemical analyses (Fig. 27). Stainings of whole scaffold crosssections revealed a small amount of CPEP⁺ in S7 control clusters, which was in accordance to the diminished expression levels of the pancreatic and endocrine differentiation markers (Fig. 27a). In contrast, a larger number of CPEP⁺ cells was found on the PET membrane, the PanMa and the SISser. Interestingly, CPEP⁺ cells on the PanMa were predominately located in cell clusters in close proximity to the ECM border. Conversely, S7 cells on the PET membrane and the SISser exhibited a homogenous distribution without an apparent CPEP⁺ clustering. On all scaffolds, the majority of S7 cells expressing CPEP were also PDX1⁺ (Fig. 27b). Notably, the 7-stage differentiation protocol did not result in a ubiquitous expression of PDX1, as this was seen at the 5-stage protocol. Instead, larger accumulations of PDX1⁻ cells were observed on all scaffolds, suggesting an increased proportion of non-pancreatic cells in the 7-stage protocol compared to the 5-stage protocol. Large amounts of NKX6.1⁺ cells were observed in S7 cells on the PanMa, the PET membrane and the SISser and to a fewer extent in S7 control cells (Fig. 27c). Notably, co-expression of NKX6.1⁺ and CPEP⁺ cells was observed on all scaffolds, indicating an enlarged number of S7 cells with a more mature phenotype. Besides this, CPEP⁺ cells on the PanMa as well as on the PET membrane and SISser were mostly MAFA⁺, which collectively provides evidence for the generation of maturing β -cells regardless of the used scaffolds (Fig. 27d). In contrast, less MAFA⁺ cells were observed in



the S7 control. Staining for the pancreatic hormones GCG and SST together with CPEP revealed a predominant monohormonal phenotype among the endocrine cells on the PET membrane, the PanMa and the SISser (Fig. 27e). On all scaffolds, the proportion of CPEP⁺ cells appeared to be slightly higher compared to GCG⁺ cells, while SST⁺ cells were detected only to a small extent. According to the qualitative assessment of the stained sections, no difference in the frequency of CPEP⁺, GCG⁺ and SST⁺ cells was apparent between S7 cells generated on the PanMa, the PET membrane or the SISser. In contrast, S7 control cells harbored a smaller amount of hormone⁺ cells compared to S7 cells, which additionally showed a polyhormonal phenotype.

Taken together, these data demonstrate that β -cell differentiation of hiPSCs according to the 7-stage protocol on the PanMa and SISser resulted in a shift of hormone gene expression in favor of *INS*. Thereby, no difference between PanMa and SISser was observed. However, this finding could not be confirmed by immunohistochemical analyses.

6.4.5 Pancreatic differentiation on the PanMa does not affect GSIS of the generated S7 cells

In order to test, whether the changes in hormone gene expression observed in S7 cells differentiated on the PanMa and SISser result in an altered β -cell function, insulin secretion of the generated cells was measured at 3 and 15 mM glucose (Fig. 28). S7 cells of all conditions lacked an adapted insulin secretion in response to rising glucose levels (Fig. 28a). The total amount of secreted insulin at 3 and 15 mM glucose was comparable between S7 cells on the PET membrane (15 ± 3 and 14 ± 2 ng/ml) and SISser (14 ± 8 and 12 ± 6 ng/ml) and appeared reduced for S7 cells on the PanMa (10 ± 2 and 7 ± 1 ng/ml) and S7 control cells (1.2 ± 0.9 and 1.3 ± 1.1 ng/ml). This increased secretion was probably due to a different cell number per stimulation experiment. In order to align the amount of secreted insulin to the cell number, results were normalized to DNA content of the respective samples. The amount of extracted DNA from PanMa (1104 ± 973 ng/ml) samples was lower compared to the PET membrane (5108 ± 434 ng/ml), SISser (6526 ± 3732 ng/ml) and control samples (1810 ± 837 ng/ml), although not statistically significant (Fig. 28b). Consequently, normalization of insulin secretion to the amount of isolated

Figure 27 Stage 7 cells generated on the PanMa show a β -like phenotype. **a** Representative crosssections of S7 cells generated according the standard 7-stage differentiation protocol (CTRL), as well as S7 cells differentiated on PET membranes, the PanMa or SISser. Cells are stained for the β -cell marker CPEP (green) and nuclei are counterstained with DAPI (grey) (n = 2). **b – e** Representative immunofluorescent stainings of standard S7 cells (CTRL) as well as S7 cells differentiated on the different scaffolds (PET, PanMa, SISser) for the transcription factors (red) PDX1 (b), NKX6.1 (c), MAFA (d) as well as the pancreatic hormones CPEP (green, b – e), GCG (blue, e) and SST (red, e). Cell nuclei are labelled with DAPI (grey, b – e). Higher magnification images show frequently observed cell types according to the qualitative evaluation of the biological replicates (n = 3). Enlarged image sections that are rotated by 90 ° compared to the overview image are annotated accordingly. **Scale bars:** If not annotated in the picture, the image size refers to the scale bar displayed in the picture in the right bottom corner in the same figure part.

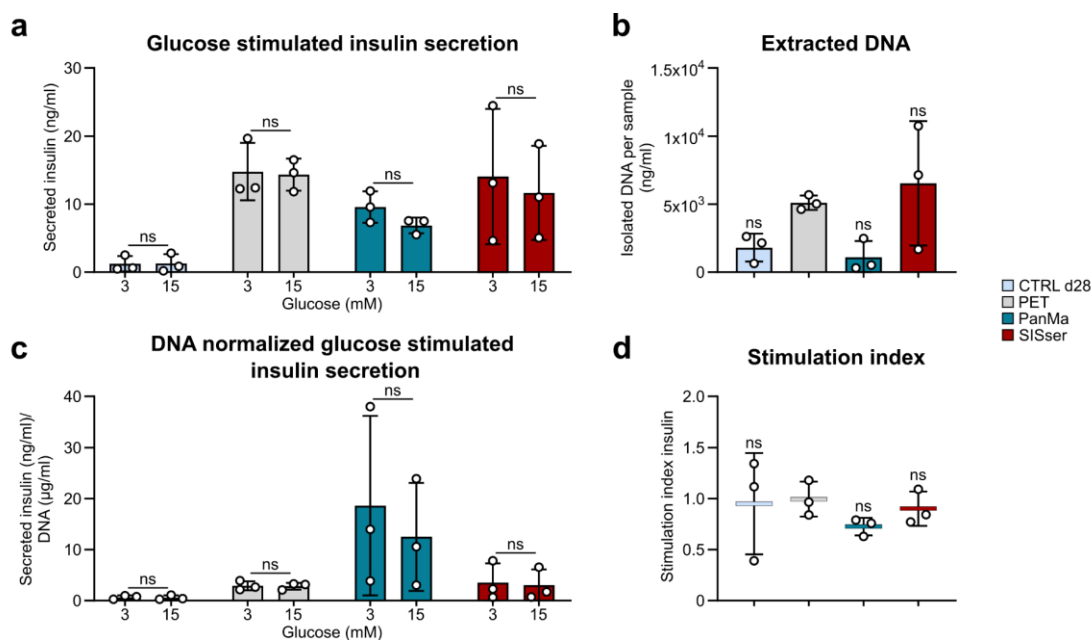


Figure 28 Measurement of glucose stimulated insulin secretion of S7 cells on the PanMa and SISser leads to false measurements. **a** Amount of recovered DNA per sample after DNA extraction from S7 cells differentiated according to the standard differentiation protocol (CTRL) or differentiated on PET, PanMa or SISser ($n = 3$). **b** Insulin secretion from S7 differentiated on the different scaffolds in response to 3 mM and 15 mM glucose ($n = 3$). **c** Insulin secretion in response to 3 mM and 15 mM glucose normalized to the DNA content ($n = 3$). **d** Stimulation index (insulin secretion at 15 mM glucose/ insulin secretion at 3 mM glucose, of S7 cells under the respective differentiation conditions ($n = 3$)). **Statistics:** Data represent mean \pm SD. ns (not significant) $P > 0.05$, one-way Anova with Dunnet's multiple comparisons test (a, d; all samples vs. PET) or two-way Anova with Sidak's multiple comparisons test (b, c; 3 mM vs. 15 mM).

DNA resulted in higher insulin secretions levels at 3 and 15 mM for S7 cells on the PanMa (19 ± 14 and 13 ± 9 ng/ml insulin/ μ g/ml DNA) than for S7 cells on PET membranes (2.9 ± 0.7 and 2.8 ± 0.5 ng/ml insulin/ μ g/ml DNA), on the SISser (3.6 ± 3.1 and 3 ± 2.6 ng/ml insulin/ μ g/ml DNA) and for S7 control cells (0.7 ± 0.3 and 0.6 ± 0.3 ng/ml insulin/ μ g/ml DNA) (Fig. 28c). This elevated normalized insulin secretion levels detected for cells on the PanMa were probably due to false measurement results caused by the ECM, which is discussed in detail in section 7.10. Calculation of the stimulation index for the S7 cells confirmed a lacking insulin response of cells in all conditions (Fig. 28d). S7 cells generated on the PanMa exhibited an insignificantly lower stimulation index (0.73 ± 0.07) compared to control S7 cells (0.95 ± 0.4), S7 cells on PET membranes (0.99 ± 0.14) and on SISser (0.9 ± 0.14).

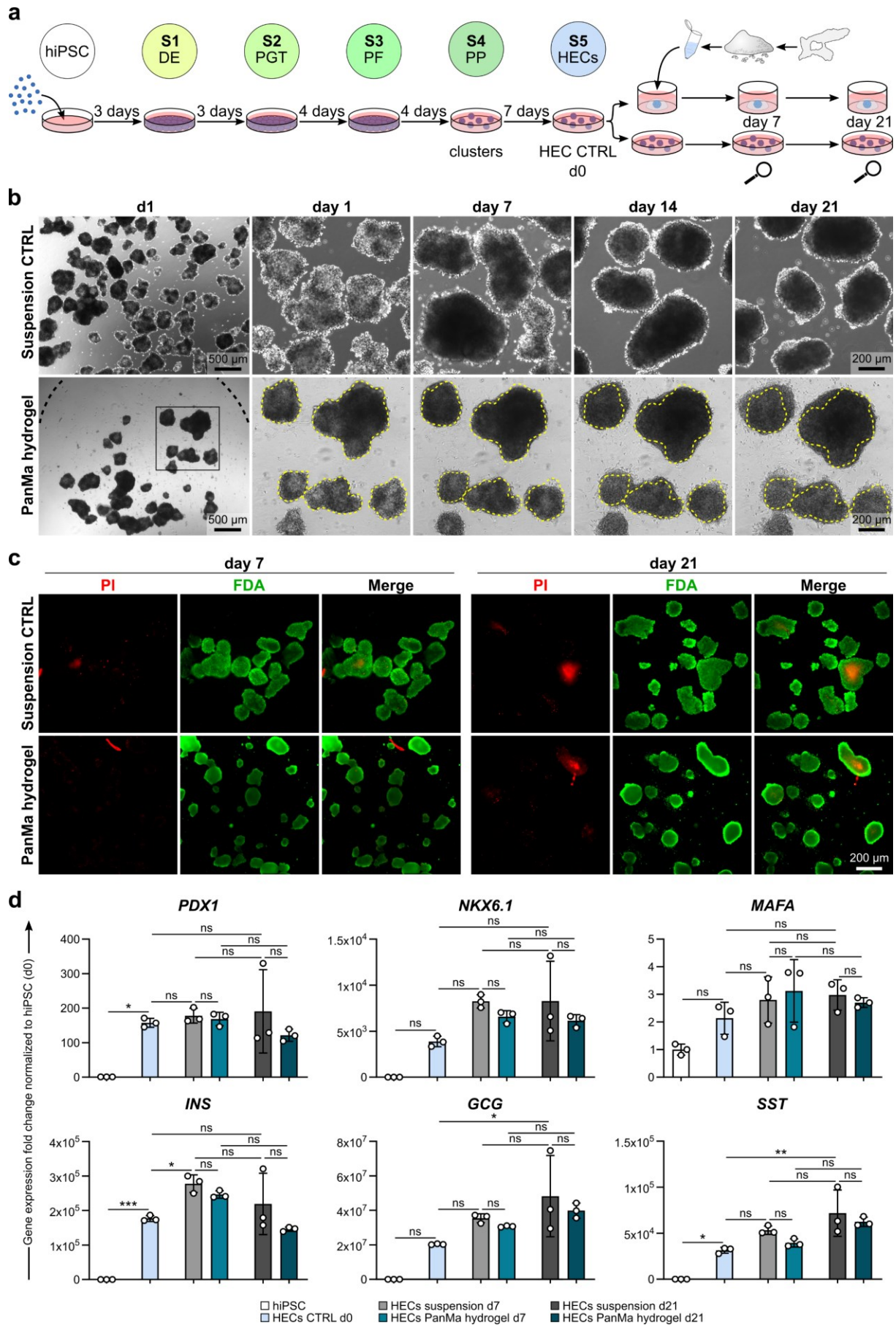
Altogether, these data show that differentiation of hiPSCs towards β -like cells on the PanMa does not alter GSIS of the generated cells and highlight the limitations of the assay when applied to ECM-cultured cells.

6.5 Establishment of a pancreatic organ model

6.5.1 A PanMa-derived hydrogel allows encapsulation and prolonged culture of S5 HECs

Pancreatic *in vitro* organ models resembling endocrine function are of high interest for the development of new therapeutic drugs as well as for disease modelling. However, in order to obtain a realistic cell model, the recreation of the sophisticated *in vivo* environment is an important prerequisite. In this part of the thesis, the suitability of the PanMa ECM as a tissue surrogate for the long-term *in vitro* culture of hiPSC derived HECs was tested. To this purpose, a PanMa derived hydrogel was established with the aim to combine the advantages of a hydrogel (3D culture, hydrophilic, modifiable, improved standardization) with the benefits of a tissue-specific ECM (natural, specific ECM composition). The generated PanMa hydrogel was subsequently used for the encapsulation of hiPSC derived S5 HECs.

The obtained HEC-laden PanMa hydrogels models were cultivated statically in S5 medium for 21 days. Differentiated S5 HECs cultured in suspension served as a control (Fig. 29a). HEC-laden PanMa hydrogel droplets solidified at 37 °C after approximately 15 min resulting in roundish hydrogel droplets with encapsulated, immobilized HECs (Fig. 29b). Despite the solid nature of the PanMa hydrogel, reshaping of the encapsulated HECs towards circular spheroids with an increased size was observed with progressing culture, highlighting the generated hydrogel as a stable, but flexible scaffold. The restructuring of HEC clusters was similarly observed in control cells cultured in suspension. At day 14, increased outgrowth of encapsulated S5 cells at the culture plate bottom was detected, demonstrating that some HECs settled at the bottom either during seeding or with ongoing culture. In contrast to control S5 cells, from day 14 on borders of especially small-sized HECs were less demarcated and HECs appeared less compact, indicating a loss of cellular cohesion. This was contrary to control cells that maintained clear contours and a consistent density until day 21. To further confirm the cytocompatibility of the PanMa hydrogel, the viability of the encapsulated HECs was examined by fluorescein diacetate (FDA; viable)/propidium iodide (PI, dead) staining (Fig. 29c). The majority of S5 cells of both, suspension and hydrogel culture, were viable and only few dead cells were detectable at day 7 and day 21, proving the cytocompatibility of the PanMa hydrogel. While the FDA signal could be allocated to single cells in the suspension control, S5 cells in the PanMa hydrogel exhibited a blurred signal, which was probably due to an altered light refraction by the hydrogel. In order to assess the impact of the PanMa hydrogel culture on the cell identity of the cultured S5 clusters, expression of the pancreatic genes was analyzed next (Fig. 29d). Suspension cultured S5 cells at day 7 exhibited slightly increased expression levels of *NKX6.1* (2.1-fold), *INS* (1.5-fold), *GCG* (1.7-fold) and *SST* (1.7-fold) compared to S5 cells after differentiation (day 0), indicating a progressing differentiation within the first 7 days of continued culture. However, these data were not



significant. A similar increase was observed in S5 cells cultured in the PanMa hydrogel (*NKX6.1*: 1.7-fold, *INS*: 1.4-fold, *GCG*: 1.5-fold, *SST*: 1.3-fold), but to a slightly lower extent compared to the suspension control. Interestingly, after 21 days, suspension cultured S5 cells showed a slightly reduced *INS* expression (0.8-fold) compared to the suspension cultured S5 cells at day 7 and a continuous increase in transcript levels of *GCG* (1.4-fold) and *SST* (1.3-fold), while expression of *PDX1*, *NKX6.1* and *MAFA* remained largely unchanged. Again, these differences were not statistically significant. A similar tendency was observed in S5 cells cultured for 21 days in the PanMa hydrogel (*INS*: 0.5-fold, *GCG*: 1.1-fold, *SST*: 1.2-fold), whereas expression levels were slightly lower compared to suspension cultured cells at day 21, although not statistically significant. In addition, *PDX1* expression appeared reduced in S5 cells cultured in the hydrogel after d21 compared to all suspension cultured cells at day 21 (0.6-fold).

Taken together, the data prove the cytocompatibility of the PanMa hydrogel. However, prolonged culture of S5 cells seemed to result in an increase of non- β -cell genes, which appeared more pronounced after prolonged culture in the PanMa hydrogel.

6.5.2 Culture in a PanMa-derived hydrogel affects the cytomorphology of HEC clusters

In order to assess the impact of the PanMa hydrogel on the occurrence of pancreatic markers, immunofluorescent stainings of the cultured cells were conducted (Fig. 30). *PDX1* was detected in most of the S5 cells after differentiation (day 0) and was co-expressed in the majority of CPEP⁺ cells (Fig. 30a). Interestingly, the generated HEC clusters revealed a high number of HEC clusters with CPEP⁺ cells located at the spheroid border after differentiation (day 0). *NKX6.1*⁺ S5 cells at day 0 clustered in the centre of the HEC clusters and showed no co-expression of CPEP (Fig. 30b), other than *MAFA*, which was frequently found in cells at the spheroid border together with CPEP (Fig. 30c). With continued suspension culture, a cytomorphological change occurred. At day 7, the

Figure 29 A PanMa-derived hydrogel is suitable for encapsulation and culture of S5 HECs **a.** Graphic representation of the experimental procedure. HECs were generated according to the 5-stage differentiation protocol (CTRL d0) and encapsulated in a PanMa derived Hydrogel. Encapsulated HECs were 21 days in compared to HECs cultivated in suspension at day 7 and day 21 of culture. **b** Brightfield images of HECs at day 1, 7, 14 and 21 after PanMa hydrogel encapsulation (lower panel) compared to HECs in suspension culture (upper panel). Images of the hydrogel culture show the same cells at different time points. Dashed yellow lines in each picture show the contours of the clusters at day 1 (n = 4). **c** Live (FDA, green)/dead (PI, red) staining of HECs at day 7 and 21 after hydrogel encapsulation (lower panel) in comparison to suspension cultured HECs (upper panel) (n = 3). **d** Gene expression profiles of HECs cultured in the PanMa hydrogel at day 7 and 21 in comparison to HECs cultured in suspension and HECs at d0 (HECs CTRL d0). Expression of *PDX1*, *NKX6.1*, *MAFA*, *INS*, *GCG* and *SST* is shown as the fold change of hiPSC expression (n = 3). **Statistics:** Data represent mean \pm SD. ns (not significant) $P > 0.05$, * $P < 0.05$, ** $P < 0.01$, *** $P < 0.001$, one-way Anova with Sidak's multiple comparisons test (hiPSC vs. CTRL d0, CTRL d0 vs. HECs suspension d7 and d21, HECs suspension d7 vs HECs suspension d21, HECs suspension d7 vs HECs PanMa hydrogel d7, HECs suspension d21 vs. HECs PanMa hydrogel d21, HECs PanMa hydrogel d7 vs. HECs PanMa hydrogel d21). **Scale bars:** If not annotated in the picture, the image size refers to the scale bar displayed in the same figure part. **Abbreviations:** DE: definitive endoderm; PGT: posterior gut tube, PF: posterior foregut, PP: pancreatic progenitor, HECs: hormone-expressing cells.

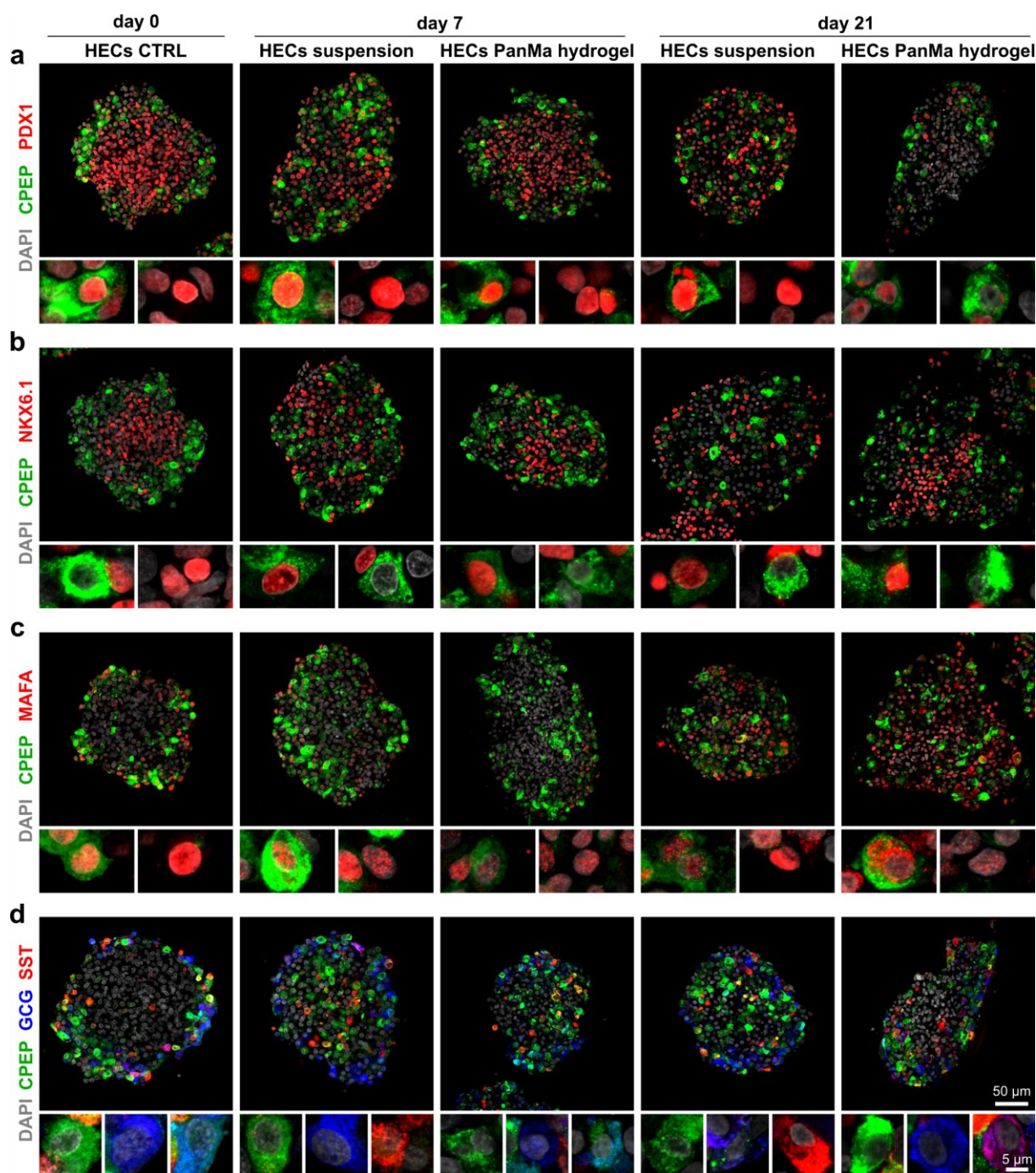


Figure 30 HECs cultured in a PanMa-derived hydrogel exhibit a different distribution of NKX6.1⁺ cells. a – d Representative immunofluorescent images of Stage 5 HECs (day 0) as well as of HECs after 7 and 21 days culture in the PanMa hydrogel or in suspension. HECs are stained for the transcription factors (red) PDX1 (a), NKX6.1 (b), MAFA (c), as well as for the pancreatic hormones GCG (blue) and SST (red) (d). Cells in all images (a – d) are co-stained with the β -cell marker CPEP (green) and counterstained with DAPI (grey). Images with higher magnifications show frequently appearing cell types according to a qualitative assessment of biological replicates (n = 3). **Scale bars:** If not annotated in the picture, the image size refers to the scale bar displayed in the picture in the right bottom corner in the same figure part.

clusters seemed to contain a higher number of CPEP⁺ cells, which were no longer restricted to the spheroid border, but were also found in the centre of day 7 suspension cultured HEC clusters. Similarly, PDX1⁺ (Fig. 30a) and NKX6.1⁺ cells (Fig. 30b) were scattered throughout the organoid. Interestingly, at day 7 NKX6.1⁺/CPEP⁺ cells were detected for the first time, demonstrating the

occurrence of cells with an advanced β -cell phenotype. In hydrogel-cultured HECs, NKX6.1⁺/CPEP⁺ cells were likewise detected at day 7 as well as an increase in CPEP⁺ cells, which were found throughout the entire spheroid, similar to the suspension control. However, in contrast to the suspension control, NKX6.1⁺ (Fig. 30b) and PDX1⁺ (Fig. 30a) cells remained clustered in the spheroid centre at day 7 of hydrogel cultured HECs. Thus, the hydrogel-S5 cells in the spheroids did not undergo a similar cytomorphological reorganization as this was seen in the suspension control. At day 21, suspension cultured HECs seemed to contain a reduced number of CPEP⁺, PDX1⁺ and NKX6.1⁺ cells in comparison to day 7 (Fig. 30a, b), while MAFA⁺ cells were more frequently abundant (Fig. 30c). The same change was observed in hydrogel-cultured HECs at day 21. However, in contrast to the day 21 suspension control, PDX1⁺ and NKX6.1⁺ cells in the hydrogel were still restricted to the centre of the HEC clusters (Fig. 30a, b). Furthermore, staining of the pancreatic hormones GCG and SST in combination with CPEP was conducted (Fig. 30d). After differentiation (day 0), the generated spheroids contained monohormonal CPEP⁺ and GCG⁺ cells, as well as a smaller proportion of bihormonal CPEP⁺/GCG⁺ and CPEP⁺/SST⁺ cells. Interestingly, all kinds of HECs were mostly located in distal spheroid regions. Continued suspension culture resulted in a decreased frequency of bihormonal cells. At day 7, suspension cultured cells harboured an increased number of monohormonal CPEP⁺, GCG⁺ and SST⁺ cells. Interestingly, GCG⁺ cells retained in distal locations of the spheroids, while CPEP⁺ and SST⁺ cells were found throughout the entire organoid. S5 cells cultured in the hydrogel showed a similar distribution of HECs at day 7. However, the number of bihormonal CPEP⁺/GCG⁺ and CPEP⁺/SST⁺ cells appeared higher and were more similar to HEC clusters at day 0 than to HECs at day 7. Prolonged suspension culture was accompanied by a slight reduction in HECs, of which the majority was CPEP⁺ or GCG⁺ at day 21. HECs cultured in the PanMa hydrogel for 21 days showed a higher loss of HECs compared to the suspension control. Moreover, an increased number of bihormonal GCG⁺/SST⁺ cells was observed in the PanMa hydrogel culture at day 21.

Taken together, these data indicate that prolonged culture in the PanMa hydrogel affects the cytomorphological changes of HECs during continued culture and impairs the efficient generation of monohormonal cell types. To allow a definitive statement, quantitative analyses are required.

6.5.3 *Prolonged culture in the PanMa hydrogel marginally impairs the functional maturation of S5 HECs*

In order to test whether the reduced number of HECs observed in S5 cells after 21 days culture in the PanMa hydrogel manifest in an altered β -cell function, the glucose stimulated insulin secretion of the cultured cells was examined (Fig. 31). Similar to the previous experiments, insulin secretion at 3 mM glucose concentrations were higher compared to 15 mM glucose in S5 cells of all

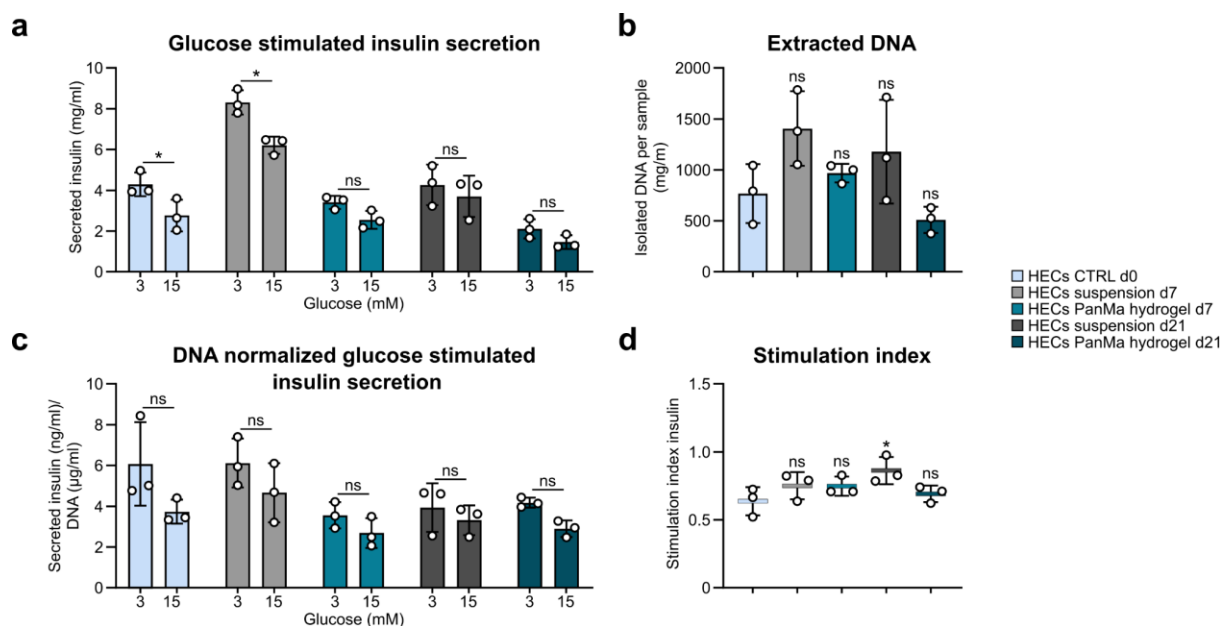


Figure 31 HECs reveal a reduced glucose stimulated insulin secretion after culture in the PanMa-derived hydrogel. **a** Amount of extracted DNA per sample after DNA isolation from HECs at d0 and from HECs after 7 or 21 days culture in the PanMa hydrogel or suspension ($n = 3$). **b** Insulin secretion of the cultured cells in response to 3 mM and 15 mM glucose at day 0, 7 or 21 in the respective culture conditions ($n = 3$). **c** Insulin secretion of the cultured HECs normalized to the amount of extracted DNA ($n = 3$). **d** Stimulation index for insulin (insulin secretion at 15 mM/insulin secretion at 3 mM) of HECs at the different experimental conditions. **Statistics:** Data represent mean \pm SD. ns (not significant) $P > 0.05$, * $P < 0.05$, one-way Anova with Dunnett's multiple comparisons test (a, d; all samples vs. PET) or two-way Anova with Sidak's multiple comparisons test (b, c; 3mM vs. 15mM).

conditions, demonstrating an immature β -cell phenotype of the generated cells (Fig. 31a). For normalization of the insulin secretion to the number of stimulated cells, DNA was extracted from each sample. Higher amounts of DNA were extracted from the suspension cultures at day 7 (1406 ± 299 ng/ml) and day 21 (1178 ± 415 ng/ml) compared to the day 0 HECs (767 ± 236 ng/ml), which correlated with the approximated amount of stimulated cells (Fig. 31b). Unlike in the previous stimulation experiments with solid matrices, normalization of insulin secretion to the DNA content resulted in reasonable amounts, indicating that the PanMa hydrogel did not interfere with the stimulation experiments. Interestingly, suspension cultured HECs showed a similar insulin secretion at 3 mM and 15 mM at day 7 (6.1 ± 1 and 4.7 ± 1.2 ng/ml insulin/ μ g/ml DNA) compared to day 0 control HECs (6.1 ± 1.7 and 3.7 ± 0.5 ng/ml insulin/ μ g/ml DNA), whereas prolonged suspension culture led to a drop of released insulin at day 21 (3.9 ± 1 and 3.3 ± 0.6 ng/ml insulin/ μ g/ml DNA) (Fig. 31c). In contrast, insulin secretion from hydrogel cultured cells was already decreased at day 7 (3.6 ± 0.5 and 2.7 ± 0.6 ng/ml insulin/ μ g/ml DNA) and showed no further decrease with prolonged culture at day 21 (4.2 ± 0.2 and 2.9 ± 0.3 ng/ml insulin/ μ g/ml DNA). Determination of the stimulation index revealed a steady increase of the stimulation response with ongoing suspension culture (day 0: 0.64 ± 0.08 , day 7: 0.75 ± 0.08 , day 21: 0.86 ± 0.08) (Fig. 31d). In contrast, hydrogel-

cultured HECs exhibited an increased stimulation index at day 7 (0.75 ± 0.05), whereas prolonged culture reversed the stimulation index to the initial values of day 0 HECs (0.69 ± 0.05).

Taken together, these data show that the PanMa hydrogel has minor negative effects on the β -cell function of cultured S5 HECs in terms of a reduced stimulation index, which suggests a negative impact of the PanMa hydrogel on β -cell maturation.

7 Discussion

7.1 The generated PanMa on the test bench

Tissue engineering-inspired approaches aim to re-build the *in vivo* microenvironment in order to resemble sophisticated cellular functions in a more physiological environment. In this regard, biomimetic ECMs derived by tissue decellularization are of increasing interest for tissue engineering approaches as they allow re-creating a large part of the *in vivo* microniche *in vitro* (Tran et al. 2020). For this purpose, an acellular pancreas scaffold with largely preserved ECM characteristics was generated in this study using whole-organ decellularization. Previous studies have demonstrated the feasibility of this approach using rodent (Carlo 2009; Goh et al. 2013; Napierala et al. 2017), human (Peloso et al. 2016) or porcine pancreata (Mirmalek-Sani et al. 2013; Katsuki et al. 2016; Elebring et al. 2017; Kuna et al. 2018). In these studies, pancreas decellularization was mostly achieved by chemical treatment using Triton X-100, sodium dodecyl sulfate (SDS) or SDC. Triton-X is reported as a mild decellularization agent, which results in efficient cell removal and a good preservation of tissue structures but which largely depends on the properties of the respective tissue, such as size and density (White et al. 2017). In contrast, the use of SDS is generally associated with enhanced damaging of ECM structures and requires thorough washing, as remnants of SDS are highly cell toxic. In the present study, SDC resulted in an efficient cell removal and a good preservation of ECM structures such as collagen I, III and IV. However, the laminin network was largely destroyed in the PanMa scaffold. Interestingly, in the course of a supervised bachelor thesis performed in 2019 at the Chair of Tissue Engineering and Regenerative Medicine (University Hospital Würzburg) Mrs. Anna-Lena Ziegler discovered that the destruction of the laminin network is not an issue of the decellularization agent, but is presumably caused by pancreatic enzymes that are liberated from acinar cells already before decellularization (Ziegler 2019). While laminin was only rarely detectable by immunohistochemical staining, proteome analysis of the PanMa, which were conducted in collaboration with the group of Prof. Helge Ræder from the department of Pediatrics at the Haukeland University Hospital in Bergen, revealed that laminin was enriched in comparison to the native pancreas (Berger et al. 2020). Collectively, these findings suggest rather a destruction of the laminin network, but the retention of laminin peptide sequences in the PanMa. Furthermore, this example emphasizes the necessity of multi-scale approaches for the thorough characterization of decellularized organs, as single detection methods may not be capable of providing an entire picture of biological ECM scaffold properties. To prevent the disruption of the laminin network in future studies, the use of proteinase inhibitors should be considered. These should be applied at the first perfusion step to inhibit proteases soon after explantation and thereby to prevent an advanced digestion of the tissue.

Furthermore, this study shows that the PanMa exhibit preserved duct and vessel structures. By the recellularization of the arterial system of the PanMa's splenic lobe the potential use of the PanMa as a revascularized biological ECM scaffold could be demonstrated. ECM scaffolds with a functional vascular system are of particular interest for tissue engineering approaches (Kress et al. 2018) as an intact vascularization facilitates nutrient supply of residing cells and reanastomosis of the scaffold to an existing vasculature or external fluidic systems. Recellularization of vessel structures has been demonstrated earlier for ECM scaffolds derived from rodent pancreata (Goh et al. 2013; Napierala et al. 2017), but not for pancreas scaffolds of larger sizes such as the porcine pancreas. Furthermore, the present study shows that the PanMa vessels provided a supportive environment for ECs as demonstrated by the cell type specific arrangement within the preserved vessel structures and their expression of characteristic EC markers. To verify the integrity of the recellularized PanMa, perfusion tests with FITC Dextran should be carried out in follow up studies.

For a standardized assessment of the generated PanMa, the PancScore was developed during this study, which represents a novelty in the field. Altogether, the application of the PancScore in this study demonstrated a good practicability, which allows an inter-laboratory comparison of generated scaffolds. Further advancement of the PancScore should aim for the inclusion of quantitative measurements evaluating the extent of ECM preservation. In this regard, proteome analysis presents a method of choice. However, more proteome datasets of PanMas generated with different decellularization protocols are required to define measuring frames for a reasonable grading of the ECMs.

Moreover, by using the PancScore for evaluating the here generated PanMas, the residual DNA content was identified as a major weak point of the applied decellularization protocol. By definition, minimal criteria for a suitable acellular scaffold are a DNA fragment length of less than 200 bp, no visible nuclear material in sections stained with DAPI or H&E and a residual DNA content of less than 50 ng/mg ECM dry weight (Crapo et al. 2011). While the PanMa fulfills the first two of the mentioned criteria, it exceeds the threshold for the residual DNA (306 ± 204 ng DNA/mg dry weight). However, these criteria count particularly for scaffolds with an intended use for transplantation. Furthermore, the validity of these criteria is currently highly debated, as scaffolds with residual DNA contents exceeding the threshold still show desired clinical performance (Aamodt and Grainger 2016). As the PanMa is in the first line used for *in vitro* approaches, the high DNA content should not be a major issue. However, if desired, reduction of DNA remnants could be achieved by an adjustment of the DNase concentration and duration of the digest.

7.2 Softer, fiber-based, hygroscopic – uncovering the PanMa's biophysical profile

The ECMs of different native tissues vary in their biochemical composition and in their biophysical and physico-structural properties (Travascio 2016). This study demonstrates that the generated PanMa likewise represents a unique ECM scaffold with specific characteristics. Thorough analysis characterized the PanMa as a soft, fiber-based scaffold that is permeable for low and high weight molecules and binds large amounts of water. Moreover, this study shows that SISser and LungMa likewise exhibit significant differences in water content and rigidity compared to the PanMa emphasizing that the tissue origin is an important determinant for the features of a biological ECM scaffold. From numerous studies, it is known that compositional, biophysical and physico-structural properties of an ECM are decisive factors for the ECM signaling profile and its regulatory function on cellular processes (Wang et al. 2020). Thereby, the ECM can have a direct influence on cells by interacting with cell surface receptors, most importantly integrins, but can also mediate indirect effects via the modulation of other cell-regulating factors, such as the interstitial availability of signaling proteins or the regulation of water content.

One important characteristic of the ECM is its stiffness, which is defined as the capacity of a material to withstand mechanical deformation. Mediated via integrins and the actin cytoskeleton, ECM rigidity regulates cellular functions, such as proliferation (Liu et al. 2018), differentiation (Engler et al. 2006) and migration (Plotnikov et al. 2012). In the present study scaffold stiffness was examined by rheological measurements and classified the PanMa as a very soft scaffold ($G' = < 0.1$ kPa). A direct comparison to the stiffness of native tissues or other biomimetic or bio-inspired scaffolds is limited by the fact that the measured rigidities largely depend on the methodical approach and the used test systems. Nevertheless, it seems that the PanMa in general is more similar to soft tissues, including native brain ($E = 0.1 - 1$ kPa) or fat ($E = 0.02$ kPa) tissue and the mammary gland ($E = 0.2$ kPa) than to native liver ($E = 640$ kPa) or kidney ($E = 2.5$ kPa) tissue (Levental et al. 2007). Studies comparing the viscoelastic properties of the native porcine pancreas to kidney, lung and spleen, report that the native pancreas exhibits the strongest viscous character among the tested abdominal organs, which coincides with the observations made for the PanMa (Nicolle et al. 2013; Wex et al. 2015). This indirectly provides evidence for a preservation of biophysical properties of the PanMa after decellularization compared to the native pancreas. In the present study, a comparison of the rheological properties to other biological ECM to SISser and LungMa showed that the rigidity of the PanMa ($G' = < 0.089$ kPa) was about 12-times lower compared to the SISser ($G' = 1.1$ kPa) and 3-times lower compared to the LungMa ($G' = 0.24$ kPa), which was statistically significant. However, when comparing the obtained values for the material stiffness of the ECMs investigated in this study to the published data for the rigidity of native tissues and other biological scaffolds, it is apparent that PanMa, SISser and LungMa altogether represent soft scaffolds. In light of the huge stiffness differences between organs of the

body, which range from soft tissue (0.1 – 10 kPa) such as brain or liver, intermediate tissue (10 – 20 kPa) such as muscle to hard tissue such as bone (1 – 2 GPa) (Guimarães et al. 2020), the differences between PanMa, SISser and LungMa appear to be only marginally. Against this background, it might be that the relatively low differences in rigidities of the here used scaffolds might not have a relevant biological effect.

Moreover, investigations of the water binding capacity in the present study demonstrated that the generated PanMa exhibits a strong hygroscopic character. The increased water content of the PanMa could be due to an increased amount of GAGs, which bind large amounts of water due their polar structure (Mouw et al. 2014). Quantification of the GAG content was attempted using colorimetric assays. However, measurements could not be realized due to a large amount of insoluble components of the PanMa, leaving the question of an increased GAG amount in the PanMa open. Another possibility that could account for the elevated water binding capacity of the PanMa is the enhanced degradation of collagens. In native tissues, such as cartilage, fibrillar collagen restricts the swelling of the tissue by limiting the diffusion of water (Knauss et al. 1999). The partial fragmentation of the collagen network due to degradation abolishes this function resulting in a less restricted water uptake (Knauss et al. 1999). This theory could apply for the PanMa, since the pancreas is prone to self-digestion due to the liberation of aggressive enzymatic peptides during decellularization, as mentioned before. Although intact networks of collagen I, III and IV were detected in the PanMa, it cannot be excluded that other collagens might be slightly degraded. Hence, it could be that the observed water binding content of the PanMa does not reflect the native state but is induced either by an enrichment of GAGs, by a partially degraded collagen networks or a combinatorial effect of both.

In another part of this study, it was shown that the PanMa is permeable for small and high weight molecules, similar to SISser and LungMa. Marginally slower diffusion through the PanMa at the beginning of the assay in comparison to the SISser further indicate that the PanMa might represent a slightly increased barrier for particle diffusion compared to the SISser. Contrary, at later time points, a slightly larger amount of molecules was detected in the basal compartment. This observation might result from an increased trapping of dissolved molecules in the PanMa. According to this presumption, initial molecular diffusion through the PanMa is decreased as molecules are deposited in the PanMa until the binding sites of the PanMa are saturated. At later time points, the amount of molecules reaching the basal compartment is increased due to an augmented release from the scaffold. A similar observation was made for the LungMa. Following this idea, the PanMa and LungMa could act as a reservoir for water and dissolved molecules, which would be a relevant aspect for cell culture. The capacity of the PanMa/LungMa to bind solubilized proteins could have a decisive impact on the availability of signaling proteins as well as the establishment of protein gradients, which might be a crucial aspect especially in the performed

differentiation experiments using hiPSCs. However, since the obtained data showed only marginal differences between the ECM scaffolds, which were not significant, more tests are required to confirm this presumption. To determine the reservoir function of the PanMa and LungMa, the diffusion test could be repeated with different fluorescent molecules or nanobeads, which can later be quantified by optic measurement. Thereby, the amount of trapped molecules per ECM weight could be determined and should give an indication about the reservoir function of the ECMs.

Another attribute that was found to be different for the PanMa compared to SISser and LungMa was the ECM topography. The surface properties of the ECM can be classified in microscale and nanoscale features. Topographical cues on the microscale comprise for instance the direction of larger collagen bundles and particularly affects the collective cell behaviour and migration (Galli et al. 2020), while nanoscale features rather result from the assembly of single ECM components and regulate single cell processes such as proliferation, differentiation and function (Dalby et al. 2014). The microscale topography of the PanMa is characterized by a fiber-based structure with a poor fiber alignment compared to the SISser. In contrast, the LungMa showed a rough topography without an apparent fiber orientation. From several studies it is known that fiber direction is an important orientation mark for cellular migration (Fraley et al. 2015). In line with that, visualization of the distribution of hiPSCs seeded on the ECM scaffolds by MTT showed that hiPSCs seeded on the PanMa and LungMa appeared to exhibit a slightly reduced spreading in contrast to hiPSCs cultured on the SISser. Instead, culture of cells on the PanMa and LungMa appeared to promote invasion of differentiating cells into the scaffold, as seen during spontaneous differentiation. However, these findings base only on qualitative observations and require quantitative analyses to allow for definitive statements. In order to quantify the migration behavior of cells, cell-tracking experiments on the scaffolds should be carried out.

While on the microscale level, poor fiber-alignment appears to limit cell migration on the PanMa, analyses of the nanoscale topography revealed a specific binding of hiPSC-derived EBs to collagen fibers and bundles of the PanMa. hiPSC-PanMa interactions were limited to few adhesion spots. Attachment of hiPSC to the LungMa was less, while hiPSCs on the SISser exhibited more adhesion spots. This suggests that the ECM proteins provided by the PanMa or LungMa do not match very well to the integrin receptors of the differentiating hiPSCs. Indeed, it has been shown that hiPSCs, similar to hESCs, predominantly express the integrin subunits $\alpha 5$, $\alpha 6$, αv , $\beta 1$, and $\beta 5$, which preferably bind to laminin-511 ($\alpha 6\beta 1$), vitronectin ($\alpha v\beta 5$) and the laminin-rich Matrigel® ($\alpha x\beta 1$) (Rowland et al. 2010; Villa-Diaz et al. 2016). In line with that, the present study shows a strong adhesion of hiPSCs to the basal lamina of the SISser, which largely composes of laminins, indicating that the ECM components of the SISser present a suitable match for the hiPSC-expressed integrins.

Besides the importance of single constituents for surface receptor mediated cell attachment, the ECM composition mainly defines all the properties of an ECM. In collaboration with the group of Prof. Helge Ræder from the department of Pediatrics at the Haukeland University Hospital in Bergen the composition of the PanMa was decoded using proteome analysis (Berger et al. 2020). At this, it could be shown, that the ECM composition of the PanMa is specific compared to SISser and LungMa. In contrast to the presumption that laminin is absent in the PanMa, which was deduced from the missing laminin signal in immunohistochemical and SEM analyses, an enrichment of laminin subunits in the PanMa compared to the native pancreas was observed in the proteome analysis (Berger et al. 2020). This indicates a destruction of the laminin network in the PanMa rather than a complete loss of the protein. Interestingly, Miyazaki et al. showed that short E8 fragments of heterotrimeric laminins (-332, and -511) are sufficient to mediate integrin-dependent adhesion and sustain self-renewal of hPSCs (Miyazaki et al. 2012). Thus, it might be that, despite a loss of laminin-assembled structures, laminins still contribute to the PanMa signaling axis. However, in comparison to the SISser and LungMa, the PanMa revealed a reduced laminin abundance, especially of β 1, β 2 and γ 1 subunits (Berger et al. 2020), which play an important role for interactions with PSCs due to their participation in the formation of laminin-511 and -521 (Miyazaki et al. 2008; Miyazaki et al. 2012). This is in line with the SEM analyses in the present study, showing laminins in form of a basal lamina on the SISser and LungMa, but not on the PanMa.

7.3 *Culture on ECM scaffolds appears to have a minor impact on the hiPSC pluripotency network*

Pluripotent stem cells are defined by the ability to self-renew and give rise to all cells of an organism (Atala et al. 2019). Thereby, the genetic program maintaining stemness is in large part governed by the nuanced interplay of OCT4, SOX2 and NANOG, which govern the downstream expression of stemness-promoting genes while simultaneously suppressing pro-differentiation genes (Pan and Thomson 2007). Changes in the expression levels of one factor can lead to an imbalance of the pluripotency core network and induce a loss of the self-renewal capacity and/or multi-lineage capacity (Niwa et al. 2005; Kopp et al. 2008). The present study proves that the PanMa is suitable for the culture of hiPSCs. However, maintenance culture of hiPSCs on the PanMa, appears to come along with a slight impact on hiPSC stemness, detectable as a minor change in the gene expression levels of the pluripotency genes *OCT4*, *SOX2* and *NANOG*, as well as reduced NANOG signals in immunofluorescent stainings. From previous studies, the ECM is known to represent one of several factors regulating stem cell function (Dakhore et al. 2018). For instance, the use of feeder cells, formerly required for the in vitro maintenance of murine and human PSCs, could be rendered obsolete by the application of basement membrane coatings, such as the

laminin-rich Matrigel® (Xu et al. 2001), which in combination with an appropriate cell culture media are able to replace the stimulatory effects provided by feeder cells. Single components such as Laminin-111, -332 and -511 as well as vitronectin have been shown to effectively support the pluripotency of iPSCs, while collagen IV and fibronectin do not (Xu et al. 2001; Dakhore et al. 2018). Interestingly, the here used PanMa missed an intact laminin network, as demonstrated by the immunohistochemical stainings and SEM analyses. Furthermore, proteome analyses revealed a lower abundance of laminins as well as vitronectin compared to the SISser and LungMa (Berger et al. 2020). In consequence, iPSC interactions with the ECM were limited to collagen fibers and bundles. These observations indicate that the slight changes in expression of the core pluripotency genes seen in iPSCs cultured on the PanMa could be due to the specific ECM composition of the PanMa, especially to the low abundance of laminins and vitronectin. Indeed, it has been shown that the activation of certain integrins, particularly receptors comprising a $\beta 1$ subunit such as $\alpha 6\beta 1$, by specific laminins, mostly -511, support pluripotency stronger than others (Villa-Diaz et al. 2016). Therefore, especially the low detection level of the laminin subunits $\beta 1$, $\beta 2$ and $\gamma 1$ in the PanMa (Berger et al. 2020), which are part of the laminins -511 and -521 would emerge as a reason for the minor changes in the expression of pluripotency genes (Miyazaki et al. 2008; Villa-Diaz et al. 2016). In contrast, proteome data reveal high abundance of the laminin $\beta 1$, $\beta 2$ and $\gamma 1$ subunits in the LungMa compared to the PanMa and SISser (Berger et al. 2020). The hypothesized elevated abundance of laminin- $\alpha 11$ could therefore explain the relatively stable expression of *SOX2* and *OCT4* seen in iPSCs on the LungMa compared to the PanMa and the SISser. Furthermore, SEM analyses clearly demonstrated the presence of laminins in form of a basal membrane on top of the SISser. Nevertheless, iPSCs on the SISser exhibited the same expression pattern for *OCT4* and *SOX2* as iPSCs on the PanMa. This raises the question whether the specific laminins abundant in the basal lamina are capable of supporting stemness. To examine whether the laminins of the basal lamina of the SISser support stemness in iPSCs or not, a deeper insight into the ECM composition regarding the abundance of different laminins in the ECM scaffolds and their specialized function is required, which could be achieved by the detection of single laminin subunits using immunohistochemical analysis (Virtanen et al. 2008).

Despite the integrin-mediated signaling of single ECM components, the ECM can regulate cellular function also via the deposition and release of ECM-binding bioactive molecules. Next to a number of other factors, the ECM has been shown to bind to FGF2 (Bossard et al. 2004) and TGF- β (Horiguchi et al. 2012). Both proteins are essential factors in the maintenance medium (mTeSR-1™) of iPSCs and contribute largely to the preservation of a SC character (Ludwig et al. 2006). Thus, it might be that the minor changes in *OCT4*, *SOX2* and *NANOG* expression are caused by an altered activity of FGF2 and TGF- β due to binding of both proteins to the ECM. Two scenarios are therefore conceivable: Binding of the proteins to the ECM could lead either to a withdrawal of free

protein from the medium, resulting in a lower signaling activity or to an accumulation of FGF2 and TGF- β at the matrix surface. To explore this possibility, attachment of both factors to the PanMa, SISser and LungMa should be investigated. This could be done by immunohistochemical staining of the cultured scaffolds for the mentioned peptides.

Furthermore, NANOG protein was weakly detectable in hiPSCs cultured on the ECM-scaffolds, while NANOG transcripts were only slightly altered. However, as the reduction of NANOG was only observed by qualitative immunofluorescent, the conclusion that NANOG is absent needs to be considered with caution. Provided that the results from the immunofluorescent analysis can be confirmed and NANOG is indeed less abundant in hiPSCs cultured on the ECMs, this suggests that hiPSCs cultured on the ECM initiate posttranscriptional or posttranslational modifications of NANOG, which result in reduced NANOG protein levels. In this context, studies have demonstrated that NANOG exhibits a relatively short half-life time of only 120 min due to a PEST-sequence targeting it for ubiquitin- proteasome-mediated degradation (Ramakrishna et al. 2011). External signaling can stabilize NANOG by phosphorylation and subsequent binding to other proteins or by enhancing the deubiquitylation of NANOG, which both reduces the probability of NANOG degradation. Hence, the stability of NANOG, and thereby the maintenance of the pluripotent state, appears to be tightly regulated by posttranslational modifications in terms of phosphorylation as well as ubi- and deubiquitylation (Liu et al. 2016). Other studies hypothesize that the OCT4-SOX2-NANOG circuitry is dependent on E-Cadherin formation, which might represent the link between ECM- and mechanic-mediated changes in the pluripotency of hPSCs (Li et al. 2010). Follow up studies of the present thesis should first aim to confirm the downregulation of NANOG in hiPSCs cultured on the ECMs by quantitative methods, such as Western blot or flow cytometry. In case the NANOG reduction can be confirmed, it would be interesting to investigate E-Cadherin as a possible mediator of the ECM signals in hiPSCs cultured on the ECMs at gene and protein level in order to see whether the ECM leads to a change in E-Cadherin expression or localization. Following studies should then also focus on the examination of posttranslational modification presumably causing the presumed reduced NANOG abundancy. This could be achieved, for instance, by taking a closer look at the ubiquitination-status of NANOG in cells cultured on ECM scaffolds by Western blot.

Eventually, the loss of NANOG in hESCs results in a decreased self-replication and an increased propensity to differentiation (Chambers et al. 2003; Mitsui et al. 2003). Accordingly, the weak NANOG signal observed in this study in nearly all hiPSCs cultured on the ECM scaffolds, should have led to an increased differentiation. However, this was not observed during the 6-day culture of hiPSCs on the ECM scaffolds. The reason for the absence of differentiation events despite reduced NANOG signals are open for speculations. It might be that the experiment duration was simply too short to allow for an apparent differentiation of hiPSCs to occur. Therefore, an

extension of the culture period of hiPSCs on the ECM scaffold might be necessary in order to observe differentiation events. Furthermore, it cannot be ruled out that the missing NANOG signal is due to a technical issue. Although this is unlikely since the used NANOG antibody is verified for the applied analysis by the manufacturer and the results were reproduced in two independent experiments, the absence of NANOG should be confirmed by quantitative methods, such as flow cytometry or Western Blot.

7.4 *The PanMa affects hiPSC differentiation – A matter of stiffness, composition, attachment or a combinatorial effect?*

hPSCs have the ability to generate any cell type of the human body. The first step is the generation of cells of one of the three germ layers ectoderm, mesoderm and endoderm. Following this initial fate choice event, differentiation of the germ layer committed cells can be directed towards any cell type of the respective germ layer lineage. Although the ECM is known to control PSC self-replication and differentiation potential *in vivo* and *in vitro* (Walma and Yamada 2020), the use of specific ECMs for directed differentiation of hiPSCs was largely neglected so far. The experiments conducted in this study suggest that tissue-specific ECMs have the capacity to guide hiPSC differentiation to a certain extent during early development. While spontaneous differentiation of hiPSCs on the PanMa promoted cellular characteristics indicating an endodermal phenotype, hiPSCs cultivated on the SISser exhibited features associated with an ectodermal phenotype. In contrast, hiPSCs cultured on the LungMa during spontaneous differentiation showed no tendency towards a certain lineage. Considering the uncovered differences between the ECM scaffolds in terms of their biophysical and physico-structural properties, a number of potential factors come into question for leading to this result.

One of them is the ECM stiffness, which slightly differed between PanMa and SISser (Smith et al. 2018). In comparison, the PanMa showed a rather soft structure ($G' = 0.089$ kPa) and more viscous behavior while the SISser ($G' = 1.1$ kPa) was more rigid, but still soft. The LungMa exhibited an intermediate rigidity ($G' = 0.24$ kPa) compared to PanMa and SISser. Substrate stiffness is known to be a crucial determinant for guiding stem cell behavior at different stages of development (Smith et al. 2018). For instance, it has been shown that matrix elasticity directs the differentiation of mesenchymal stem cells towards neural (soft matrix), muscle (intermediate) or bone cell types (stiff matrix) (Engler et al. 2006). Furthermore, in an approach similar to the here conducted experiment Zoldan et al. demonstrated that the *in vitro* multi-lineage differentiation of hESCs is mechano-responsive (Zoldan et al. 2011). Thereby, stiff synthetic polymers with a high elastic modulus ($E = 1.5 - 6$ MPa) resulted in an enhanced mesoderm formation, while intermediate rigidities ($E = 0.1 - 1$ MPa) promoted an endoderm- and soft scaffolds ($E < 0.1$ MPa) an ectoderm-

associated phenotype (Zoldan et al. 2011). This coincides with another study, showing that electrospun scaffolds with an Young's modulus of $E = 20$ kPa support the directed differentiation of hiPSCs into ectodermal cells, while culture on stiffer substrates ($E = 300$ kPa) promotes an endodermal formation (Maldonado et al. 2017). On a first view, both studies are in contrast to the present study. Here, endoderm-associated phenotypes were increasingly detected on the soft PanMa ($G' = 0.089$ kPa), while ectoderm signatures were elevated on the slightly stiffer SISser ($G' = 1.1$ kPa). However, it must be noticed that the scaffolds, which are termed stiff in the present study (SISser) would be defined as a soft substrate compared to the scaffold rigidities used by Zoldan et al. or Maldonado et al. Thus, the discrepancies to these studies might arise from the different range of used substrate stiffness. Furthermore, in the present work the effect of stiffness on hiPSC differentiation was not examined as an isolated parameter, but in context of a whole ECM-profile. Therefore, it is conceivable that other ECM properties also alter the differentiation outcome and cause the difference to other studies. Whether the relatively small differences between the three scaffolds have a relevant biological impact that could account for the observed lineage bias of hiPSCs is speculative and requires further tests. Therefore, it would be recommended to repeat the spontaneous differentiation of hiPSCs under conditions that only differ in substrate rigidity. This could be achieved by using gelatin coating of different height allowing an adjustment of substrate stiffness in order to resemble the stiffness's of PanMa, SISser and LungMa.

Proteome analysis of the here generated PanMa demonstrated a unique composition of the PanMa (Berger et al. 2020). Thus, it might be that the observed endoderm shift of the hiPSCs cultured in the PanMa might be also affected by the presence or absence of single ECM components in the PanMa. Indeed studies report that individual ECM proteins are capable of guiding hiPSC development. In a screen of several combinations of ECM components, including collagen I, III, IV, V, laminin, fibronectin and vitronectin, Brafman et al. identified vitronectin and fibronectin as effective promoters for endoderm commitment of hESCs (Brafman et al. 2013). This process is mediated by the specific binding to the integrin subunits $\alpha 5$ (fibronectin) and αV (vitronectin). Other studies confirm the beneficial effect of fibronectin on endoderm formation of hESCs and mESCs and further claim other ECM proteins, such as collagen I and laminin to support an endodermal development (Taylor-Weiner et al. 2013; Rasmussen et al. 2015). As demonstrated by the proteome analysis, the PanMa exhibited a lower abundancy of fibronectin and vitronectin, as well as laminin compared to the SISser (Berger et al. 2020). Nevertheless, an enhanced endodermal phenotype was observed on the PanMa. Again, the findings of the present work are in contrast to other studies (Brafman et al. 2013; Taylor-Weiner et al. 2013; Rasmussen et al. 2015). However, once more it is important to note that in the present study, differentiation was investigated in a multifactorial complex, whereas the mentioned studies investigated the

influence of single proteins. It has been shown that the combination of ECM proteins can have synergistic and antagonistic effects (Brafman et al. 2013; Rasmussen et al. 2015). It is therefore reasonable that the assembled ECM acts differentially on cells than single components.

The complex composition of PanMa, SISser and LungMa further plays a decisive role for the specific attachment of the differentiating hiPSC to the ECMs, as revealed by SEM analysis. Differentiating hiPSCs adhered to collagen bundles and fibers on the PanMa via thin stretched filopodia, while cells on the SISser adhered additionally to laminins via flat, spread out cell protrusions. Thereby, the cells on the SISser showed an increased contact area to the ECM surface than cells seeded on the PanMa. Cells on the LungMa exhibited the least contact area to the ECM. It is known that the density of adhesion spots largely defines how cells perceive biophysical cues of a material (Oria et al. 2017; Kechagia et al. 2019). Accordingly, a high density of integrin binding spots reduces the force, which is applied to every single integrin receptor. In consequence, an increased force is required to reach the thresholds at which intracellular mechanisms are triggered. On the contrary, a reduced ligand density enhances the probability for integrin downstream signaling (Kechagia et al. 2019). Accordingly, it might be assumed that integrin signaling on the PanMa and LungMa is facilitated by a reduced number of adhesion spots. In consequence, this could lead to an altered signaling in hiPSCs on the PanMa and LungMa compared to the SISser during differentiation, which might regulate lineage commitment. To investigate this issue, the performance of the PanMa, LungMa and SISser should be analyzed under conditions of applied force, as this stresses the signaling differences resulting from the diverging adhesion spot density. For this, dynamic flow systems in bioreactors present one possibility. Particularly, qualitative analysis of intermediate filaments, especially actin, should be carried out to examine the effect of adhesion spot density of the ECMs on the state of the cytoskeleton.

7.5 *A role of the ECM as a selective factor for lineage biased cell attachment*

Interestingly, all of the aforementioned studies assume that the ECM-mediated effects on differentiation base on an inductive signal of the ECM. According to this theory, cell attachment to the ECM is followed by integrin signaling which promotes differentiation (Wong et al. 2010). Apart from this accepted paradigm, the ECM could also act as a selection factor for cells according to their set of surface integrins. Following this idea, cells that express integrins matching to the provided ECM proteins adhere more efficiently than cells with a “non-suitable” integrin subset. In consequence, cells with a poor ECM attachment are lost with ongoing culture. Interestingly, studies show that integrin expression is changing during differentiation (Wang et al. 2015). Cells of the definitive endoderm express αV and $\beta 5$ integrins, while simultaneously downregulating the integrin $\alpha 6$, which is abundant in PSCs (Wong et al. 2010). In contrast, the differentiation of cells

with an ectodermal origin, such as neural tube and neural crest cells, involves amongst others the expression of the integrins $\alpha3\beta1$, $\alpha6\beta1$, $\alpha1\beta1$, $\alphaV\beta5$, $\alpha5\beta1$ (Goh et al. 1997; Lee et al. 2007; Ma et al. 2008; Li et al. 2014). Against this background, it might be that some ECM proteins selectively bind cells that are prone to differentiation into a certain lineage, while other cells fail to bind and are lost during culture. Thus, it could be that the PanMa represents the preferred binding target of hiPSCs with a destined but not manifested endodermal phenotype, while the SISser promotes attachment of cells, which will develop an ectodermal phenotype. Given the fact that hiPSCs were cultured for four days in spontaneous differentiation medium prior to seeding and therefore presumably contain cells with primed cell states, further substantiates this presumption. In order to test this hypothesis, EBs of day 6 (before seeding) should be stained for different integrin subunits, sorted via flow cytometry and subsequently characterized for a lineage bias using gene expression analysis.

7.6 Pancreatic differentiation on the PanMa does not improve β -cell function

In vitro differentiation of hiPSCs towards β -like cells by the concerted administration of growth factors or small molecules in 2D or 3D culture results in β -like cells with an impaired insulin secretion (D'Amour et al. 2006; Reznania et al. 2012; Reznania et al. 2014). However, the *in vivo* development of mature islets shows, that processes involving the ECM, such as migration and delamination, play an important role for the generation of mature islets (Jennings et al. 2013). To test, whether a tissue specific ECM can improve the pancreatic differentiation of hiPSCs, the PanMa was applied in different scenarios of pancreatic *in vitro* differentiation.

In terms of β -cell function, neither culture on the PanMa, nor on the SISser resulted in an improved glucose-stimulated insulin secretion. Therefore, the hypothesized role of the ECM as an inducer of functional maturation of hiPSC-derived β -cells could not be confirmed. The generated S5 and S7 cells showed no response to rising glucose levels, irrespective of whether an ECM scaffold was used or not. This is in line with the data of the original publications (Reznania et al. 2012; Reznania et al. 2014) and presents a common problem in the field of pancreatic tissue engineering. However, recent studies, which were published during this work, overcame this limitation by the reaggregation of immature β -like cells as well as the permission of TGF β signaling by omission of ALK5 inhibitor at the β -cell maturation stage (Nair et al. 2019; Velazco-Cruz et al. 2019). The refinement of the differentiation protocols resulted in the generation of mature β -cells that display a robust glucose-stimulated insulin secretion similar to human islets (Nair et al. 2019; Velazco-Cruz et al. 2019). A comparison of the differentiation protocols used in this study (Reznania et al. 2012; Reznania et al. 2014) and the refined protocols (Nair et al. 2019; Velazco-Cruz et al. 2019) suggests that the prolonged application of ALK5 inhibitor suppressed the maturation of the

here generated S5 and S7 cells. Furthermore, it has been shown that early induction of the endocrine lineage marker NGN3 results in an increased number of polyhormonal cells with a predestined α -cell fate (Veres et al. 2019; Hogrebe et al. 2020), which is discussed in more detail in section 7.8.

7.7 *Indications for an involvement of the PanMa in endocrine commitment*

In order to test the effect of the PanMa at different stages of pancreatic development, the PanMa was applied in several experimental set-ups: 1) as a liquid medium supplement to examine the non-mechanical signaling of the PanMa, 2) as a solid scaffold during the 5-stage pancreatic differentiation protocol (Rezania et al. 2012; Rezania et al. 2014) to analyze its effect on premature HECs, 3) as a solid scaffold during the 7-stage pancreatic differentiation protocol (Rezania et al. 2014) to investigate its effect on maturing β -cells and 4) as a hydrogel to evaluate the PanMa as a substrate for long term culture of HECs.

No effect on the generated S5 cells was observed when the PanMa was applied as a liquid medium supplement during pancreatic differentiation of hiPSCs. This indicates either that a mechano-independent signaling of the solubilized PanMa components is not possible, or that the induced signals are insufficient to alter intracellular processes. Whether ECM components are able to mediate a mechano-independent signaling is questionable when considering the operation mode of integrin receptors. Thereby, binding to an ECM ligand alone is insufficient to induce an intracellular signal. Instead, an additional mechanical stimuli is required which drives the formation of a focal adhesion complex and the eventual activation of intracellular signaling pathways (Kechagia et al. 2019). Hence, solubilized ECM particles are unlikely to induce intracellular signaling, as they do not provide any mechanical cues. Apart from integrin-binding components, ECMs can contain other molecules, for instance growth factors, that can indeed mediate an integrin-independent signaling (Taipale and Keski-Oja 1997). However, the applied concentration of solubilized ECM (100 – 800 ng/ml) appears quite low considering the low amount of growth factors that might be present in the PanMa, although this is not shown yet. Therefore, it is conceivable that the putative amount of non-ECM signaling molecules applied with the liquid PanMa is not sufficient to trigger an integrin-independent signaling. Therefore, the application of bigger ECM particles at higher concentrations should be considered to test whether a signaling of solubilized ECM is possible or not.

Moreover, it must be stressed that the differentiation efficiency of control S5 cells in this study was much lower compared to the original protocol. Rezania et al. reported that 50% of the generated S5 cells were NKX6.1⁺/INS⁺/GCG⁺. In contrast, the differentiation experiments conducted in the present study resulted in only a few NKX6.1⁺/CPEP⁺ S5 cells at day 21. However,

continued culture led to an increase in NKX6.1⁺/CPEP⁺, indicating a delayed differentiation in the present study. The diverging differentiation course might be due to the usage of another PSC type in comparison to the original publication. Rezania et al. obtained their results using a hESC-cell line (H1) and further showed that use of a hiPSC line (Gibco, A18945) resulted most notably in a less efficient generation of NKX6.1⁺/INS⁺ cells. Thus, it is reasonable that the here used hiPSCs (iMR-90-4) possesses a reduced capacity for a pancreatic differentiation compared to the cell lines used in the original publication.

PanMa and SISser was furthermore applied as a solid scaffold during pancreatic differentiation using a 5-stage protocol (Rezania et al. 2012; Rezania et al. 2014), which resulted in a markedly reduced gene and protein expression of INS, GCG and SST. These observations indicate a negative effect of the PanMa and SISser on endocrine commitment of the differentiating cells. One reason for this outcome might be the adherent culture during S5, which is actually designed for the suspension culture of S4 cell clusters (Rezania et al. 2012; Rezania et al. 2014). Furthermore, it might be possible that attachment to the ECM suppresses the endocrine commitment of cells, leading to an enhanced proportion of pancreatic-non endocrine cells. In a recent study, Mamidi et al. conclusively demonstrated that the commitment of bipotent ductal endocrine progenitors to the endocrine or the ductal lineage indeed is controlled in an ECM-dependent manner (Mamidi et al. 2018). In detail, a ductal fate choice was promoted by the attachment of bipotent ductal endocrine progenitors to fibronectin or vitronectin via integrin $\alpha 5$. In contrast, laminin and collagen resulted in a reduced $\alpha 5$ expression and an increased endocrinogenesis. The results of the present study support the ECM-dependent regulation of endocrine commitment. However, according to the data from Mamidi et al. (Mamidi et al. 2018), culture on the PanMa, which has been shown to contain a reduced content of fibronectin and vitronectin (Berger et al. 2020), should have led to an increased amount of endocrine cells. Similarly, differentiation of hiPSCs on the laminin-rich SISser should theoretically have led to an enhanced endocrine phenotype. Instead, differentiation of hiPSCs on the PanMa and SISser reduced the amount of HECs. A possible explanation for this contrary result is, again, the multifactorial composition of the ECM scaffolds. Furthermore, the presented results were obtained using the S5 differentiation protocol from Rezania et al., whereas Mamidi et al. used the more sophisticated 7-stage protocol (Mamidi et al. 2018).

Qualitative analysis of the hormone expression by immunofluorescent analysis further confirmed the reduced number of HECs but was also indicative for a slightly increased abundance of monohormonal cells. This observation is a first indication that the PanMa or SISser might regulate the specification into α -, β - and δ -cells. Recently, it has been shown that the basis for the later specification into α - and β -cells is partially established during endocrine commitment (Sharon et al. 2019; Veres et al. 2019). Application of the PanMa during the 7-stage protocol further

corroborated the presumption of an involvement of the PanMa in endocrine commitment and or terminal cell type specification.

7.8 *The right timing for PanMa signaling might boost endocrine development*

When using the similar 7-stage protocol for differentiating hiPSCs towards β -like cells on the PanMa and SISser, an impact on hormone expression in terms of reduced *GCG* and *SST* transcript levels compared to Matrigel®-coated PET membranes was observed. This strongly suggests an influence of the PanMa and SISser on endocrine commitment or specification and indicates a regulatory effect on the endocrine inducing factor *NGN3*, which covers a crucial role during endocrine lineage commitment. Recently, studies revealed that *NGN3*-mediated endocrinogenesis occurs in two waves during pancreatic *in vitro* differentiation of hESCs (Sharon et al. 2019; Veres et al. 2019). Thereby, it was shown that the development into α - and β -cells largely depends on the timing of *NGN3* expression. An early onset of *NGN3* in S4 cells prior to *NKX6.1* expression results in polyhormonal cells, which are prone to an α -cell fate (Sharon et al. 2019; Veres et al. 2019; Hoglebe et al. 2020). In contrast, if *NGN3* turns on after *NKX6.1* (around S5), the probability of β -cell development is increased (Sharon et al. 2019; Veres et al. 2019; Hoglebe et al. 2020). Considering the fact that S7 cells on the PanMa and SISser exhibit a decrease in *GCG*, but not *INS* expression, hypothesizes an ECM-dependent effect on the activation of *NGN3*. In line with this discovery, recent studies demonstrate an ECM-dependent regulation mechanism of *NGN3* (Mamidi et al. 2018; Hoglebe et al. 2020). According to the proposed model, ECM-mediated integrin $\alpha 5$ signaling increases the polymerization state of the actin cytoskeleton state and promotes the establishment of stress fibers which alter the nuclear translocation of mechanoresponsive transcription factors (Mamidi et al. 2018). In consequence, YAP1 enters the nucleus where it suppresses *NGN3* by directly binding to the *NGN3* promoter as well as by driving the expression of the *NGN3* repressor *HES1* (Mamidi et al. 2018; Hoglebe et al. 2020). Hence, a polymerized cytoskeleton state blocks *NGN3*-mediated endocrinogenesis and promotes a ductal commitment of bipotent ductal endocrine progenitor cells. Conversely, a depolymerization of the cytoskeleton abrogates *NGN3* suppression by YAP1 thereby inducing an endocrine commitment (Cebola et al. 2015; Mamidi et al. 2018; Hoglebe et al. 2020). *In vivo*, *NGN3* expression could be triggered by the attachment of S4 cells to laminin and collagen, but not fibronectin and vitronectin (Mamidi et al. 2018). Thus, it might be that the collagen-based and environment of the PanMa and the laminin-rich SISser, stimulate *NGN3* expression at S5. However, if the ECM composition would be the inducing factor, diverging results would be expected for S7 cells generated on the PanMa and the SISser, due to their specific abundance of single ECM constituents. Furthermore, similar results would then have been expected for the Matrigel®-coated PET membranes, since Matrigel®

is composed of around 60% laminin, 30% collagens and only trace amount of vitronectin and fibronectin (according to manufacturer's information, Corning 2020). Thus, it is conceivable that the observed reduction in GCG and SST expression is not a PanMa-specific phenomenon, but is rather caused by a general ECM mechanism.

In the mentioned studies, a depolymerization of the actin cytoskeleton and the resulting promotion of *NGN3* expression was further achieved by chemical cytoskeleton modulators, such as Latrunculin A (Hogrebe et al. 2020) and could be reproduced by culturing the differentiating cells on soft substrates (Mamidi et al. 2018; Hogrebe et al. 2020). Most strikingly, the substrate rigidity is the main difference between the biological ECMs and the Matrigel[®]-coated PET membranes. In fact, the stiffness of PanMa and SISser ($G' = 0.089$ kPa and 1.2 kPa) is about six order of magnitudes lower than that of uncoated PET membranes ($E = 2 - 2.7$ GPa) (Kreuder et al. 2020). Hence, the soft ECM structure could reduce actin polymerization of the seeded cells during pancreatic differentiation and thereby promote a late endocrinogenesis. The relatively small discrepancies between stiffness of the PanMa and the SISser (10-fold compared to the huge differences to the Matrigel[®]-coated PET membrane (10⁶-fold) also explain why no ECM-specific impact on the differentiation was observed. In order to test this hypothesis, the cytoskeleton state of S5 cells cultured on the ECM scaffolds should be analyzed by determining the ratio of filamentous actin (F-actin; \triangleq polymerized) and glomerular actin (G-actin; \triangleq depolymerized) using Western Blot. Furthermore, it should be examined, if the ECM-dependent phenotype of S7 cells can be reverted using chemical compounds that induce a cytoskeleton polymerization, such as Jasplakinolide (Coué et al. 1987). Eventually, expression of *NGN3* should be investigated at S4 and S5 in cells on the Matrigel[®]-coated PET membrane in comparison to PanMa and SISser, as well as the downstream targets of *NGN3*, such as *NKX2.2* and *NEUROD1*. *NGN3* expression was not assessed in the present study, since analyses were performed at S7 and *NGN3* is only activated transiently during endocrinogenesis (S4 – S6) (Hogrebe et al. 2020).

The hypothesis that an ECM-cytoskeleton-YAP1-*NGN3* regulatory loop is causative for the shift in hormone gene expression in favor of *INS* seen in S7 cells differentiated on PanMa and SISser, raises several questions. One mayor problem of this theory is that the proposed PanMa/SISser-induced cytoskeleton depolymerization would be continuously present, meaning that *NGN3* is supposed to be triggered already at early stages (S4) of pancreatic differentiation, which should result in an increased generation of polyhormonal cells with an ultimately α -cell phenotype. However, this is not seen on the ECM scaffolds. It might be that other attributes of the scaffolds interfere with the *NGN3* expression and block a premature endocrinogenesis. Indeed, Mamidi et al. demonstrated that cell shape and spreading are further aspects which affect YAP1-controlled *NGN3* expression by altering the cytoskeleton tension (Mamidi et al. 2018). Thereby, cell spreading suppresses *NGN3* expression while cell confinement increases *NGN3* expression (Mamidi et al. 2018). One

observation made in the present study is that the PanMa and SISser provide ECM cues for cellular migration, which requires cellular spreading. It could be that S4 cells exhibit an increased motional behavior, which is promoted by the ECM culture, whereas S5 cells represent a resident, confined cell type. To investigate this issue, the migration activity of S4 and S5 cells should be compared in 2D by live cell imaging. Moreover, it would be interesting to see whether a time dependent seeding of cells on the ECM scaffolds at different stages of the 7-stage protocol promotes endocrinogenesis and the development of α - or β -cells.

Furthermore, it is possible that the ECM alone is not sufficient to induce the observed gene expression shift, but rather acts in synergy with one of the soluble factors of the differentiation medium. One interesting candidate in this regard is the γ -secretase inhibitor XX, which inhibits Notch signaling by preventing the γ -secretase-mediated cleavage of the intracellular domain of the Notch receptor, which is required for Notch signaling. γ -secretase inhibitor XX is applied during S6 and S7 of culture in the Rezia protocol and during S5 in the Hoglebe protocol to promote endocrinogenesis (Rezia et al. 2014; Hoglebe et al. 2020). *In vivo*, Notch signaling plays an important role for the tip-trunk decision of MPPs and thereby largely affects endocrine commitment (Jennings et al. 2013). *In vitro*, the inhibition of Notch signaling by the γ -secretase inhibitor XX induces endocrine commitment not only in cells of the pancreatic but also the intestinal lineage (Hald et al. 2003; Murtaugh et al. 2003). Studies in mice suggest that YAP1 acts upstream of Notch and can bind to the *Notch* promoter in an inducing manner (Mamidi et al. 2018). This presumption implies that the ECM and γ -secretase inhibitor XX interfere at different levels of the Notch-mediated *NGN3* suppression machinery: the ECM by inhibiting the nuclear transfer of YAP1, thereby repressing *Notch* expression, and the γ -secretase inhibitor XX by reducing Notch signaling. This further shows that the application of γ -secretase inhibitor XX alone abolishes the Notch mediated repression of *NGN3* but not the YAP1 induced inhibition of *NGN3*. In contrast, the ECM induced mechanism blocks YAP1 and thereby reduces Notch signaling, which likewise results in an upregulation of *NGN3*. Therefore, it is conceivable that the ECM-mediated modulation of the cytoskeleton and γ -secretase inhibition potentially inhibit Notch signaling in a synergistic manner. To test this hypothesis, γ -secretase inhibitor XX treated or non-treated S5 ECM cultures should be analyzed for the total amount and the nuclear/cytoplasmic localization of YAP using Western Blot on cytoplasmic/nuclear fractions. Furthermore, expression of *NGN3* and its downstream targets *NKX2.2* and *NEUROD1* should be examined.

7.9 Using the PanMa hydrogel as a platform for the establishment of an islet-endothelial co-culture model

Functional organ models hold great promise to render the development chain of new drugs and medical products more efficient and thereby reduce the number of animal experiments (Russel and Burch 1959). The establishment of pancreatic organ models was so far largely restricted by the limited availability of functional islet cells. Isolated islets of high quality are mostly used for transplantation purposes and islets that come into question for *in vitro* assays are mostly rejects of lower quality. 2D cell lines, such as MIN-6 or INS-1 (Skelin et al. 2010), reflect endocrine function only to a little amount, as they lack the complex islet environment and *in vitro* generated islets were not much useful due to an immature phenotype with limited functional capacity (Pagliuca et al. 2014; Rezanian et al. 2014). Due to these restrictions, only a limited number of studies investigating the possibilities of pancreatic organ models are available to date (Daoud et al. 2010). The recent establishment of next generation β -cells displaying functions similar to their *bona fide* counterpart could render this issue obsolete.

In light of this groundbreaking achievement, improved *in vitro* organ models are likely to be realized soon. However, such models require culture systems that allow for the establishment of standardized models with a sophisticated cellular environment. The recreation of the microenvironment using solid biological or bio-inspired scaffolds (Tran et al. 2020) remains a challenging task as demonstrated in the present study. In this regard, hydrogels have emerged as a promising compromise as they enable the recreation of an *in vivo* like environment in a more standardized fashion. Several studies demonstrated the feasibility of hydrogel-based islet culture using biomimetic ECM-derived (Weber and Anseth 2008; Davis et al. 2012) or synthetic hydrogels (Liese N. Beenken-Rothkopf et al. 2013; Phelps et al. 2015; Knobloch et al. 2017) and further showed a beneficial influence of the hydrogel culture on islet function. Recently, Sackett et al. reported about the establishment of a hydrogel derived from human pancreata (Sackett et al. 2018). The generated hydrogel was successfully tested for the *in vitro* culture of hESC as well as hESC-derived HECs. However, encapsulated hydrogels were cultured for only 9 days, which does not allow any statement about the long-term effects of the hydrogel on HECs (Sackett et al. 2018).

In the presents study, a PanMa-derived hydrogel was developed allowing culture of pancreatic cells for 21 days, which, however, showed an altered islet morphology as well as a slightly decreased glucose stimulated insulin secretion at day 21. Furthermore, this study demonstrates that the PanMa hydrogel does not interfere with functional read outs, such as gene expression analysis or glucose-stimulated insulin secretion measurements. A preliminary approach to characterize the PanMa hydrogel has been addressed by Anna-Lena Ziegler in the course of her bachelor thesis (Ziegler 2019). Thereby, it could be shown that the gelation process of the PanMa

hydrogel is different compared to Matrigel[®], indicating that crosslinking of the PanMa hydrogel rests on different protein groups compared to Matrigel[®] (Ziegler 2019). Furthermore, the PanMa hydrogel exhibited a higher storage modulus ($G' = 200$ Pa) than the solid PanMa ($G' = 89$ Pa) but was slightly less rigid than 50% (v/v) Matrigel[®] ($G' = 300$ Pa) (Ziegler 2019). To optimize the application of the PanMa hydrogel, a much greater understanding of its compositional and biophysical properties is required. Proteome analysis of the PanMa hydrogel is recommended to decipher its composition and to show which proteins are lost during hydrogel preparation. Also, measurement of the GAG content should be taken into consideration as the GAG content correlates with the water binding capacity of the hydrogel and thereby contributes largely to its viscous behavior (Mouw et al. 2014). Other than for the solid PanMa, quantification of the GAG content should be feasible for the PanMa hydrogel, as insoluble components are removed from the hydrogel in beforehand.

Using the PanMa hydrogel for the culture of isolated porcine neonatal islet-like cells clusters (NICCs) (Ziegler 2019), led to the same difficulties as observed in the present study. Firstly, clusters partially settled at the plate bottom leading to an increased spreading of attached cells. This is due to a low viscosity of the neutralized hydrogel and long gelation time (15 – 20 min) compared to Matrigel[®] (5 – 10 min). The viscosity of the hydrogel could be increased by the addition of viscous components, such as cellulose or agarose. Furthermore, delipidization of the pancreas should be carried out to remove residual fat, as lipids have been shown to inhibit the hydrogel generation (Young et al. 2011). To this purpose, the decellularization process for the generation of PanMa for hydrogels could be adapted to the protocol from Sackett et al., who achieved an efficient delipidization by tissue homogenization and subsequent centrifugation (Sackett et al. 2018). Fewer lipid content per ECM dry mass would also reduce the batch-dependent variations of the protein content and thereby facilitate the optimization of the hydrogel ECM concentration, which was shown to require a precise adjustment to ensure the suitability of the PanMa hydrogel for cell culture (Ziegler 2019). It will be interesting to see, whether the refined PanMa hydrogel shows an improved performance for the maintenance of HECs, since this is a prerequisite for the advancement of this system.

So far, the PanMa hydrogel is not suitable for the establishment of an *in vitro* model due to a negative impact on the morphology and endocrine signature of HECs. Due to its properties as a biomimetic pancreas-specific ECM scaffold, it is nevertheless of interest for future projects. A refined PanMa hydrogel would present a good basis for the contemporary realization of a sophisticated *in vitro* organ model. In this regard, it would be very interesting to study the new generation of hPSC-derived β -cells that were recently established (Nair et al. 2019; Velazco-Cruz et al. 2019). Thereby, the effects of the pancreatic ECM on mature β -cells with a functional insulin secretion could be studied in more detail. Encapsulation of the functional β -cells would further

allow for a non-invasively monitoring of islet morphology and insulin secretion over a period in a consistent microenvironment. Another feature that could possibly be implemented in the hydrogel organ model is an endothelial network of primary or hiPSC-derived ECs. Arterial ECs can routinely be generated from hiPSCs and demonstrate functional similarity to human ECs such as network formation in a Matrigel®-based 3D culture (Zhang et al. 2017). The feasibility of this approach has been demonstrated in the course of a side-project during this work (Fig. S4). Whether a refined PanMa hydrogel supports the network formation similar to Matrigel® needs to be studied. As physical contact of β -cells to the vasculature interface in murine islets has been demonstrated to contribute to cell polarization by relocalization of the insulin vesicle pool (Low et al. 2014; Gan et al. 2018), the maintenance of functional hiPSC-derived islets in co-culture with endothelial cells is a highly interesting aspect. A hydrogel-based islet-endothelial co-culture would represent the first *in vitro* system allowing for investigating islet-endothelial interactions. Furthermore, this would be a first step towards the formation of a vascularized pancreatic model, which is of high interest for both *in vitro* test systems and *in vivo* cell replacement strategies.

7.10 Limitations of this study

The high complexity of the here generated PanMa scaffold allows to investigate the function of cells in a sophisticated ECM environment, which cannot be resembled to this extent by other approaches published so far. However, the ECM complexity is also a major drawback of the ECM for some methodical techniques, especially when encountering approaches with a basic research questioning.

In this study, specific effects of ECM scaffolds derived from different tissues on hiPSC differentiation were observed. However, this study was not able to resolve which property of the ECM caused this effect due to the high ECM complexity. By comparing the here obtained data with current literature, probable candidates could be identified that come into question to be responsible for certain observations. Nevertheless, the here applied top-down approach is not suitable to connect cellular responses to certain ECM properties. In order to resolve this link, simplified approaches are required, which allow investigating the effect of ECM properties in an isolated manner. Subsequently, stepwise combination of defined ECM cues in a bottom-up approach would help to decipher the relationship of ECM properties among each other and their combinatorial effect on cellular physiology. This has partially been executed in some studies (Engler et al. 2006; Brafman et al. 2013) but more data are required to complete the picture of the ECM-mediated signaling on cells.

Another limitation of this study is the fact that the generated PanMa resembles the ECM of the entire pancreas and not particularly the islet-specific environment. As mentioned, the pancreas

mostly consists of acinar tissue, whereas the endocrine part in forms of Langerhans islets accounts for only 1% of the cell mass (Beger 2018). Therefore, the PanMa rather represents the ECM of the acinar tissue and not of the islet niche. While some properties, such as the bulk rigidity or the water content should be comparable between both compartments, others, like the biochemical composition, are likely to exhibit a larger discrepancy. Thus, the generation of an islet-specific ECM would be a desirable achievement. However, the small amount of pancreatic islets strongly limits the amount of ECM generated by islet decellularization. Therefore, designed ECMs that resemble islet-ECM composition according to proteome studies (Waanders et al. 2009; Asthana et al. 2020) represent a more effective method for generating an ECM scaffold with an islet-niche signature. Furthermore, it is important to note that the here used PanMa was generated from the porcine pancreas. However, it can be assumed that there might be interspecies differences. Therefore, a comparison of human and porcine pancreas ECMs is recommended to decipher differences and similarities between both species. This could be realized with less effort as proteome data sets of both the human (Danielsson et al. 2014) and the porcine (Berger et al. 2020) pancreata already exist.

Moreover, application of the PanMa complicated some experimental approaches and largely restricted the choice and validity of some analytical methods. For instance, the expression of protein markers in this study was only assessed qualitatively by immunofluorescent staining, as quantification of cell numbers, especially in regard of the number of mono- and polyhormonal cells generated by pancreatic differentiation on the PanMa, was impeded by the culture conditions on the PanMa. Apart from elaborate manual quantification by cell counting, which was conducted in this study to determine the number of GATA4⁺ and PAX6⁺ cells on the scaffolds after spontaneous differentiation, flow cytometry experiments would be the preferable choice. However, therefore cells need to be detached first, which might work for cells that adhere to the surface of the ECM, but not for those that migrated into the scaffold. One possible strategy would be a digest of the scaffold using collagenase. However, whether this can be executed without harming the cells needs to be tested.

Similarly, analyses of the glucose-stimulated insulin secretion were largely impaired by the solid ECM scaffolds and led to false measurement results. There are two possible explanations for an ECM-dependent impact on the outcome of this assay. First, it is likely that exogenous insulin, contained in the culture medium, bound to the PanMa-TWs and resulted in an increased measurement of insulin, as observed by increased insulin values measured for PanMa and SISser. This hypothesis is further corroborated by the high water binding capacity of the PanMa. To solve this issue, a more thorough washing prior to the assay as well as the measurement of empty scaffolds incubated with cell culture medium should be carried out. Secondly, normalization of the secreted insulin to the number of assayed cells poses a problem. Usually, normalization is carried

out by determining the ratio of measured insulin and the amount of extracted DNA after cell lysis. However, DNA extraction from cells cultured on the PanMa resulted in lower amounts compared to the control and the SISser. This could be an indication for a much lower number of cells, but is more likely to be explained by an insufficient DNA extraction from cells cultured on the PanMa. Probably, DNA isolation from cells could be improved by using column-based DNA purification. However, this is elaborate and costly and entails the risk of a loss of DNA during the purification process. Another possibility would be to detach the cells from the scaffold and determine the cell number by automated counting. As mentioned above, this is difficult for cells that are located inside the scaffold. Therefore, other normalization strategies have to be developed to ensure reliable insulin measurements in PanMa-based systems.

8 Conclusion

The overall aim of this thesis was to investigate the influence of the pancreas ECM on the directed *in vitro* pancreatic differentiation of hiPSCs.

In the first part of this thesis, the successful generation of the PanMa using whole organ decellularization was demonstrated. Furthermore, it could be shown that important macro-, micro- and ultrastructural ECM features of the native tissue were preserved in the PanMa. A comparison with the SISser and the LungMa characterized the PanMa as a very soft, hygroscopic, fiber-based ECM scaffold and indicated that the generated ECM scaffolds contain tissue-specific biophysical and physico-structural properties. Moreover, the data of this study indicate that these ECM-specific properties have a relevant influence on the multi-lineage differentiation of hiPSCs.

Furthermore, it was postulated that the PanMa has a beneficial impact on the pancreatic differentiation of hiPSCs and particularly on the terminal maturation of insulin producing cells towards mature β -cells. Contrary to this hypothesis, the PanMa did not result in an enhanced β -cell maturation in terms of an improved glucose-stimulated insulin secretion. However, directed differentiation of hiPSCs towards islet-like cells on the PanMa and the SISser resulted in a gene expression shift of pancreatic hormones in favor of *INS*. Consideration of the current literature indicate a possible role of the PanMa for regulating endocrinogenesis by a cytoskeleton-mediated upregulation of *NGN3*. These findings suggest that the ECM might be a relevant factor for pancreatic *in vitro* differentiation and imply that the PanMa and SISser could be used to enhance the number of β -like cells by improving endocrine commitment.

Another aim of this study was the establishment of a pancreas-specific *in vitro* culture system of HECs. In this regard, a PanMa-derived hydrogel could be established and used for a hydrogel-based *in vitro* culture of hiPSC-derived HECs for 21 days. However, hydrogel encapsulation and culture resulted in accelerated decrease of cells with a β -cell-like phenotype and an altered cluster cytomorphology of HECs. Taken together, these data proof the concept of the PanMa hydrogel-based pancreas *in vitro* model but further demonstrate that a more detailed characterization and refinement of the hydrogel is required to realize this aim.

In conclusion, this thesis demonstrates a biological effect of the ECM on the *in vitro* differentiation of hiPSCs. Furthermore, the results of this study indicate a possible role of tissue-specific ECM properties for the regulation of ECM-mediated hiPSC functions. Thereby, these findings underline the relevance of the ECM for *in vitro* cell culture and emphasize a stronger consideration of organ-specific microenvironmental features for tissue engineering-inspired approaches.

9 *Future Perspectives*

In order to elaborate more on the ECM-mediated signaling on hiPSC differentiation, a profound understanding how individual biophysical and physico-structural properties of the ECM regulate cell functions is indispensable. Future studies should therefore aim for resolving the effect of ECM properties, such as rigidity, porosity and composition on the cellular processes regulating differentiation. For this, simplified ECM structures will be necessary that allow analyzing the cellular function in response to individual ECM properties. Apart from this, uncovering the interconnection of ECM characteristics will be essential in order to understand piece by piece how ECM scaffolds with certain properties can be generated.

Tissue-derived ECM scaffolds such as the here generated PanMa provide a unique environmental complexity which cannot be resembled by any other approach so far. However, a major drawback of such scaffolds is their heterogeneity. ECM-derived hydrogels present a promising compromise as they combine a more standardized application while maintaining the compositional complexity and tissue-specificity of the ECM. Furthermore, hydrogels allow a modification of certain properties such as rigidity and composition as well as an implementation of other cell types. Due to these advantages, ECM-derived hydrogels are designated to play a central role for future *in vitro* tissue engineering approaches.

With the generation of the PanMa hydrogel, a suitable scaffold for creating a pancreas-specific environment for *in vitro* organ models has been established. Follow-up studies should focus on a further refinement of the PanMa hydrogel to aim for the generation of a more defined and reproducible biomimetic scaffold. An optimized PanMa hydrogel would represent a promising starting point for the stepwise development of an *in vivo*-like pancreas *in vitro* model. The most important step in this approach represents the implementation of pancreatic endocrine cells, which will benefit from the recent establishment of improved hiPSC-derived islet-like cells. Moreover, the addition of other cell types, such as acinar, ductal or endothelial cells is desirable to investigate the impact of cellular interaction on the islet-cell function.

As emphasized by this study, biomimetic scaffolds with tissue-specific ECM cues could play a major role in future tissue engineering approaches. Especially the establishment of ECM-derived hydrogels is an exciting achievement, which has a huge potential to improve *in vitro* cell culture models. With the here generated PanMa and the PanMa-derived hydrogel two scaffolds have been established which could be of use to realize such projects.

10 References

- Aamodt, Joseph M.; Grainger, David W. (2016): Extracellular matrix-based biomaterial scaffolds and the host response. In *Biomaterials* 86, pp. 68–82. DOI: 10.1016/j.biomaterials.2016.02.003.
- Agulnick, Alan D.; Ambruzs, Dana M.; Moorman, Mark A.; Bhoomik, Anindita; Cesario, Rosemary M.; Payne, Janice K. et al. (2015): Insulin-Producing Endocrine Cells Differentiated In Vitro From Human Embryonic Stem Cells Function in Macroencapsulation Devices In Vivo. In *Stem cells translational medicine* 4 (10), pp. 1214–1222. DOI: 10.5966/sctm.2015-0079.
- Alcazar, Oscar; Buchwald, Peter (2019): Concentration-Dependency and Time Profile of Insulin Secretion: Dynamic Perfusion Studies With Human and Murine Islets. In *Frontiers in Endocrinology* 10, p. 680. DOI: 10.3389/fendo.2019.00680.
- An, Duo; Chiu, Alan; Flanders, James A.; Song, Wei; Shou, Dahua; Lu, Yen-Chun et al. (2018): Designing a retrievable and scalable cell encapsulation device for potential treatment of type 1 diabetes. In *PNAS* 115 (2), E263-E272. DOI: 10.1073/pnas.1708806115.
- Anazawa, Takayuki; Okajima, Hideaki; Masui, Toshihiko; Uemoto, Shinji (2019): Current state and future evolution of pancreatic islet transplantation. In *Annals of gastroenterological surgery* 3 (1), pp. 34–42. DOI: 10.1002/ags3.12214.
- Asthana, Amish; Tamburrini, Riccardo; Chaimov, Deborah; Walker, Stephen J.; van Dyke, Mark; Tomei, Alice et al. (2020): Comprehensive characterization of the human pancreatic proteome for bioengineering applications. In *Biomaterials*, p. 120613. DOI: 10.1016/j.biomaterials.2020.120613.
- Atala, Anthony; Lanza, Robert Paul; Nerem, Robert M.; Mikos, Tony (Eds.) (2019): Principles of regenerative medicine. Third edition. London, United Kingdom: Academic Press an imprint of Elsevier. Available online at <https://www.sciencedirect.com/science/book/9780128098806>.
- Baggio, Laurie L.; Drucker, Daniel J. (2007): Biology of incretins: GLP-1 and GIP. In *Gastroenterology* 132 (6), pp. 2131–2157. DOI: 10.1053/j.gastro.2007.03.054.
- Baker, Christopher L.; Pera, Martin F. (2018): Capturing Totipotent Stem Cells. In *Cell Stem Cell* 22 (1), pp. 25–34. DOI: 10.1016/j.stem.2017.12.011.
- Bansal, Nidhi; Weinstock, Ruth S. (Eds.) (2020): Endotext [Internet]: MDText.com, Inc.
- Beger, Hans G. (Ed.) (2018): The pancreas. An integrated textbook of basic science, medicine, and surgery. Third edition. Hoboken, NJ: Wiley Blackwell. Available online at <https://onlinelibrary.wiley.com/doi/book/10.1002/9781119188421>.
- Bella, Jordi; Hulmes, David J. S. (2017): Fibrillar Collagens. In David A.D. Parry, John M. Squire (Eds.): *Fibrous Proteins: Structures and Mechanisms*. Cham, s.l.: Springer International Publishing (Subcellular Biochemistry, 82), pp. 457–490.
- Bennet, W.; Groth, C. G.; Larsson, R.; Nilsson, B.; Korsgren, O. (2000): Isolated human islets trigger an instant blood mediated inflammatory reaction: implications for intraportal islet transplantation as a treatment for patients with type 1 diabetes. In *Uppsala journal of medical sciences* 105 (2), pp. 125–133. DOI: 10.1517/03009734000000059.
- Berger, Constantin; Bjørlykke, Yngvild; Hahn, Lukas; Mühlemann, Markus; Kress, Sebastian; Walles, Heike et al. (2020): Matrix decoded - A pancreatic extracellular matrix with organ specific cues guiding human iPSC differentiation. In *Biomaterials* 244, p. 119766. DOI: 10.1016/j.biomaterials.2020.119766.
- Bertau, Martin; Mosekilde, Erik; Westerhoff, Hans V. (2007): *Biosimulation in Drug Development*: Wiley.
- Bock, Christoph; Kiskinis, Evangelos; Verstappen, Griet; Gu, Hongcang; Boulting, Gabriella; Smith, Zachary D. et al. (2011): Reference Maps of human ES and iPS cell variation enable high-throughput characterization of pluripotent cell lines. In *Cell* 144 (3), pp. 439–452. DOI: 10.1016/j.cell.2010.12.032.
- Bone, Heather K.; Nelson, Adam S.; Goldring, Christopher E.; Tosh, David; Welham, Melanie J. (2011): A novel chemically directed route for the generation of definitive endoderm from human embryonic stem cells based on inhibition of GSK-3. In *Journal of Cell Science* 124 (Pt 12), pp. 1992–2000. DOI: 10.1242/jcs.081679.
- Bonfanti, Paola; Nobecourt, Estelle; Oshima, Masaya; Albagli-Curiel, Olivier; Laurysens, Veerle; Stangé, Geert et al. (2015): Ex Vivo Expansion and Differentiation of Human and Mouse Fetal Pancreatic Progenitors Are Modulated by Epidermal Growth Factor. In *Stem cells and development* 24 (15), pp. 1766–1778. DOI: 10.1089/scd.2014.0550.
- Bonnans, Caroline; Chou, Jonathan; Werb, Zena (2014): Remodelling the extracellular matrix in development and disease. In *Nat Rev Mol Cell Biol* 15 (12), pp. 786–801. DOI: 10.1038/nrm3904.
- Bossard, Carine; van den Berghe, Loic; Laurell, Henrik; Castano, Caroline; Cerutti, Martine; Prats, Anne-Catherine; Prats, Hervé (2004): Antiangiogenic properties of fibstatin, an extracellular FGF-2-binding polypeptide. In *Cancer research* 64 (20), pp. 7507–7512. DOI: 10.1158/0008-5472.CAN-04-0287.

- Bouchi, Ryotaro; Foo, Kylie S.; Hua, Haiqing; Tsuchiya, Kyoichiro; Ohmura, Yoshiaki; Sandoval, P. Rodrigo et al. (2014): FOXO1 inhibition yields functional insulin-producing cells in human gut organoid cultures. In *Nat Commun* 5 (1), p. 4242. DOI: 10.1038/ncomms5242.
- Brafman, D. A.; Phung, C.; Kumar, N.; Willert, K. (2013): Regulation of endodermal differentiation of human embryonic stem cells through integrin-ECM interactions. In *Cell Death Differ* 20 (3), pp. 369–381. DOI: 10.1038/cdd.2012.138.
- Brissova, Marcela; Fowler, Michael J.; Nicholson, Wendell E.; Chu, Anita; Hirshberg, Boaz; Harlan, David M.; Powers, Alvin C. (2005): Assessment of human pancreatic islet architecture and composition by laser scanning confocal microscopy. In *The journal of histochemistry and cytochemistry : official journal of the Histochemistry Society* 53 (9), pp. 1087–1097. DOI: 10.1369/jhc.5C6684.2005.
- Brown, Stephanie; Teo, Adrian; Pauklin, Siim; Hannan, Nicholas; Cho, Candy H-H; Lim, Bing et al. (2011): Activin/Nodal signaling controls divergent transcriptional networks in human embryonic stem cells and in endoderm progenitors. In *Stem cells (Dayton, Ohio)* 29 (8), pp. 1176–1185. DOI: 10.1002/stem.666.
- de Carlo (2009): Pancreatic acellular matrix supports islet survival and function in a synthetic tubular device: In vitro and in vivo studies. In *Int J Mol Med* 25 (2), pp. 195–202. DOI: 10.3892/ijmm_00000330.
- Castaing, Muriel; Duvillié, Bertrand; Quemeneur, Eric; Basmaciogullari, Annie; Scharfmann, Raphael (2005): Ex vivo analysis of acinar and endocrine cell development in the human embryonic pancreas. In *Developmental dynamics : an official publication of the American Association of Anatomists* 234 (2), pp. 339–345. DOI: 10.1002/dvdy.20547.
- Cebola, Inês; Rodríguez-Seguí, Santiago A.; Cho, Candy H-H; Bessa, José; Rovira, Meritxell; Luengo, Mario et al. (2015): TEAD and YAP regulate the enhancer network of human embryonic pancreatic progenitors. In *Nat Cell Biol* 17 (5), pp. 615–626. DOI: 10.1038/ncb3160.
- Chambers, Ian; Colby, Douglas; Robertson, Morag; Nichols, Jennifer; Lee, Sonia; Tweedie, Susan; Smith, Austin (2003): Functional Expression Cloning of Nanog, a Pluripotency Sustaining Factor in Embryonic Stem Cells. In *Cell* 113 (5), pp. 643–655. DOI: 10.1016/s0092-8674(03)00392-1.
- Chang, Lei; Azzolin, Luca; Di Biagio, Daniele; Zanconato, Francesca; Battilana, Giusy; Lucon Xiccatto, Romy et al. (2018): The SWI/SNF complex is a mechanoregulated inhibitor of YAP and TAZ. In *Nature* 563 (7730), pp. 265–269. DOI: 10.1038/s41586-018-0658-1.
- Cheng, Jennifer Y. C.; Raghunath, Michael; Whitelock, John; Poole-Warren, Laura (2011): Matrix components and scaffolds for sustained islet function. In *Tissue engineering. Part B, Reviews* 17 (4), pp. 235–247. DOI: 10.1089/ten.TEB.2011.0004.
- Collombat, Patrick; Hecksher-Sørensen, Jacob; Broccoli, Vania; Krull, Jens; Ponte, Ilaria; Mundiger, Tabea et al. (2005): The simultaneous loss of Arx and Pax4 genes promotes a somatostatin-producing cell fate specification at the expense of the alpha- and beta-cell lineages in the mouse endocrine pancreas. In *Development (Cambridge, England)* 132 (13), pp. 2969–2980. DOI: 10.1242/dev.01870.
- Collombat, Patrick; Mansouri, Ahmed; Hecksher-Sorensen, Jacob; Serup, Palle; Krull, Jens; Gradwohl, Gerard; Gruss, Peter (2003): Opposing actions of Arx and Pax4 in endocrine pancreas development. In *Genes & development* 17 (20), pp. 2591–2603. DOI: 10.1101/gad.269003.
- Cooper-Jones, Brit; Ford, Caitlyn (Eds.) (2017): CADTH Issues in Emerging Health Technologies: Canadian Agency for Drugs and Technologies in Health.
- Corning (2020): Corning® Matrigel® Matrix - Frequently Asked Questions. Available online at <https://www.corning.com/catalog/cls/documents/faqs/CLS-DL-CC-026.pdf>, checked on 12/17/2020.
- Coué, Martine; Brenner, Stephen L.; Spector, Ilan; Korn, Edward D. (1987): Inhibition of actin polymerization by latrunculin A. In *FEBS Letters* 213 (2), pp. 316–318. DOI: 10.1016/0014-5793(87)81513-2.
- Crapo, Peter M.; Gilbert, Thomas W.; Badylak, Stephen F. (2011): An overview of tissue and whole organ decellularization processes. In *Biomaterials* 32 (12), pp. 3233–3243. DOI: 10.1016/j.biomaterials.2011.01.057.
- Cross, S. E.; Vaughan, R. H.; Willcox, A. J.; McBride, A. J.; Abraham, A. A.; Han, B. et al. (2017): Key Matrix Proteins Within the Pancreatic Islet Basement Membrane Are Differentially Digested During Human Islet Isolation. In *American journal of transplantation : official journal of the American Society of Transplantation and the American Society of Transplant Surgeons* 17 (2), pp. 451–461. DOI: 10.1111/ajt.13975.
- Dakhore, Sushrut; Nayer, Bhavana; Hasegawa, Kouichi (2018): Human Pluripotent Stem Cell Culture: Current Status, Challenges, and Advancement. In *Stem cells international* 2018, p. 7396905. DOI: 10.1155/2018/7396905.
- Dalby, Matthew J.; Gadegaard, Nikolaj; Orefo, Richard O. C. (2014): Harnessing nanotopography and integrin-matrix interactions to influence stem cell fate. In *Nature materials* 13 (6), pp. 558–569. DOI: 10.1038/nmat3980.
- D'Amour, Kevin A.; Agulnick, Alan D.; Eliazer, Susan; Kelly, Olivia G.; Kroon, Evert; Baetge, Emmanuel E. (2005): Efficient differentiation of human embryonic stem cells to definitive endoderm. In *Nature biotechnology* 23 (12), pp. 1534–1541. DOI: 10.1038/nbt1163.

- D'Amour, Kevin A.; Bang, Anne G.; Eliazar, Susan; Kelly, Olivia G.; Agulnick, Alan D.; Smart, Nora G. et al. (2006): Production of pancreatic hormone-expressing endocrine cells from human embryonic stem cells. In *Nature biotechnology* 24 (11), pp. 1392–1401. DOI: 10.1038/nbt1259.
- Daneman, Denis (2006): Type 1 diabetes. In *The Lancet* 367 (9513), pp. 847–858. DOI: 10.1016/S0140-6736(06)68341-4.
- Danielsson, Angelika; Pontén, Fredrik; Fagerberg, Linn; Hallström, Björn M.; Schwenk, Jochen M.; Uhlén, Mathias et al. (2014): The human pancreas proteome defined by transcriptomics and antibody-based profiling. In *PLOS ONE* 9 (12), e115421. DOI: 10.1371/journal.pone.0115421.
- D'Antonio, Matteo; Woodruff, Grace; Nathanson, Jason L.; D'Antonio-Chronowska, Agnieszka; Arias, Angelo; Matsui, Hiroko et al. (2017): High-Throughput and Cost-Effective Characterization of Induced Pluripotent Stem Cells. *Stem Cell Reports*, 8(4), 1101–1111. In *Stem cell reports* 8 (4), pp. 1101–1111. DOI: 10.1016/J.STEMCR.2017.03.011.
- Daoud, Jamal; Rosenberg, Lawrence; Tabrizian, Maryam (2010): Pancreatic islet culture and preservation strategies: advances, challenges, and future outlook. In *Cell transplantation* 19 (12), pp. 1523–1535. DOI: 10.3727/096368910X515872.
- Davenport, Claudia; Diekmann, Ulf; Budde, Insa; Detering, Nora; Naujok, Ortwin (2016): Anterior-Posterior Patterning of Definitive Endoderm Generated from Human Embryonic Stem Cells Depends on the Differential Signaling of Retinoic Acid, Wnt-, and BMP-Signaling. In *Stem cells (Dayton, Ohio)* 34 (11), pp. 2635–2647. DOI: 10.1002/stem.2428.
- Davis, Nicolynn E.; Beenken-Rothkopf, Liese N.; Mirsoian, Annie; Kojic, Nikola; Kaplan, David L.; Barron, Annelise E.; Fontaine, Magali J. (2012): Enhanced function of pancreatic islets co-encapsulated with ECM proteins and mesenchymal stromal cells in a silk hydrogel. In *Biomaterials* 33 (28), pp. 6691–6697. DOI: 10.1016/j.biomaterials.2012.06.015.
- del Rio, Armando; Perez-Jimenez, Raul; Liu, Ruchuan; Roca-Cusachs, Pere; Fernandez, Julio M.; Sheetz, Michael P. (2009): Stretching single talin rod molecules activates vinculin binding. In *Science* 323 (5914), pp. 638–641. DOI: 10.1126/science.1162912.
- Dor, Yuval; Brown, Juliana; Martinez, Olga I.; Melton, Douglas A. (2004): Adult pancreatic beta-cells are formed by self-duplication rather than stem-cell differentiation. In *Nature* 429 (6987), pp. 41–46. DOI: 10.1038/nature02520.
- Doyle, Andrew D.; Yamada, Kenneth M. (2016): Mechanosensing via cell-matrix adhesions in 3D microenvironments. In *Experimental Cell Research* 343 (1), pp. 60–66. DOI: 10.1016/j.yexcr.2015.10.033.
- Duca, Lindsey M.; Reboussin, Beth A.; Pihoker, Catherine; Imperatore, Giuseppina; Saydah, Sharon; Mayer-Davis, Elizabeth et al. (2019): Diabetic ketoacidosis at diagnosis of type 1 diabetes and glycemic control over time: The SEARCH for diabetes in youth study. In *Pediatric diabetes* 20 (2), pp. 172–179. DOI: 10.1111/pedi.12809.
- Dyballa, Michael P.; Hara, Manami (2019): Heterogeneity of the Human Pancreatic Islet. In *Diabetes* 68 (6), pp. 1230–1239. DOI: 10.2337/db19-0072.
- Eguchi, Goro; Kodama, Ryuji (1993): Transdifferentiation. In *Current Opinion in Cell Biology* 5 (6), pp. 1023–1028. DOI: 10.1016/0955-0674(93)90087-7.
- El, Kimberley; Campbell, Jonathan E. (2020): The role of GIP in α -cells and glucagon secretion. In *Peptides* 125, p. 170213. DOI: 10.1016/j.peptides.2019.170213.
- Elebring, Erik; Kuna, Vijay K.; Kvarnström, Niclas; Sumitran-Holgersson, Suchitra (2017): Cold-perfusion decellularization of whole-organ porcine pancreas supports human fetal pancreatic cell attachment and expression of endocrine and exocrine markers. In *Journal of tissue engineering* 8, 2041731417738145. DOI: 10.1177/2041731417738145.
- Elosegui-Artola, Alberto; Andreu, Ion; Beedle, Amy E. M.; Lezamiz, Ainhoa; Uroz, Marina; Kosmalska, Anita J. et al. (2017): Force Triggers YAP Nuclear Entry by Regulating Transport across Nuclear Pores. In *Cell* 171 (6), 1397–1410.e14. DOI: 10.1016/j.cell.2017.10.008.
- Engler, Adam J.; Sen, Shamik; Sweeney, H. Lee; Discher, Dennis E. (2006): Matrix elasticity directs stem cell lineage specification. In *Cell* 126 (4), pp. 677–689. DOI: 10.1016/j.cell.2006.06.044.
- Frale, Stephanie I.; Wu, Pei-Hsun; He, Lijuan; Feng, Yunfeng; Krisnamurthy, Ranjini; Longmore, Gregory D.; Wirtz, Denis (2015): Three-dimensional matrix fiber alignment modulates cell migration and MT1-MMP utility by spatially and temporally directing protrusions. In *Sci Rep* 5 (1), p. 14580. DOI: 10.1038/srep14580.
- Freckmann, Guido; Hagenlocher, Sven; Baumstark, Annette; Jendrike, Nina; Gillen, Ralph C.; Rössner, Katja; Haug, Cornelia (2007): Continuous glucose profiles in healthy subjects under everyday life conditions and after different meals. In *Journal of diabetes science and technology (Online)* 1 (5), pp. 695–703. DOI: 10.1177/193229680700100513.
- Furuyama, Kenichiro; Chera, Simona; van Gurp, Léon; Oropeza, Daniel; Ghila, Luiza; Damond, Nicolas et al. (2019): Diabetes relief in mice by glucose-sensing insulin-secreting human α -cells. In *Nature* 567 (7746), pp. 43–48. DOI: 10.1038/s41586-019-0942-8.

- Galivo, Feorillo; Benedetti, Eric; Wang, Yuhan; Pelz, Carl; Schug, Jonathan; Kaestner, Klaus H.; Grompe, Markus (2017): Reprogramming human gallbladder cells into insulin-producing β -like cells. In *PLOS ONE* 12 (8), e0181812. DOI: 10.1371/journal.pone.0181812.
- Galli, Alessandra; Algerta, Marku; Marciani, Paola; Schulte, Carsten; Lenardi, Cristina; Milani, Paolo et al. (2020): Shaping Pancreatic β -Cell Differentiation and Functioning: The Influence of Mechanotransduction. In *Cells* 9 (2), p. 413. DOI: 10.3390/cells9020413.
- Gan, Wan Jun; Do, Oanh Hoang; Cottle, Louise; Ma, Wei; Kosobrodova, Elena; Cooper-White, Justin et al. (2018): Local Integrin Activation in Pancreatic β Cells Targets Insulin Secretion to the Vasculature. In *Cell reports* 24 (11), 2819-2826.e3. DOI: 10.1016/j.celrep.2018.08.035.
- Gefen-Halevi, Shiraz; Rachmut, Itzhak H.; Molakandov, Kfir; Berneman, Dana; Mor, Eytan; Meivar-Levy, Irit; Ferber, Sarah (2010): NKX6.1 promotes PDX-1-induced liver to pancreatic β -cells reprogramming. In *Cellular reprogramming* 12 (6), pp. 655–664. DOI: 10.1089/cell.2010.0030.
- Goh, K. L.; Yang, J. T.; Hynes, R. O. (1997): Mesodermal defects and cranial neural crest apoptosis in alpha5 integrin-null embryos. In *Development (Cambridge, England)* 124 (21), pp. 4309–4319. Available online at <https://dev.biologists.org/content/124/21/4309.short>.
- Goh, Saik-Kia; Bertera, Suzanne; Olsen, Phillip; Candiello, Joseph E.; Halfter, Willi; Uechi, Guy et al. (2013): Perfusion-decellularized pancreas as a natural 3D scaffold for pancreatic tissue and whole organ engineering. In *Biomaterials* 34 (28), pp. 6760–6772. DOI: 10.1016/j.biomaterials.2013.05.066.
- Gouzi, Mathieu; Kim, Yung Hae; Katsumoto, Keiichi; Johansson, Kerstin; Grapin-Botton, Anne (2011): Neurogenin3 initiates stepwise delamination of differentiating endocrine cells during pancreas development. In *Developmental dynamics : an official publication of the American Association of Anatomists* 240 (3), pp. 589–604. DOI: 10.1002/dvdy.22544.
- Gu, Guoqiang; Dubauskaite, Jolanta; Melton, Douglas A. (2002): Direct evidence for the pancreatic lineage: NGN3+ cells are islet progenitors and are distinct from duct progenitors. In *Development (Cambridge, England)* 129 (10), pp. 2447–2457.
- Guimarães, Carlos F.; Gasperini, Luca; Marques, Alexandra P.; Reis, Rui L. (2020): The stiffness of living tissues and its implications for tissue engineering. In *Nat Rev Mater* 5 (5), pp. 351–370. DOI: 10.1038/s41578-019-0169-1.
- Gylfe, Erik (2016): Glucose control of glucagon secretion-'There's a brand-new gimmick every year'. In *Uppsala journal of medical sciences* 121 (2), pp. 120–132. DOI: 10.3109/03009734.2016.1154905.
- Habegger, Kirk M.; Heppner, Kristy M.; Geary, Nori; Bartness, Timothy J.; DiMarchi, Richard; Tschöp, Matthias H. (2010): The metabolic actions of glucagon revisited. In *Nat Rev Endocrinol* 6 (12), pp. 689–697. DOI: 10.1038/nrendo.2010.187.
- Hald, Jacob; Hjorth, J.Peter; German, Michael S.; Madsen, Ole D.; Serup, Palle; Jensen, Jan (2003): Activated Notch1 prevents differentiation of pancreatic acinar cells and attenuate endocrine development. In *Developmental Biology* 260 (2), pp. 426–437. DOI: 10.1016/S0012-1606(03)00326-9.
- Halper, Jaroslava; Kjaer, Michael (2014): Basic components of connective tissues and extracellular matrix: elastin, fibrillin, fibulins, fibrinogen, fibronectin, laminin, tenascins and thrombospondins. In *Advances in experimental medicine and biology* 802, pp. 31–47. DOI: 10.1007/978-94-007-7893-1_3.
- Hamidi, Hellyeh; Ivaska, Johanna (2018): Every step of the way: integrins in cancer progression and metastasis. In *Nature reviews. Cancer* 18 (9), pp. 533–548. DOI: 10.1038/s41568-018-0038-z.
- Hauge-Evans, Astrid C.; King, Aileen J.; Carmignac, Danielle; Richardson, Carolyn C.; Robinson, Iain C. A. F.; Low, Malcolm J. et al. (2009): Somatostatin secreted by islet delta-cells fulfills multiple roles as a paracrine regulator of islet function. In *Diabetes* 58 (2), pp. 403–411. DOI: 10.2337/db08-0792.
- Hellemans, Jan; Mortier, Geert; Paepe, Anne de; Speleman, Frank; Vandesompele, Jo (2007): qBase relative quantification framework and software for management and automated analysis of real-time quantitative PCR data. In *Genome Biol* 8 (2), R19. DOI: 10.1186/gb-2007-8-2-r19.
- Hellinger, Eva; Veszelka, Szilvia; Tóth, Andrea E.; Walter, Fruzsina; Kittel, Agnes; Bakk, Mónika Laura et al. (2012): Comparison of brain capillary endothelial cell-based and epithelial (MDCK-MDR1, Caco-2, and VB-Caco-2) cell-based surrogate blood-brain barrier penetration models. In *European journal of pharmaceuticals and biopharmaceutics : official journal of Arbeitsgemeinschaft fur Pharmazeutische Verfahrenstechnik e.V* 82 (2), pp. 340–351. DOI: 10.1016/j.ejpb.2012.07.020.
- Henquin, J. C.; Ravier, M. A.; Nenquin, M.; Jonas, J. C.; Gilon, P. (2003): Hierarchy of the beta-cell signals controlling insulin secretion. In *European journal of clinical investigation* 33 (9), pp. 742–750. DOI: 10.1046/j.1365-2362.2003.01207.x.
- Hogrebe, Nathaniel J.; Augsornworawat, Punng; Maxwell, Kristina G.; Velazco-Cruz, Leonardo; Millman, Jeffrey R. (2020): Targeting the cytoskeleton to direct pancreatic differentiation of human pluripotent stem cells. In *Nat Biotechnol* 38 (4), pp. 460–470. DOI: 10.1038/s41587-020-0430-6.
- Horiguchi, Masahito; Ota, Mitsuhiko; Rifkin, Daniel B. (2012): Matrix control of transforming growth factor- β function. In *J Biochem* 152 (4), pp. 321–329. DOI: 10.1093/jb/mvs089.

- Hovorka, Roman (2011): Closed-loop insulin delivery: from bench to clinical practice. In *Nat Rev Endocrinol* 7 (7), pp. 385–395. DOI: 10.1038/nrendo.2011.32.
- Huypens, P.; Ling, Z.; Pipeleers, D.; Schuit, F. (2000): Glucagon receptors on human islet cells contribute to glucose competence of insulin release. In *Diabetologia* 43 (8), pp. 1012–1019. DOI: 10.1007/s001250051484.
- International Diabetes Federation (2019): IDF Diabetes Atlas 2019. 9th edition. Belgium: International Diabetes Federation, 2019.
- Itoh, Masayuki; Takizawa, Yuji; Hanai, Sae; Okazaki, Shin; Miyata, Rie; Inoue, Takeshi et al. (2010): Partial loss of pancreas endocrine and exocrine cells of human ARX-null mutation: consideration of pancreas differentiation. In *Differentiation; research in biological diversity* 80 (2-3), pp. 118–122. DOI: 10.1016/j.diff.2010.05.003.
- Jacobs-Tulleneers-Thevissen, D.; Chintinne, M.; Ling, Z.; Gillard, P.; Schoonjans, L.; Delvaux, G. et al. (2013): Sustained function of alginate-encapsulated human islet cell implants in the peritoneal cavity of mice leading to a pilot study in a type 1 diabetic patient. In *Diabetologia* 56 (7), pp. 1605–1614. DOI: 10.1007/s00125-013-2906-0.
- Jennings, Rachel E.; Berry, Andrew A.; Kirkwood-Wilson, Rebecca; Roberts, Neil A.; Hearn, Thomas; Salisbury, Rachel J. et al. (2013): Development of the human pancreas from foregut to endocrine commitment. In *Diabetes* 62 (10), pp. 3514–3522. DOI: 10.2337/db12-1479.
- Johansson, Kerstin A.; Dursun, Umut; Jordan, Nathalie; Gu, Guoqiang; Beermann, Friedrich; Gradwohl, Gérard; Grapin-Botton, Anne (2007): Temporal control of neurogenin3 activity in pancreas progenitors reveals competence windows for the generation of different endocrine cell types. In *Developmental cell* 12 (3), pp. 457–465. DOI: 10.1016/j.devcel.2007.02.010.
- Jurgens, Catherine A.; Toukatly, Mirna N.; Fligner, Corinne L.; Udayasankar, Jayalakshmi; Subramanian, Shoba L.; Zraika, Sakeneh et al. (2011): β -cell loss and β -cell apoptosis in human type 2 diabetes are related to islet amyloid deposition. In *The American journal of pathology* 178 (6), pp. 2632–2640. DOI: 10.1016/j.ajpath.2011.02.036.
- Kahn, S. E.; Prigeon, R. L.; McCulloch, D. K.; Boyko, E. J.; Bergman, R. N.; Schwartz, M. W. et al. (1993): Quantification of the relationship between insulin sensitivity and beta-cell function in human subjects. Evidence for a hyperbolic function. In *Diabetes* 42 (11), pp. 1663–1672. DOI: 10.2337/diab.42.11.1663.
- Kahn, Steven E.; Cooper, Mark E.; Del Prato, Stefano (2014): Pathophysiology and treatment of type 2 diabetes: perspectives on the past, present, and future. In *The Lancet* 383 (9922), pp. 1068–1083. DOI: 10.1016/S0140-6736(13)62154-6.
- Kaido, Thomas; Yebra, Mayra; Cirulli, Vincenzo; Rhodes, Christopher; Diaferia, Giuseppe; Montgomery, Anthony M. (2006): Impact of defined matrix interactions on insulin production by cultured human beta-cells: effect on insulin content, secretion, and gene transcription. In *Diabetes* 55 (10), pp. 2723–2729. DOI: 10.2337/db06-0120.
- Kanak, Mazhar A.; Takita, Morihito; Kunnathodi, Faisal; Lawrence, Michael C.; Levy, Marlon F.; Naziruddin, Bashoo (2014): Inflammatory response in islet transplantation. In *International journal of endocrinology* 2014, p. 451035. DOI: 10.1155/2014/451035.
- Katsuki, Yusuke; Yagi, Hiroshi; Okitsu, Teru; Kitago, Minoru; Tajima, Kazuki; Kadota, Yoshie et al. (2016): Endocrine pancreas engineered using porcine islets and partial pancreatic scaffolds. In *Pancreatology* 16 (5), pp. 922–930. DOI: 10.1016/j.pan.2016.06.007.
- Kechagia, Jenny Z.; Ivaska, Johanna; Roca-Cusachs, Pere (2019): Integrins as biomechanical sensors of the microenvironment. In *Nat Rev Mol Cell Biol* 20 (8), pp. 457–473. DOI: 10.1038/s41580-019-0134-2.
- Kim, Abraham; Miller, Kevin; Jo, Junghyo; Kilimnik, German; Wojcik, Pawel; Hara, Manami (2009): Islet architecture: A comparative study. In *Islets* 1 (2), pp. 129–136. DOI: 10.4161/isl.1.2.9480.
- Knauss, R.; Schiller, J.; Fleischer, G.; Krger, J.; Arnold, K. (1999): Self-diffusion of water in cartilage and cartilage components as studied by pulsed field gradient NMR. In *Magn. Reson. Med.* 41 (2), pp. 285–292. DOI: 10.1002/(sici)1522-2594(199902)41:2<285::aid-mrm11>3.0.co;2-3.
- Knobeloch, Tracy; Abadi, Sakineh Esmaeili Mohsen; Bruns, Joseph; Zustiak, Silviya Petrova; Kwon, Guim (2017): Injectable Polyethylene Glycol Hydrogel for Islet Encapsulation: an in vitro and in vivo Characterization. In *Biomedical physics & engineering express* 3. DOI: 10.1088/2057-1976/aa742b.
- Kopp, Janel L.; Dubois, Claire L.; Schaffer, Ashleigh E.; Hao, Ergeng; Shih, Hung Ping; Seymour, Philip A. et al. (2011): Sox9+ ductal cells are multipotent progenitors throughout development but do not produce new endocrine cells in the normal or injured adult pancreas. In *Development* 138 (4), pp. 653–665. DOI: 10.1242/dev.056499.
- Kopp, Janel L.; Ormsbee, Briana D.; Desler, Michelle; Rizzino, Angie (2008): Small increases in the level of Sox2 trigger the differentiation of mouse embryonic stem cells. In *Stem cells (Dayton, Ohio)* 26 (4), pp. 903–911. DOI: 10.1634/stemcells.2007-0951.

- Kress, Sebastian; Baur, Johannes; Otto, Christoph; Burkard, Natalie; Braspenning, Joris; Walles, Heike et al. (2018): Evaluation of a Miniaturized Biologically Vascularized Scaffold in vitro and in vivo. In *Sci Rep* 8 (1), p. 4719. DOI: 10.1038/s41598-018-22688-w.
- Kreuder, Anna-Elisabeth; Bolaños-Rosales, Aramis; Palmer, Christopher; Thomas, Alexander; Geiger, Michel-Andreas; Lam, Tobias et al. (2020): Inspired by the human placenta: a novel 3D bioprinted membrane system to create barrier models. In *Sci Rep* 10 (1), p. 15606. DOI: 10.1038/s41598-020-72559-6.
- Kroon, Evert; Martinson, Laura A.; Kadoya, Kuniko; Bang, Anne G.; Kelly, Olivia G.; Eliazar, Susan et al. (2008): Pancreatic endoderm derived from human embryonic stem cells generates glucose-responsive insulin-secreting cells in vivo. In *Nat Biotechnol* 26 (4), pp. 443–452. DOI: 10.1038/nbt1393.
- Kruegel, Jenny; Miosge, Nicolai (2010): Basement membrane components are key players in specialized extracellular matrices. In *Cell. Mol. Life Sci.* 67 (17), pp. 2879–2895. DOI: 10.1007/s00018-010-0367-x.
- Kuehn, Carina; Dubiel, Evan A.; Sabra, Georges; Vermette, Patrick (2012): Culturing INS-1 cells on CDPGYIGSR-, RGD- and fibronectin surfaces improves insulin secretion and cell proliferation. In *Acta biomaterialia* 8 (2), pp. 619–626. DOI: 10.1016/j.actbio.2011.10.036.
- Kumar, M. (2003): Pancreas specification: a budding question. In *Current Opinion in Genetics & Development* 13 (4), pp. 401–407. DOI: 10.1016/S0959-437X(03)00089-3.
- Kuna, Vijay Kumar; Kvarnström, Niclas; Elebring, Erik; Holgersson, Suchitra Sumitran (2018): Isolation and Decellularization of a Whole Porcine Pancreas. In *JoVE (Journal of Visualized Experiments)* (140), e58302. DOI: 10.3791/58302.
- Leavesley, David I.; Kashyap, Abhishek S.; Croll, Tristan; Sivaramakrishnan, Manaswini; Shokoohmand, Ali; Hollier, Brett G.; Upton, Zee (2013): Vitronectin—master controller or micromanager? In *IUBMB life* 65 (10), pp. 807–818. DOI: 10.1002/iub.1203.
- Lee, Gabsang; Kim, Hyesoo; Elkabetz, Yechiel; Al Shamy, George; Panagiotakos, Georgia; Barberi, Tiziano et al. (2007): Isolation and directed differentiation of neural crest stem cells derived from human embryonic stem cells. In *Nat Biotechnol* 25 (12), pp. 1468–1475. DOI: 10.1038/nbt1365.
- Lee, Kuen Yong; Mooney, David J. (2012): Alginate: properties and biomedical applications. In *Progress in polymer science* 37 (1), pp. 106–126. DOI: 10.1016/j.progpolymsci.2011.06.003.
- Lehuen, Agnès; Diana, Julien; Zaccone, Paola; Cooke, Anne (2010): Immune cell crosstalk in type 1 diabetes. In *Nat Rev Immunol* 10 (7), pp. 501–513. DOI: 10.1038/nri2787.
- Levental, Ilya; Georges, Penelope C.; Janmey, Paul A. (2007): Soft biological materials and their impact on cell function. In *Soft Matter* 3 (3), pp. 299–306. DOI: 10.1039/B610522J.
- Li, Dong; Zhou, Jiayi; Wang, Lu; Shin, Myung Eun; Su, Pei; Lei, Xiaohua et al. (2010): Integrated biochemical and mechanical signals regulate multifaceted human embryonic stem cell functions. In *The Journal of Cell Biology* 191 (3), pp. 631–644. DOI: 10.1083/jcb.201006094.
- Li, Yan; Liu, Meimei; Yan, Yuanwei; Yang, Shang-Tian (2014): Neural differentiation from pluripotent stem cells: The role of natural and synthetic extracellular matrix. In *World Journal of Stem Cells* 6 (1), pp. 11–23. DOI: 10.4252/wjsc.v6.i1.11.
- Liese N. Beenken-Rothkopf; Lindsay S. Karfeld-Sulzer; Nicolynn E. Davis; Ryan Forster; Annelise E. Barron; Magali J. Fontaine (2013): The Incorporation of Extracellular Matrix Proteins in Protein Polymer Hydrogels to Improve Encapsulated Beta-cell Function. In *Ann Clin Lab Sci* 43 (2), pp. 111–121.
- Lin, Chien-Chi; Anseth, Kristi S. (2009): PEG hydrogels for the controlled release of biomolecules in regenerative medicine. In *Pharmaceutical research* 26 (3), pp. 631–643. DOI: 10.1007/s11095-008-9801-2.
- Linke, Kirstin; Schanz, Johanna; Hansmann, Jan; Walles, Thorsten; Brunner, Herwig; Mertsching, Heike (2007): Engineered liver-like tissue on a capillarized matrix for applied research. In *Tissue engineering* 13 (11), pp. 2699–2707. DOI: 10.1089/ten.2006.0388.
- Liu, Gele; David, Brian T.; Trawczynski, Matthew; Fessler, Richard G. (2020): Advances in Pluripotent Stem Cells: History, Mechanisms, Technologies, and Applications. In *Stem Cell Rev and Rep* 16 (1), pp. 3–32. DOI: 10.1007/s12015-019-09935-x.
- Liu, Nanxin; Zhou, Mi; Zhang, Qi; Yong, Li; Zhang, Tao; Tian, Taoran et al. (2018): Effect of substrate stiffness on proliferation and differentiation of periodontal ligament stem cells. In *Cell Proliferation* 51 (5), e12478. DOI: 10.1111/cpr.12478.
- Liu, Xingyu; Yao, Yuying; Ding, Huiguo; Han, Chuanchun; Chen, Yuhan; Zhang, Yuan et al. (2016): USP21 deubiquitylates Nanog to regulate protein stability and stem cell pluripotency. In *Sig Transduct Target Ther* 1 (1), p. 16024. DOI: 10.1038/sigtrans.2016.24.
- Londono, Ricardo; Badylak, Stephen F. (2015): Biologic scaffolds for regenerative medicine: mechanisms of in vivo remodeling. In *Ann Biomed Eng* 43 (3), pp. 577–592. DOI: 10.1007/s10439-014-1103-8.

- Low, Jiun T.; Zavortink, Michael; Mitchell, Justin M.; Gan, Wan J.; Do, Oanh Hoang; Schwiening, Christof J. et al. (2014): Insulin secretion from beta cells in intact mouse islets is targeted towards the vasculature. In *Diabetologia* 57 (8), pp. 1655–1663. DOI: 10.1007/s00125-014-3252-6.
- Lucas-Clerc, C.; Massart, C.; Campion, J. P.; Launois, B.; Nicol, M. (1993): Long-term culture of human pancreatic islets in an extracellular matrix: morphological and metabolic effects. In *Molecular and Cellular Endocrinology* 94 (1), pp. 9–20. DOI: 10.1016/0303-7207(93)90046-M.
- Ludwig, Tenneille E.; Levenstein, Mark E.; Jones, Jeffrey M.; Berggren, W. Travis; Mitchen, Erika R.; Frane, Jennifer L. et al. (2006): Derivation of human embryonic stem cells in defined conditions. In *Nature biotechnology* 24 (2), pp. 185–187. DOI: 10.1038/nbt1177.
- Ma, Wu; Tavakoli, Tara; Derby, Eric; Serebryakova, Yevgeniya; Rao, Mahendra S.; Mattson, Mark P. (2008): Cell-extracellular matrix interactions regulate neural differentiation of human embryonic stem cells. In *BMC Dev Biol* 8 (1), p. 90. DOI: 10.1186/1471-213X-8-90.
- Magisson, Jordan; Sassi, Aladin; Xhema, Daela; Kobalyan, Aram; Gianello, Pierre; Mourer, Brice et al. (2020): Safety and function of a new pre-vascularized bioartificial pancreas in an allogeneic rat model. In *Journal of tissue engineering* 11, 2041731420924818. DOI: 10.1177/2041731420924818.
- Maldonado, Maricela; Luu, Rebecca J.; Ico, Gerardo; Ospina, Alex; Myung, Danielle; Shih, Hung Ping; Nam, Jin (2017): Lineage- and developmental stage-specific mechanomodulation of induced pluripotent stem cell differentiation. In *Stem Cell Res Ther* 8 (1), p. 216. DOI: 10.1186/s13287-017-0667-2.
- Mamidi, Anant; Prawiro, Christy; Seymour, Philip A.; Lichtenberg, Kristian Honnens de; Jackson, Abigail; Serup, Palle; Semb, Henrik (2018): Mechanosignalling via integrins directs fate decisions of pancreatic progenitors. In *Nature* 564 (7734), pp. 114–118. DOI: 10.1038/s41586-018-0762-2.
- Marín-Peñalver, Juan José; Martín-Timón, Iciar; Sevillano-Collantes, Cristina; Del Cañizo-Gómez, Francisco Javier (2016): Update on the treatment of type 2 diabetes mellitus. In *World journal of diabetes* 7 (17), pp. 354–395. DOI: 10.4239/wjd.v7.i17.354.
- Markert, Sebastian Matthias; Britz, Sebastian; Proppert, Sven; Lang, Marietta; Witvliet, Daniel; Mulcahy, Ben et al. (2016): Filling the gap: adding super-resolution to array tomography for correlated ultrastructural and molecular identification of electrical synapses at the *C. elegans* connectome. In *Neurophotonics* 3 (4), p. 41802. DOI: 10.1117/1.NPh.3.4.041802.
- Matsuoka, Taka-aki; Artner, Isabella; Henderson, Eva; Means, Anna; Sander, Maïke; Stein, Roland (2004): The MafA transcription factor appears to be responsible for tissue-specific expression of insulin. In *Proceedings of the National Academy of Sciences of the United States of America* 101 (9), pp. 2930–2933. DOI: 10.1073/pnas.0306233101.
- Miner, Jeffrey H.; Yurchenco, Peter D. (2004): Laminin functions in tissue morphogenesis. In *Annual review of cell and developmental biology* 20, pp. 255–284. DOI: 10.1146/annurev.cellbio.20.010403.094555.
- Mirmalek-Sani, Sayed-Hadi; Orlando, Giuseppe; McQuilling, John P.; Pareta, Rajesh; Mack, David L.; Salvatori, Marcus et al. (2013): Porcine pancreas extracellular matrix as a platform for endocrine pancreas bioengineering. In *Biomaterials* 34 (22), pp. 5488–5495. DOI: 10.1016/j.biomaterials.2013.03.054.
- Mirzaei, Hamed; Sahebkar, Amirhossein; Sichani, Laleh Shiri; Moridikia, Abdullah; Nazari, Sara; Sadri Nahand, Javid et al. (2018): Therapeutic application of multipotent stem cells. In *Journal of cellular physiology* 233 (4), pp. 2815–2823. DOI: 10.1002/jcp.25990.
- Mitsui, Kaoru; Tokuzawa, Yoshimi; Itoh, Hiroaki; Segawa, Kohichi; Murakami, Mirei; Takahashi, Kazutoshi et al. (2003): The Homeoprotein Nanog Is Required for Maintenance of Pluripotency in Mouse Epiblast and ES Cells. In *Cell* 113 (5), pp. 631–642. DOI: 10.1016/S0092-8674(03)00393-3.
- Miyatsuka, Takeshi; Kosaka, Yasuhiro; Kim, Hail; German, Michael S. (2011): Neurogenin3 inhibits proliferation in endocrine progenitors by inducing Cdkn1a. In *Proceedings of the National Academy of Sciences of the United States of America* 108 (1), pp. 185–190. DOI: 10.1073/pnas.1004842108.
- Miyazaki, Takamichi; Futaki, Sugiko; Hasegawa, Kouichi; Kawasaki, Miwa; Sanzen, Noriko; Hayashi, Maria et al. (2008): Recombinant human laminin isoforms can support the undifferentiated growth of human embryonic stem cells. In *Biochemical and biophysical research communications* 375 (1), pp. 27–32. DOI: 10.1016/j.bbrc.2008.07.111.
- Miyazaki, Takamichi; Futaki, Sugiko; Suemori, Hirofumi; Taniguchi, Yukimasa; Yamada, Masashi; Kawasaki, Miwa et al. (2012): Laminin E8 fragments support efficient adhesion and expansion of dissociated human pluripotent stem cells. In *Nat Commun* 3 (1), p. 1236. DOI: 10.1038/ncomms2231.
- Morris, Andrew P.; Voight, Benjamin F.; Teslovich, Tanya M.; Ferreira, Teresa; Segrè, Ayellet V.; Steinthorsdottir, Valgerdur et al. (2012): Large-scale association analysis provides insights into the genetic architecture and pathophysiology of type 2 diabetes. In *Nature genetics* 44 (9), pp. 981–990. DOI: 10.1038/ng.2383.

- Mouw, Janna K.; Ou, Guanqing; Weaver, Valerie M. (2014): Extracellular matrix assembly: a multiscale deconstruction. In *Nat Rev Mol Cell Biol* 15 (12), pp. 771–785. DOI: 10.1038/nrm3902.
- Murtaugh, L. Charles; Stanger, Ben Z.; Kwan, Kristen M.; Melton, Douglas A. (2003): Notch signaling controls multiple steps of pancreatic differentiation. In *Proceedings of the National Academy of Sciences of the United States of America* 100 (25), pp. 14920–14925. DOI: 10.1073/pnas.2436557100.
- Musah, Samira; Morin, Stephen A.; Wrighton, Paul J.; Zwick, Daniel B.; Jin, Song; Kiessling, Laura L. (2012): Glycosaminoglycan-binding hydrogels enable mechanical control of human pluripotent stem cell self-renewal. In *ACS nano* 6 (11), pp. 10168–10177. DOI: 10.1021/nn3039148.
- Nair, Gopika G.; Liu, Jennifer S.; Russ, Holger A.; Tran, Stella; Saxton, Michael S.; Chen, Richard et al. (2019): Recapitulating endocrine cell clustering in culture promotes maturation of human stem-cell-derived β cells. In *Nat Cell Biol* 21 (2), pp. 263–274. DOI: 10.1038/s41556-018-0271-4.
- Nalbach, Lisa; Roma, Leticia P.; Schmitt, Beate M.; Becker, Vivien; Körbel, Christina; Wrublewsky, Selina et al. (2020): Improvement of islet transplantation by the fusion of islet cells with functional blood vessels. In *EMBO molecular medicine*, e12616. DOI: 10.15252/emmm.202012616.
- Napierala, H.; Hillebrandt, K-H; Haep, N.; Tang, P.; Tintemann, M.; Gassner, J. et al. (2017): Engineering an endocrine Neo-Pancreas by repopulation of a decellularized rat pancreas with islets of Langerhans. In *Sci Rep* 7 (1), p. 41777. DOI: 10.1038/srep41777.
- Nguyen, Anh Tuan; Sathe, Sharvari R.; Yim, Evelyn K. F. (2016): From nano to micro: topographical scale and its impact on cell adhesion, morphology and contact guidance. In *Journal of physics. Condensed matter : an Institute of Physics journal* 28 (18), p. 183001. DOI: 10.1088/0953-8984/28/18/183001.
- Nicolle, S.; Noguier, L.; Paliere, J-F (2013): Shear mechanical properties of the porcine pancreas: experiment and analytical modelling. In *Journal of the mechanical behavior of biomedical materials* 26, pp. 90–97. DOI: 10.1016/j.jmbbm.2013.05.029.
- Nir, Tomer; Melton, Douglas A.; Dor, Yuval (2007): Recovery from diabetes in mice by beta cell regeneration. In *The Journal of clinical investigation* 117 (9), pp. 2553–2561. DOI: 10.1172/JCI32959.
- Niwa, Hitoshi; Toyooka, Yayoi; Shimosato, Daisuke; Strumpf, Dan; Takahashi, Kadue; Yagi, Rika; Rossant, Janet (2005): Interaction between Oct3/4 and Cdx2 determines trophoblast differentiation. In *Cell* 123 (5), pp. 917–929. DOI: 10.1016/j.cell.2005.08.040.
- Nyitray, Crystal E.; Chavez, Miquella G.; Desai, Tejal A. (2014): Compliant 3D microenvironment improves β -cell cluster insulin expression through mechanosensing and β -catenin signaling. In *Tissue engineering. Part A* 20 (13-14), pp. 1888–1895. DOI: 10.1089/ten.TEA.2013.0692.
- Oliver-Krasinski, Jennifer M.; Kasner, Margaret T.; Yang, Juxiang; Crutchlow, Michael F.; Rustgi, Anil K.; Kaestner, Klaus H.; Stoffers, Doris A. (2009): The diabetes gene Pdx1 regulates the transcriptional network of pancreatic endocrine progenitor cells in mice. In *The Journal of clinical investigation* 119 (7), pp. 1888–1898. DOI: 10.1172/JCI37028.
- Oria, Roger; Wiegand, Tina; Escribano, Jorge; Elosegui-Artola, Alberto; Uriarte, Juan Jose; Moreno-Pulido, Cristian et al. (2017): Force loading explains spatial sensing of ligands by cells. In *Nature* 552 (7684), pp. 219–224. DOI: 10.1038/nature24662.
- Pagliuca, Felicia W.; Millman, Jeffrey R.; Gürtler, Mads; Segel, Michael; van Dervort, Alana; Ryu, Jennifer Hyoje et al. (2014): Generation of functional human pancreatic β cells in vitro. In *Cell* 159 (2), pp. 428–439. DOI: 10.1016/j.cell.2014.09.040.
- Pan, Guangjin; Thomson, James A. (2007): Nanog and transcriptional networks in embryonic stem cell pluripotency. In *Cell Res* 17 (1), pp. 42–49. DOI: 10.1038/sj.cr.7310125.
- Papatheodorou, Konstantinos; Banach, Maciej; Bekiari, Eleni; Rizzo, Manfredi; Edmonds, Michael (2018): Complications of Diabetes 2017. In *Journal of Diabetes Research* 2018, p. 3086167. DOI: 10.1155/2018/3086167.
- Parnaud, Geraldine; Hammar, Eva; Rouiller, Dominique G.; Armanet, Mathieu; Halban, Philippe A.; Bosco, Domenico (2006): Blockade of beta1 integrin-laminin-5 interaction affects spreading and insulin secretion of rat beta-cells attached on extracellular matrix. In *Diabetes* 55 (5), pp. 1413–1420. DOI: 10.2337/db05-1388.
- Peloso, Andrea; Urbani, Luca; Cravedi, Paolo; Katari, Ravi; Maghsoudlou, Panagiotis; Fallas, Mario Enrique Alvarez et al. (2016): The Human Pancreas as a Source of Protolerogenic Extracellular Matrix Scaffold for a New-generation Bioartificial Endocrine Pancreas. In *Annals of surgery* 264 (1), pp. 169–179. DOI: 10.1097/SLA.0000000000001364.
- Perl, S.; Kushner, J. A.; Buchholz, B. A.; Meeker, A. K.; Stein, G. M.; Hsieh, M. et al. (2010): Significant human beta-cell turnover is limited to the first three decades of life as determined by in vivo thymidine analog incorporation and radiocarbon dating. In *The Journal of clinical endocrinology and metabolism* 95 (10), E234–9. DOI: 10.1210/jc.2010-0932.
- Petersen, Maja B.K.; Gonçalves, Carla A.C.; Kim, Yung Hae; Grapin-Botton, Anne (2018): Chapter Six - Recapitulating and Deciphering Human Pancreas Development From Human Pluripotent Stem Cells in a Dish. In Ali H. Brivanlou (Ed.): *Current*

- Topics in Developmental Biology : Human Embryonic Stem Cells in Development, vol. 129: Academic Press, pp. 143–190. Available online at <http://www.sciencedirect.com/science/article/pii/S0070215318300413>.
- Petersen, Maja Borup Kjær; Azad, Ajuna; Ingvorsen, Camilla; Hess, Katja; Hansson, Mattias; Grapin-Botton, Anne; Honoré, Christian (2017): Single-Cell Gene Expression Analysis of a Human ESC Model of Pancreatic Endocrine Development Reveals Different Paths to β -Cell Differentiation. In *Stem cell reports* 9 (4), pp.1246–1261. DOI: 10.1016/j.stemcr.2017.08.009.
- Petersen, Max C.; Shulman, Gerald I. (2018): Mechanisms of Insulin Action and Insulin Resistance. In *Physiological reviews* 98 (4), pp. 2133–2223. DOI: 10.1152/physrev.00063.2017.
- Phelps, Edward A.; Templeman, Kellie L.; Thulé, Peter M.; García, Andrés J. (2015): Engineered VEGF-releasing PEG-MAL hydrogel for pancreatic islet vascularization. In *Drug delivery and translational research* 5 (2), pp. 125–136. DOI: 10.1007/s13346-013-0142-2.
- Piper, K.; Brickwood, S.; Turnpenny, L. W.; Cameron, I. T.; Ball, S. G.; Wilson, D. I.; Hanley, N. A. (2004): Beta cell differentiation during early human pancreas development. In *The Journal of endocrinology* 181 (1), pp.11–23. DOI: 10.1677/joe.0.1810011.
- Plotnikov, Sergey V.; Pasapera, Ana M.; Sabass, Benedikt; Waterman, Clare M. (2012): Force fluctuations within focal adhesions mediate ECM-rigidity sensing to guide directed cell migration. In *Cell* 151 (7), pp. 1513–1527. DOI: 10.1016/j.cell.2012.11.034.
- Poitout, Vincent; Robertson, R. Paul (2008): Glucolipototoxicity: fuel excess and beta-cell dysfunction. In *Endocrine reviews* 29 (3), pp. 351–366. DOI: 10.1210/er.2007-0023.
- Pozzi, Ambra; Yurchenco, Peter D.; Iozzo, Renato V. (2017): The nature and biology of basement membranes. In *Matrix biology : journal of the International Society for Matrix Biology* 57-58, pp. 1–11. DOI: 10.1016/j.matbio.2016.12.009.
- Ramakrishna, Suresh; Suresh, Bharathi; Lim, Key-Hwan; Cha, Byung-Hyun; Lee, Soo-Hong; Kim, Kwang-Soo; Baek, Kwang-Hyun (2011): PEST motif sequence regulating human NANOG for proteasomal degradation. In *Stem cells and development* 20 (9), pp. 1511–1519. DOI: 10.1089/scd.2010.0410.
- Ramracheya, Reshma; Chapman, Caroline; Chibalina, Margarita; Dou, Haiqiang; Miranda, Caroline; González, Alejandro et al. (2018): GLP-1 suppresses glucagon secretion in human pancreatic alpha-cells by inhibition of P/Q-type Ca²⁺ channels. In *Physiological reports* 6 (17), e13852. DOI: 10.14814/phy2.13852.
- Rasmussen, Camilla Holzmann; Petersen, Dorthe Roenn; Moeller, Jonas Bech; Hansson, Mattias; Dufva, Martin (2015): Collagen Type I Improves the Differentiation of Human Embryonic Stem Cells towards Definitive Endoderm. In *PLOS ONE* 10 (12), e0145389. DOI: 10.1371/journal.pone.0145389.
- Rezania, Alireza; Bruin, Jennifer E.; Arora, Payal; Rubin, Allison; Batushansky, Irina; Asadi, Ali et al. (2014): Reversal of diabetes with insulin-producing cells derived in vitro from human pluripotent stem cells. In *Nat Biotechnol* 32 (11), pp. 1121–1133. DOI: 10.1038/nbt.3033.
- Rezania, Alireza; Bruin, Jennifer E.; Riedel, Michael J.; Mojibian, Majid; Asadi, Ali; Xu, Jean et al. (2012): Maturation of human embryonic stem cell-derived pancreatic progenitors into functional islets capable of treating pre-existing diabetes in mice. In *Diabetes* 61 (8), pp. 2016–2029. DOI: 10.2337/db11-1711.
- Ricard-Blum, Sylvie; Ruggiero, Florence (2005): The collagen superfamily: from the extracellular matrix to the cell membrane. In *Pathologie-biologie* 53 (7), pp. 430–442. DOI: 10.1016/j.patbio.2004.12.024.
- Ricordi, C.; Gray, D. W.; Hering, B. J.; Kaufman, D. B.; Warnock, G. L.; Kneteman, N. M. et al. (1990): Islet isolation assessment in man and large animals. In *Acta diabetologica latina* 27 (3), pp. 185–195. DOI: 10.1007/BF02581331.
- Ris, F.; Hammar, E.; Bosco, D.; Pilloud, C.; Maedler, K.; Donath, M. Y. et al. (2002): Impact of integrin-matrix matching and inhibition of apoptosis on the survival of purified human beta-cells in vitro. In *Diabetologia* 45 (6), pp. 841–850. DOI: 10.1007/s00125-002-0840-7.
- Romito, Antonio; Cobellis, Gilda (2016): Pluripotent Stem Cells: Current Understanding and Future Directions. In *Stem cells international* 2016, p. 9451492. DOI: 10.1155/2016/9451492.
- Rowland, Teisha J.; Miller, Liane M.; Blaschke, Alison J.; Doss, E. Lauren; Bonham, Andrew J.; Hikita, Sherry T. et al. (2010): Roles of integrins in human induced pluripotent stem cell growth on Matrigel and vitronectin. In *Stem cells and development* 19 (8), pp. 1231–1240. DOI: 10.1089/scd.2009.0328.
- Ruiz, Sergio; Brennand, Kristen; Panopoulos, Athanasia D.; Herrerías, Aída; Gage, Fred H.; Izpisua-Belmonte, Juan Carlos (2010): High-efficient generation of induced pluripotent stem cells from human astrocytes. In *PLoS one* 5 (12), e15526. DOI: 10.1371/journal.pone.0015526.
- Rukstalis, J. Michael; Habener, Joel F. (2009): Neurogenin3: a master regulator of pancreatic islet differentiation and regeneration. In *Islets* 1 (3), pp. 177–184. DOI: 10.4161/isl.1.3.9877.

- Russ, Holger A.; Parent, Audrey V.; Ringler, Jennifer J.; Hennings, Thomas G.; Nair, Gopika G.; Shveygert, Mayya et al. (2015): Controlled induction of human pancreatic progenitors produces functional beta-like cells in vitro. In *The EMBO Journal* 34 (13), pp. 1759–1772. DOI: 10.15252/embj.201591058.
- Russel, W. M. S.; Burch, R. L. (1959): The Principles of Humane Experimental Technique. In *Methuen & Co. Limited* 1 (13), p. 500. DOI: 10.5694/j.1326-5377.1960.tb73127.x.
- Rutter, Guy A. (2009): Regulating glucagon secretion: somatostatin in the spotlight. In *Diabetes* 58 (2), pp. 299–301. DOI: 10.2337/db08-1534.
- Sackett, Sara Dutton; Tremmel, Daniel M.; Ma, Fengfei; Feeney, Austin K.; Maguire, Rachel M.; Brown, Matthew E. et al. (2018): Extracellular matrix scaffold and hydrogel derived from decellularized and delipidized human pancreas. In *Sci Rep* 8 (1), p. 10452. DOI: 10.1038/s41598-018-28857-1.
- Saeedi, Pouya; Petersohn, Inga; Salpea, Paraskevi; Malanda, Belma; Karuranga, Suvi; Unwin, Nigel et al. (2019): Global and regional diabetes prevalence estimates for 2019 and projections for 2030 and 2045: Results from the International Diabetes Federation Diabetes Atlas, 9th edition. In *Diabetes research and clinical practice* 157, p. 107843. DOI: 10.1016/j.diabres.2019.107843.
- Salisbury, Rachel J.; Blaylock, Jennifer; Berry, Andrew A.; Jennings, Rachel E.; Krijger, Ronald de; Piper Hanley, Karen; Hanley, Neil A. (2014): The window period of NEUROGENIN3 during human gestation. In *Islets* 6 (3), e954436. DOI: 10.4161/19382014.2014.954436.
- Schaffer, Ashleigh E.; Taylor, Brandon L.; Benthuisen, Jacqueline R.; Liu, Jingxuan; Thorel, Fabrizio; Yuan, Weiping et al. (2013): Nkx6.1 controls a gene regulatory network required for establishing and maintaining pancreatic Beta cell identity. In *PLoS Genetics* 9 (1), e1003274. DOI: 10.1371/journal.pgen.1003274.
- Scharp, D. W.; Lacy, P. E.; Santiago, J. V.; McCullough, C. S.; Weide, L. G.; Falqui, L. et al. (1990): Insulin independence after islet transplantation into type I diabetic patient. In *Diabetes* 39 (4), pp. 515–518. DOI: 10.2337/diab.39.4.515.
- Seydoux, Geraldine; Braun, Robert E. (2006): Pathway to totipotency: lessons from germ cells. In *Cell* 127 (5), pp. 891–904. DOI: 10.1016/j.cell.2006.11.016.
- Shanik, Michael H.; Xu, Yuping; Skrha, Jan; Dankner, Rachel; Zick, Yehiel; Roth, Jesse (2008): Insulin resistance and hyperinsulinemia: is hyperinsulinemia the cart or the horse? In *Diabetes Care* 31 Suppl 2 (Supplement 2), S262-8. DOI: 10.2337/dc08-s264.
- Shapiro, A. M.; Lakey, J. R.; Ryan, E. A.; Korbitt, G. S.; Toth, E.; Warnock, G. L. et al. (2000): Islet transplantation in seven patients with type 1 diabetes mellitus using a glucocorticoid-free immunosuppressive regimen. In *The New England journal of medicine* 343 (4), pp. 230–238. DOI: 10.1056/NEJM200007273430401.
- Shapiro, A. M. James; Ricordi, Camillo; Hering, Bernhard J.; Auchincloss, Hugh; Lindblad, Robert; Robertson, R. Paul et al. (2006): International trial of the Edmonton protocol for islet transplantation. In *The New England journal of medicine* 355 (13), pp. 1318–1330. DOI: 10.1056/NEJMoa061267.
- Sharon, Nadav; Vanderhoof, Jordan; Straubhaar, Juerg; Mueller, Jonas; Chawla, Raghav; Zhou, Quan et al. (2019): Wnt Signaling Separates the Progenitor and Endocrine Compartments during Pancreas Development. In *Cell reports* 27 (8), 2281-2291.e5. DOI: 10.1016/j.celrep.2019.04.083.
- Skelin, Masa; Rupnik, Marjan; Cencic, Avreljia (2010): Pancreatic beta cell lines and their applications in diabetes mellitus research. In *ALTEX* 27 (2), pp. 105–113. DOI: 10.14573/altex.2010.2.105.
- Skelin Klemen, Maša; Dolenšek, Jurij; Slak Rupnik, Marjan; Stožer, Andraž (2017): The triggering pathway to insulin secretion: Functional similarities and differences between the human and the mouse β cells and their translational relevance. In *Islets* 9 (6), pp. 109–139. DOI: 10.1080/19382014.2017.1342022.
- Smith, Lucas R.; Cho, Sangkyun; Discher, Dennis E. (2018): Stem Cell Differentiation is Regulated by Extracellular Matrix Mechanics. In *Physiology (Bethesda, Md.)* 33 (1), pp. 16–25. DOI: 10.1152/physiol.00026.2017.
- Solar, Myriam; Cardalda, Carina; Houbracken, Isabelle; Martín, Mercè; Maestro, Miguel Angel; Medts, Nele de et al. (2009): Pancreatic exocrine duct cells give rise to insulin-producing beta cells during embryogenesis but not after birth. In *Developmental cell* 17 (6), pp. 849–860. DOI: 10.1016/j.devcel.2009.11.003.
- Spagnoli, Francesca M. (2015): Simply the right time to turn on insulin. In *The EMBO Journal* 34 (13), pp. 1740–1742. DOI: 10.15252/embj.201591894.
- Steiner, Donald J.; Kim, Abraham; Miller, Kevin; Hara, Manami (2010): Pancreatic islet plasticity: interspecies comparison of islet architecture and composition. In *Islets* 2 (3), pp. 135–145. DOI: 10.4161/isl.2.3.11815.
- Stendahl, John C.; Kaufman, Dixon B.; Stupp, Samuel I. (2009): Extracellular matrix in pancreatic islets: relevance to scaffold design and transplantation. In *Cell transplantation* 18 (1), pp. 1–12. DOI: 10.3727/096368909788237195.

- Taipale, J.; Keski-Oja, J. (1997): Growth factors in the extracellular matrix. In *FASEB journal : official publication of the Federation of American Societies for Experimental Biology* 11 (1), pp. 51–59. DOI: 10.1096/fasebj.11.1.9034166.
- Tajik, Arash; Zhang, Yuejin; Wei, Fuxiang; Sun, Jian; Jia, Qiong; Zhou, Wenwen et al. (2016): Transcription upregulation via force-induced direct stretching of chromatin. In *Nature materials* 15 (12), pp. 1287–1296. DOI: 10.1038/nmat4729.
- Takahashi, Kazutoshi; Tanabe, Koji; Ohnuki, Mari; Narita, Megumi; Ichisaka, Tomoko; Tomoda, Kiichiro; Yamanaka, Shinya (2007): Induction of pluripotent stem cells from adult human fibroblasts by defined factors. *Cell*, 131(5), 861–872. In *Cell* 131 (5), pp. 861–872. DOI: 10.1016/J.CELL.2007.11.019.
- Taylor-Weiner, Hermes; Schwarzbauer, Jean E.; Engler, Adam J. (2013): Defined extracellular matrix components are necessary for definitive endoderm induction. In *STEM CELLS* 31 (10), pp. 2084–2094. DOI: 10.1002/stem.1453.
- Thomas, Francis T.; Contreras, Juan L.; Bilbao, Guadalupe; Ricordi, Camillo; Curiel, David; Thomas, Judith M. (1999): Anoikis, extracellular matrix, and apoptosis factors in isolated cell transplantation. In *Surgery* 126 (2), pp. 299–304. DOI: 10.1016/S0039-6060(99)70169-8.
- Thomson, J. A.; Itskovitz-Eldor, J.; Shapiro, S. S.; Waknitz, M. A.; Swiergiel, J. J.; Marshall, V. S.; Jones, J. M. (1998): Embryonic stem cell lines derived from human blastocysts. In *Science (New York, N.Y.)* 282 (5391), pp. 1145–1147. DOI: 10.1126/science.282.5391.1145.
- Tran, Raymond; Moraes, Christopher; Hoesli, Corinne A. (2020): Developmentally-Inspired Biomimetic Culture Models to Produce Functional Islet-Like Cells From Pluripotent Precursors. In *Frontiers in Bioengineering and Biotechnology* 8, p. 583970. DOI: 10.3389/fbioe.2020.583970.
- Travascio, Francesco (2016): Composition and Function of the Extracellular Matrix in the Human Body: InTech.
- Umpierrez, Guillermo E.; Klonoff, David C. (2018): Diabetes Technology Update: Use of Insulin Pumps and Continuous Glucose Monitoring in the Hospital. In *Diabetes Care* 41 (8), pp. 1579–1589. DOI: 10.2337/dci18-0002.
- van Deijnen, J. H.; van Suylichem, P. T.; Wolters, G. H.; van Schilfgaarde, R. (1994): Distribution of collagens type I, type III and type V in the pancreas of rat, dog, pig and man. In *Cell Tissue Res* 277 (1), pp. 115–121. DOI: 10.1007/BF00303087.
- Vantuyghem, Marie-Christine; Chetboun, Mikael; Gmyr, Valéry; Jannin, Arnaud; Espiard, Stéphanie; Le Mapihan, Kristell et al. (2019): Ten-Year Outcome of Islet Alone or Islet After Kidney Transplantation in Type 1 Diabetes: A Prospective Parallel-Arm Cohort Study. In *Diabetes Care* 42 (11), pp. 2042–2049. DOI: 10.2337/dc19-0401.
- Velazco-Cruz, Leonardo; Song, Jiwon; Maxwell, Kristina G.; Goedegebuure, Madeleine M.; Augsnornworawat, Punn; Hogrebe, Nathaniel J.; Millman, Jeffrey R. (2019): Acquisition of Dynamic Function in Human Stem Cell-Derived β Cells. In *Stem cell reports* 12 (2), pp. 351–365. DOI: 10.1016/j.stemcr.2018.12.012.
- Veres, Adrian; Faust, Aubrey L.; Bushnell, Henry L.; Engquist, Elise N.; Kenty, Jennifer Hyoje-Ryu; Harb, George et al. (2019): Charting cellular identity during human in vitro β -cell differentiation. In *Nature* 569 (7756), pp. 368–373. DOI: 10.1038/s41586-019-1168-5.
- Vergari, Elisa; Knudsen, Jakob G.; Ramracheya, Reshma; Salehi, Albert; Zhang, Quan; Adam, Julie et al. (2019): Insulin inhibits glucagon release by SGLT2-induced stimulation of somatostatin secretion. In *Nat Commun* 10 (1), p. 139. DOI: 10.1038/s41467-018-08193-8.
- Villa-Diaz, Luis G.; Kim, Jin Koo; Laperle, Alex; Palecek, Sean P.; Krebsbach, Paul H. (2016): Inhibition of Focal Adhesion Kinase Signaling by Integrin $\alpha\beta 1$ Supports Human Pluripotent Stem Cell Self-Renewal. In *STEM CELLS* 34 (7), pp. 1753–1764. DOI: 10.1002/stem.2349.
- Virtanen, I.; Banerjee, M.; Palgi, J.; Korsgren, O.; Lukinius, A.; Thornell, L-E et al. (2008): Blood vessels of human islets of Langerhans are surrounded by a double basement membrane. In *Diabetologia* 51 (7), pp. 1181–1191. DOI: 10.1007/s00125-008-0997-9.
- Waanders, Leonie F.; Chwalek, Karolina; Monetti, Mara; Kumar, Chanchal; Lammert, Eckhard; Mann, Matthias (2009): Quantitative proteomic analysis of single pancreatic islets. In *PNAS* 106 (45), pp. 18902–18907. DOI: 10.1073/pnas.0908351106.
- Walma, David A. Cruz; Yamada, Kenneth M. (2020): The extracellular matrix in development. In *Development* 147 (10). DOI: 10.1242/dev.175596.
- Wang, Han; Luo, Xie; Leighton, Jake (2015): Extracellular Matrix and Integrins in Embryonic Stem Cell Differentiation. In *Biochemistry insights* 8 (Suppl 2), pp. 15–21. DOI: 10.4137/BCI.S30377.
- Wang, Tuntun; Nanda, Sitansu Sekhar; Papaefthymiou, Georgia C.; Yi, Dong Kee (2020): Mechanophysical Cues in Extracellular Matrix Regulation of Cell Behavior. In *ChemBioChem* 21 (9), pp. 1254–1264. DOI: 10.1002/cbic.201900686.
- Weber, Laney M.; Anseth, Kristi S. (2008): Hydrogel encapsulation environments functionalized with extracellular matrix interactions increase islet insulin secretion. In *Matrix biology : journal of the International Society for Matrix Biology* 27 (8), pp. 667–673. DOI: 10.1016/j.matbio.2008.08.001.

- Weir, G. C. (2013): Islet encapsulation: advances and obstacles. In *Diabetologia* 56 (7), pp. 1458–1461. DOI: 10.1007/s00125-013-2921-1.
- Wex, C.; Fröhlich, M.; Brandstädter, K.; Bruns, C.; Stoll, A. (2015): Experimental analysis of the mechanical behavior of the viscoelastic porcine pancreas and preliminary case study on the human pancreas. In *Journal of the mechanical behavior of biomedical materials* 41, pp. 199–207. DOI: 10.1016/j.jmbbm.2014.10.013.
- White, Lisa J.; Taylor, Adam J.; Faulk, Denver M.; Keane, Timothy J.; Saldin, Lindsey T.; Reing, Janet E. et al. (2017): The impact of detergents on the tissue decellularization process: A ToF-SIMS study. In *Acta biomaterialia* 50, pp. 207–219. DOI: 10.1016/j.actbio.2016.12.033.
- Wolf, Matthew T.; Daly, Kerry A.; Brennan-Pierce, Ellen P.; Johnson, Scott A.; Carruthers, Christopher A.; D'Amore, Antonio et al. (2012): A hydrogel derived from decellularized dermal extracellular matrix. In *Biomaterials* 33 (29), pp. 7028–7038. DOI: 10.1016/j.biomaterials.2012.06.051.
- Wong, Jennifer C. Y.; Gao, Steven Y.; Lees, Justin G.; Best, Marie B.; Wang, Rennian; Tuch, Bernard E. (2010): Definitive endoderm derived from human embryonic stem cells highly express the integrin receptors α V and β 5. In *Cell Adhesion & Migration* 4 (1), pp. 39–45. DOI: 10.4161/cam.4.1.10627.
- Wu, Yanling; Ding, Yanping; Tanaka, Yoshimasa; Zhang, Wen (2014): Risk factors contributing to type 2 diabetes and recent advances in the treatment and prevention. In *International Journal of Medical Sciences* 11 (11), pp. 1185–1200. DOI: 10.7150/ijms.10001.
- Xu, C.; Inokuma, M. S.; Denham, J.; Golds, K.; Kundu, P.; Gold, J. D.; Carpenter, M. K. (2001): Feeder-free growth of undifferentiated human embryonic stem cells. In *Nature biotechnology* 19 (10), pp. 971–974. DOI: 10.1038/nbt1001-971.
- Ye, F.; Duvillié, B.; Scharfmann, R. (2005): Fibroblast growth factors 7 and 10 are expressed in the human embryonic pancreatic mesenchyme and promote the proliferation of embryonic pancreatic epithelial cells. In *Diabetologia* 48 (2), pp. 277–281. DOI: 10.1007/s00125-004-1638-6.
- Young, D. Adam; Ibrahim, Dina O.; Hu, Diane; Christman, Karen L. (2011): Injectable hydrogel scaffold from decellularized human lipoaspirate. In *Acta biomaterialia* 7 (3), pp. 1040–1049. DOI: 10.1016/j.actbio.2010.09.035.
- Zakrzewski, Wojciech; Dobrzyński, Maciej; Szymonowicz, Maria; Rybak, Zbigniew (2019): Stem cells: past, present, and future. In *Stem cell research & therapy* 10 (1), p. 68. DOI: 10.1186/s13287-019-1165-5.
- Zhang, Donghui; Jiang, Wei; Liu, Meng; Sui, Xin; Yin, Xiaolei; Chen, Song et al. (2009): Highly efficient differentiation of human ES cells and iPS cells into mature pancreatic insulin-producing cells. In *Cell research* 19 (4), pp. 429–438. DOI: 10.1038/cr.2009.28.
- Zhang, Jue; Chu, Li-Fang; Hou, Zhonggang; Schwartz, Michael P.; Hacker, Timothy; Vickerman, Vernella et al. (2017): Functional characterization of human pluripotent stem cell-derived arterial endothelial cells. In *PNAS* 114 (30), E6072–E6078. DOI: 10.1073/pnas.1702295114.
- Zhou, Qiao; Melton, Douglas A. (2018): Pancreas regeneration. In *Nature* 557 (7705), pp. 351–358. DOI: 10.1038/s41586-018-0088-0.
- Ziegler, Anna-Lena (2019): Establishment and characterization of organ-specific hydrogels derived from natural extracellular matrices. Bachelor Thesis. Julius Maximilians University, Würzburg. Chair for Tissue Engineering and Regenerative Medicine.
- Zoldan, Janet; Karagiannis, Emmanouil D.; Lee, Christopher Y.; Anderson, Daniel G.; Langer, Robert; Levenberg, Shulamit (2011): The influence of scaffold elasticity on germ layer specification of human embryonic stem cells. In *Biomaterials* 32 (36), pp. 9612–9621. DOI: 10.1016/j.biomaterials.2011.09.012.

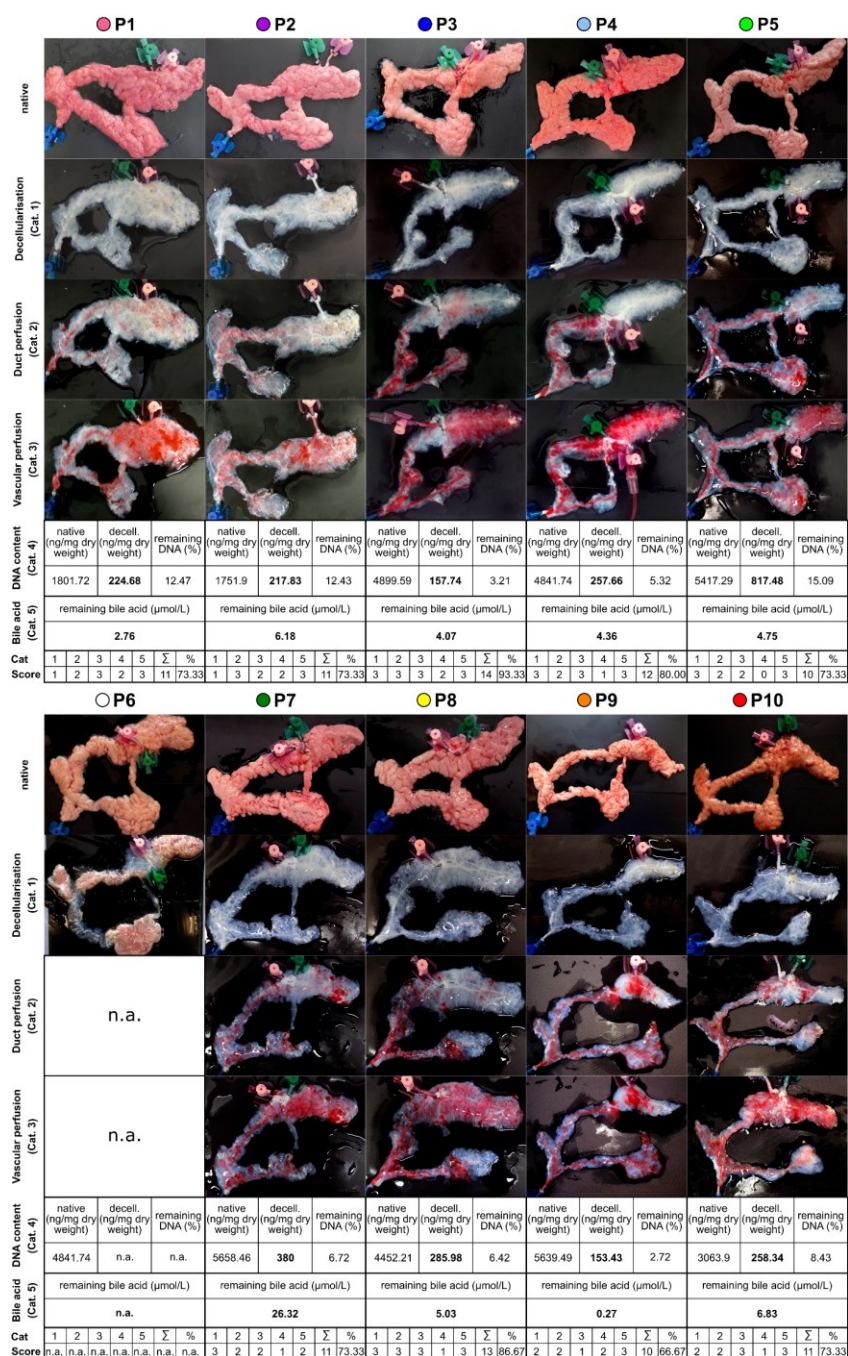
11 *Tables and Figures*

Figure 1 Anatomy of the human pancreas. _____	7
Figure 2 Glucose homeostasis of the human body. _____	9
Figure 3 Therapeutic strategies for the treatment of diabetes mellitus. _____	14
Figure 4 Development of the human pancreas and derived protocols for the directed in vitro differentiation of hiPSC towards insulin producing cells. _____	18
Figure 5 Extracellular matrix assembly and integrin signaling. _____	22
Figure 6 Generation of the PanMa by whole organ perfusion decellularization. _____	45
Figure 7 The PanMa represents an acellular scaffold with a largely preserved ECM structure. _____	46
Figure 8 Collagens are preserved in the PanMa while laminins are lost. _____	47
Figure 9 The PanMa exhibits a well-preserved ultrastructure. _____	47
Figure 10 Preservation of the PanMa's vessel system allows recellularization of the splenic lobe arterial vasculature with human ECs. _____	49
Figure 11 Application of the newly established PancScore for the evaluation of generated PanMas. _____	52
Figure 12 The microscale topography of the PanMa is characterized by a homogenous fiber-based network. _____	53
Figure 13 The PanMa represents a hygroscopic scaffold permeable for low and high weight molecules. _____	54
Figure 14 Rheological measurements highlight the PanMa as a soft scaffold. _____	55
Figure 15 Marginal changes in the gene expression of pluripotency markers and weak NANOG signals in hiPSCs maintained on the ECM scaffolds. _____	58
Figure 16 Culture of hiPSC on the PanMa slightly enhances the expression of endoderm-associated genes during spontaneous differentiation. _____	61
Figure 17 Distribution of GATA4+ and PAX6+ cells after spontaneous differentiation on the ECM scaffolds. _____	63
Figure 18 Spontaneous differentiation of hiPSCs on the PanMa results in an elevated number of GATA4+ cells. _____	64
Figure 19 Spontaneous differentiation of hiPSCs on the PanMa leads to an increased expression of endoderm lineage genes. _____	65
Figure 20 Attachment of hiPSCs to the PanMa is mediated by binding to collagen fibers. _____	66
Figure 21 Supplementation of the PanMa as a liquid medium supplement has no effect on the differentiation of hiPSCs towards pancreatic HECs. _____	68

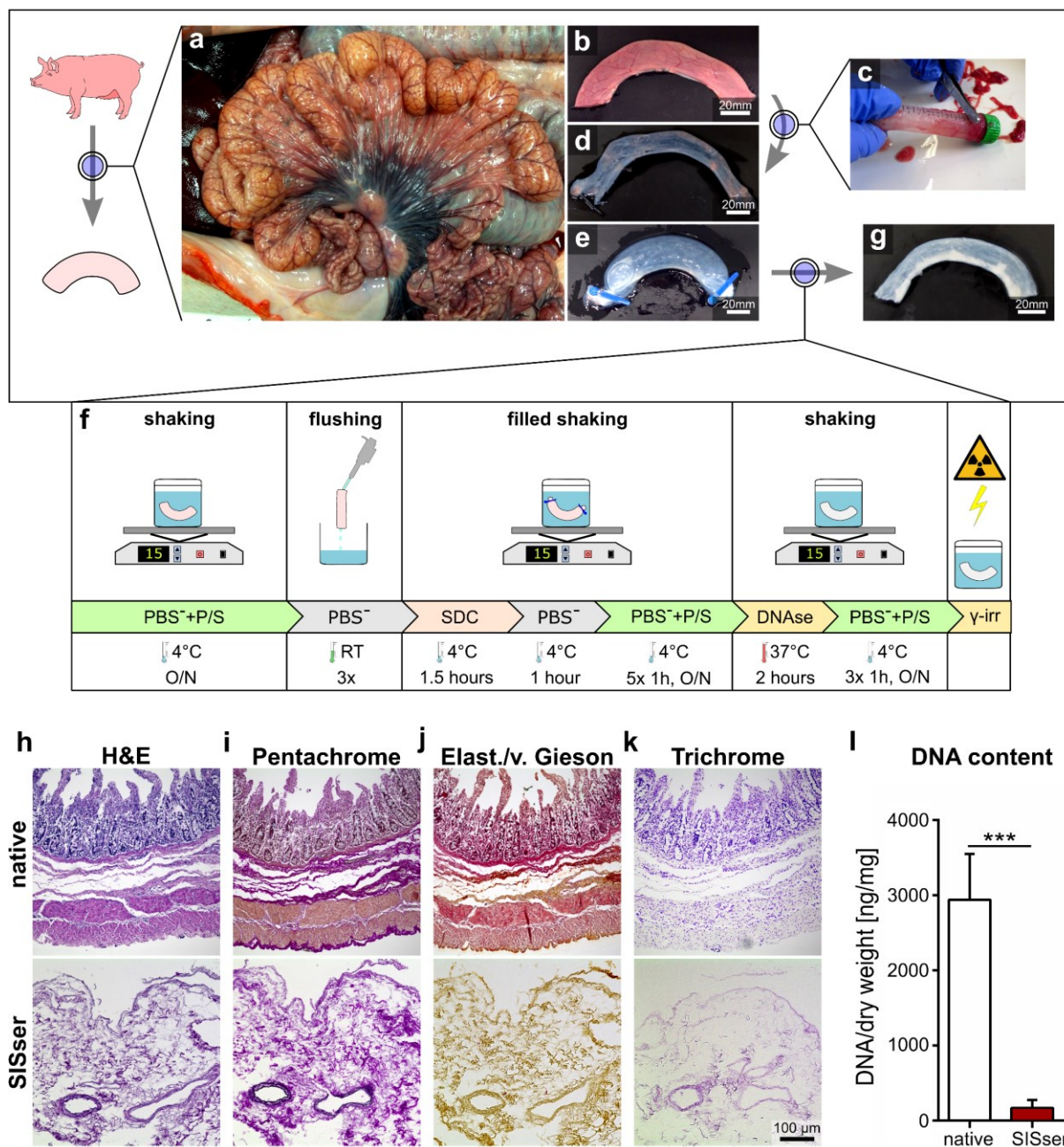
Figure 22 Supplementation of liquid PanMa during pancreatic differentiation has no influence on the phenotype of hiPSC derived HECs. _____	69
Figure 23 Directed differentiation of hiPSCs towards HECs on the PanMa leads to a diminished hormone gene expression. _____	71
Figure 24 Fig. 19 hiPSC-derived HECs generated on the PanMa display a typical marker expression. _____	72
Figure 25 Analysis of the glucose stimulated insulin secretion of HECs on the PanMa and SISser delivers false measurement results. _____	73
Figure 26 Differentiation of hiPSCs towards β -like cells on the PanMa reduces the expression of glucagon and somatostatin. _____	75
Figure 27 Stage 7 cells generated on the PanMa show a β -like phenotype. _____	78
Figure 28 Measurement of glucose stimulated insulin secretion of S7 cells on the PanMa and SISser leads to false measurements. _____	79
Figure 29 A PanMa-derived hydrogel is suitable for encapsulation and culture of S5 HECs _____	82
Figure 30 HECs cultured in a PanMa-derived hydrogel exhibit a different distribution of NKX6.1 ⁺ cells. _____	83
Figure 31 HECs reveal a reduced glucose stimulated insulin secretion after culture in the PanMa-derived hydrogel. _____	85
Supplementary Figure 1 PanMas evaluated with the PancScore. _____	125
Supplementary Figure 2 Generation and basal characterization of the SISser. _____	126
Supplementary Figure 3 Generation and basal characterization of the LungMa. _____	127
Supplementary Figure 4 Characterization of the hiPSC-derived arterial endothelial cells (AECs). _____	128
Table 1 Protocol for cDNA synthesis _____	40
Table 2 Protocol for RT-qPCR _____	40
Table 3 Criteria of the PancScore. _____	50
Table 4 Scoring of the single PanMas. _____	51

12 Appendix

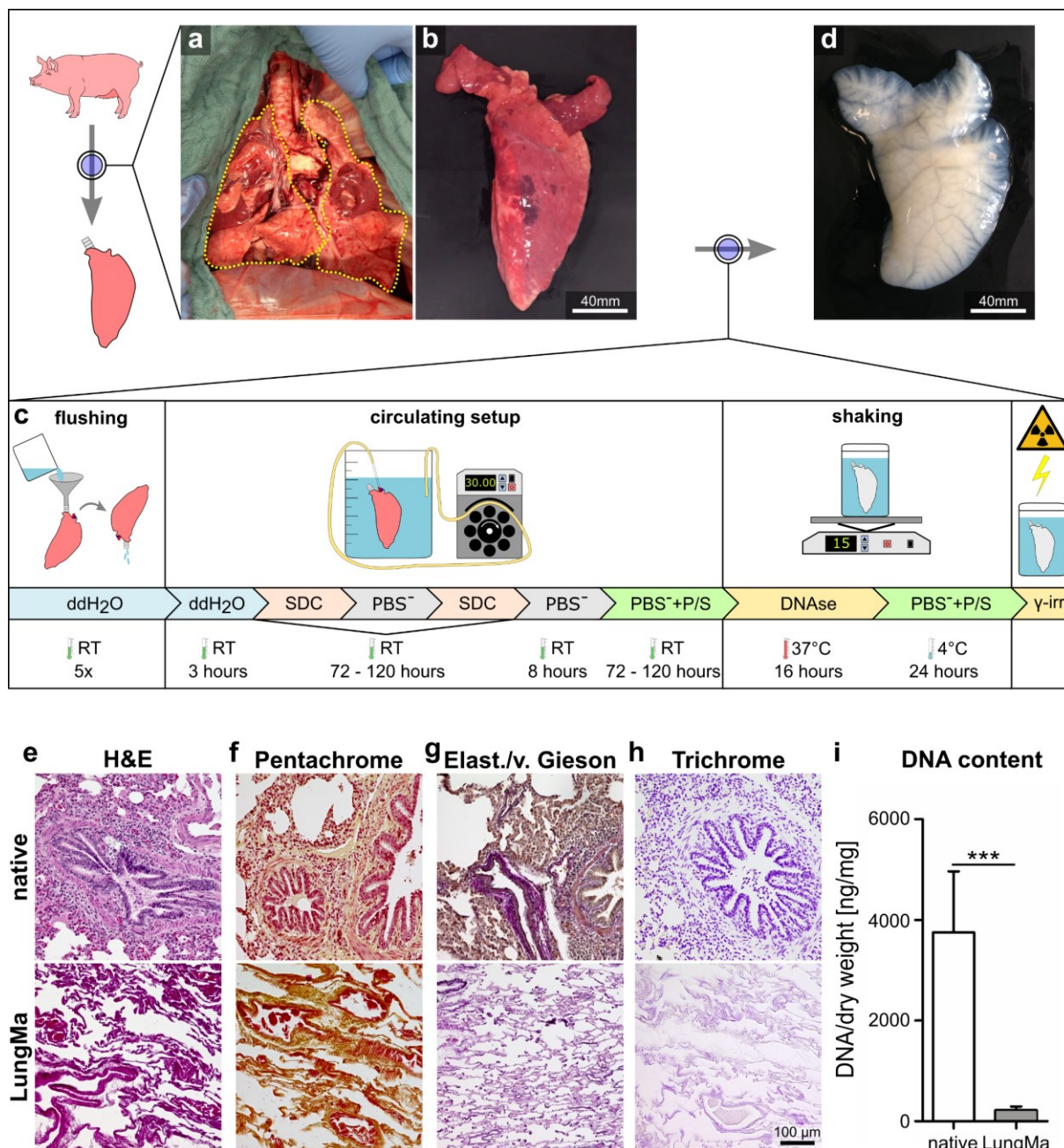
12.1 Suplementary Figures



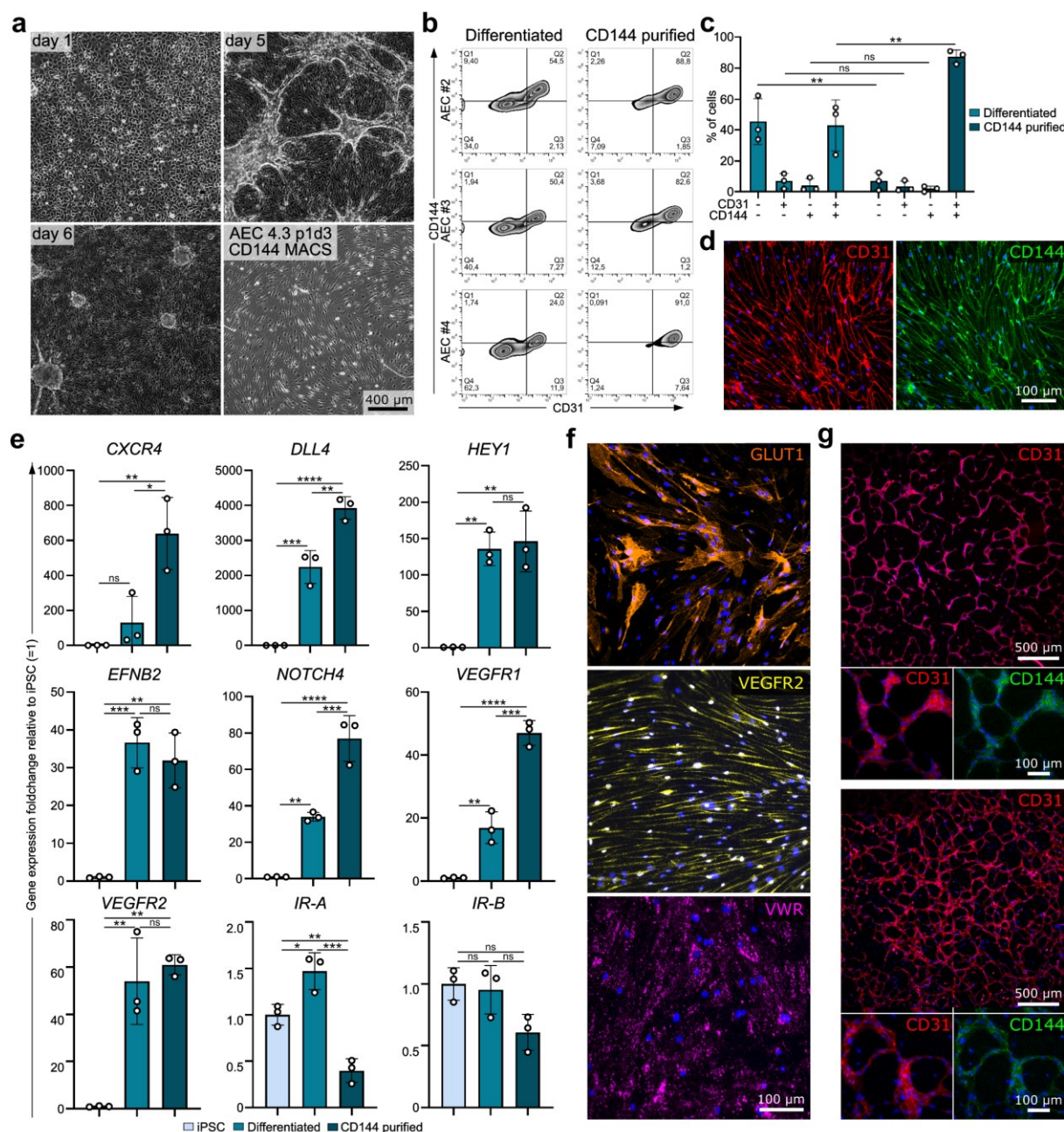
Supplementary Figure 1 PanMAs evaluated with the PancScore. Shown are the PanMAs used for Scoring displayed in Fig. XX. The color-coding corresponds to the colors used in Fig. XX. The upper row shows native pancreata before decellularization. The images below were used to evaluate the PanMa for decellularization (category 1), duct perfusion (category 2), vascular perfusion (category 3). The data below show the DNA content (category 4) in ng/mg dry weight of the native pancreas and the derived PanMa. The remaining bile acid (category 5) is shown in $\mu\text{mol/l}$. The lowest row of each column shows the scores of the respective PanMa for each category as well as the sum of scored points and the ratio. Figure taken from Berger et al. 2020.



Supplementary Figure 2 Generation and basal characterization of the SISser. **a** Exposed small intestine in the peritoneal cavity. **b** Segment of the native jejunum. **c** Manual removal of mucosal parts by scraping. **d** Jejunal segment after removal of the mucosa. **e** Filled jejunal segment as it is used for washing and decellularization. **f** Scheme of the decellularization process. Shown are the different set-ups used for decellularization and washing. The timeline beneath illustrates the used agents, temperature and duration of the individual steps. **g** Jejunal segment after decellularization. **h** – **k** Images of sections of native jejunal segments (upper panel) and the SISser (lower panel) analyzed by Hematoxylin & Eosin (**h**), Pentachrom (**i**), Elastica/van Gieson (**j**) and Feulgen staining (**k**). **l** DNA content of native jejunal segment ($n = 4$) and the SISser ($n = 4$) given as ng DNA/mg dry weight. **Statistics:** Data represent mean \pm SD. *** $P < 0.001$, unpaired two-tailed t-Test. **Scale bars:** If not annotated in the picture, the image size refers to the scale bar displayed in the picture at the right bottom corner in the same figure part. Figure taken from Berger et al. 2020.



Supplementary Figure 3 Generation and basal characterization of the LungMa. **a** Exposed lobes of the lung (yellow lining) in the opened thorax. **b** Explanted lung lobe after removal of connective tissue. **c** Illustration of the decellularization process. The cartoon shows the different set-ups used for decellularization and washing. The timeline beneath illustrates the used agents, temperature and duration of the individual steps. **d** Lung lobe after decellularization. **e - h** Images of sections of native lung (upper panel) and the LungMa (lower panel) analyzed by Hematoxylin & Eosin (**e**), Pentachrom (**f**), Elastica/van Gieson (**g**) and Feulgen staining (**h**). **i** DNA content of native lung ($n = 5$) and the SISser ($n = 5$) given as ng DNA/mg dry weight. **Statistics:** Data represent mean \pm SD. *** $P < 0.001$, unpaired two-tailed t-Test. **Scale bars:** If not annotated in the picture, the image size refers to the scale bar displayed in the picture at the right bottom corner in the same figure part. Figure taken from Berger et al. 2020.



Supplementary Figure 4 Characterization of the hiPSC-derived arterial endothelial cells (AECs). **a** Micrographs of the cellular morphology during differentiation and at passage 1 after CD144 magnetic cell sorting (MACS). **b** Density plots of FACS measurements showing the amount CD144 and CD31 labelled cells after differentiation (left panel) and after MACS sorting and expansion (right panel) ($n = 3$). **c** Quantification of the cell population according to the expression of CD31 and CD144 after differentiation (blue) and after MACS sorting and expansion (dark blue) shown as bar graph. Data are shown as mean \pm SD. Single data points represent individual biological replicates ($n = 3$). **d** Representative images of MACS sorted AECs at passage 1 stained for CD31 (red) and CD144 (green) counterstained with DAPI (blue) ($n = 3$). **e** Fold change gene expression of endothelial celltype-specific markers of AECs relative to the expression of hiPSCs. Data are shown as mean \pm SD. Single data points represent individual biological replicates ($n = 3$). **f** Representative images of AECs treated with antibodies against GLUT1 (orange), VEGFR2 (yellow), and VWR (magenta) with DAPI counterstaining (blue) ($n = 3$). **g** Images of Matrigel encapsulated HUVECs and AECs labelled with antibodies against CD31 (red) and CD144 (green), counterstained with DAPI (HUVECs: $n = 1$; AECs: $n = 3$). ns, not significant, * $P < 0.05$, ** $P < 0.01$, *** $P < 0.001$, **** $P < 0.0001$, one-way Anova with Tukey's multiple comparison test (d) or two-way Anova with Sidak's multiple comparison (c).

12.2 List of abbreviations

12.2.1 Protein and gene abbreviations

AFP	alpha fetoprotein	MAF	V-Maf avian musculoaponeurotic fibrosarcoma oncogene homolog
ALDH1A1	aldehyde dehydrogenase 1 family, member A1	NEUROD1	neuronal differentiation 1
ALK	activin receptor-like kinase	NGN3	neurogenin (also: NEUROG3)
ARX	aristaless related homeobox	NKX2.2	homeobox protein NK-2 homolog B
BMP	bone morphogenetic protein	NKX6.1	homeobox protein NK-6 homolog A
C-MYC	avian myelocytomatosis virus oncogene cellular homolog	OCT	octamer-binding transcription factor
COL	collagen	PAX	paired box
CPA1	carboxypeptidase A1	PDX1	pancreatic and duodenal homeobox 1
CPEP	connecting peptide	PKC	protein kinase C
DCN	decorin	RFP	red fluorescent protein
FGF	fibroblast growth factor	RPL	ribosomal protein L
FOX	forkhead box protein	RPS	ribosomal protein S
GATA	GATA binding protein	SHH	sonic hedgehog
GCG	glucagon	SOX	sex determining region Y-box
GIP	gastric inhibitory polypeptide	SST	somatostatin
GLP-1	glucagon like peptide-1	TAZ	tafazzin
IGF	insulin like growth factor	TGF	transforming growth factor
INS	insulin	WNT	cingless-related integration site
KLF	kruppel-like Factor	YAP	yes1 associated transcriptional regulator
LAM	laminin		

12.2.2 Other abbreviations

2D	two-dimensional	DAPI	4',6-diamidino-2-phenylindole
3D	three-dimensional	DE	definitive endoderm
AA	ascorbic acid	DMEM	Dulbecco's modified Eagle's medium
BL	basal lamina	DNA	deoxyribonucleic acid
BSA	bovine serum albumin	DNase	desoxyribonuclease
cDNA	complementary DNA	Du	duodenum
CL	connecting lobe		

DuL	duodenal lobe	PE	pancreatic endoderm
EC	human dermal microvascular endothelial cell	PF	posterior foregut
ECM	extracellular matrix	PGT	primitive gut tube
ESC	embryonic stem cell	PP	pancreatic progenitor
FCS	fetal calve serum	PSC	pluripotent stem cell
GAGs	glucosaminoglycans	RA	retinoic acid
H&E	hematoxylin and eosin	RNA	ribonucleic acid
hESC	human embryonic stem cell	RPMI	rounds per minute
hiPSC	human induced pluripotent stem cell	RT	room temperature
hPSC	human pluripotent stem cell	RT-qPCR	Real-Time quantitative PCR
IBMIR	instant blood mediated inflammatory reaction	S	spleen
INS-1	rat insulinoma-1	SA	spleen artery
iPSC	induced pluripotent stem cell	SC	stem cell
LungMa	lung specific extracellular matrix scaffold	SD	standard deviation
MIN6	mouse insulinoma 6	SDC	sodium deoxycholate
MPP	multipotent pancreatic progenitor	SDS	sodium dodecyl sulfate
MTT	3-(4,5-dimethylthiazol-2-yl)-2,5-diphenyl-2H-tetrazolium bromide	SI	stimulation index
P/S	penicillin/streptomycin	SISser	small intestinal submucosa serosa matrix
PanMa	pancreas specific extracellular matrix scaffold	SL	splenic lobe
PBS ⁻	phosphate buffered solution without Ca ²⁺ and Mg ²⁺ pH 7.4	SV	spleen vein
PBS ⁺	phosphate buffered solution with Ca ²⁺ and Mg ²⁺ pH 7.4	T1DM	type 1 diabetes mellitus
PD	pancreatic duct	T2DM	type 2 diabetes mellitus
PDBu	phorbol 12,13-dibutyrate	T3	Triiodo-L-Thyronine
		TPB	α -Amyloid Precursor Protein Modulator
		v/v	<u>volume percent</u>
		w/v	mass/volume percent
		WST	1-methoxy-5-methyl-phenazinium methyl sulfate

12.2.3 Units and symbols

°	degree	μm	micrometer
μg	microgram	μM	micromolar
μl	microliter	bp	base pairs

bp	base pairs	min	minute
C°	°celsius	ml	milliliter
Ca ²⁺	Calcium-Kation	mm	millimeter
cm	centimeter	mM	millimolar
E	Young's modulus	mmol	millimol
g	gram	MPa	megapascal
g	gravitational force	N	normality
G'	storage modulus	ng	nanogram
G''	loss modulus	nm	nanometer
GPa	gigapascal	Pa	pascal
h	hour	s	second
Hz	Hertz	T	temperature
kPa	kilopascal	γ	amplitude
l	liter	γ̇	shear rate
M	molar	η	viscosity
mg	milligram	τ	shear stress
Mg ²⁺	Magnesium-Kation	ω	angular frequency

13 Materials

13.1 Buffers and Solutions

1x Citrate Buffer, pH 6.0 (1 l)

Citric acid	3.84 g	\cong 20 mM
Aqua dest.	800 ml	
→ Adjust to pH 6		
Aqua dest.	Ad 1 l	

Digest buffer (10 ml)

1 M Hydrochloric Acid	100 μ l	\cong 0.1 M
Milli-Q® H ₂ O	Ad 10 ml	
Pepsin	10 mg	\cong 0.1% (w/v)

1x Krebs Ringer Buffer (1 l)

Sodium chloride	7.54 g	\cong 129 mM
Potassium chloride	358.4 mg	\cong 4.8 mM
Magnesium sulfate	144.5 mg	\cong 1.2 mM
Sodium phosphate dibasic dihydrate	177.9 mg	\cong 1 mM
Potassium phosphate monobasic	163.3 mg	\cong 1.2 mM
Hepes	2.38 g	\cong 10 mM
Sodium bicarbonate	420 mg	\cong 5 mM
BSA	1 g	\cong 0.1% (w/v)
Milli-Q® H ₂ O	800 ml	
	Dissolve	
Calcium chloride dihydrate	367.5 mg	\cong 2.5 mM
→ Adjust to pH 7.4		
Milli-Q® H ₂ O	Ad 1 l	

6x Loading Buffer (10 ml)

1 M Tris-HCl solution	100 μ l	\cong 10 mM
1% Bromphenolblau	500 μ l	\cong 0.05% (v/v)
Glycerin	6 ml	\cong 60% (v/v)
EDTA disodium salt dihydrate	223.32 mg	\cong 60 mM
Aqua dest.	Ad 10 ml	

1x PBS (1 l)

PBS powder		
Aqua dest.	Ad 1 l	

SEM fixation buffer (100 ml)

0.2 M Sorensen Phosphate Buffer	50 ml	\cong 0.1 M
---------------------------------	-------	---------------

25% Glutaraldehyde	25 ml	≅ 6.25% (v/v)
Milli-Q® H ₂ O	25 ml	

Sonication buffer for liquid PanMa (10 ml)

Sodium-Dodecyl-Sulfate	400 mg	≅ 4% (w/v)
1 M Tris-HCl solution	500 µl	≅ 50 mM
Milli-Q® H ₂ O	Ad 10 ml	

0.2 M Sorensen Phosphate Buffer (1 l)

Sodium phosphate dibasic dihydrate	12.82 g	≅ 72 mM
Sodium phosphate monobasic	3.36 g	≅ 28 mM
Milli-Q® H ₂ O	800 ml	
→ Adjust to pH 7.2		
Milli-Q® H ₂ O	Ad 1 l	

0.1 M Sorensen Phosphate Buffer (1 l)

0.2 M Sorensen Phosphate Buffer	500 ml	≅ 0.1 M
Milli-Q® H ₂ O	500 ml	

1x TAE Buffer (1 l)

Tris	4.84 g	≅ 40 mM
Acetic acid (100%)	1.14 ml	≅ 20 mM
EDTA disodium salt dihydrate	370 mg	≅ 1 mM
Aqua dest.	Ad 1 l	

TE buffer, pH 7.4 (1 l)

1 M Tris-HCl solution	1 ml	≅ 10 mM
EDTA disodium salt dihydrate	0.37 g	≅ 1 mM
Milli-Q® H ₂ O	800 ml	
→ Adjust to pH 7.4		
Milli-Q® H ₂ O	ad 1 l	

1x TE Buffer, pH 9.0 (1 l)

Tris	1.21 g	≅ 10 mM
EDTA disodium salt dihydrate	370 mg	≅ 1 mM
Aqua dest.	800 ml	
→ Adjust to pH 9.0		
Aqua dest.	Ad 1 l	

13.2 Cell culture media composition

HECs differentiation protocol (Rezania et al. 2012; Rezania et al. 2014)

Stage	day	Basal medium	Supplements
R-S1 (DE)	d0	RPMI, Glutamax™	1% P/S, 0.2% FCS, 100 ng/ml Activin A, 2 µM CHIR99021
	d1 – d2	RPMI, Glutamax™	1% P/S, 0.5% FCS, 100 ng/ml Activin A
R-S2 (PGT)	d3 – d5	DMEM/F-12, Glutamax™	1% P/S, 2% FCS, 50 ng/ml FGF7
R-S3 (PF)	d6 – d9	DMEM, high glucose, Glutamax™	1% P/S, 1% B27™, 250 nM SANT-1, 2 µM Retinoic Acid, 100 ng/ml Noggin
R-S4 (PP)	d10 – d13	DMEM, high glucose, Glutamax™	1% P/S, 1% B27™, 100 ng/ml Noggin, 1 µM ALK5 inh. II, 50nM TBP
R-S5 (HE)	d14 – d21	DMEM, high glucose, Glutamax™	1% P/S, 1% B27™, 10 µM ALK5 inh. II, 100nM LDN193189, 1 µM T3, 100 nM γ-secretase inh. XX, 10 µg/ml (= 1 U/ml) Heparin

β-cell differentiation protocol (referred to as Bergen Airlift protocol) (Rezania et al. 2014)

Stage	day	Basal medium	Supplements
B-S1 (DE)	d0	MCDB 131	1% P/S, 1x Glutamax™, 1.5g/l Sodium Bicarbonate, 10 mM Glucose, 0.5% BSA, 100 ng/ml Activin A, 3 µM CHIR99021
	d1	MCDB 131	1% P/S, 1x Glutamax™, 1.5g/l Sodium Bicarbonate, 10 mM Glucose, 0.5% BSA, 100 ng/ml Activin A, 0.3 µM CHIR99021
	d2	MCDB 131	1% P/S, 1x Glutamax™, 1.5g/l Sodium Bicarbonate, 10 mM Glucose, 0.5% BSA, 100 ng/ml Activin A
B-S2 (PGT)	d3 – d4	MCDB 131	1% P/S, 1x Glutamax™, 1.5g/l Sodium Bicarbonate, 10 mM Glucose, 0.5% BSA, 0.25 mM ascorbic acid, 50 ng/ml FGF7
B-S3 (PF)	d5 – d6	MCDB 131	1% P/S, 1x Glutamax™, 1.5g/l Sodium Bicarbonate, 10 mM Glucose, 2% BSA, 0.25 mM ascorbic acid, 50 ng/ml FGF7, 0.25 µM SANT-1, 1 µM Retinoic acid, 100nM LDN193189, 200 nM TBP, 0.5% ITS-X
B-S4 (PE)	d7 – d9	MCDB 131	1% P/S, 1x Glutamax™, 1.5g/l Sodium Bicarbonate, 10 mM Glucose, 2% BSA, 0.25 mM ascorbic acid, 2 ng/ml FGF7, 0.25 µM SANT-1, 0.1 µM Retinoic acid, 200 nM LDN193189, 100 nM TBP, 0.5% ITS-X
B-S5 (HE)	d10 – d12	MCDB 131	1% P/S, 1x Glutamax™, 1.5g/l Sodium Bicarbonate, 20 mM Glucose, 2% BSA, 0.25 mM ascorbic acid, 0.25 µM SANT-1, 0.05 µM Retinoic acid, 100 nM

			LDN193189, 0.5% ITS-X, 1 μ M T3, 10 μ M ALK5 II inh., 10 μ M zinc sulfate
B-S6	d13 – d20	MCDB 131	1% P/S, 1x Glutamax TM , 1.5g/l Sodium Bicarbonate, 20 mM Glucose, 2% BSA, 100 nM LDN193189, 0.5% ITS-X, 1 μ M T3, 10 μ M ALK5 II inh., 10 μ M zinc sulfate, 10 μ g/ml Heparin (1 U/ml), 100 nM γ -secretase inh. XX
B-S7	d21 – d27	MCDB 131	1% P/S, 1x Glutamax TM , 1.5g/l Sodium Bicarbonate, 20 mM Glucose, 2% BSA, 0.5% ITS-X, 1 μ M T3, 10 μ M ALK5 II inh., 10 μ M zinc sulfate, 10 μ g/ml Heparin (1 U/ml), 1mM N-Acetyl Cysteine, 10 μ M Trolox, 2 μ M R428

Spontaneous Differentiation (SD) medium

	<i>Basal medium</i>	<i>Supplements</i>
Spontaneous Differentiation	DMEM/F12	1% P/S, 20% Knockout TM Serum replacement, 2 mM L-Glutamine, 100 mM non-essential amino acids, 0.1 mM 2-Mercaptoethanol

13.3 Cell lines

<i>Cell line</i>	<i>Information</i>	<i>Vendor/Company</i>
ECs (RFP expressing)	human dermal microvascular endothelial cells (transduced lentivirally with RFP)	University Würzburg, AG Nickel
iMR 90-4	iPS(IMR90)-clone(4)-DL-1	WiCell

13.4 Cell culture media and solutions

<i>Material name</i>	<i>Vendor</i>	<i>Catalogue #</i>
DMEM, high glucose, Glutamax TM	ThermoFisher	61965-026
DMEM/F-12	ThermoFisher	21331-020
DMEM/F-12, Glutamax TM	ThermoFisher	31331-028
Dulbecco's Phosphate Buffered Saline with MgCl ₂ and CaCl ₂ (PBS ⁺)	Sigma-Aldrich	D8662-500ML
Dulbecco's Phosphate Buffered Saline without MgCl ₂ and CaCl ₂ (PBS ⁻)	Sigma-Aldrich	D8537-500ML
Dulbecco's Phosphate Buffered Saline without MgCl ₂ and CaCl ₂ , 10x (PBS ⁻)	Sigma-Aldrich	D1283-500ML
MCDB 131	ThermoFisher	10372019
mTeSR TM 1	Stemcell Tech.	85850
RPMI, Glutamax TM	ThermoFisher	61870-010
Vasculife®	Cellsystems	LL-0005

13.5 Medium supplements

Material name	Vendor	Catalogue #
2-Mercaptoethanol (cell culture)	ThermoFisher	31350010
Activin A	Peptotech	120-14E-250
ALK5 inhibitor II	Enzo life sciences	ALX-270-445-M005
B27™ (without Vitamin A)	ThermoFisher	12587010
BSA (for cell culture)	Sigma	A7030-100G
BSA (for histology)	Biofrox	1126GR500
CHIR99021	Biomol	Cay-13122
FCS	Bio & Sell	FCS.ADD.0500
Glucose	Sigma-Aldrich	G8270-1KG
Glutamax™	ThermoFisher	35050038
Heparin sodium salt	Sigma-Aldrich	H3149-10KU
ITS-X	ThermoFisher	51500056
KGF (FGF7)	Peptotech	100-19-100
Knockout™ serum replacement	ThermoFisher	10828028
L-Ascorbic Acid	Sigma-Aldrich	A4544-25G
LDN193189	Stemcell	72146-1mg
L-Glutamine	Sigma-Aldrich	G7513-100ML
MEM NEAAs	ThermoFisher	11140035
N-Acetyl Cysteine	Sigma	A9165-5G
Noggin	Peptotech	AF-250-38
P/S (Penicillin/Streptomycin)	Sigma-Aldrich	P4333-100ML
Phenol Red solution, 0.5%	Sigma-Aldrich	P0290-100ML
R428 (Bemcentinib)	Selleckchem	S2841-1mg
Retinoic Acid	Sigma-Aldrich	R2625-50MG
SANT-1	Sigma-Aldrich	S4572-5MG
Sodium bicarbonate, solution	ThermoFisher	S8761-500ML
T3 (3,3',5-Triiodo-L-thyronine sodium salt)	Sigma-Aldrich	T6397-250MG
TPB	R&D	5343/1
Trolox	EMD Millipore	648471-500MG
Y-27632 (ROCK inhibitor)	Bio-Techne	1254/10
Zinc sulfate heptahydrate	Sigma-Aldrich	Z0251-100G
γ-secretase inhibitor XX	EMD Millipore	565789-1mg

13.6 Cell culture surface coatings

Material name	Vendor	Catalogue #
Gelatine	Seva	22151
Matrigel®	Corning	356231

13.7 Enzymes

Enzyme	Vendor	Catalogue #
Accutase® Solution	Sigma-Aldrich	A6964-100ML
Dispase II, Powder	ThermoFisher	17105-041
DNase I (for decellularization)	Roche	10104159001
DNase I (for RNA Iso)	Qiagen	79254
Pepsin	Sigma-Aldrich	77160-25G
Trypsin-EDTA	ThermoFisher	15400054

13.8 Commercial kits

Material name	Vendor	Catalogue #
BCA Protein Assay Kit	Merck	71285-3
DNeasy Blood & Tissue Kits	Qiagen	69506
Human Glucagon ELISA Kit	Mercodia	10-1271-01
Human Insulin ELISA Kit	Mercodia	10-1113-01
iScript™ cDNA Synthesis Kit	Bio-Rad	1708891
Quant-iT™ PicoGreen™ dsDNA Assay-Kit	ThermoFisher	P11496
RNeasy Micro Kit	Qiagen	74004
RNeasy Mini Kit	Qiagen	74104
SsoFast™ Eva Green® Supermix	Bio-Rad	1725201
Total bile acids Assay	Diazyme	DZ042A-K

13.9 Chemicals and solutions for histology and molecular biology

Component	Vendor	Catalogue #
1% alcian blue	Morphisto	10126.00500
25% Glutaraldehyde	Sigma-Aldrich	G5882-50ML
2-Mercaptoethanol (RNA isolation)	Sigma-Aldrich	M3148-100ML
4 kD FITC-Dextran	Sigma-Aldrich	46944-100MG-F
40 kD FITC Dextran	Sigma-Aldrich	FD40S-100MG
Acetic acid	Applichem	A8020,2500PE*
Agarose	Genaxxon bioscience	M3044.0500
Alkaline alcohol	Morphisto	10132.01000
Antibody dilution solution	DCS diagnostics	AL120R500
Brilliant Crocein-acid fuchsin	Morphisto	10156.01000
Calcium chloride dihydrate (CaCl ₂ · 2 H ₂ O)	Sigma-Aldrich	C7902-500G
Citric acid (C ₆ H ₈ O ₇)	Sigma-Aldrich	W230618-10KG-K
Dimethyl sulfoxide (DMSO)	Sigma-Aldrich	D8418-500ML
DNA ladder (100 – 3000 bp)	VWR Peqlab	25-2020
Donkey serum	Sigma-Aldrich	S30-100ml
Entellan®	Merck	107960.0500
Eosin 1%, aqueous	Morphisto	10177.00500

Ethanol (absolute)	ChemSolute	2246.1000
Ethanol (denatured)	Carl Roth	K928.4
Ethylenediaminetetraacetic acid (EDTA), disodium salt dihydrate ($C_{10}H_{14}N_2Na_2O_8 \cdot 2H_2O$)	Sigma-Aldrich	E5134-1KG
Fluoresceindiacetate (FDA)	Sigma-Aldrich	F7378-5G
Fluoromount-G™, with DAPI	ThermoFisher	00-4959-52
GelRed®	Genaxxon bioscience	M3199.0500
Hematoxylin acid acc. to Mayer	Morphisto	10231.01000
Heparin Natrium	Ratiopharm®	-
Hepes ($C_8H_{18}N_2O_4S$)	Sigma-Aldrich	H4034-100G
Histogel	ThermoFisher	HG-4000-012
Hydrochloric Acid, 1 N	Carl Roth	K025.1
Isopropanol	Carl Roth	6752.2
Light green	Morphisto	10267.01000
Magnesium sulfate ($MgSO_4$)	Carl Roth	0261.1
MTT (3-(4,5-Dimethyl-2-thiazolyl)-2,5-diphenyl-2H-tetrazolium·bromide) ($C_{18}H_{16}BrN_5S$)	Serva	20395.04
Phosphomolybdic acid - Orange G - (A)	Morphisto	11195.00.500
Phosphotungstic acid	Morphisto	10324.00500
Ponceau acid Fuchsin	Morphisto	10366.01000
Potassium chloride (KCl)	Applichem	A3582*
Potassium phosphate monobasic (KH_2PO_4)	Merck	1.04873.1000
Propidiumiodide (PI)	Sigma-Aldrich	P4170-10MG
Resorcin-Fuchsin	Morphisto	10354.01000
Roti® 4% Histofix	Carl Roth	P087.3
Safron du Gatinais	Morphisto	10369.00250
Schiff's reagent	Merck	107907/2
Sodium bicarbonate, solid ($NaHCO_3$)	Carl Roth	HN01.2
Sodium chloride (NaCl)	Carl Roth	P029.4
Sodium deoxycholate	Sigma-Aldrich	30970-500G
Sodium hydroxide, 1N	Sigma-Aldrich	1.09137.1000
Sodium metabisulfite	Merck	107907/3
Sodium phosphate dibasic dihydrate ($Na_2HPO_4 \cdot 2 H_2O$)	Merck	1.06580.1000
Sodium phosphate monobasic (NaH_2PO_4)	Sigma-Aldrich	S8282-500G
Sodium-dodecyl-sulfate ($NaC_{12}H_{25}SO_4$)	Carl Roth	CN30.4
Stresnil®	Elanco	-
T61®	MSD Animal Health	-
Tris ($C_4H_{11}NO_3$)	Serva	37181.02
Tris-HCl solution, 1M	Applichem	A4577,1000
Triton® X 100	Carl Roth	3051.2
Trypan Blue solution	Sigma-Aldrich	T8154-20ML
Tween® 20	Sigma-Aldrich	P1379-500ML
Ultrapure water (PCR Grade)	Braun	CE 0123

Ursotamin®	Serumwerk, Bernburg	-
Van Gieson Picrofuchsin solution	Morphisto	11486.02500
Weigert's iron hematoxyline solution A	Morphisto	10225A.01000
Weigert's iron hematoxyline solution B	Morphisto	10225B.01000
WST-1	Sigma-Aldrich	11644807001
Xylene (isomers)	Carl Roth	9713.3

*no longer available

13.10 Primary Antibodies

Antigen	Marker	host	Antigen retr.	dil.	vendor	Catalogue #
COL I	ECM component	ms	Citrate pH 6	1:500	Abcam	ab90395
COL III	ECM component	ms	Citrate pH 6	1:250	Abcam	ab90395
COL IV	ECM component	rb	Citrate pH 6	1:200	Abcam	ab6586
CPEP	β-cell	rt	Citrate pH 6	1:500	DSHB	GN-ID4
GATA4	Endoderm	rb	Citrate pH 6	1:500	Abcam	ab5790
GCG	α-cell	ms	Citrate pH 6	1:1000	Abcam	ab10988
INS	β-cell	gp	Citrate pH 6	1:100	Dako	A0564*
LAM	ECM component	rb	Citrate pH 6	1:200	Abcam	ab11575
MAFA	Maturing β-cell	rb	Citrate pH 6	1:250	Abcam	ab26405
NANOG	Pluripotency	rb	Citrate pH 6	1:150	Abcam	ab80892
NKX6.1	β-cell lineage	gt	Citrate pH 6	1:250	R&D	AF5857
OCT4	Pluripotency	gt	Citrate pH 6	1:100	Abcam	ab27985
PAX6	Ectoderm	rb	TE pH 9	1:500	Abcam	ab124265
PDX1	Pancreatic prog.	gt	Citrate pH 6	1:250	R&D	AF2419
SOX2	Pluripotency	rb	Citrate pH 6	1:50	Abcam	ab137385
SST	δ-cell	rb	Citrate pH 6	1:250	Sigma-Ald.	HPA019472
TRA 1-60	Pluripotency	ms	Citrate pH 6	1:250	Abcam	ab16288
VWF	Endothelium	rb	Citrate pH 6	1:100	Abcam	ab9378

*no longer available

13.11 Secondary Antibodies

Antigen	Fluorophor	host	dilution	vendor	Catalogue #
gp	Alexa488	gt	1:400	Life Technologies	A11073
gt	Alexa647	dk	1:400	Life Technologies	A21447
ms	Alexa555	dk	1:400	Life Technologies	A31570
ms	Alexa647	dk	1:400	Life Technologies	A31571
rb	Alexa647	dk	1:400	Life Technologies	A31573
rb	Alexa555	dk	1:400	Life Technologies	A31572
rt	Alexa488	dk	1:400	Life Technologies	A21208

13.12 Primers

Gene/RefSeq	Reference	T [C°]	Primer sequence (5'-3')
<i>AFP</i> NM_001134.3	(D'Antonio et al. 2017)	60	f TGAGCACTGTTGCAGAGGAG r TTGTTTGACAGAGTGTCTTGTGGA
<i>ALDH1A1</i> NM_000689.5	(D'Antonio et al. 2017)	60	f CTGCTGGCGACAATGGAGT r CGCAATGTTTTGATGCAGCCT
<i>BMP4</i> NM_001202.6	(Bock et al. 2011)	60	f GCACTGGTCTTGAGTATCCTG r TGCTGAGGTTAAAGAGGAAACG
<i>CDX2</i> NM_001265.6	-	60	f CCCTCGGCAGCCAAGTGAAA r TCCTCCGGATGGTGTAGTAG
<i>COL1A1</i> NM_000088.4	(D'Antonio et al. 2017)	60	f GAGGGCCAAGACGAAGACATC r CAGATCACGTCATCGCACAAAC
<i>CXCR4</i> NM_003467.3	(D'Amour et al. 2006)	60	f CACCGCATCTGGAGAACCA r GCCCATTTCCCTCGGTGTAGTT
<i>DCN</i> NM_001920.5	(D'Antonio et al. 2017)	60	f AGAGTACCTGGTGGGCTGG r GTGGGCAGAAGTCACTTGAT
<i>FOXA2</i> NM_153675.3	-	60	f GGGAGCGGTGAAGATGGA r TCATGTTGCTCACGGAGGAGTA
<i>GATA1</i> NM_002049.4	(Bock et al. 2011)	60	f TGCGGCCTCTATCACAAGATG r CTGCCCGTTTACTGACAATCA
<i>GATA2</i> NM_032638.5	(D'Antonio et al. 2017)	60	f CTGTCTGCAACGCCTGTG r GTTCCGAGTCTGGATCCCTT
<i>GATA4</i> NM_001308093.3	(Ruiz et al. 2010)	60	f ACACCCCAATCTCGATATGTTTG r GTTGCACAGATAGTGACCCGT
<i>GATA6</i> NM_005257.6	(Ruiz et al. 2010)	60	f AGGGCTCGGTGAGTCCAAT r CGCTGCTGGTGAATAAAAAGGA
<i>GCG</i> NM_002054.5	(D'Amour et al. 2006)	60	f AAGCATTTA CTTTGTGGCTGGATT r TGATCTGGATTTCTCCTCTGTGTCT
<i>HNF1b</i> NM_000458.4	(D'Amour et al. 2006)	60	f TCACAGATACCAGCAGCATCAGT r GGGCATCACCAGGCTTGTA
<i>HNF4a</i> NM_000457.5	(D'Amour et al. 2006)	60	f CGAAGGTCAAGCTATGAGGACA r ATCTGCGATGCTGGCAATCT
<i>HOXC5</i> NM_018953.4	-	60	f CACATGAGCCACGAGACGG r TCCACTTCATCCTGCGGTTT
<i>IGF2</i> NM_000612.6	(D'Antonio et al. 2017)	60	f AGACGTA CTGTGCTACCCC r TGCTTCCAGGTGTCATATTGG
<i>INS</i> NM_000207.3	(Zhang et al. 2009)	62	f GCAGCCTTTGTGAACCAACAC r CCCCACACTAGGTAGAGA
<i>INS (primer: CB-1)</i> NM_000207.3	-	60	f TCTACACACCCAAGACCCGC r GTTCCACAATGCCACGCTTC
<i>MAFA</i> NM_201589.4	(Zhang et al. 2009)	60	f CTTTCAAGCAAGGAGGAGTTCATC r CTCGTATTTCTCCTTGTACAGGTCC
<i>NANOG</i> NM_024865.4	-	60	f CCAAATTCTCCTGCCAGTGAC r CACGTGGTTTCCAACAAGAAA

<i>NKX2.1</i> NM_001079668.3	-	60	f AGGACACCATGAGGAACAGC r CATGAAGCGGGAGATGGCG
<i>NKX6.1</i> NM_006168.3	(Zhang et al. 2009)	60	f AGACCCACTTTTTCCGGACA r CCAACGAATAGGCCAAACGA
<i>OCT4</i> NM_002701.6	-	60	f CCTCACTTCACTGCACTGTA r CAGGTTTTCTTTCCCTAGCT
<i>PAX6</i> NM_001127612.3	(Bock et al. 2011)	60	f AACGATAACATACCAAGCGTGT r GGTCTGCCCGTTCAACATC
<i>PAX9</i> NM_001372076.1	-	60	f GTTATGTTGCTGGACATGGGT r GAAGCCGTGACAGAATGACTAC
<i>PDX1</i> NM_000209.4	(D'Amour et al. 2006)	62	f AAGTCTACCAAAGTCCACGCG r GTAGGCGCCGCCTGC
<i>PTF1α</i> NM_178161.3	-	60	f CTCAACAGCAAATCTTCCTTCAACAAC r CTTCAGCCGAGTCTGGGACTTC
<i>RPL4</i> NM_000968.4	-	60	f GCCTGCTGTATTCAAGGCTC r GGTTGGTGCAAACATTCGGC
<i>RPL6</i> NM_001024662	-	60	f ATTCCCGATCTGCCATGTATTC r TACCGCCGTTCTTGTCACC
<i>RPS29</i> NM_001032.5	(D'Antonio et al. 2017)	60	f AATATGTGCCGCCAGTGTTTT r CCCGGATAATCCTCTGAAGG
<i>SOX2</i> NM_003106.4	-	60	f CCCAGCAGACTTCACATGT r CCTCCCATTTCCCTCGTTTT
<i>SOX17</i> NM_022454.4	-	60	f GGCGCAGCAGAATCCAGA r CCACGACTTGCCCAGCAT
<i>SST</i> NM_001048.4	(Zhang et al. 2009)	60	f CCCAGACTCCGTGAGTTTCT r ATCATTTCTCCGTCTGGTTGG

13.13 Expandable materials

Item name	Vendor	Catalogue #
24-well plates	TPP	92024
3 kD Amicon® Ultra Centrifugal filters	Merck	UFC900324
30 kD Amicon® Ultra Centrifugal filters	Merck	UFC903024
48-well plates	TPP	92048
96-well plates black bottom	VWR	82050-728
Biopsy punch	pfm medical	48201
Catheter 18G	Braun	4269136
Catheter 20G	Braun	4269110
Catheter 22G	Braun	4269102
Cell crowns (reusable)	Kuhn GmbH	-
Costar® 6-well ultra-low attachment plates	Corning	3471
Filter-Inserts, 12-well, 3.0 μ m	Costar	3402
Hydrophobic Pen	Science Services	N71310
NUNC™ 6-well Plates	ThermoFisher	140675

PET-Inserts, 24 well, 0.4 µm, translucent	Greiner bio-one	662640
Poly-l-lysine-coated glass slides	VWR	631-1349
Qiashredder	Qiagen	79656
Superfrost Glass slides	VWR	631-0650
T150 cell culture flasks	TPP	90151
145 mm Petridish	Greiner bio-one	639161

13.14 Machines

<i>Machine</i>	<i>Model</i>	<i>Company</i>
Binocular	SteREO Discovery.V12	Zeiss
Cell culture CO ₂ Incubator	BBD 6220	ThermoFisher
Cell culture hood	Safe 2020	ThermoFisher
Centrifuge (Cell culture)	Sorvall Legend X1R	ThermoFisher
Centrifuge (Molecular Biology)	Centrifuge 5424 R	Eppendorf
Digital Camera	DS126191	Canon
Embedding machine	Microm STP 120	ThermoFisher
Lyophilizer	Alpha 1-2 LO Plus	Christ
Micro balance	MSE3.6P-000-DM	Sartorius
Microscope, brightfield (Cell culture)	EVOS XL	ThermoFisher
Microscope, confocal	TCS SP8	Leica Microsystems CMS GmbH
Microscope, fluorescence	BZ-9000	Keyence Corporation
Microscope, scanning electron	JEOL JSM 7500F	Jeol Ltd.
Microtome	SM2010 R	Leica Microsystems CMS GmbH
Milli-Q® water treatment system	Milli-Q® Advantage A10	Merck
Orbital Shaker	KM-2 Akku	Edmund Bühler GmbH
Plate Reader	Infinite M200	Tecan Group
Power supply	EV243	PEQLAB Biotechnologie GmbH
Pumps	MCP Standard	Ismatec
qPCR Cycler	CFX96 RT System	Bio-Rad
Sonicator (for cells)	Sonopuls HD 4100	Bandelin
Sonicator (for tissue)	Digital sonifier; 102-C (CE)	Branson
Sonotrode (for Branson sonicator)	Micro Tip 3/16	Branson
Sonotrode (for Sonopuls sonicator)	TS103	Bandelin
Steam cooker	Type 3216	Braun
Thermocycler cDNA	Labcycler 48	Sensoquest
Thermomixer	Thermomixer comfort	Eppendorf
Tissue Lyser	TissueLyser LT	Qiagen
Tissue Rupture	TissueRuptor	Qiagen

13.15 *Software*

<i>Software (version)</i>	<i>Company</i>
BZ-II Analyzer (2.1)	Keyence Corporation
BZ-II Viewer	Keyence Corporation
CFX Manager (3.1.1517.0823)	Bio-Rad
GraphPad Prism (8.4.3 (686))	GraphPad Software Inc.
i-control (3.9.1.0)	Tecan Group
Image J (1.51n + Biovoxxel toolbox)	W. Rasband., National Institute of Health
Inkscape (0.92.4)	open source
Leica Application Suite X (3.5.6.21594)	Leica Microsystems CMS GmbH
Mega-Capt (15,14)	Vilber Lourmat
Microsoft Excel (Office 2016)	Microsoft
Microsoft Word (Office 2016)	Microsoft
OriginPro 2020 (9.7.0.188 (Lehre))	OriginLab Corporation

14 Acknowledgment

Writing the acknowledgement is at least some productive way of procrastination. Currently, I am far away from finishing this thesis. So, I type this text in the optimistic speculation that I will successfully submit my thesis in due time. If you read these lines, I apparently made it.

During my time in the lab and while writing this thesis, I experienced tremendous support from many different people.

First and foremost, I would like Dr. Daniela Zdzieblo for your great support, your time, your patience, your enthusiasm, for turning off the electronic ankle tag every fourth weekend and for eventually **paving the way** to the completion of my PhD. Please, never lose your passion for science and please do not get lost in the office. The bench needs you.

Furthermore, I thank the members of my thesis committee for their steady support. PD Dr. Marco Metzger for your fruitful input during our meetings and for keeping me off the streets for four years by keeping the institute running, Prof. Heike Walles for your helpful suggestions and your humorous comments during our meetings and Prof. Faßnacht-Capeller for being an attentive supervisor and for sparing your time to support this work. I am sorry you only made it to the second place, but Daniela is undisputedly No. 1 – otherwise my electronic tag will send me shocks...

I also thank Prof. Manfred Gessler for filling in the function of the chairman. I sincerely hope that you will not surprise me with a “biochemistry-quickie-test” at the end of my defense.

I would further like to grant my biggest gratitude to the people who accompanied me during my time at the institute and who fill the chair with life: Sanjana, my brother in hip David, Philipp O. and P., Christina, Heike, Renate, Maria, Joachim, Olli, Sabrina, Antje, Kirsten, Heidi and Heide, Martina, Florian, Christian, Anna, Maxi, Matthias, Rinu, Ji, Marius, Tobi S. und W., Antje, Basti, the true emperors of this institute Anna-Kristina and Özlem, Marc, Shabaz, the second best football manager Thomas, Patrick, Mona, Kirsten, Gudrun, Sarah, Franzi, Tamás and all those who already left us. To another city. Not – they are still alive: Florentin, David F., Christoph R., Claudia, Matthias S., Marion, Elke. You all made a lasting impression and were one of the reasons why I enjoyed (almost) every day of my PhD.

A special thanks goes to Tom, for many good discussions and funny Schafkopf evenings, to Alevtina for being a great support in the cell culture, to Franze for being a tremendous help with the pancreas and in the lab, to Markus for your great support and inspiring discussion, to Anna-Lena for being an excellent bachelor student, to Jonas for being a student (kidding – he also did a

great job in the lab) and to the former Pankreat and now Punk-pirate Sebastian Kress for doing NICCs with me. Thank you!

I especially do **not** thank COVID-19, who made 2020 horrible. Furthermore, I unacknowledge the bursted tube that ruined one decellularization experiment and made me clean the lab for 2 hours. Also thanks for nothing to all the cells that didn't grow, to the bacteria that did grow and to the student who switched the labels for Trypsin and Pen/Strep.

While some things cannot pass quickly enough, others should never be forgotten. I would therefore like to point out that pigs were sacrificed during this study for scientific purposes. Remembering that every day we work with these materials is the least we can do and I sincerely hope that their sacrifice was not in vain.

I would also like to thank many people from outside the lab. First of all, I want express my greatest to my parents, my grandpa and his wife for all your support. Knowing that you are always there gives me so much strength, confidence and energy. Dear grandpas and grandmas: thank you for everything you gave to me. Also, I would like to thank my friends outside the lab. You all supported me and kept me in balance. I am particularly honoured to be a member of the best club in the world TSV Grombühl and to coach a wonderful football team. Never give up! 90+4!

I further owe un grande merci to Kim, who suddenly appeared and luckily stayed. As John Lennon once said: "Love is all you need" ... and food. So thank you so much for keeping me alive with your delicious food – and love.

Consti out! **mic drop**

15 Curriculum Vitae

16 List of Publications

C. Berger, D. Zdzieblo. „Glucose Transporters in Pancreas in Health and Disease.” Review, *Pflugers Archive – European Journal of Physiology* 2020

C. Berger*, Y. Bjørlykke*, L. Hahn, M. Mühlemann, S. Kress, H. Walles, R. Luxenhofer, H. Ræder, M. Metzger, D. Zdzieblo. „Matrix decoded – A pancreatic extracellular matrix with organ specific cues guiding human iPSC differentiation.” *Biomaterials*, 2020(*shared 1st authorship)

T. Däullary, C. Fey, **C. Berger**, M. Metzger, D. Zdzieblo. “Bioartificial gut – current state of small intestinal tissue engineering.” Book Chapter, *Woodhead publishing series in Biomaterials*, 2020

I. Schwedhelm, D. Zdzieblo, A. Appelt-Menzel, **C. Berger**, T. Schmitz, B. Schuldt, A. Franke, F. J. Müller, O. Pless, T. Schwarz, P. Wiedemann, H. Walles, J. Hansmann. „ Automated real-time monitoring of human pluripotent stem cell aggregation in stirred tank reactors” *Scientific Reports*, 2019

M. Mühlemann, D. Zdzieblo, A. Friedrich, **C. Berger**, C. Otto, H. Walles, H. Koepsell, M. Metzger. “Altered pancreatic islet morphology and function in SGLT1 knockout mice on a glucose-deficient, fat-enriched diet.” *Molecular Metabolism*, 2018

C. Berger, F. Helmprobst, P. Chapouton, C. Lillesaar, C. Stigloher. “sept8a and sept8b mRNA expression in the developing and adult zebrafish.” *Gene Expression Patterns*, 2017

R. Blumroeder, A. Glunz, B. Dunkelberger, C. Serway, **C. Berger**, B. Mentzel, S. de Belle, T. Raabe. “MCM3 replicative helicase mutation impairs neuroblast proliferation and memory in *Drosophila*.” *Genes, Brain and Behaviour*, 2016

17 Affidavit

I hereby confirm that my thesis entitled "*Influence of the pancreatic extracellular matrix on pancreatic differentiation of human induced pluripotent stem cells and establishment of 3D organ models*" is the result of my own work. I did not receive any help or support from commercial consultants. All sources and / or materials applied are listed and specified in the thesis.

Furthermore, I confirm that this thesis has not yet been submitted as part of another examination process neither in identical nor in similar form.

Place, Date

Signature

18 Eidesstattliche Erklärung

Hiermit erkläre ich an Eides statt, die Dissertation „*Einfluss der Extrazellulärmatrix des Pankreas auf die pankreatische Differenzierung induziert pluripotenter Stammzellen und Etablierung von 3D Organmodellen*“ eigenständig, d.h. insbesondere selbständig und ohne Hilfe eines kommerziellen Promotionsberaters, angefertigt und keine anderen als die von mir angegebenen Quellen und Hilfsmittel verwendet zu haben.

Ich erkläre außerdem, dass die Dissertation weder in gleicher noch in ähnlicher Form bereits in einem anderen Prüfungsverfahren vorgelegen hat.

Ort, Datum

Unterschrift